NASA-CR-120831
AI-72-1

HIGH TEMPERATURE (1200°C) CERAMIC-TO-METAL SEAL DEVELOPMENT

By
R. L. McKisson and G. Ervin, Jr.

Atomics International
North American Rockwell

Prepared for

NATIONAL AERONAUTICS AND SPACE ADMINISTRATION
NASA LEWIS RESEARCH CENTER
Under Contract No. NAS3-11840

1. Report No.	2. Government Accession No.	3. Recipient's Catalog No.
NASA-CR-120831		

4. Title and Subtitle	5. Report Date
High Temperature (1200°C) Ceramic-to-Metal Seal Development	December 15, 1972
	6. Performing Organization Code AI-72-1

7. Author(s)	8. Performing Organization Report No.
R. L. McKisson and G. Ervin, Jr.	
	10. Work Unit No.

9. Performing Organization Name and Address	11. Contract or Grant No.
Atomics International Post Office Box 309 Canoga Park, California 91304	NAS-3-11840
	13. Type of Report and Period Covered: Contractor Report

12. Sponsoring Agency Name and Address	14. Sponsoring Agency Code
National Aeronautics and Space Administration Lewis Research Center 21000 Brookpark Road, Cleveland, Ohio	

15. Supplementary Notes

Project Manager, Russell A. Lindberg, Non-Destructive Evaluations Section, Materials Applications Branch, Materials and Structures Division, NASA-Lewis Research Center, Cleveland, Ohio.

16. Abstract

Two phases have been completed, of a program whose ultimate objective is the development of an alkali metal resistant, thermal shock resistant, leak-tight, and neutron radiation resistant ceramic-to-metal seal capable of operation at 1200°C for three to five years. The first phase involved the screening of platinum-base, vanadium-base and vanadium-niobium base brazes for the joining of Cb-1Zr or T-111 alloys to high purity alumina. The second phase involved studies of the performance of sealed capsule samples during 5000-hour aging tests at 800°, 1000°, and 1200°C in high vacuum.

Sealed capsules which were made using pure vanadium braze, and were brazed at 1850°C for one minute, survived 64 thermal cycles to 1200°C at the heating/cooling rate of 100°C/minute. Vanadium braze samples survived 5000-hour aging tests at 800°, 1000°, and 1200°C. One thermally cycled sample survived a subsequent 5000-hour aging period at 1000°C, but another, at 1200°C, did not survive.

It is concluded that a pure vanadium braze used to bond high purity alumina to Cb-1Zr alloy is the best of the systems studied, but that additional studies must be performed to establish its service temperature limitations for the desired three to five years' service.

17. Key Words (Suggested by Author(s))	18. Distribution Statement
Seals, ceramic, braze, high temperature, alumina, Cb-1Zr alloy.	Unclassified, unlimited

19. Security Classif. (of this report)	20. Security Classif. (of this page)	21. No. of Pages	22. Price*
Unclassified	Unclassified	292	$3.00

* For sale by the National Technical Information Service, Springfield, Virginia 22151

FOREWORD

The work described herein, which was conducted by Atomics International, a Division of North American Rockwell Corporation, was performed under NASA Contract NAS3-11840. The Project Manager for NASA was Mr. Russell A. Lindberg, Non-Destructive Evaluations Section, Applications Branch, Materials and Structures Division, NASA-Lewis Research Center, Cleveland, Ohio.

ACKNOWLEDGEMENT

The authors wish to express their appreciation to, and to acknowledge the contributions of: R. A. Lindberg, the NASA Project Manager for the program, for the frequent discussions and many useful suggestions relating to the work, and to its presentation in this report; and to L. Cooper, for his valued assistance and consultations regarding the electron microprobe work and his authorship of the sections in the report dealing with those studies.

TABLE OF CONTENTS

TABLE OF CONTENTS

TABLE OF CONTENTS

LIST OF TABLES

LIST OF TABLES

LIST OF TABLES

LIST OF FIGURES

LIST OF FIGURES

SUMMARY

A program whose ultimate objective is the development of an alkali metal resistant, thermal shock resistant, leak-tight, and neutron radiation resistant ceramic-to-metal seal capable of operation at 1200° C for three to five years has been completed. The program consisted of a screening phase in which candidate braze systems were evaluated on the basis of the metallurgical and strength characteristics of simple braze specimens and their behavior in a 1000-hour aging test sequence followed by a more demanding test sequence involving thermal cycling and 5000-hour aging of capsule specimens. Although the probable attainment of the ultimate goal of five-year service at 1200° C has not been demonstrated for any of the braze systems examined, significant and relevant information and additional new technology which is applicable to the further pursuit of the ultimate objective has been developed.

Alloys of the nominal compositions Pt-1Ce, Pt-2Hf, V-2Ce, V-2Hf, V-1Zr, V-2Ti, 64V-34Cb-2Zr, 64V-34Cb-2Ti, and pure V were tested for their ability to form a braze seal between very high purity alumina ceramic and Cb-1Zr alloy; and alloys of the nominal compositions V-10Mo, 65V-35Cb, V-10Mo-2Zr, V-2Hf, and 64V-34Cb-2Zr were tested for their ability to form a braze seal between very high purity alumina ceramic and T-111 alloy (Ta-8W-2Hf).

Two hundred sixty-two braze test specimens were prepared and evaluated. Of these, 224 were tests involving alumina and the Cb-1Zr alloy; 35 were tests involving alumina and the T-111 alloy; and three were tests involving beryllia and the Cb-1Zr alloy. These specimens were involved in a variety of tests, including 161 ultrasonic tests, 178 shear tests, 188 visual examinations of the broken surfaces, 52 metallurgical examinations, 47 microhardness profiles, and 40 electron microprobe examination series. Each of these electron microprobe examinations involved the measurement of the apparent concentration traces of six elements plus one or more back-scattered electron and area scan measurements. In addition, eighty modulus of rupture test specimens were prepared and tested.

None of the attempts to bond alumina and T-111 alloy were successful. Bonding between the ceramic and the T-111 is achieved at the braze temperatures of 1850-1950° C. Because of the thermal expansion differences, tensile forces are set up in the alumina as it cools, and because the brazes are not sufficiently ductile or plastic to accomodate these forces, the alumina cracks.

The platinum brazes typically dissolve large amounts of the Cb-1Zr alloy, and the resultant brazes contain two or three Pt-Cb alloys or compound compositions.

The vanadium and vanadium-niobium (columbium) base alloy brazes also dissolve large amounts of Cb-1Zr alloy, but the resultant braze alloy is single phase, and characteristically freezes to form

crystallites which are continuations of crystallites in the Cb-1Zr alloy. In addition, the vanadium and vanadium-niobium (columbium) base brazes tend to dissolve alumina, so that the final brazes contain appreciable amounts of aluminum, and presumably, oxygen, as well.

Fourteen bulb samples were prepared using two brazes with alumina and Cb-1Zr alloy. These bulb specimens were used in 14 thermal shock test evaluations, two thermal cycling tests, one cesium-vapor aging test, and six simple aging tests. Vacuum integrity measurements, metallographic examinations and microhardness traverse measurements were used in the evaluations of these bulb test samples.

These bulb samples were made using the V-2Ti and the pure V brazes. The samples formed by the V-2Ti brazes were found not to be vacuum tight. Those formed by the pure vanadium braze were vacuum tight and were demonstrated to be capable of undergoing 64 thermal cycles to 1200° C at 100° C/min. Uncycled vanadium brazed samples also survived the 5000-hour aging treatments at 800° C, 1000° C, and 1200° C. One sample survived the 64 thermal cycle treatment followed by a 5000-hour aging exposure at 1000° C without loss of vacuum integrity.

A bulb sample fitted with a cesium-filled reservoir which was held at 338° C (calculated cesium vapor pressure, 5 torr) survived a 1000-hour aging period at 1200° C, but developed a vacuum leak before completing a 5000-hour aging period.

In the final analysis, use of an active metal ceramic wetting promoter such as zirconium or titanium was found not to be necessary to effect a good bond to high-purity alumina ceramic. In fact, the pure vanadium braze was found to have adequate wetting capability. Further, the vanadium-base brazes which did contain one or two percent of a wetting promoter were found to be too active, and did not form vacuum-tight seal joints.

It is concluded that a pure vanadium braze, used to bond tungsten-coated high-purity alumina to high quality columbium-1% zirconium alloy, represents a ceramic-to-metal seal system capable of at least a year's operation in cesium vapor at a minimum temperature of 1000° C.

INTRODUCTION

The ultimate objectives of this ceramic-to-metal seal program are: "to provide long life (3 to 5 years), high temperature (1200°C), alkali metal resistant, thermal shock resistant, leak-tight, and neutron radiation resistant seals suitable for application in in-pile or out-of-pile nuclear thermionic space power systems," (Ref. 1). To this end, ceramic-to-metal seal systems were to be defined, prepared, and tested under conditions of thermal shock, high temperature aging to 5000 hours, and exposure to cesium metal vapor in order to evaluate their potential for long service life at 800°C, 1000°C, 1200°C, and 1400°C. The ceramic-metal combinations to be tested to 1200°C were high purity alumina with Cb-1Zr alloy, and high purity alumina with T-111 (Ta-8W-2Hf) alloy. In addition, if the Al_2O_3/T-111 tests were successful at 1200°C, the combination of high purity beryllia with T-111 alloy was to be tested to 1400°C.

The program study sequence involved two phases. In Phase I, thirteen braze systems, each consisting of a very high purity (99.99%) alumina ceramic braze alloy-refractory metal alloy combination, were carried through a brazing operation and a screening evaluation of the resultant braze joints. Each of the braze alloys was used with both a tungsten and a molybdenum barrier on the ceramic, so that in this initial series, twenty-six systems were examined. The evaluation of these twenty-six systems was made and the ten most promising systems were examined further in the second part of the Phase I study. This consisted of aging tests at 1200°C for times of 10, 100, 500, and 1000 hours (3.6×10^4, 3.6×10^5, 1.8×10^6, and 3.6×10^6s).* The analyses of the aged samples included Modulus of Rupture measurements, and microstructural, microhardness, and electron microprobe examinations.

Based upon these findings, the best braze system was selected for testing in the Phase II part of the program. This involved the fabrication of bulb-type samples using Al_2O_3 ceramic rings and refractory metal end caps, and the evaluation of these bulbs for their vacuum integrity in thermal shock, their aging behavior to 5000 hours (1.8×10^7s), and their long-term resistance to cesium vapor at temperatures to 1200°C. Figure 1 is a test sequence diagram for the program.

The preparation of early ceramic-to-metal seals involved a metallizing step by which a thin deposit of a metal such as molybdenum, rhenium, tungsten, iron, chromium, nickel and/or manganese was deposited on the ceramic material. (Ref. 2) The seal between this metal deposit and the ceramic is formed by the development of a thin glassy bond. The metal member of the seal is then brazed to the metallized surface. For service temperatures up to about 500°C, copper- or silver-base braze alloys are commonly used. For service in the 500-800°C range, nickel- or palladium-

*In this report, the commonly used engineering units are used as the primary units. The International System (SI) units are shown in parentheses. Appendix I gives the pertinent conversion factors.

(PHASE I)

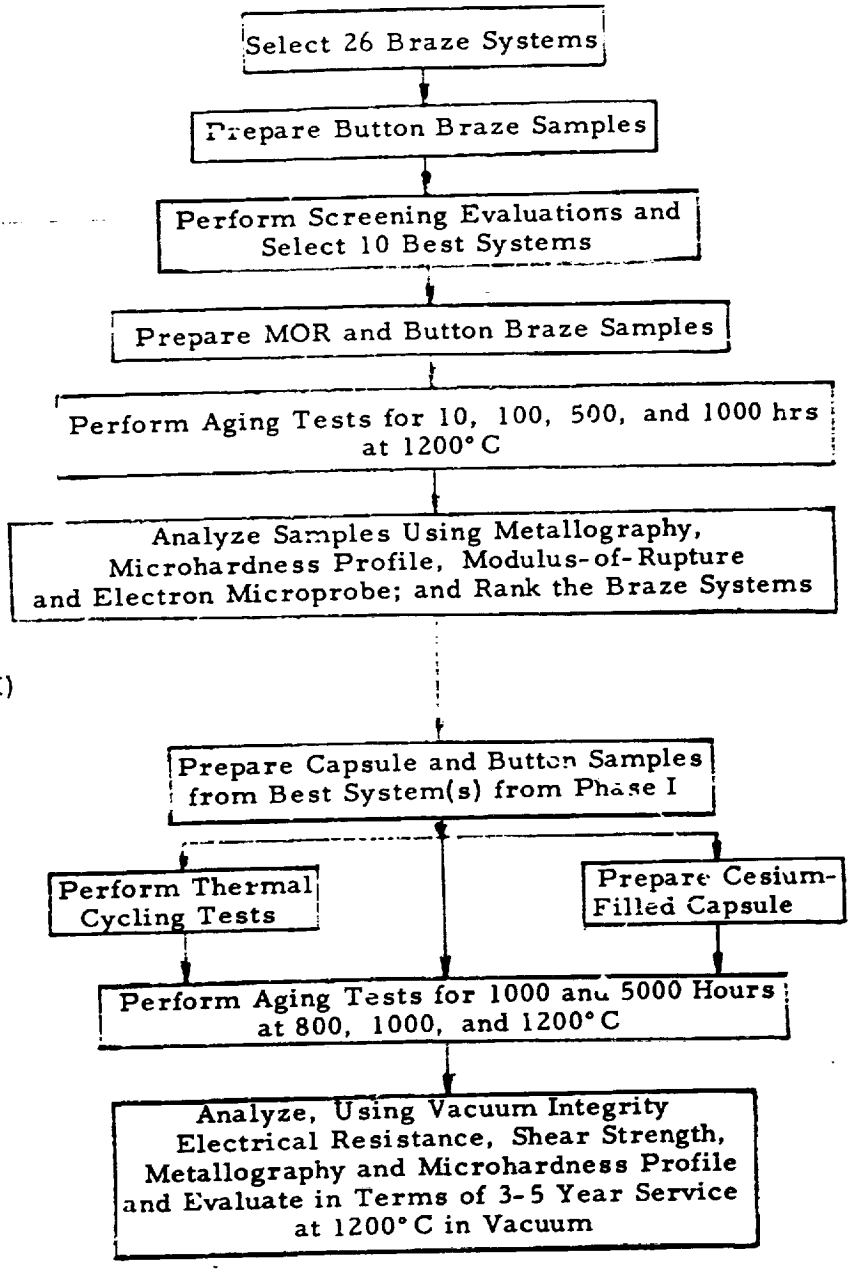

Figure 1. Test Sequence Diagram

base brazes are useful. This type of seal is quite adequate for many applications, but the presence of the glassy phase, which is usually a silica-base glass, makes these seals unsuitable for service with alkali metals.

One must turn to the use of highly purified ceramics when alkali-metal resistance is a requirement. In particular, the silica contents of ceramics such as Al_2O_3 or BeO must be kept below 100 ppm if attack is to be avoided. Such high purity materials require a joining technique other than the use of a silicate glass in order to maintain their alkali metal resistance.

One method that has been examined in some detail, and has shown success, is the formation of graded seals (Ref. 3). Here one uses several layers of mixtures of highly purified oxide and metal powders grading from a mostly-oxide to a mostly-metal layer. These mixtures are bonded and densified by hot pressing, or by cold pressing and sintering.

A second method of forming ceramic-to-metal seals involves the use of an active metal, such as a Group IV metal, that will react with and wet a ceramic. This ability of the Group IV metals to wet a ceramic is not materially diminished by dilution in less active metals. An alloy containing only a few percent of zirconium or titanium readily wets alumina or beryllia surfaces. Once the surfaces are wet, the braze will adhere to them, and if there is no major mismatch in expansion behavior, a joint will be formed.

The most persistent problem associated with active-metal seals is the tendency of the braze alloy to continue reacting with the ceramic. While the reaction itself may not be deleterious, compounds or phases may be produced in the braze or at the interface. Some phases, particularly the intermetallics, are typically hard and brittle, and are prone to crack under stress.

This tendency to continue reacting, and the tendency to undergo an excessive interaction during the brazing cycle have been experienced by several investigators (Ref. 2, Ref. 4, Ref. 5). However, the alloys tested all had rather large amounts of titanium and/or zirconium, such as Ti-48Zr-4Be, Ti-49Cu-2Be, Zr-23Cu-2Be, Zr-5Be, Zr-6Ni-6Cr-6Fe, Zr-19Nb-6Be, Zr-28V-16Ti, and various Ti-V-Zr alloys. During the brazing period, only a small fraction of the braze alloy reacts with the ceramic, so that a large reservoir of active metal remains in the frozen braze. Therefore, because the chemical stabilities of the Group IV oxides are somewhat greater than that of Al_2O_3, the condition for continued reaction is present.

In the present study, whose goals are to produce a ceramic-to-metal seal suitable for use for extended periods at 1200° C, smaller amounts of reactive metals were to have been used, so that only a small amount of active metal would remain in the braze after the completion of the brazing operation.

MATERIALS

The materials used in this program were special high purity (low silica) ceramics, zone-refined braze stock elements, and very good quality refractory alloys. The specifications for the alumina bodies were that they be 99.9+% pure with a maximum of 50 wppm SiO_2, and that the bodies have less than five percent porosity. The analyses of the materials used are given in Appendix II, which shows the alumina to be nominally 99.99% pure with <43 ppm SiO_2. The specifications for the beryllia bodies were that they be 99.9+% pure with a maximum of 75 wppm SiO_2, and that the bodies have less than five percent porosity. The analyses of the materials procured are given in Appendix II, which shows the beryllia to be nominally 99.98% pure with 64 wppm SiO_2.

The braze materials used in the program were prepared from triple-pass zone-refined elements of the highest commercially available purities. The thirteen braze alloys originally specified for the test program and their braze systems are shown in Table I. Some of these brazes proved to be very difficult to form into the desired 5-mil foils. They were replaced by the more tractable alloys which are indicated by the "A" designations in Table I. The details of the materials compositions and braze preparation are given in Appendix II, as are the details of the compositions of the Cb-1Zr and the T-111 (Ta-8W-2Hf) alloys.

Pure vanadium, the braze found to be the best in these studies, is listed as #14 in Table 1.

TABLE I

CERAMIC-TO-METAL BRAZE SYSTEMS

System No.	Nominal Braze Composition	Ceramic	Alloy
1*	98Pt-2Ce	Al_2O_3	Cb-1Zr
1 A	99Pt-1Ce	Al_2O_3	Cb-1Zr
2	98Pt-2Hf	Al_2O_3	Cb-1Zr
3	98V-2Ce	Al_2O_3	Cb-1Zr
4	98V-2Hf	Al_2O_3	Cb-1Zr
5	99V-1Zr	Al_2O_3	Cb-1Zr
6	98V-2Ti	Al_2O_3	Cb-1Zr
7	90V-10Mo	Al_2O_3	T-111
8	65V-35Cb	Al_2O_3	T-111
9	64V-34Cb-2Zr	Al_2O_3	Cb-1Zr
10	64V-34Cb-2Ti	Al_2O_3	Cb-1Zr
11*	60Zr-25V-15Cb	Al_2O_3	T-111
11A	98V-2Hf	Al_2O_3	T-111
12*	49Cb-36Zr-15V	Al_2O_3	T-111
12A	64V-34Cb-2Zr	Al_2O_3	T-111
13*	59Re-40V-1Zr	Al_2O_3	T-111
13A	90V-8Mo-2Zr	Al_2O_3	T-111
14**	Pure V	Al_2O_3	Cb-1Zr

*These compositions were not readily formable as 0.005-inch foil and were replaced by the "A" materials shown.

**This material was not among those initially examined in the program.

GENERAL LABORATORY EQUIPMENT

The general laboratory equipment used to carry out the program included aging furnaces and their appurtenances, vacuum chambers and their appurtenances, a clean bench, and a brazing furnace. These equipment items are described in detail in Appendix III.

PHASE I TEST PROGRAM

The Phase I Test Program goal was to determine the best braze-alloy-ceramic combinations on the basis of measurements and observations of the nature of the thirteen braze alloys shown in Table I. Each braze alloy was to be tested with both a tungsten and a molybdenum barrier on the alumina ceramic. A minimum matrix of three braze temperatures and two hold times was to be examined for each of the twenty-six braze systems. The completed brazes were to be examined and tested for wetting, braze reaction with the ceramic, fillet characteristics, ultrasonic response, and shear strength. The sequence of testing of the Phase I braze materials is shown on the test flow sheet in Figure 2, and the details of the various tests and their evaluations follows.

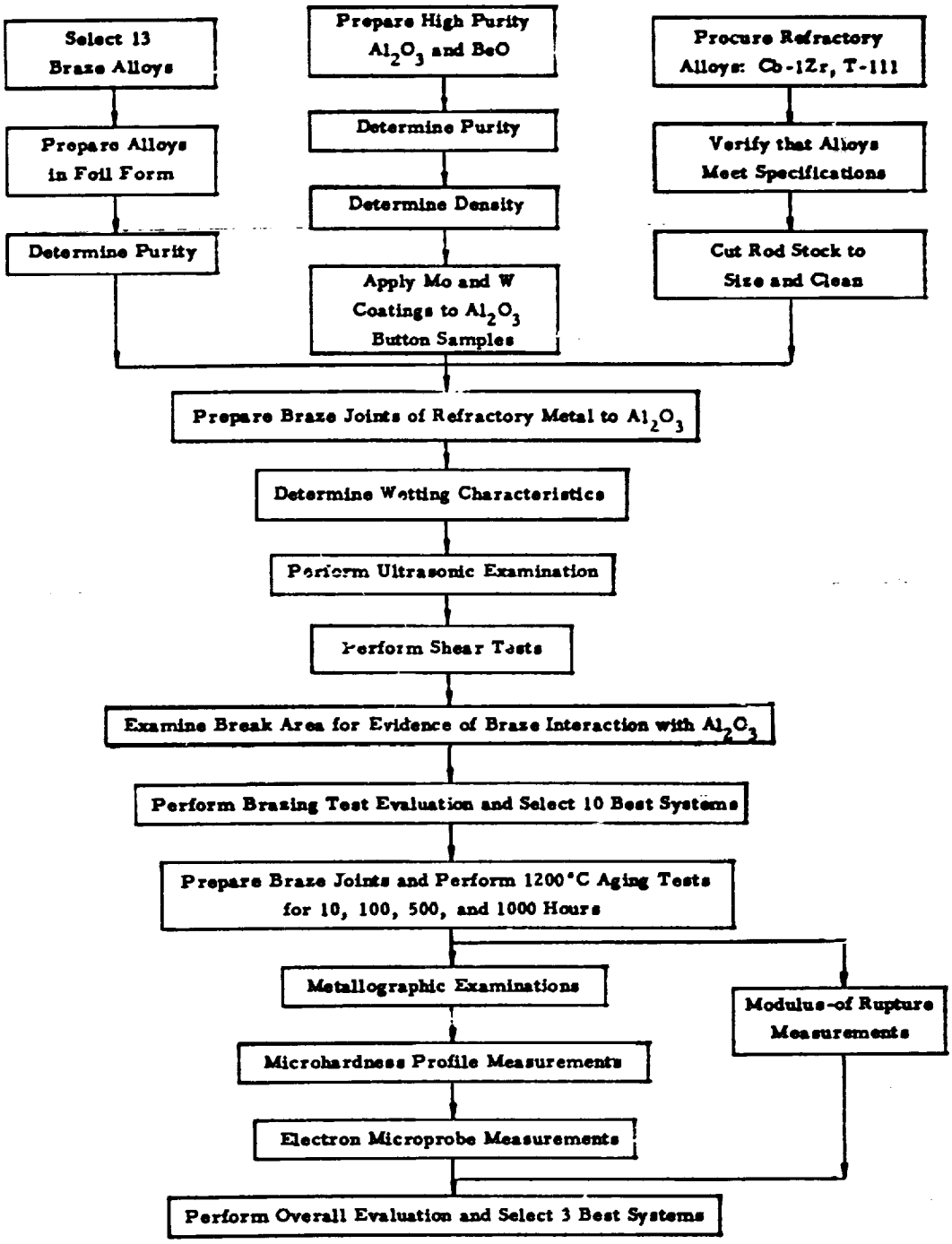

Figure 2. Brazing Test Flow Sheet

PHASE I TEST PROCEDURES AND SPECIAL TEST EQUIPMENT

Brazing. – The brazing jigs used in the Phase I studies were built for their particular purposes using tantalum, T-111 alloy, or Cb-1Zr alloy. Figures 3 and 4 are photographs of the brazing jigs. Appendices IV and V show the details of these button sample and MOR sample jigs, respectively.

The selection of the brazing test conditions was based on the phase diagram data for the braze alloys. In general, the liquidus temperature of the braze alloy was chosen as one of the braze temperatures. Then, recognizing that the braze alloys might tend to dissolve some of the refractory alloy, a lower temperature was tentatively selected. Also, a higher temperature limit was tentatively chosen at 20°C above the liquidus temperature. These temperatures are shown in Table II, together with the temperature ranges actually tested.

The brazing test duration at temperature was varied from 30 to 120 sec for most systems, but in a few cases the brazing periods were 300 seconds.

Ultrasonic Scanning Tests.– The unit used in this program was a Model 1177 Hi-Res System manufactured by the Don Erdman Company. A Nortec CZ3-22-8 transducer was used. This is a 3/16-inch (0.476 cm) diameter unit tuned at 22 Megahertz and shaped to yield a 1/2-inch (1.27 cm) water path focal length. The transducer was shaped to focus its pulse on a spot 0.040 inch (1.0 mm) in diameter. The output from the receiver was photographed from a Model 545A Tectronix oscilloscope.

The brazed test samples were tested by two different methods using an ultrasonic pulse-echo technique. The first technique used had a go/no-go character, and involved the measurement of the intensity of a reflected longitudinal sonic pulse which had passed through the braze joint twice.

The pulse first enters the Al_2O_3 from above, passes through the Al_2O_3 to the braze interface, passes through the braze region into the Cb-1Zr (or T-111) alloy, reflects off the end of the sample and then traverses upward in the alloy back to the braze. It again passes through the braze into the Al_2O_3 and thence moves through the Al_2O_3 to the water interface and back to be detected and measured in the transmitting/receiving head. Based on the transmission through a metal sample, the detector is set to respond to a minimum intensity of the reflected sonic pulse, and to actuate a pen to trace when the signal strength exceeds the set point value. By moving the transmitter/receiver head over the sample, one can trace a pattern of go/no-go response over the surface of the sample in the form of continuous or interrupted parallel lines. In order to evaluate these ultrasonic scan-trace patterns, a five-unit scale of G, GF, F, FP, and P was adopted as an interpretation scale. However, the interpretations of these traces were complicated by the existence of the ever-present edge-effects and it was not always possible to interpret the diagrams in a quantitative way.

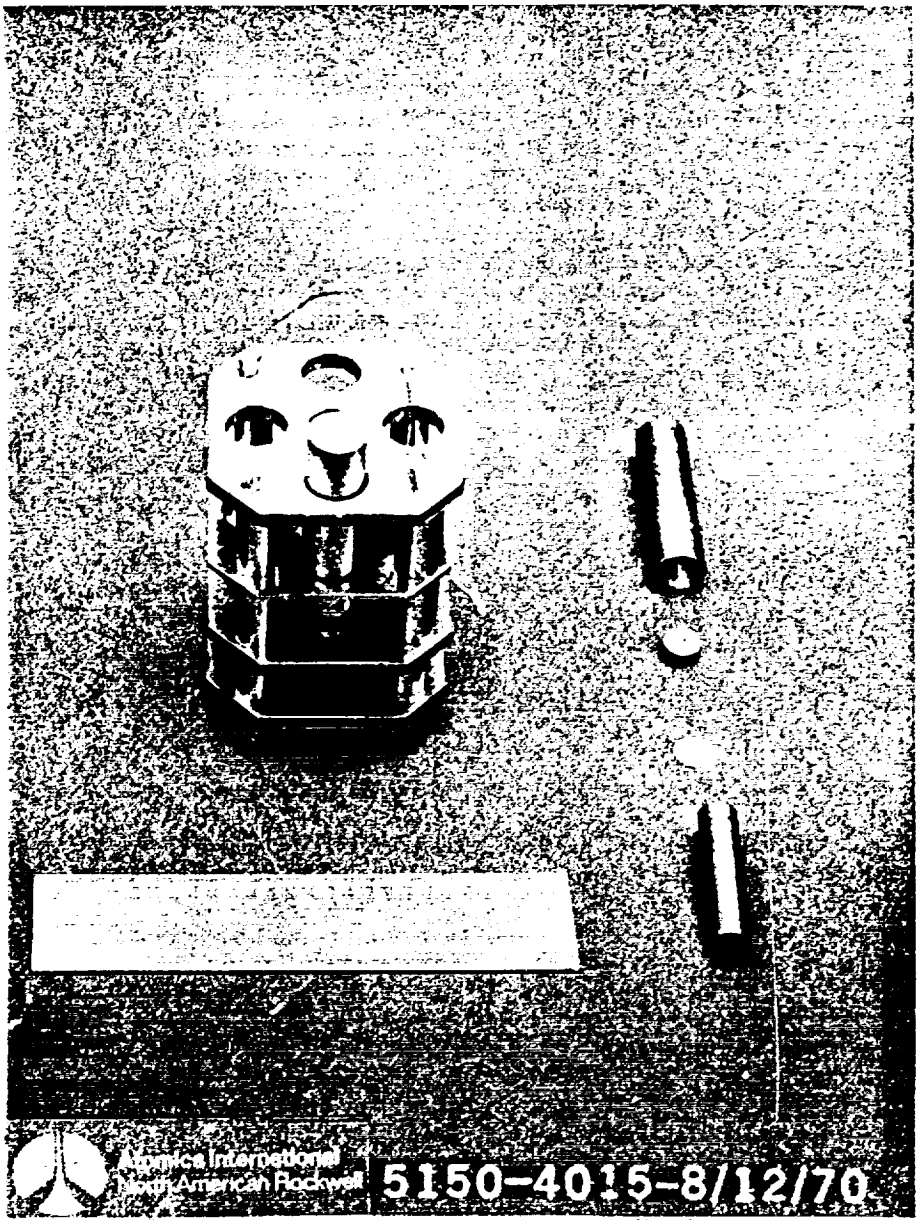

Figure 3. Brazing Jig, Button Samples

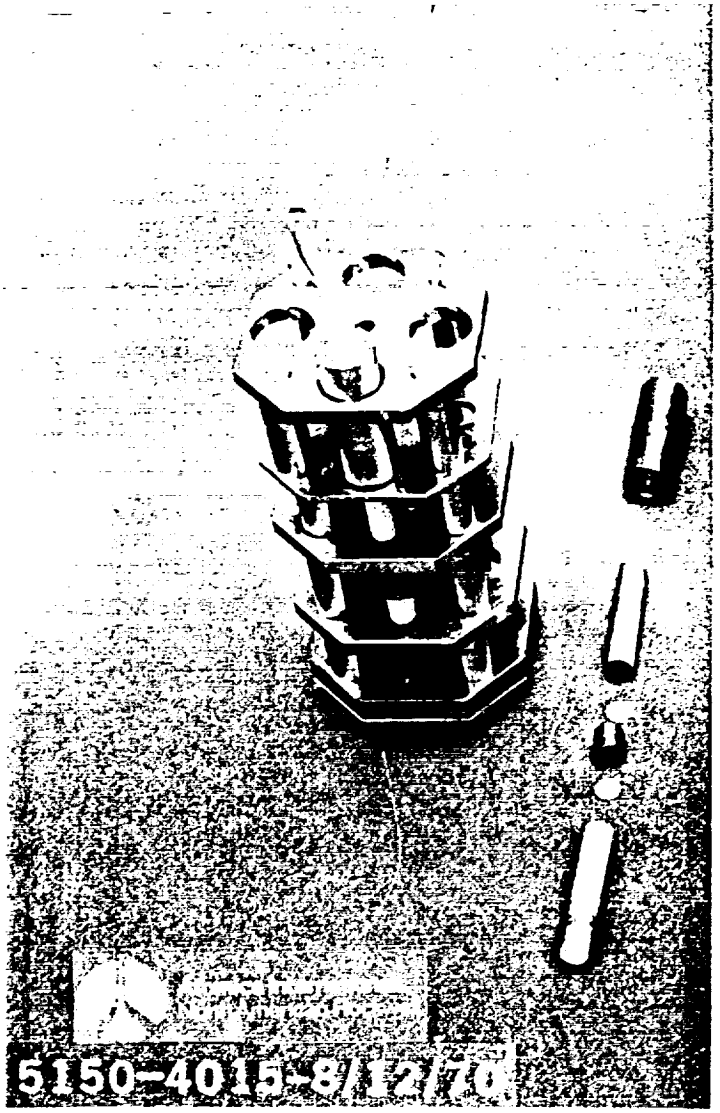

Figure 4. Brazing Jig, MOR Samples

TABLE II

BRAZE TEMPERATURES

No.	Braze Comp.	Alloy*	Tentative Temperatures, °C	Actual Temperature Range Tested, °C
1A	98Pt - 1Ce	C	1690, 1720, 1740	1690-1740
2	98Pt - 2Hf	C	1700, 1720, 1740	1680-1740
3	98V - 2Ce	C	1850, 1870, 1890	1842-1885
4	98V - 2Hf	C	1850, 1870, 1890	1842-1885
5	98V - 1Zr	C	1850, 1870, 1890	1842-1885
6	98V - 2Ti	C	1850, 1870, 1890	1842-1885
7	90V - 10Mo	T	1940, 1960, 1980	1850-1980
8	65V - 35Cb	T	1830, 1850, 1870	1820-1885
9	64V - 34Cb-2Zr	C	1830, 1850, 1870	1840-1885
10	64V - 34Cb-2Ti	C	1830, 1850, 1870	1820-1885
11A	98V - 2Hf	T	1850, 1870, 1890	1855-1885
12A	64V - 34Cb-2Zr	T	1830, 1850, 1870	1855-1885
13A	90V - 8Mo-2Zr	T	1940, 1960, 1980	1940-1960

* Alloy Code: C is Cb-1Zr, T is T-111.

Because of this difficulty, an alternate mode of operation of the ultrasonic pulse-echo technique was developed. Basically, this technique is a modification of the pulse-echo go/no-go record used in the early examinations of button brazes. The ultrasonic transducer is positioned over the sample and the echo-trace is displayed on an oscilloscope such that the echo from the top of the ceramic button is located near the left side of the screen, and the echo from the bottom of the metal rod is displayed near the middle of the screen. Then the transducer is moved to locate it at the position of the maximum bottom-echo response for the test reading. The echo signal passes through an amplifier before it is fed to the oscilloscope. In the test, the gain of the amplifier is adjusted to produce a bottom-echo response of four volts (a two-cm peak on the vertical scale at two volts/cm). Then the entire echo trace is photographed at this gain setting. The photograph and the amplifier gain dial reading constitute the record taken for each sample.

Thus, the echo signal from the bottom of the sample is used as an internal standard in this comparative echo-display analysis method. This is a good standard because it is present in all samples, and the behavior of the Cb-1Zr alloy is a constant from sample-to-sample (as is the behavior of the T-111 in those samples). Since the water-ceramic interface is also a constant from sample to sample, the single factor which most affects the echo from the bottom of the sample is the braze joint itself. The pulse enters the ceramic at the water-ceramic interface, passes through the 1/8-inch (0.318 cm) thick ceramic to the braze interface, through that interface, through the braze metal [0.004 to 0.006 inches (0.104 to 0.152 mm) thick], through the braze-refractory alloy interface, and proceeds to the bottom of the sample. At the bottom, the pulse is partly reflected and the echo reverses its path and emerges again from the ceramic-water interface to be picked up in the detector. If the braze interface is a sound one, the pulse will pass through it with a minimum of degradation and reflection, but if there is no metallurgical bond, the pulse suffers a major reflection from the joint, and the transmitted pulse is markedly diminished in amplitude. Upon its return, the echo also suffers a diminution in intensity as it traverses the poor bond, so that its intensity as it emerges into the water is relatively weak. However, it can be amplified by turning up the gain of the amplifier, to produce the required standard pulse height of four volts at the oscilloscope. Weak echo pulses therefore require more amplification. For such a sample, all of the echo pulses from the braze joint (and any other discontinuities in the sample) are displayed on the oscilloscope trace. They appear as pulses between the first echo pulse from the ceramic surface and the echo pulse from the bottom. For samples in which the bond is a good pulse transmitter (and is therefore presumably a sound bond) the base-line on the oscilloscope photograph is essentially clear between the limiting pulses.

By examining the photographs and the amplifier dial settings, an evaluation of the braze joint integrity can be made. In order to maintain the same evaluation scale for this mode of operation as that used in the scan-trace mode of operation, the same five-unit scale G, GF, F, FP, and P was used to rate the photographic traces. Figures 5, 6, 7, 8, and 9 show

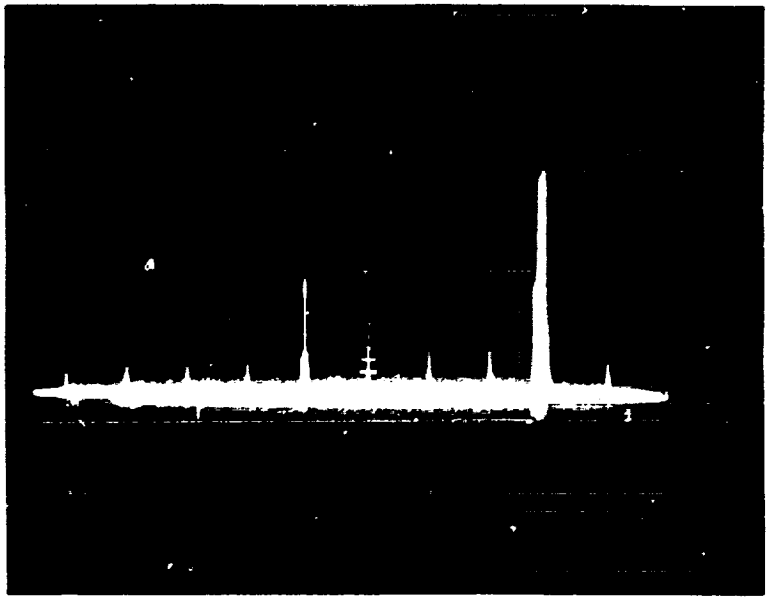

Figure 5. Ultrasonic Test Pattern, Typical "G" Evaluation

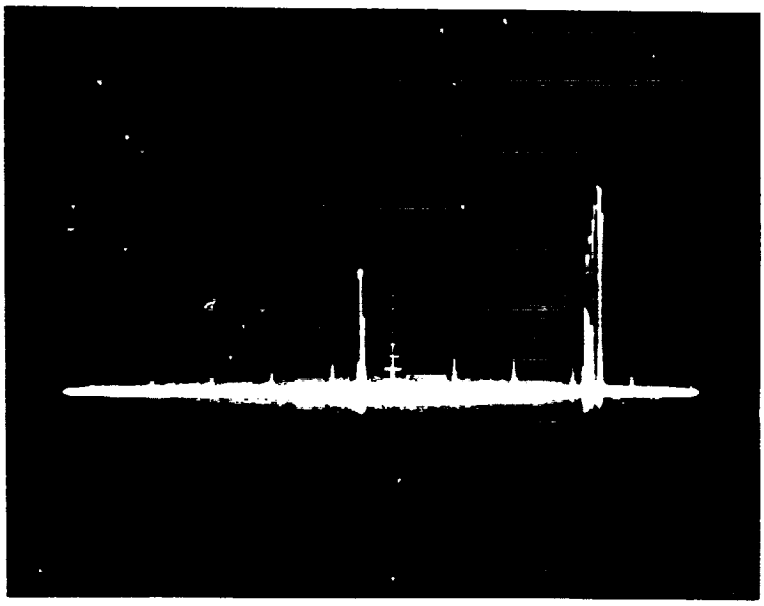

Figure 6. Ultrasonic Test Pattern, Typical "GF" Evaluation

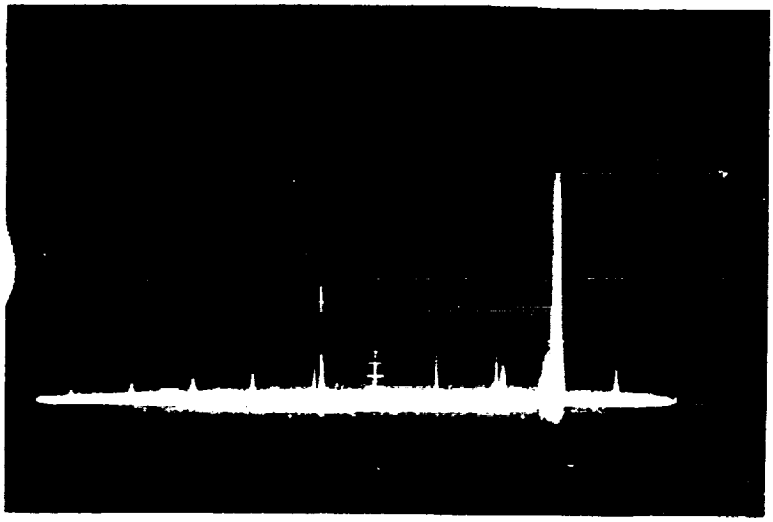

Figure 7. Ultrasonic Test Pattern, Typical "F" Evaluation

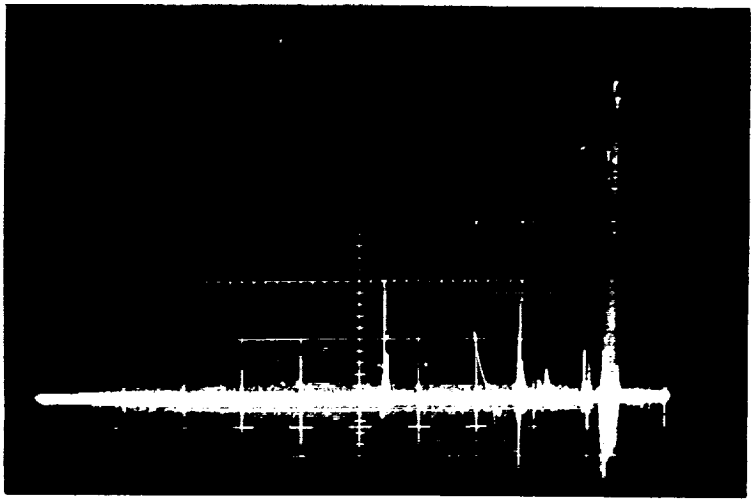

Figure 8. Ultrasonic Test Pattern, Typical "FP" Evaluation

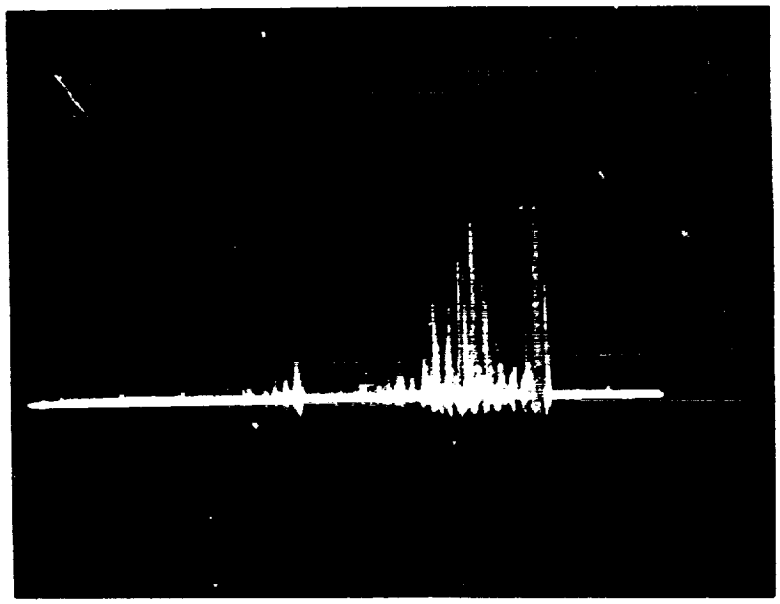

Figure 9. Ultrasonic Test Pattern, Typical "P" Evaluation

typical oscilloscope traces designated as G, GF, F, FP, and P, respectively. As can be seen in the photographs, the base line shows no evidence of a reflected sonic pulse between the rather tight group on the right and the single spike in Figure 5, a "G" designation. Time runs from right to left in these photographs, so that during the time the pulse enters the sample, is reflected from the bottom, and emerges to be observed in the detecting head, there is no indication of any reflection in this "G" sample. The group of pulses which represents the pulse injection is thought to be multiple reflections between the top of the sample and the detector head. Each time the sonic pulse reverberates between the two surfaces, it is detected and recorded to form the multi-peaked figure shown. As was noted above, the pulse reflected from the bottom of the sample is amplified to a constant 4-volts to provide the internal reference pulse intensity.

If there are defects in the sample which reflect part of the energy, then a greater amplification of the reflected pulse is needed, but the imperfections also send back reflected signals which appear in the pattern as pulses between the initial group and the bottom-reflection. This effect is shown in a graded way in Figures 6, 7, 8, and 9 in which the internal imperfections increase and the evaluations range from GF through P, respectively.

Appendix VI shows a comparison of these two methods of ultrasonic scanning technique. Although the latter method is shown to be better, it remains, on the basis of the present amount of testing, less than ideally effective.

Shear Tests. — The shear test unit used in the program was built to accomodate the button samples used in Phase I. Figure 10 shows the jig with a sample in place. Appendix VII shows the details of the unit. The knife is driven by an Instron test unit at a speed of 0.050 in./min (0.0212mm/s) and the developed loads are recorded on a strip chart.

The shear tests were performed using the button braze samples with the unit shown in Figure 10. Any braze material which had run out of the braze region onto the cylindrical area of the refractory metal was carefully filed away with a fine-cut file so that the external surface of the sample was smooth and as cylindrical as possible. Then the sample was inserted in the block so that the braze joint was positioned just at the edge of the block. The positioning screw and the holding spring were adjusted to hold the sample in place. A piece of 0.010-inch (0.254 mm) aluminum foil was placed over the alumina button and then the shear knife was lowered into place. The foil provides a cushion to distribute the load of the knife evenly over the surface of the alumina, and prevents the development of extreme local stresses.

The loaded shear test jig was then placed in a bench Instron and the knife moved downward at 0.050 inch per minute (0.0212 mm/s). The load cell output was recorded on a strip chart on a scale of 0-1000 pounds (0-4448N). The shear stress on a 0.25-inch (0.635 cm) diameter braze

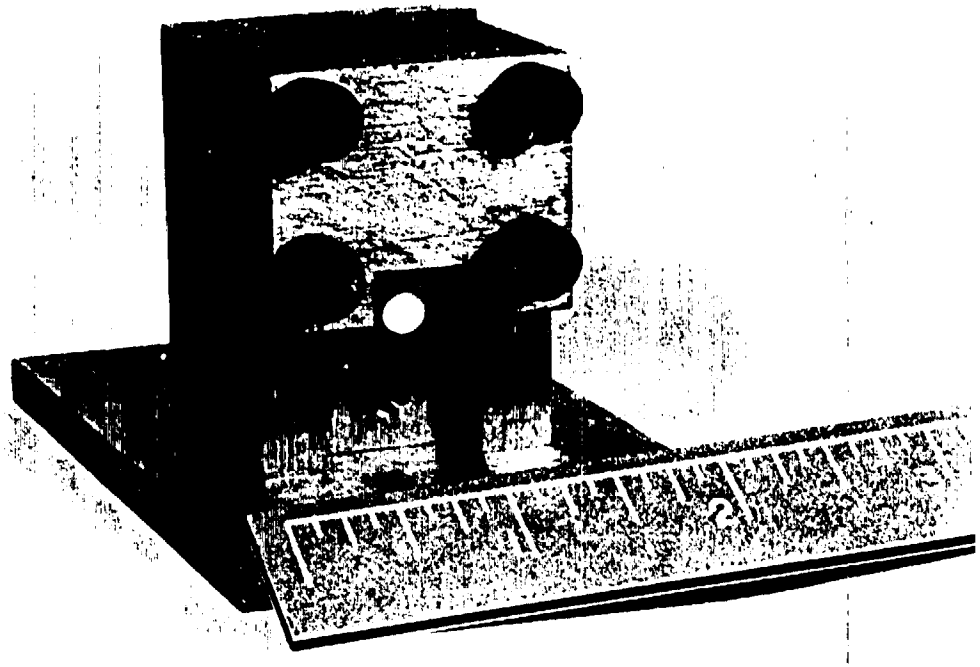

Figure 10. Shear Test Jig

area is given by:

$$\sigma = 4\,P/(0.25^2\pi) = 20.4\,P \text{ psi or } 1.406 \times 10^5 P \text{ N/m}^2 \qquad (1)$$

where P is the breaking load in pounds.

Microhardness. - The unit used in these tests was a Leitz Miniload Hardness Tester, with a Vickers type (square) diamond point indenter. The tests were performed using a 100 gram weight, which permits the evaluation of DPH (Vickers) hardnesses ranging from 19.7 to 1097 units.

The microhardness tests were performed on aged button samples which had previously been mounted in epoxy, polished, etched, and photographed. The interface between the braze and the alumina was used as the reference, and indents were made at nominal one-mil (0.0254 mm) intervals in the braze, and then at greater intervals in the refractory metal. The indents were measured and converted to DPH hardness units using tabular data.

Modulus of Rupture (MOR). - The MOR test unit used in the program was built to accomodate the 0.200-inch (0.508 cm) diameter x 2.2 inch (5.6 cm) long test sample. Dense graphite was used as the basic structural material, and sapphire rods were used as the bearing elements to transmit the bending forces. These materials have high compressive strength and show minimal creep at elevated temperatures, and were chosen in preference to refractory metal for 1200°C service. Four-point loading was employed with 0.5 inch (1.27 cm) equal spacing of load points. The characteristic bending moment for symmetrical four-point loading is a constant between the two center load points. Since the specimen consists of two one-inch (2.54 cm) lengths of ceramic bonded to a nominal 0.2 inch (0.508 mm) length of metal, both braze regions are within the center region of constant bending moment. Thus, the maximum fiber stress is also constant over this region, and can be evaluated from the standard formula:

$$\text{Modulus of Rupture} = \frac{Mc}{I} \quad \text{(force/area)}$$

where M is the bending moment measured in in.-lbf or m.N; c is the distance from the neutral axis to the fiber at maximum stress; i.e., c is the radius of a circular bar specimen measured in inches or meters; and I is the moment of inertia of the sample cross section, measured in inches^4 or meters^4.

Thus, the units of MOR are psi or N/m^2. Figure 11 shows the MOR jig, and Appendix VIII shows the details of the parts.

Modulus of rupture tests were performed at room temperature on as-brazed, on 100-hour (3.6×10^5s) and on 1000-hour (3.6×10^6s) 1200°C aged samples. Modulus of rupture tests were also performed at 1200°C on as-brazed samples. The MOR samples were visually examined following the brazing step and any braze metal which had run out of the joint was

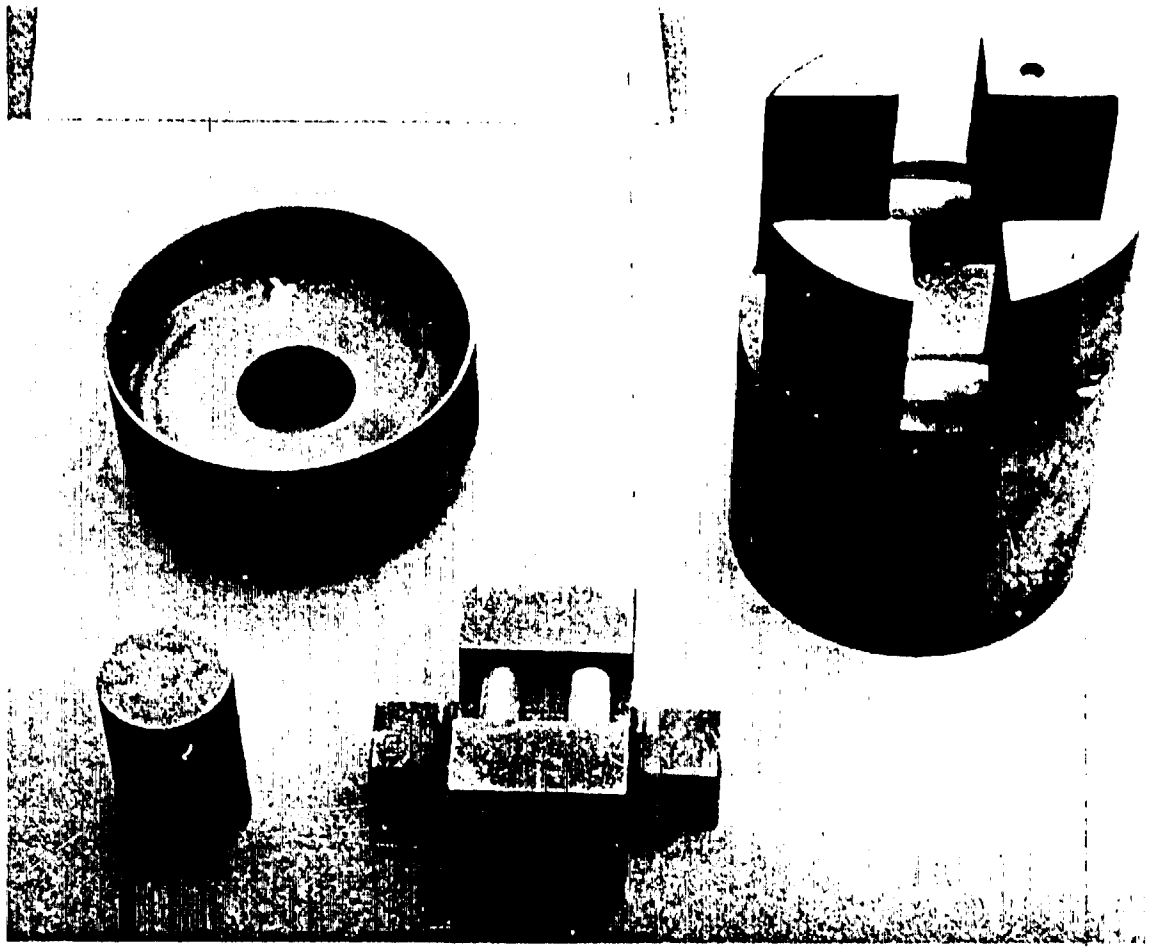

Figure 11. MOR Test Unit

carefully removed with a fine-cut file so that the test specimens were smooth and cylindrical. The specimens were placed in the test rig (Figure 11) so that the metal section was midway between the loading points. The room temperature samples were then broken using a crosshead speed of 0.050 inches/min (0.0212 mm/s). The loading force was recorded on a strip chart recorder using an 0-5000 lb (0-22241 N) load cell. The 1200°C test temperature was achieved by using a tantalum strip heater operating in vacuum, and located around the test rig. Samples were loaded, brought to temperature and then tested. The breaking load was read from the strip chart.

Electron Microprobe. — The unit* used in this program employs a bombarding beam of electrons having a preselected energy in the range 0-50 kev, with a specimen current on the order of 0.05 μA, and a minimum beam diameter of 1-2 microns. The unit can be operated in four basic modes.

The first mode is an area scan of back-scattered electrons. Here, the heavier atoms (large Z) elastically scatter the incoming electrons to a greater degree than do the atoms of smaller Z. The electrons that are reflected at approximately 58° from the plane of the sample surface are detected on film as a function of the position of the electron beam on the sample. The resulting film will show light and dark regions. The light regions correspond to higher average atomic number and the dark regions to lower average atomic number in the sample scan area.

The second mode of operation involves the detection (at 52-1/2°) of the characteristic x-rays of the elements in the sample area scan. One characteristic x-ray for each element is selected and the presence of that element is recorded on a film as a light spot. Therefore, in this element area scan, the lightest areas are those having the greatest concentrations of the element being detected.

The third mode of operation involves the development of a line profile of the intensity of the selected characteristic x-ray of a particular element. The intensity is nominally proportional to the amount of the particular element present. In this mode, the electron beam is moved along a straight line path across the stationary sample and the intensity of the x-rays sought is recorded on a film. In this way the intensity versus position along a linear traverse of the sample is obtained.

The fourth mode of operation involves a counting technique. The electron beam is held in a fixed position, and the sample is moved stepwise under the beam. At each position the x-rays are counted for a set time. This technique permits a more precise and accurate measure of the amount of a given element at a particular location because it is possible to accumulate a large number of counts and to thereby get good statistics. The weakness in this operation mode is the fact that the sample is moved by a micrometer screw, and there is a positional uncertainty from this source. If a sharp diffusion gradient is being examined, the positional uncertainty

*Manufactured by Applied Research Laboratories, Inc.

may make the counting data questionable. The operations involved in converting the raw data to quantitative concentration profiles are described in Appendix IX.

The electron microprobe measurements of the test samples were made on the mounted samples after the microhardness tests were complete. The first examination made of the sample was the back-scattered electron pattern. Then, area scans of the major elements in the braze and the refractory alloy were made. The third measurement was a series of line profiles of the intensities of the various elements in the braze system. Two elements are shown on each profile trace, and in order to have a constant reference for traces in each system, the aluminum trace is used as one of these two elements. All line profile films were taken at a magnification of 800x (about 11-1/4u per large division). In addition, a constant scale factor (the reciprocal of electronic sensitivity) was used for each element's oscilloscope trace. In all cases the Al trace was recorded at 5 v/cm as the reference trace. The other elements were recorded at the following settings: Pt, 1v/cm; Nb, 1 v/cm; V, 1 v/cm; Ce, 0.2 v/cm; Mo, 0.2 v/cm; Hf, 0.2 v/cm; Zr, 0.2 v/cm; W, 0.2 v/cm; and Ti, 0.1 v/cm. These traces are only semi-quantitative in nature, because they show the uncorrected intensities of the characteristic x-rays from the different elements. Two comments are appropriate in comparing the line profile films: (1) it should be kept in mind that the recording sensitivities for Ce, Mo, Hf, Zr, W, and Ti are more than an order of magnitude greater than the recording sensitivity for Al; and (2) the presence and distribution of elements can be compared from sample-to-sample, however, their amplitudes should not be compared. The reason is that, for the purpose for which the line profiling examinations were made (namely, a scoping operation), it was not necessary to attempt to hold constant microprobe operating conditions (e.g., specimen current) from day-to-day.

Finally, selected samples were examined by the point-counting technique. These data were corrected as described in Appendix IX to obtain quantitative weight percent concentrations, which have been reported in tabular form.

EVALUATION OF PHASE I BRAZING TESTS

A total of 189 button braze screening tests were made on the thirteen braze systems. All of the brazes were formed as 0.004-0.005" (0.102-0.127 mm) thick foil, although two of them, #9 (64V-34Cb-2Zr) and #13A (90V-8Mo-2Zr) were formed with some difficulty, as is indicated in Figure 25, Appendix II. Each of the 189 tests was evaluated on six bases: (1) Braze Visual, which describes the external appearance of the joints; (2) Ultrasonic, which describes the evaluation of this test on the G, GF, F, FP and P scale: (3) Ceramic Visual, which describes the color in the ceramic at the braze break surface; (4) Shear, which is the shear failure load; (5) Break, which describes the location of the break along the ceramic-braze-alloy unit; and (6) Braze, which describes the appearance of the fracture surface of the braze. These terms are defined in detail in Appendix X, in which all the braze evaluation test data are presented in tabular form. Each of the twenty-six braze systems is discussed and evaluated in Appendix X.

The approach taken involved reducing the test data into three principal categories; Strength, Ultrasonic, and Visual. Each braze system was compared and assigned a letter-evaluation in the series G, GF, FG, F, FP, and P on the basis of the average performance of the best braze specimens of that system. These individual category ratings are shown in Table III, in which the braze systems are designated as 1AM, 1AW, 2M, etc., to indicate the braze and the metal coating used on the alumina ceramic. (Braze compositions are shown in Table II.)

The tabular data for the "Strength Evaluation" and the "Ultrasonic (US) Evaluation" were derived from Table XXXIX in Appendix X. The designations for the "Visual Evaluation" were established by evaluating the data in Tables XXV through XXXVIII in Appendix X.

The "Overall Evaluation" column data of Table III are the judgment-averages of the three factors translated into a single evaluation designation, and the "Category Number" column merely shows the final overall evaluation in a numerical scale of one to seven.

Examination of Table III indicates that there is one braze in the G(1) category, six in the GF(2) category, three in the FG(3) category and two in the F(4) category, which accounts for the best braze systems. The remaining braze systems shown in Table III are rated FP(5), PF(6), or P(7), and are not recommended for further consideration.

The ten braze systems shown in Table IV were selected for the Phase I aging studies. The table also shows the temperatures, pressures, and times selected for the second part of the Phase I test program.

It should be noted that Table IV does not show any T-111 alloy samples. In every case in the samples tested and reported in Tables XXXI, XXXII, XXXV, XXXVI, XXXVII and XXXVIII in Appendix X, the ceramic button was found to have one or more radial cracks at the periphery. The BeO cracked

TABLE III

SCREENING TEST OVERALL EVALUATION SUMMARY					
Braze System	Strength Eval.	Ultrasonic Eval.	Visual Eval.	Overall Eval.	Category No.
1A-M	PF	FP	FP	FP	5
1A-W	FP	P	PF	PF	6
2-M	GF	FP	FP	F	4
2-W	FP	PF	PF	PF	6
3-M	GF	GF	F	FG	3
3-W	F	FP	GF	F	4
4-M	G	GF	G	G	1
4-W	G	GF	GF	GF	2
5-M	GF	FG	FG	FG	3
5-W	GF	GF	F	FG	3
6-M	GF	GF	F	FG	3
6-W	G	F	GF	FG	2
*7-M	P	P	PF	P	7
*7-W	P	PF	PF	PF	6
*8-M	PF	PF	F	FP	5
*8-W	PF	PF	F	FP	5
9-M	GF	GF	GF	GF	2
9-W	GF	GF	GF	GF	2
10-M	G	GF	GF	GF	2
10-W	GF	FG	FG	FG	3
*11A-M	P	FG	F	PF	6
*11A-W	PF	FG	F	FP	5
*12A-M	PF	GF	F	FP	5
*12A-W	PF	GF	F	FP	5
*13A-M	PF	FG	F	FP	5
*13A-W	PF	F	F	FP	5
*5-M	P	GF	F	PF	6
*5-W	PF	GF	F	PF	6
*10-M	FP	FG	PF	FP	5
*10-W	FP	FG	PF	FP	5

*Brazes with T-111 alloy; all others are with Cb-1Zr alloy.

TABLE IV

SELECTED BRAZE SYSTEMS AND BRAZE CONDITIONS

Braze System		Temp. °C	Time sec	Pressure psi	Pressure N/m^2
4M	Al_2O_3/Mo : V-2Hf : Cb-1Zr	1860	60	2	13,790
4W	Al_2O_3/W : V-2Hf : Cb-1Zr	1870	60	2	13,790
5W	Al_2O_3/W : V-1Zr : Cb-1Zr	1870	60	2	13,790
6W	Al_2O_3/W : V-2Ti : Cb-1Zr	1870	60	2	13,790
9M	Al_2O_3/Mo : 64V-34Cb-2Zr : Cb-1Zr	1860	60	2	13,790
9W	Al_2O_3/W : 64V-34Cb-2Zr : Cb-1Zr	1870	60	2	13,790
10M	Al_2O_3/Mo : 64V-34Cb-2Ti : Cb-1Zr	1870	120	2	13,790
3M	Al_2O_3/Mo : V-2Ce : Cb-1Zr	1860	60	2	13,790
10W	Al_2O_3/W : 64V-34Cb-2Ti : Cb-1Zr	1870	120	2	13,790
2M	Al_2O_3/Mo : Pt-2Hf : Cb-1Zr	1720	60	2	13,790

worse than the Al_2O_3. This difference in cracking propensity is ascribed to the greater thermal expansion of BeO than that of Al_2O_3. This, plus the fact that T-111 alloy is quite strong at elevated temperatures, and the fact that these brazes are rather hard, causes the tension stress levels in the BeO to exceed its strength during the first cool-down from the brazing temperature. Because the Cb-1Zr alloy is materially weaker than T-111 alloy, and because the expansion differences between Cb-1Zr and Al_2O_3 are very small, the stress levels in the Al_2O_3 do not exceed its strength. In a BeO vs. Cb-1Zr alloy braze system, one finds the expansion differences are greater than for the Al_2O_3 : Cb-1Zr alloy system. However, the low strength of the alloy is expected to prevent the development of excessive tensile stresses in the BeO, although it does appear marginal, because of the necessity of brazing at 1850°C, a very high temperature.

EVALUATION OF PHASE I AGING TESTS

Tests. — Four button samples of each of the ten braze systems shown in Table IV were prepared for the aging tests. One button sample of each braze system was aged at 1200°C in a vacuum of 10^{-7} to 10^{-8} torr (1.33×10^{-5} to 1.33×10^{-6} N/m^2) for 10 hours (3.6×10^4s), 100 hours (3.6×10^5s), 500 hours (1.8×10^6s) and 1000 hours (3.6×10^6s). After aging, these samples were sectioned across the joint, mounted, polished, etched and photographed at 100X. Then their hardness profiles were measured, and finally each sample was examined, using the electron microprobe as described above. In all, forty button samples were prepared and tested.

Duplicate MOR samples of each of the ten braze systems were prepared and aged at 1200°C in a vacuum of 10^{-7} to 10^{-8} torr (1.33×10^{-5} to 1.33×10^{-6} N/m^2) for 100 hours (3.6×10^5 s) and 1000 hours (3.6×10^6s). These samples were tested at room temperature in the unit shown in Figure 11. In addition, duplicate MOR specimens of each system were prepared and tested at room temperature and at 1200°C before aging. In all, eighty MOR samples were prepared and tested.

MOR Test Results. — The MOR test results are shown and discussed in Appendix XI. Figure 12 shows the data in graphical form. The figure shows ten groups of four bars each. The first bar, with solid dots at its ends, represents the as-brazed samples broken at room temperature; the second bar, with the crosses at its ends, represents the as-brazed samples broken at 1200°C. The third bar, with open circles at its ends, represents the samples aged at 1200°C for 100 hours (3.6×10^5s) and broken at room temperature; and the fourth bar, with open circles with cross bars at its ends represents the samples aged at 1200°C for 1000 hours (3.6×10^6s) and broken at room temperature.

From this figure, one sees that Brazes 2M, 4M, 6W, and 10M appear to have fairly consistent MOR measurements in that there is no suggestion of degradation in the MOR value with aging, and the 1200°C MOR measurement shows values comparable with or higher than the room temperature values. Brazes 3M, 4W, 5W, 9M, and 9W all show higher MOR values in the 1200°C tests than the room temperature values, but their 1000-hour (3.6×10^6s) aged values are generally lower than the as-brazed and the 100-hour (3.6×10^5s) aged values. This suggests that there may be a deterioration occurring in these braze joints as they age at high temperature. Finally, Braze 10W is the only braze which shows distinctly lower values in the 1200°C test than were found in the room temperature tests. In addition, there is an aging effect in this sample as evidenced by the large difference in the MOR values between the 100-hour (3.6×10^5s) and the 1000-hour (3.6×10^6s) data.

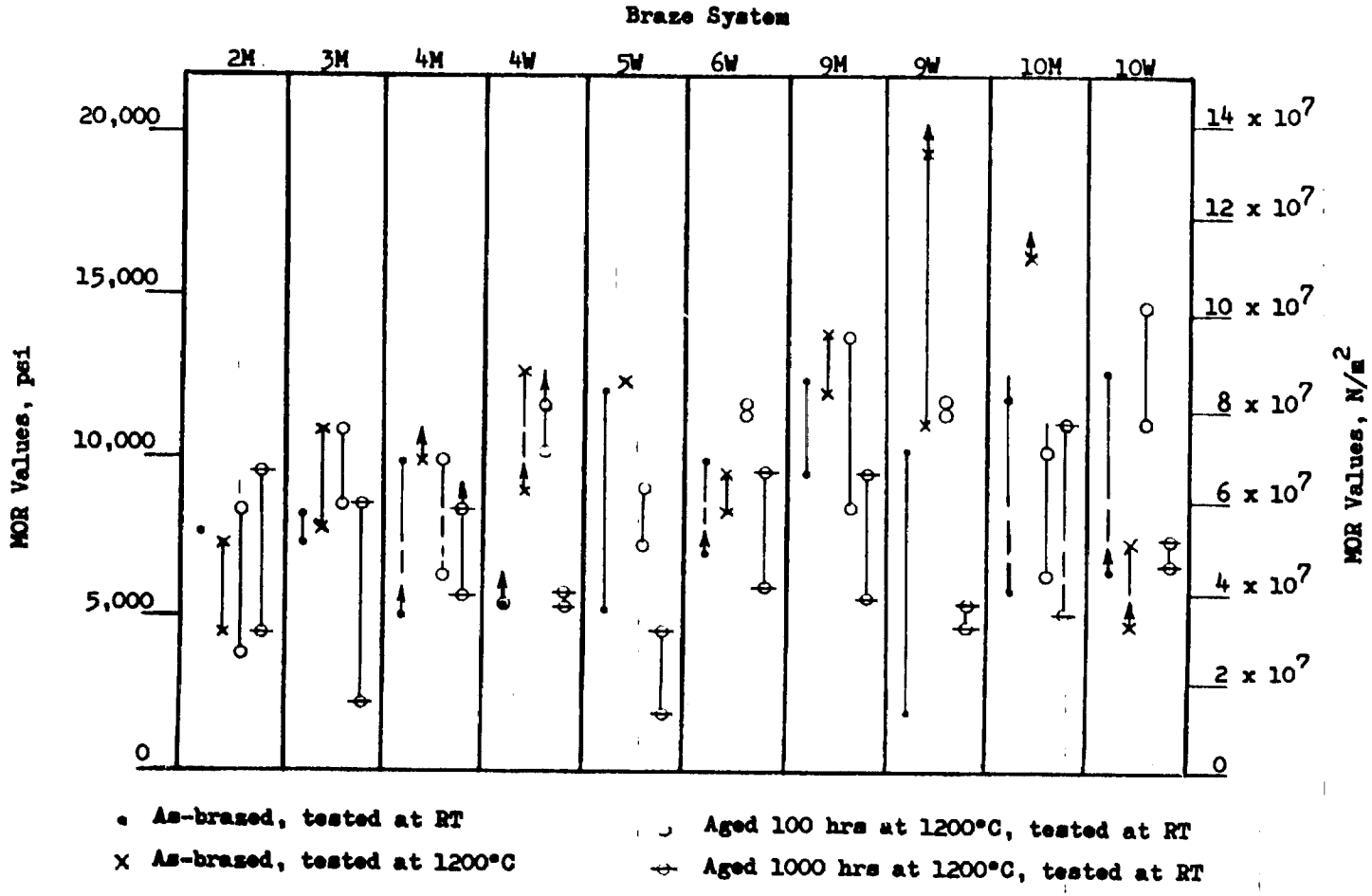

Figure 12. MOR Test Results

Therefore, based upon these rather few values of MOR data, the systems 2M, 4M and 6W appear to be the most stable, and give a tighter pattern of test values than the others. Probably, system 10M should also be included in this group even though it shows a high 1200°C test result. It is not unlikely that that particular test (or any single test, for that matter) is anomalous.

Metallographic, Microhardness, and Electron Microprobe Results

Each of the ten braze system samples selected for the 10-hour, 100-hour, 500-hour, and 1000-hour aging test sequence was examined after testing using metallography, microhardness traverses, and electron microprobe studies as the means of evaluation. These test data are presented in detail in Appendix XII. In order to best illustrate and interpret the relationship of the metallographic record and the microhardness profile, both are aligned on the same figure. In addition, in each figure is presented a listing of the locations of either the actual electron microprobe trace for the particular sample, or the location of a representative electron microprobe trace. The referencing technique was adopted in order to reduce the number of figures to be shown, but because many of the traces are essentially identical, no loss in the interpretation of the data results from this practice.

In general, the examinations of these data show that the braze alloys dissolved rather large amounts of the Cb-1Zr alloy with the result that the final braze compositions had Nb (Cb) as a major constituent regardless of the starting composition of the braze. Further, the electron microprobe data indicates in all cases that some alumina was dissolved by the braze and appears as aluminum. It follows, therefore, that the associated oxygen from the Al_2O_3 is also in the braze, particularly in view of the fact that vanadium and niobium (columbium) are capable of dissolving rather large amounts of oxygen in solid solution. This hypothesis is at least in part supported by the observation in these [Nb(Cb)-V]-base and V-base braze alloys that the brazes have hardness values of 350-400 units as compared to 750 units for the base Cb-1Zr alloy.

Another general observation is that the molybdenum and the tungsten "barrier" materials which were initially deposited on the alumina were invariably totally dissolved and the Mo and W appeared uniformly distributed through the final braze thickness. This, of course, makes the alumina more susceptible to attack by the braze. Further, a concentration of the additives Ce, Zr, and Hf is frequently found adjacent to the alumina. The titanium additive did not show this tendency, probably because its chemical affinity for the oxygen (which is more concentrated near the Al_2O_3) is not significantly greater than that of the vanadium. However, the affinities of Ce, Hf, and Zr for oxygen greatly exceed that of vanadium, so that the concentration of Ce, Hf, or Zr in the braze region adjacent to the alumina probably results from the formation of the stable oxides of these active elements.

The following paragraphs give a summary of the observations of the ten systems examined. The test sample designations are coded with a number designating the braze alloy as listed in Table II, and a letter designation, M or W, to indicate the presence of a molybdenum or tungsten barrier on the alumina.

The aging test duration coding is:

A for the 10-hour (3.6×10^4s) exposure;

B for the 100-hour (3.6×10^5s) exposure;

C for the 500-hour (1.8×10^6s) exposure; and

D for the 1000-hour (3.6×10^6s) exposure.

The 2M braze, (Cb-1Zr/Pt-2Hf/Mo/Al_2O_3), typically is seen to dissolve significant amounts of Cb-1Zr, and to form Cb-Pt phases of at least three different compositions. The Hf in the braze and the Zr from the dissolved Cb-1Zr alloy become concentrated at the Al_2O_3-braze interface, presumably as a result of reaction with the Al_2O_3. The thickness of the final braze is smaller than that of the original braze wafer, and the drops of braze alloy are frequently found to have run out of the braze region. This would account for the generally reduced braze thickness, although it is not a particularly desirable characteristic for the braze to have.

In general, this braze has undesirable properties because of the formation of intermetallic phases, and the attendant hardening and embrittling effects. These difficulties are compounded by the tendency of the active elements to concentrate at the alumina-braze interface.

The 3M braze, (Cb-1Zr/V-2Ce/Mo/Al_2O_3), is seen to dissolve rather large amounts of Cb-1Zr, but in contrast to the 2M braze alloy, the 3M brazes tend to remain in the joint. Upon freezing, the braze tends to crystallize beginning at the Cb-1Zr surface, and to grow on the existing crystal surfaces, so that a gross epitaxial growth occurs. Some of the braze crystals extend across the full thickness of the braze.

The tendency of the reactive elements Ce and Zr which are dissolved in the braze to react with the Al_2O_3 is not pronounced, although some reaction was observed in the 10-hour (3.6×10^4s) and the 500-hour (1.8×10^6s) samples.

The 4M braze, (Cb-1Zr/V-2Hf/Mo/Al_2O_3), appears to have a variable character. In some cases a hard interface layer is found, while in other cases, there is none. Some of the brazes are quite thick, but the A braze (10-hour exposure) is only about 2 mils (0.051 mm) thick. The hardness at the interface may be associated with the presence of high Zr and Hf at that location, with the presumption that a reaction with Al_2O_3 has occurred to form Zr and Hf oxides in the reaction zone. However, there is a lack of consistency in this hypothesis too, in that the C sample (500-hour exposure) which showed no Zr and Hf concentration at the surface, did show a high DPH hardness value near the interface, while the D sample (1000-hour exposure) in which there was a marked Zr and Hf concentration effect, showed a rather level DPH profile through the braze.

The 4W braze (Cb-1Zr/V-2Hf/W/Al_2O_3), is characterized by having moderately wide to very wide braze joints, with generally uniform hardness profiles showing DPH values in the 300-400 range. No tendency for the segregation of the Group IV elements at the Al_2O_3 was seen, and the braze-Al_2O_3 interface regions were all good-appearing. The V-2Hf braze is a good solvent for Cb-1Zr alloy and major amounts of Nb (Cb) are found in the braze joint.

The 5W braze (Cb-1Zr/V-1Zr/W/Al_2O_3), does not show a really consistent pattern. The A and D samples show rather large interaction regions, but the B and C samples do not. The A and B samples show nominally level hardness profiles, but C and D samples show a slope. There is an indication of a concentration of Zr at the interface in Sample C, but it does not appear in the other samples. Finally, there is evidence in the D sample of the development of a ternary Nb (Cb)-V-Al phase.

The 6W braze (Cb-1Zr/V-2Ti/W/Al_2O_3), system produces brazes which range from 5 to 10 mils (0.127 to 0.254 mm) in thickness and show very small reaction zones. The DPH microhardness values measured within the braze layers are in the range 300 to 425. The electron microprobe line profiles are all rather regular and no anomalies appear to be present in the system.

The 9M braze (Cb-1Zr/64V-34Cb-2Zr/Mo/Al_2O_3), is characterized by the presence of substantial interaction regions, which in the 1000-hour (3.6×10^6s) D sample approach a mil (0.0254 mm) in width. It is not clear whether the D sample's wide reaction zone was the result of the aging treatment, but it is one of the thickest reaction zones seen in any braze system. The DPH hardness values of these brazes are generally below 400, although one value of 750 was found. Epitaxial growth of the braze alloy on the Cb-1Zr grains is common.

The 9W braze (Cb-1Zr/64V-34Cb-2Zr/W/Al_2O_3), is characterized by the presence of a zirconium concentration at the Al_2O_3 interface, except that it does not appear in the D sample. The D sample, however, does show a a rather wide reaction zone, and the others have only a small zone or essentially none at all. The DPH hardness values are, in general, moderate at 300-375, except for the D sample, whose hardness approaches 500 near the Al_2O_3 interface. The most plausible reason for the large reaction zone in the D sample appears to be that it is the result of aging. No evidence of a ternary Nb (Cb)-V-Al phase was found in these samples, which one would think should closely parallel the 9M braze behavior.

The 10M braze (Cb-1Zr/64V-34Cb-2Ti/Mo/Al_2O_3), is characterized by the presence of a modest-sized interfacial layer at the Al_2O_3 surface, and by a thick braze region. The DPH hardnesses are not all consistent, although the values are below 500. No deleterious effects are observed in the aged Al_2O_3.

The 10W braze (Cb-1Zr/64V-34Cb-2Ti/W/Al_2O_3), yields wide braze regions, but with varying hardness character. Some of the DPH hardness values reach 600, although most are below 450. A modest tendency to form a reaction region is shown in Sample C, but the other three samples have rather thin reaction zone thicknesses. There is no tendency for the concentration of Zr or Ti at the Al_2O_3 surface, and the Nb (Cb) profiles are generally smooth and regular. A few indicationf of the presence of very small Al_2O_3 particles in the braze were found.

Concentration Profiles and Diffusion Effects. — In order to evaluate the prospects for long-term service of a braze system, and to aid in the selection of the system to have been examined in the Phase II 5000-hour aging studies, the concentration profiles of the major alloy elements of three systems were measured using the electron microprobe. The basis for the analysis of the data is given in Appendix IX, and the data obtained from the test systems 4W (Cb-1Zr/V-2Hf/W/Al_2O_3), 6W (Cb-1Zr/V-2Ti/W/Al_2O_3), and 10M (Cb-1Zr/64V-34Cb-2Ti/Mo/Al_2O_3) are shown in Appendix XII. The final form of these data is a graphical representation of the concentration profiles of Nb(Cb), V, and Al.

At the outset of the study, it was expected that these profiles would be amenable to analysis and that pertinent diffusion coefficients could be derived. The analysis of diffusion gradients and the evaluation of D-values from unsteady-state concentration gradients is based upon the application of Fick's second law of diffusion:

$$\frac{\partial c}{\partial t} = \frac{\partial}{\partial x}\left(D\frac{\partial c}{\partial x}\right) \qquad (2)$$

When the diffusion coefficient D is a constant, this equation can be simplified,

$$\frac{dc}{dt} = D\frac{d^2c}{dx^2} \qquad (3)$$

Equation (3) can be solved analytically (Ref. 6, 7, 8) for the concentration c in terms of the position x and time t, for a system meeting certain boundary conditions. These are that D be constant, and that at $t = 0$, c is constant at c_1 for $x<0$, and c is constant at c_2 for $x>0$; i.e., that the initial concentration profile of the element in question be a step function changing at the $x = 0$ origin. For these conditions,

$$2\,c\,(x,t) = (c_1-c_2)\left[1 - \mathrm{erf}\ x/2(Dt)^{1/2}\right] + 2\,c_2 \qquad (4)$$

The curves described by Equation (4) all pass through the point $c = (c_1 + c_2)/2$ at $x = 0$ and show symmetry of the form

$$[c(+ x_i, t) - (c_1 + c_2)/2] = - [c(- x_i, t) - (c_1 + c_2)/2] \qquad (5)$$

for any pair of positions x_i and $-x_i$ at any time t. The evaluation of the constant D, given values of c (x, t), follows from arithmetical manipulations of Equation (4).

If D is not a constant, and varies with c, as is frequently the case, an analytical solution of Equation (2) is not usually possible. However, Matano (Ref. 9), gives a solution of Equation (2) using a graphical approach, and the use of his technique permits the determination of D at any point along the concentration profile. Matano's solution to Equation 2 is:

$$D = (1/2\,t)\ (dx/dc) \int x\,dc. \qquad (6)$$

In applying Equation (6) to concentration gradient data, one must first find a neutral position along the x axis at which the amount of the diffusing element leaving the region of higher concentration equals the amount entering the region of lower concentration. This position is called the Matano interface and is the reference position on the x-axis. However, the implication of the Matano interface is that the assumed starting point for the diffusional process was a step function concentration gradient of the element whose D-values are sought.

No analytical evaluation of D's in systems with other than initial step function concentration gradients is possible. Because all of these braze systems show unmistakable evidence of having begun their aging test periods with concentration profiles which were far from a step-function character, and because each sample of a braze is different from any other sample of that braze, no further attempt to evaluate diffusion coefficients was made.

Braze Chemistry. — In the foregoing sections, it was noted that a significant amount of aluminum is present in the braze material. The only source of aluminum in these systems is the Al_2O_3 ceramic. Therefore, a significant amount of ceramic must react with the braze. It is of interest to examine the various mechanisms by which Al_2O_3 could be dissolved by the product vanadium-niobium "braze" alloys resulting from the dissolution of the Cb-1Zr alloy by the vanadium-base and the vanadium-niobium-base braze alloys.

The starting braze materials in the studies of the ten Phase I systems all contained about two percent of Ce, Ti, Zr, or Hf, which metals are more active chemically than vanadium or niobium (columbium), and whose purpose was to initiate a wetting action on the alumina. The choice of these elements was dictated by the examination of the free energies of formation of the most stable oxides which could form in these systems. These are shown in Table V. In the table the three groups of oxides are listed in order of increasing ΔF_f (decreasing chemical stability). Thus, in the upper group, one can see that the Ce, the tetravalent Zr and Hf, and the bivalent Ti oxides are more stable than Al_2O_3, and that TiO_2, VO, V_2O_3 and NbO are significantly less stable than is Al_2O_3. The direct ΔF differences are representative of the energy effect of the complete transfer of oxygen from one metal oxide to another. However, the chemical systems of concern here do not, for the most part, involve the full exchange of oxygen in this manner; rather, these systems involve the transfer of the aluminum and oxygen from the [Al_2O_3 compound + V-Nb alloy] system to the [V-Nb-Al-O alloy] system. That is, the Al_2O_3 dissolves in the V-Nb alloy (V-Cb alloy) to produce a quaternary metal system in which some oxygen is dissolved. In these systems, one expects that the small amounts of Hf and Zr become essentially saturated with oxygen, perhaps with some concentration at grain boundaries, so they are, in effect, no longer chemically active.

The reactions of the Zr and Hf to become closely associated with oxygen are readily predicted from Table V but the solution of oxygen (originally associated with aluminum as Al_2O_3) in the V-Nb-base (V-Cb) alloy, whose oxides are less stable than is Al_2O_3, involves chemical solution effects in the alloy. It is well known that the partial molal free energy of solution of oxygen in a metal at low oxygen concentrations can be substantially more negative than is the ΔF_f of the oxide itself. For example, if one considers the case of a one-percent saturated solution of a metal monoxide in the metal, and assumes ideal solution, the ΔF_f of the monoxide in this 1% saturated solution becomes:

$$\Delta F_f \text{ (monoxide in solution, } a = 0.01) = \Delta F_f^\circ + RT \log (0.01) \quad (7)$$

$$= \Delta F_f^\circ + 4.575\ T\ (-2), \quad (8)$$

or, at 2000°K, the ΔF_f°(monoxide in sol'n) becomes 18.3 Kcal/g atom 0 more negative than ΔF_f (2000). This has the effect of making nearly every oxide at least slightly soluble in every liquid metal. The smaller the ΔF_f°-value differences between the metal oxides the more readily the more stable oxide will dissolve in the other metal. Another factor regulating the end-point of dissolution is the solubility limit of oxygen in the alloy. If this limiting value is high, then, obviously, one can obtain substantial amounts of oxygen in the solution. Although a phase diagram of the V-Nb-O system is not available, there are some measurements of the binary systems V-O and Nb-O. Shunk (Ref. 12) summarizes the work on the Nb-O (Cb-O) system, and indicates the solid solubility of oxygen in Nb(Cb) at 1900°C is 9 atom percent O. Hansen (Ref. 13) shows two somewhat conflicting phase diagrams for the V-O system. However, each shows a metallic vanadium phase which

TABLE V

FREE ENERGIES OF FORMATION OF SELECTED OXIDES

Oxide	ΔF_f°, Kcal/g atom O				
	1100°K	1300°K	1500°K	1700°K	Ref.
1/3 Ce_2O_3	-121.0	-116.0	-111.5	-107.5	(10)
BeO	-117.4	-112.8	-108.3	-103.5	(9)
1/2 HfO_2	-108.0	-103.5	- 98.5	- 94.5	(10)
1/2 ZrO_2	-106.2	-101.7	- 97.3	- 93.0	(9)
TiO	-103.2	- 99.7	- 96.3	- 93.0	(9)
1/3 Al_2O_3	-105.8	-100.6	- 95.3	- 90.2	(9)
1/2 TiO_2	- 88.9	- 84.6	- 80.3	- 76.0	(9)
VO	- 77.5	- 73.8	- 69.0	- 65.0	(10)
1/3 V_2O_3	- 77.0	- 73.5	- 68.8	- 65.0	(10)
NbO	- 76.0	- 72.0	- 68.0	- 64.0	(10)
1/2 WO_2	- 46.6	- 42.5	- 38.5	- 34.6	(9)
1/2 MoO_2	- 44.0	- 40.0	- 36.5	- 33.0	(10)
1/3 Na_2SiO_3	- 95.9	- 89.4	- 82.3(ℓ)	- 75.6(ℓ)	(9)
1/5 $Na_2Si_2O_5$	- 92.3	- 87.1(ℓ)	- 81.5(ℓ)	- 75.9(ℓ)	(9)
1/2 SiO_2	- 85.1	- 81.0	- 76.9	- 72.8	(9)
Na_2O	- 63.6	- 53.6(ℓ)	- 41.7(ℓ)	- 30.1(ℓ)	(9)
1/2 $NaAlO_2$	-106.5	- 99.8	- 92.5	- 85.2	(9)

has a large atom percent oxygen. In one case, a very broad γ-phase ranging from pure V to 40 atom percent oxygen in the temperature range 1450° to ~1700° C is shown. In the second diagram, a vanadium metal β-phase is shown with a range of 17 to 28 atom percent oxygen at temperatures to 1800° C. At lower oxygen concentrations, a vanadium metal α-phase is stable with up to 5 atom percent oxygen at 1820° C. A two-phase region exists between the metallic α-V and β-V phases in the oxygen concentration range 5 to 17 atom percent.

With such wide-range oxygen-containing single phases in the V-O and Nb-O systems, one can reasonably expect a substantial oxygen solubility to exist in V-Nb (V-Cb) alloys, so that solubility of oxygen in the braze alloy is a contributing factor in the solution of Al_2O_3.

Another contributing factor is the energetics of the solution of the aluminum in the alloy. Aluminum forms compounds with V and Nb(Cb), such as Nb_3Al, Nb_2Al, and V_5Al_8. Aluminum intermetallics have heats of formation ranging from -4 to -12 kcal/g atom (Ref. 14), and one would expect the free energies of formation to be in the same range. Thus the partial molal free energies of solution of aluminum in V-Nb alloys to form dilute Al solutions can be significant in the overall energetics of the simplified reaction.

$$n\,Al_2O_3 + \text{Nb-V alloy} = 2n\,Al(\text{sol'n in Nb-V alloy}) + 3n\,O(\text{sol'n in Nb-V alloy}) \quad (9)$$

for which one can write,

$$\Delta F\,(\text{solution reaction}) = 2n\,\Delta F\,(\text{solution of Al in alloy}) + 3n\,\Delta F\,(\text{solution of O in alloy}) - n\,\Delta F\,(\text{formation of } Al_2O_3) \quad (10)$$

For these systems, then, the net ΔF (solution reaction) becomes negative, so that the reaction proceeds during the brazing process.

The presence of Group IV elements in 1-2% amounts in the alloy will reduce the amount of oxygen in solution to the extent that TiO_2, ZrO_2, or HfO_2 compounds are formed, and the removal of the oxygen from the alloy phase will tend to make the integral free energy of solution of the remaining oxygen in the alloy more negative, because its chemical activity will be lower.

Therefore, one sees that braze systems involving V-Cb (V-Nb) base alloys will tend to dissolve even the most stable oxides, and that the resulting braze will contain dissolved oxygen. Thus a hardening effect in the braze is to be expected, although, if the system remains single phase, the amount or degree of hardening may be tolerable. Therefore, it is desirable that the braze period be minimized, and that the braze alloy contain a minimum of Group IV elements. Both of these factors will tend to minimize the amount of Al_2O_3 which will react during brazing, and the presence of only small amounts of Group IV elements will minimize the tendency for the braze and the ceramic to continue to react during service.

It has been noted above that great care was taken to obtain ceramic materials having very low silica contents in order to ensure that the ceramic has good resistance to alkali metal. The chemical basis for this is illustrated by the examination of the Na_2O, the SiO_2, and the silicate data shown in Table V. The chemical stabilities (i.e., their negative free energies of formation per g atom O) of the sodium silicates (which are representative of other alkali silicates) are seen to be greater than those of either Na_2O or SiO_2. Because of this, the formation of silicates is thermodynamically favored both from the addition reaction of the oxides and from the displacement of silicon by sodium. This is illustrated in Table VI, which shows all such reactions to have a negative $\Delta F(Rx)$ at all temperatures. This, then, explains why impure alumina (which commonly contains silica as its major impurity) is not resistant to alkali metals.

Experimentally, pure alumina is resistant to alkali metals at all temperatures. However, according to the published thermodynamic data for sodium aluminate, $NaAlO_2$, the formation of $NaAlO_2$ from elemental sodium and Al_2O_3 is slightly favored at temperatures below 1200°K. Above 1200°K, Al_2O_3 is expected to be stable in sodium. Sodium aluminate is thermodynamically favored in systems of Na_2O (or oxygen-saturated sodium) and pure Al_2O_3 at all temperatures (Table VI).

These observations for the sodium silicates and sodium aluminate are typical of those for the alkali metals and silica and alumina. However, the potassium, rubidium, and cesium silicates and aluminates (for which no thermodynamic data were found) are expected to be less stable than are the corresponding sodium compounds. There is some qualitative evidence that cesium metal will attack impure alumina and beryllia, so that one must conclude that the cesium silicates are quite stable relative to SiO_2 and Cs_2O. However, cesium aluminate is expected to be relatively less stable, so that pure Al_2O_3 is quite probably thermodynamically stable in cesium at all temperatures.

Phase I Test Results - Overall Evaluation. — The foregoing sections describe the test results of the ten aged samples. In order to select the three best braze systems, assignments of the performance ratings of each of the brazes in the various tests have been made. The first of these is the evaluation of the micrographic information. The braze alloys used were initially

TABLE VI

FREE ENERGIES OF REACTIONS

Reaction	T °K	ΔF (Reaction)* kcal	ΔF (Reaction)* kcal/g atom O
$Na_2O + SiO_2 = Na_2SiO_3$	1100	-53.9	-18.0
	1500	-51.4	-17.1
$4Na + 3\ SiO_2 = 2\ Na_2\ SiO_3 + Si$	1100	-64.8	-10.8
	1500	-32.4	- 5.4
$Na_2O + 2\ SiO_2 = Na_2Si_2O_5$	1100	-57.5	-11.5
	1500	-58.2	-11.6
$4\ Na + 5\ SiO_2 = 2\ Na_2Si_2O_5 + Si$	1100	-72.0	- 7.2
	1500	-46.0	- 4.6
$Na_2O + Al_2O_3 = 2\ NaAlO_2$	1100	-45.0	-11.3
	1500	-42.4	-10.6
$3\ Na + 2\ Al_2O_3 = 3\ NaAlO_2 + Al$	1100	- 4.2	- 0.7
	1300	+ 4.8	+ 0.8
	1500	+16.8	+ 2.8

*ΔF - values for compounds are given in Table V.

5 mils (0.127 mm) thick, and, as has been shown above, the molten brazes dissolve some of the Cb-1Zr alloy. The resultant molten mixture, if it remains in the joint, should be thicker than the original braze, so that braze zone thicknesses are expected to be 5 mils (0.127 mm) or more. However, if the braze alloy becomes highly fluid, it may run out of the joint and leave a braze thickness of less than, say, four mils (0.10 mm). Both excessive solution of the refractory alloy with the formation of a very thick braze zone, and excessive fluidity of the braze with the loss of braze from the joint are undesirable.

A second factor which is observable in the micrographs is the extent of the interaction or reaction zone between the braze and the alumina. Extensive reaction leads to the formation of a brittle region adjacent to the alumina, and is undesirable. A third feature that can be evaluated is the behavior of the alumina adjacent to the braze. Here, the presence of cracks is the most serious problem. The presence of pores is not necessarily deleterious, and certainly some pores will be evident because the Al_2O_3 used was only 96-98% dense.

Table VII summarizes the observations of the micrographs, and shows the evaluations of these data in terms of a five-unit scale; G, GF, F, FP, and P.

The microhardness traverse data is presented in Appendix XII. These data serve two purposes. First, they indicate the hardnesses and the hardness profiles of the braze. Second, they help in defining the width of the braze region. A ductile braze is desired so that it can absorb the deformations produced by thermal expansion differences between the alumina (or beryllia) and the Cb-1Zr (or T-111) alloy. It would also be helpful in this regard if the braze region were thick, because this will allow the maximum amount of deformation to be accomodated with the least strain in the braze. Therefore, the ideal microhardness profile for the expected service for these brazes is a low hardness value over a wide region. Table VIII shows the evaluations of the microhardness data in the five-unit scale.

The modulus of rupture (MOR) data obtained from rod samples is shown in Appendix XI. The majority of the MOR values fall in the 4000 to 12,000 psi (27 600 000 to 82 800 000 N/m^2) range. These values are lower than one would expect to obtain from 95+% dense alumina, although, as is indicated on the tables, 33 of the 80 samples broke at least partly in the ceramic, and 16 of the 33 were breaks which occurred entirely within the ceramic. Because one would expect MOR values of 35 000 psi (241 000 000 N/m^2) or more for the alumina, the question is raised regarding the possibility of the braze's interaction on the alumina, possibly by the diffusion of foreign atoms. Another possibility is that there may be some residual stresses in the alumina after the brazing operation is completed. Although the Al_2O_3 and Cb-1Zr materials show a good thermal expansion match,

TABLE VII

EVALUATION OF PHOTOMICROGRAPHS

Braze		Fig. No.	Braze thickness mil	Braze thickness mm	Nature of Braze	Interaction	Alumina Effect	Rating	Overall Rating
2M	A	26	2.0	0.051	two phase	Slight	none	FP	
	B	26	3.0	0.076	two phase	negligible	none	F	
	C	27	2.5	0.063	two phase	slight	none	FP	FP
	D	27	1.5	0.038	two phase	negligible	crack	P	
3M	A	34	7.0	0.178	epitaxy	large	pores (?)	P	
	B	34	8.0	0.203	epitaxy	negligible	none	F	
	C	35	10.0	0.254	epitaxy	large	defects	P	FP-
	D	35	8.0	0.203	epitaxy	moderate	pores	FP	
4M	A	42	2.0	0.051	epitaxy	large	none	P	
	B	42	10.0	0.254	epitaxy	slight	none	GF	
	C	43	5.0*	0.127*	epitaxy	slight	none	GF	F
	D	43	8.0	0.203	epitaxy, pores	moderate	none	F	
4W	A	48	5.0	0.127	epitaxy	moderate	none	GF	
	B	48	3.5	0.089	epitaxy	negligible	none	G	
	C	49	10.0	0.254	epitaxy	v. slight	none	GF	G-
	D	49	5.0	0.127	epitaxy	slight	none	G	
5W	A	57	5.0	0.127	epitaxy	v. large	pores	P	
	B	57	10.0	0.254	epitaxy	negligible	none	GF	
	C	58	5.0	0.127	epitaxy	slight	pores	F	FP+
	D	58	5.0	0.127	epitaxy	extreme	few pores	P	
6W	A	64	4.0	0.101	epitaxy	slight	none	GF	
	B	64	6.5	0.165	epitaxy	negligible	none	G	
	C	65	5.0	0.127	epitaxy	slight	pores	GF	G-
	D	65	9.0	0.229	epitaxy	slight	none	G	
9M	A	73	2.0	0.051	epitaxy	moderate	lg. grain	FP	
	B	73	5.0	0.127	epitaxy	negligible	none	GF	
	C	74	4.0	0.101	epitaxy	moderate	none	F	FP+
	D	74	5.0	0.127	epitaxy	v. large	pores	P	
9W	A	80	4.0	0.101	epitaxy	slight	none	GF	
	B	80	6.0	0.152	epitaxy	negligible	none	F	
	C	81	9.0	0.229	epitaxy	slight	none	GF	F+
	D	81	4.5	0.115	epitaxy	v. large	none	P	
10M	A	84	7.0	0.178	epitaxy	moderate	pores	GF	
	B	84	5.0	0.127	epitaxy	negligible	none	G	
	C	85	5.0	0.127	epitaxy	large	pores	FP	GF-
	D	85	8.5	0.216	epitaxy	moderate	none	GF	
10W	A	92	6.5	0.165	epitaxy	negligible	pores	F	
	B	92	8.0	0.203	epitaxy	negligible	none	GF	
	C	93	5.0	0.127	epitaxy	moderate	pores	F	F+
	D	93	8.0	0.203	epitaxy	slight	pores	GF	

*Not a uniform width

TABLE VIII

EVALUATION OF MICROHARDNESS DATA

Braze		Fig. No.	Type of Profile	Median Value DPH Units	Braze Thickness mil	Braze Thickness mm	Rating	Overall Rating
2M	A	26	Step, sl. slope	650	2.0	0.051	FP	FP
	B	26	Slope	375	3.0	0.076	F	
	C	27	Slope	550	2.5	0.063	FP	
	D	27	Step	825	1.5	0.038	P	
3M	A	34	Step sl. slope	300	7.0	0.178	G	G-
	B	34	Step, uniform	300	8.0	0.203	G	
	C	35	Step, uniform	350	10.0	0.254	GF	
	D	35	Step, uniform	350	8.0	0.203	GF	
4M	A	42	Slope	460	2.0	0.051	FP	F+
	B	42	Slope	225	10.0	0.254	GF	
	C	43	Irreg. slope	350	5.0*	0.127*	F	
	D	43	Step, uniform	325	8.0	0.203	G	
4W	A	48	Step, uniform	350	5.0	0.127	GF	GF-
	B	48	Slope	250	3.5	0.089	F	
	C	49	Step, slope	325	10.0	0.254	G	
	D	49	Step, slope	400	5.0	0.127	F	
5W	A	57	Step, uniform	300	5.0	0.127	G	GF
	B	57	Step, uniform	320	10.0	0.254	G	
	C	58	Step, slope	425	5.0	0.127	F	
	D	58	Slope	400	5.0	0.127	F	
6W	A	64	Slope	380	4.0	0.101	F	G-
	B	64	Step, neg. slope	325	6.5	0.165	G	
	C	65	Step, uniform	325	5.0	0.127	G	
	D	65	Step, uniform	325	9.0	0.228	G	
9M	A	73	Slope	625	2.0	0.051	FP	F+
	B	73	Slope	335	5.0	0.127	GF	
	C	74	Slope	325	4.0	0.101	F	
	D	74	Step, neg. slope	360	5.0	0.127	GF	
9W	A	80	Step, neg. slope	300	4.0	0.101	GF	GF+
	B	80	Step, slope	335	6.0	0.152	GF	
	C	81	Step, uniform	300	9.0	0.229	G	
	D	81	Step, slope	385	4.5	0.115	GF	
10M	A	84	Slope	275	7.0	0.178	GF	GF
	B	84	Step, neg. slope	315	5.0	0.127	GF	
	C	85	Steps	400	5.0	0.127	F	
	D	85	Step, slope	330	8.5	0.216	G	
10W	A	92	Slope	325	6.5	0.165	GF	GF+
	B	92	Step, uniform	350	8.0	0.203	G	
	C	93	Step, uniform	360	5.0	0.127	G	
	D	93	Slope, step, slope	400	8.0	0.203	F	

*Not a uniform width.

there is still a difference of about 0.06% in their expansions at 1850°C. This, plus the presence of reactive metals, plus heating to within 200°C of the Al_2O_3 melting point, followed by rather rapid cooling could well weaken the Al_2O_3 and leave some residual stress, which would cause low MOR values to be experienced.

The effects of aging at 1200°C are shown in Figure 12, which shows most of the samples to have lower MOR values after the 1000-hr (3.6×10^6s) exposure than after the 100-hr (3.6×10^5s) aging exposure. In general, the 100-hr (3.6×10^5s) aging exposure MOR results are equal to or higher than the as-brazed results. This can probably be attributed to an annealing effect of residual stresses, although any chemical effects of the brazing will persist.

In evaluating the MOR test patterns shown in Figure 12, the effects of aging were given the greatest weight with the "as-brazed tested at 1200°C" values being given consideration, also. A good pattern of MOR results is therefore one in which the average level of values is high, the "as-brazed, tested at 1200°C" data are equal to or higher than the as-brazed data, and the 1000-hr (3.6×10^6s) aged data are equal to or greater than the as-brazed data. On these bases, the MOR data summarized in Figure 12 have been evaluated as follows: 2M, good; 3M, poor; 4M, good; 4W, fair; 5W poor; 6W, good; 9M, good-to-fair; 9W, poor; 10M, good; and 10W, fair.

The electron microprobe data show a number of important facets of braze performance. The stability of the Al_2O_3-braze interface is shown by the presence or absence of strong peaks for the Group IV metals (or cerium), the presence of a separation, if one is present, or the existence of a stable, straightforward interface. The nature of the braze alloy itself is shown by an examination of the metal concentrations. The existence of compounds is demonstrated by the presence of characteristic flat regions in the metal profiles, and the nature of the diffusional processes can ordinarily be inferred from an examination of the concentration gradients. However, as has been noted above, these particular systems have unknown initial gradients, so that the evaluation of diffusional effects is quite difficult.

The preferred electron microprobe line profile or concentration gradient pattern for vanadium in these systems is a regular one in which there is a smooth gradient of vanadium with a maximum at the Al_2O_3 interface, a slowly decreasing concentration toward the Cb-1Zr juncture, and a smoothly dropping concentration through the juncture region. The preferred pattern for niobium (columbium) is a relatively low level at the Al_2O_3 interface, with a slowly rising concentration through the braze region and finally a smoothly rising concentration through the juncture region.

The preferred pattern for the Group IV elements and cerium is a low level through the braze with at most a small concentration increase adjacent to the alumina interface. The localized regions of small concentrations of Zr, which are indicative of a grain boundary effect, are not deleterious.

The preferred pattern for the Group VI element would be a strong concentration at the alumina interface, its original position. However, it has been found that all of the brazes used in this study dissolve both the molybdenum and the tungsten deposited on the alumina by vacuum evaporation.

Table IX summarizes the electron microprobe data and shows a composite evaluation of the performance of each braze in terms of the five-unit scale; G, GF, F, FP, and P.

The overall analysis of the performance of the ten Phase I braze systems has been made by evaluating all of the foregoing performance factors as is indicated in Table X. This table shows the individual evaluations on the five-unit scale, and from these individual performance ratings an overall ranking has been made as shown. The final rankings are shown in six groups: the best braze with a rating of G- is 6W; the two brazes with a rating of GF+ are 10M and 4W; the two brazes with a rating of GF- are 10W and 4M; the three brazes with a rating of F are 9M, 9W, and 3M; the one braze with a rating of F- is 5W; and the one braze with a rating of FP- is 2M.

TABLE IX

EVALUATION OF ELECTRON MICROPROBE DATA

Braze		Nature of Al_2O_3-braze interface	Nature of Braze	Nature of V or Pt(x) Profile	Nature of Nb(Cb) Profile	Nature of Ce, Zr, Hf, Ti Profiles	Rating	Overall Rating
2M	A	reaction	two phase	compounds*	compounds	Hf, Zr peaks at Al_2O_3	P	P
	B	reaction	two phase	compounds*	compounds	Hf, Zr peaks at Al_2O_3	P	
	C	reaction	two phase	compounds*	compounds	Hf, Zr peaks at Al_2O_3	P	
	D	reaction	two phase	compounds*	compounds	Hf, Zr peaks at Al_2O_3	P	
3M	A	v. sl. reaction	one phase	smooth	smooth	sl. Ce peak at Al_2O_3	GF	GF
	B	v. sl. reaction	one phase	smooth	smooth	sl. Ce peak at Al_2O_3	GF	
	C	v. sl. reaction	one phase	smooth	smooth	sl. Ce peak at Al_2O_3	GF	
	D	v. sl. reaction	one phase	smooth	smooth	sl. Ce peak at Al_2O_3	GF	
4M	A	reaction	one phase	smooth	smooth	Hf, Zr peaks at Al_2O_3	F	GF-
	B	reaction	one phase	smooth	smooth	Hf, Zr peaks at Al_2O_3	F	
	C	no reaction	one phase	smooth	smooth	uniform	G	
	D	reaction	one phase	smooth	smooth	Hf, Zr peaks at Al_2O_3	F	
4W	A	no reaction	one phase	smooth	smooth	uniform	G	G
	B	no reaction	one phase	smooth	smooth	uniform	G	
	C	no reaction	one phase	g.b. dip	g.b. dip	g.b. peak	G	
	D	no reaction	one phase	smooth	smooth	uniform	G	
5W	A	no reaction	one phase	smooth	smooth	Zr peak, mid-braze	GF	F+
	B	no reaction	one phase	g.b. dip	g.b. dip	g.b. peak	G	
	C	reaction	one phase	smooth	smooth	Zr peak at Al_2O_3	G	
	D	reaction	one phase	interface dip, structure	interface dip, structure	Zr groove at Al_2O_3	P	
6W	A	no reaction	one phase	smooth	smooth	Ti uniform, Zr peaks	GF	G-
	B	no reaction	one phase	smooth	smooth	uniform	G	
	C	no reaction	one phase	smooth	smooth	uniform	G	
	D	no reaction	one phase	g.b. dip	g.b. dip	g.b. peaks	G	
9M	A	reaction	one phase	smooth	smooth	Zr peak at Al_2O_3	F	FP+
	B	reaction	one phase	smooth	smooth	sl. Zr peak at Al_2O_3	F	
	C	reaction	one phase	dip at Al_2O_3	dip at Al_2O_3	Zr peak at Al_2O_3	FP	
	D	reaction	one phase	compound (?)	compound (?)	Zr, many peaks	P	
9W	A	reaction	one phase	smooth	smooth	Zr peak at Al_2O_3	F	F-
	B	reaction	one phase	smooth	smooth	Zr peak at Al_2O_3	F	
	C	reaction	one phase	smooth	smooth	Zr peak at Al_2O_3	F	
	D	much reaction	one phase	groove	groove	groove, then uniform	P	
10M	A	no reaction	one phase	occlusion	occlusion	uniform	GF	GF+
	B	no reaction	one phase	smooth	smooth	uniform	G	
	C	no reaction	one phase	spurious peaks	spurious peaks	uniform	GF	
	D	no reaction	one phase	smooth	smooth	uniform	G	
10W	A	no reaction	one phase	few dips	few dips	uniform	GF	G-
	B	no reaction	one phase	smooth	smooth	uniform	G	
	C	no reaction	one phase	smooth	smooth	uniform	G	
	D	no reaction	one phase	smooth	smooth	uniform	G	

*Platinum profile.

TABLE X

OVERALL EVALUATION

Braze	Photo-micrographs	Modulus of Rupture	Micro-hardness	Electron Micro-Probe	Overall Rating	Overall Ranking
2M	FP	G	FP	P	FP-	10
3M	FP-	P	G-	GF	F	6-7-8
4M	F	G	F+	GF-	GF-	4-5
4W	G-	F	GF-	G	GF+	2-3
5W	FP+	P	GF	F+	F-	9
6W	G-	G	G-	G-	G-	1
9M	FP+	GF	F+	FP+	F	6-7-8
9W	F+	P	GF+	F-	F	6-7-8
10M	GF-	G	GF	GF+	GF+	2-3
10W	F+	F	GF+	G-	GF-	4-5

CONCLUSIONS AND RECOMMENDATIONS

Phase I Braze Evaluation and Selection Studies

The overall evaluation of the first phase of the evaluations of twenty-six ceramic-to-metal braze seal systems for 1200°C service has indicated the best three braze systems of those tested to be:

(1) Braze System 6W (Cb-1Zr/V-2Ti/W/Al_2O_3)

(2) Braze System 10M (Cb-1Zr/64V-34Cb-2Ti/Mo/Al_2O_3)

(3) Braze System 4W (Cb-1Zr/V-2Hf/W/Al_2O_3)

Based upon the evaluations made of the structure, aging, and bonding natures of these systems, 6W is clearly the first choice. Systems 10M and 4W are nominally equal, and somewhat superior to the next two choices shown in Table X, 10W and 4M. The remainder are clearly inferior.

Several facets of the behavior of the brazes tested stand out. First, all of the brazes dissolved large amounts of the Cb-1Zr alloy, with the result that the final braze contained 40-60 weight percent niobium (columbium). This is not necessarily deleterious, but care must be taken to avoid an excessively long brazing period, so that the amount of dissolution will be minimized. In addition, one should be particularly mindful of this dissolution when thin sheets are being brazed.

Second, the successful brazes contained modest amounts (2%) of an active metal whose presence in the braze presumably aided in accomplishing good wetting of the ceramic. In the good braze systems, the amount of reaction as evidenced by the development of a layer of reaction products adjacent to the alumina was quite small. In the two best brazes, the active element was titanium, which is the least reactive of the Group IV elements. However, the third best braze, 4W, used hafnium as its reactive metal, and hafnium is significantly more reactive than titanium. Nevertheless, one is led to the conclusion that the best braze alloy would contain a minimum amount of active metal, and that titanium would be the preferred choice. All that is required is that the ceramic be wetted by the braze. Any further reaction is undesirable and can lead to the development of a reaction layer, either during the immediate brazing period, or later, during aging.

Third, the amount of aluminum found in the brazes is significant, and can only be explained by the assumption that some Al_2O_3 decomposed and dissolved in the molten braze. This conclusion is supported by the fact that there is a chemical driving force for this dissolution. Therefore, one should minimize the time during which the braze is molten. However, there is some inferred evidence that an induction period exists in the process of wetting

of the ceramic by the braze. If such a period does indeed exist, then the reproducibility of the braze reaction is difficult to control, and the final composition of the braze alloy may be quite variable.

Fourth, all of the joints attempted between alumina and T-111 alloy resulted in poor bonds, and peripheral tension-induced cracks in the ceramic. This is attributed to the effect of the larger expansion of the alumina than that of the T-111. Upon cooling from the brazing temperature the alumina tends to shrink more than the T-111 and tension cracks are developed. The test cases in which BeO buttons were brazed to T-111 alloy also showed the tension cracks. Because of the very high melting point of brazes which are to be used at 1200°C, it is essential that the metal-ceramic combinations used be very well matched in their expansion characteristics, unless the braze alloys are very ductile and can absorb the expansion mismatch.

These Phase I studies have established that at least three braze systems show promise in the 1000-hour (3.6×10^6s) 1200°C aging tests of simple button braze test specimens and in MOR tests. In order to further establish their use as high temperature braze systems, the tests of vacuum integrity under thermal cycling, the aging tests of at least 5000 hours, and the tests of alkali metal resistance as are described below in the Phase II studies were carried out.

PHASE II TEST PROGRAM

The Phase II Test program goal was to prepare bulb or capsule specimens of the best braze system determined by the Phase I studies, and to carry out a series of performance tests. These were measurements of (1) thermal shock and thermal cycling resistance; (2) aging behavior at 800°, 1000°, and 1200°C; and (3) resistance to 5 torr cesium vapor pressure at 1200°C. The sequence of testing of the Phase II studies is shown on the test flow sheet in Figure 13, and the details of the various tests and their evaluations follows.

Figure 13. Phase II Test Flow Sheet

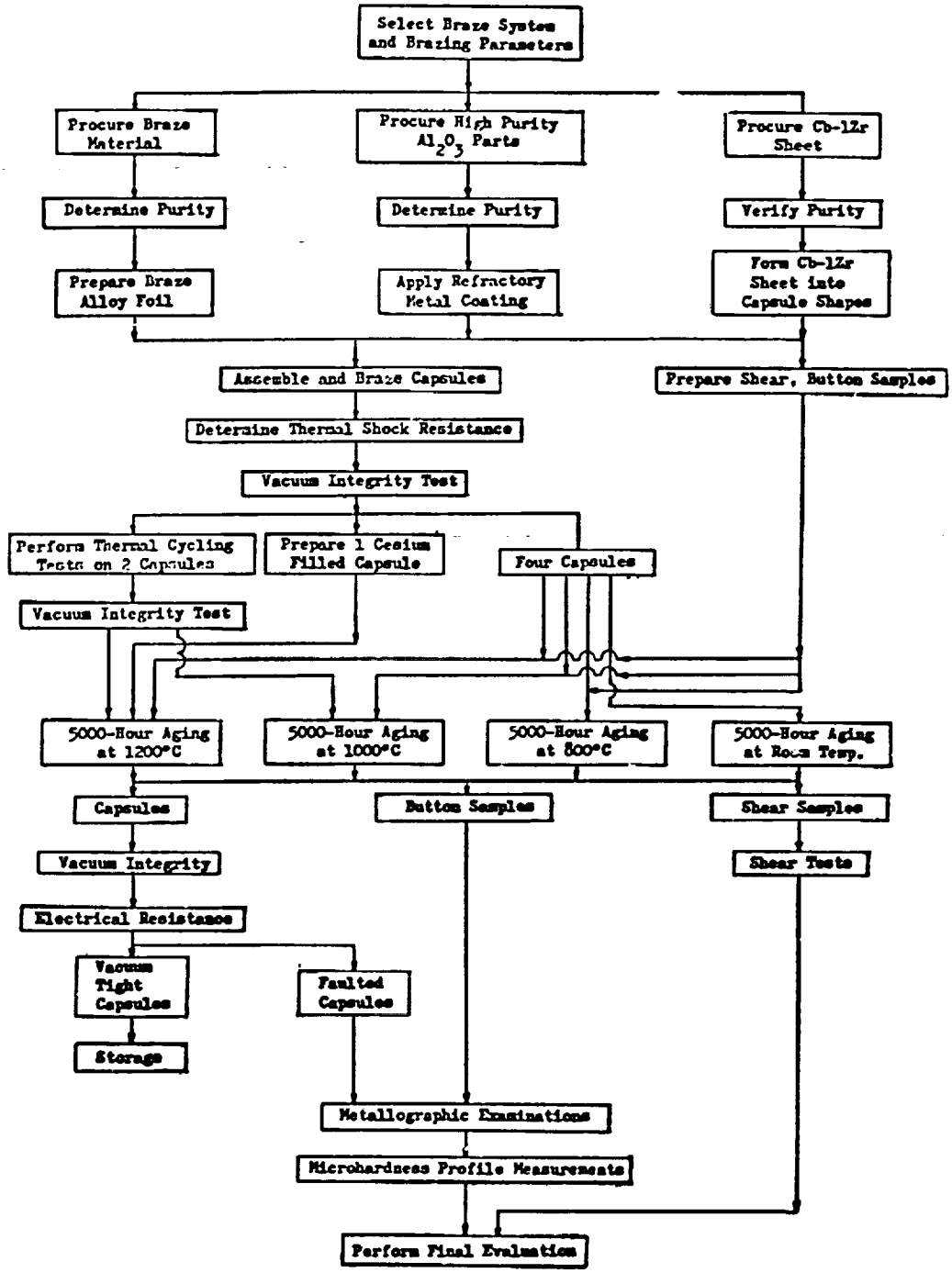

PHASE II TEST PROCEDURES AND SPECIAL TEST EQUIPMENT

Brazing (Capsule Specimens). — The brazing jig used to prepare the capsule samples for the Phase II studies was built using Cb-1Zr alloy and tungsten. Figure 14 is a photograph of the jig. Appendix XIV shows the details and dimensions of this unit in which the 0.5-inch capsule joints were brazed. The brazing conditions used were those determined to be optimum in the Phase I studies. For the system (Cb-1Zr/V-2Ti/W/Al_2O_3) the conditions were 1870°C for one minute.

Thermal Cycling Tests. — The thermal cycling test procedure involved heating the bulb samples from <250°C to 1200°C at a rate of 100°C/min holding at 1200°C for five minutes, and then cooling to <250°C at a rate no greater than 100°C/min. Figure 15 shows a typical thermal cycle temperature trace.

The test evaluation procedure involved a series of helium leak rate measurements made during the 64-cycle sequence both at <250°C and at 1200°C. This thermal cycling helium leak rate test procedure involved the installation of the samples in the furnace with a 1/4-inch (0.635 cm) diameter tube leading from each sample to a common manifold which was fitted with vacuum and helium connections. The test chamber was maintained at a nominal 1×10^{-6} torr ($1.33 \times 10^{-4} N/m^2$) pressure and a Veeco Model MS-9 helium leak detector was attached to the chamber. After establishing the background level on the leak detector, helium was introduced into the manifold to about 5 psia ($3.4 \times 10^4 N/m^2$). The vacuum pump line leading to the Turbomolecular pump was closed to prevent pumping of the vacuum chamber during the test period. Then, the helium was released into the first of the bulb samples and the leak detector reading was monitored for a period of five minutes. If there was no increase in the leak detector's reading, the helium pressure in the manifold was increased to 20 psia ($1.38 \times 10^5 N/m^2$) and held again for five minutes. The pressure was finally increased to 25 psia ($1.72 \times 10^5 N/m^2$). At each pressure level, the leak detector was monitored for five minutes and the readings were recorded.

After the 25 psia test, the manifold and the first sample were evacuated and then the sample was valved off before the testing of the second sample began. This test sequence was performed on the thermal cycling test samples at the beginning of the thermal cycling test series, at 1200°C during the first, fourth, sixteenth, and sixty-fourth cycle; and at <250°C following the first, fourth, sixteenth and sixty-fourth cycle.

Leak Tests. — Helium leak testing was used to determine the vacuum integrity of the capsule samples. Two methods of testing were used. The first, which was a qualitative technique at best, involved connecting the test instrument, a Veeco MS-9 helium leak detector, to a port on a vacuum chamber in which a capsule sample was located. Then a standard calibrated leak was used to bleed a known amount of helium into the chamber, and the leak detector was adjusted to produce a fixed meter

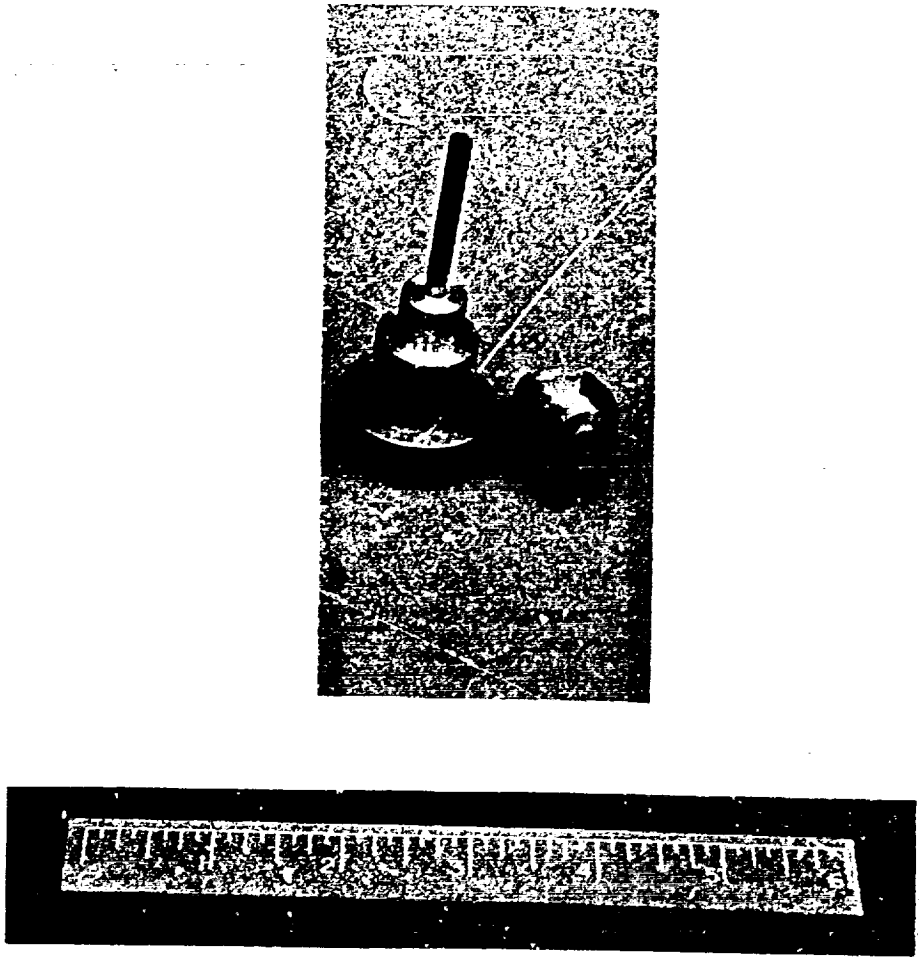

Figure 14. Brazing Jig Parts for One-Half-Inch Seal Capsule

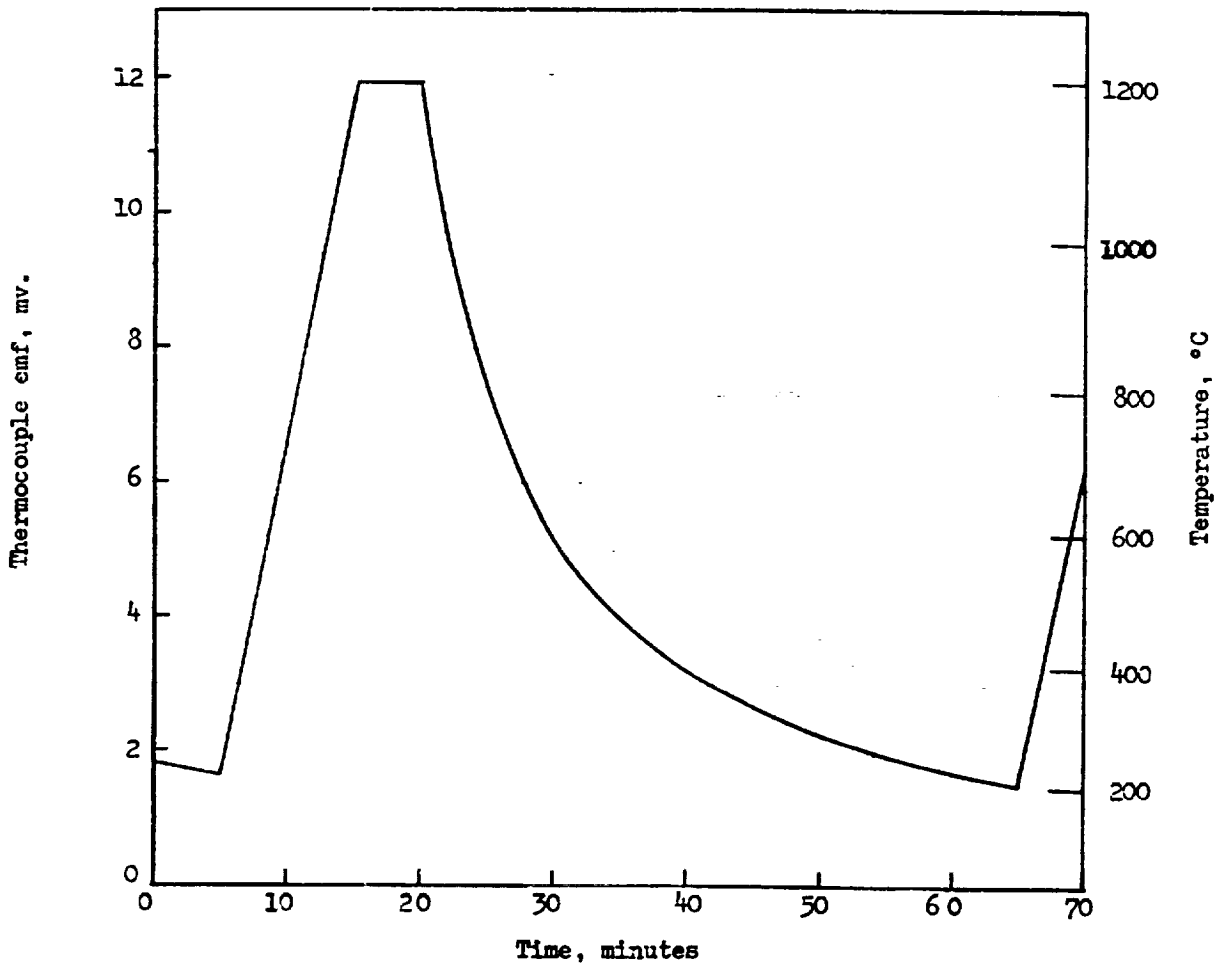

Figure 15. Typical Thermal Cycle Time-Temperature Trace (Cycle No. 53)

reading when the system reached a steady state. This meter reading was taken as that corresponding to the calibrated leak rate.

When the capsules were pressurized with helium, it was expected that a leak of the magnitude of the standard leaks (1.7×10^{-8} std cc air/sec) would produce a comparable meter reading. However, it was observed in the early tests that this was a rather insensitive method, particularly when the leak rates of the samples were expected to be two orders of magnitude less than the standard leak's rate. Therefore, the tests for the thermal cycling test series were carried out by closing the valve to the vacuum pump and, in effect, allowing any helium that might leak from the capsules to collect in the chamber, and thereby increasing the detection sensitivity of the leak detector.

The second method of performing a leak rate measurement involved mounting the sample directly on the leak detector's port. First the meter reading of a calibrated leak was determined. Also, the minimum detectable increment in the meter was identified. Then, the minimum detectable leak size is evaluated as,

$$L\,(\text{min}) = \frac{S\,(\text{min})}{S\,(\text{calib})}\,[L\,(\text{calib})] \qquad (11)$$

where

L (min) is the minimum detectable leak rate, std cc air/sec,

S (min) is the minimum readable scale difference (which was taken in this instrument at 0.02 scale divisions),

S (calib) is the scale reading for the calibrated leak,

L (calib) is the leak rate of the calibrated leak (which is 1.7×10^{-8} std cc air/sec for the Veeco #3441 standard leak used in this program).

The measured leak for any sample is then given by,

$$L\,(\text{sample}) = \frac{S\,(\text{sample})}{S\,(\text{calib})}\,[L\,(\text{calib})] \qquad (12)$$

where

L (sample) is the measured leak rate, std cc air/sec,

S (sample) is the scale reading of the sample.

Initially, a small helium probe is used to determine whether there is an easily detectable leak. If no response is obtained to the helium probe, the sample is bagged and flooded with helium to measure the leak rate to be recorded as the test data. If no response to the bagging operation is observed, the test record shows the value of [<L (min)].

Shear Tests. — The shear test unit used in the Phase II studies is shown in Figure 10 and Appendix VII. The knife is driven by an Instron test unit at a speed of 0.050 in/min (0.0212 mm/s) and the developed shear loads are recorded on a strip chart. The tests were performed as described under the Phase I studies on Page

Microhardness. — The unit used in these tests was a Leitz Miniload Hardness Tester, with a Vickers type diamond point indenter. The tests were performed using a 100 gram weight, which permits the evaluation of DPH (Vickers) hardnesses ranging from 19.7 to 1097 units (Kg/sq mm). The test procedure is described above on Page

Electrical Resistivity. — The post-test electrical resistivity of test samples was measured using a General Radio Corporation, Type 1862-C megohmeter. This unit has the capability of measuring electrical resistance in the range 1 megohms to 100,000 megohms.

Cesium Vapor Exposure Test. — The cesium vapor exposure test involved the attachment of a cesium reservoir to the tubulation of a capsule. A six-inch (15 cm) length of 1/4-inch (0.635 cm) diameter nickel tubing was welded to the end of the 15-inch (38 cm) long, 0.257-inch (0.652 cm) Cb-1Zr tube affixed to the capsule, using a mild steel sleeve to effect the joint. The steel sleeve was machined to slip over the Cb-1Zr tube, and its wall thickness was machined to 0.025 inch (0.0635 cm) to approximate that of the Cb-1Zr. The other end of the sleeve was matched to the nickel. The sleeve was then electron-beam joined to the Cb-1Zr by melting the iron and allowing it to wet and adhere to the Cb-1Zr alloy tube. A true electron-beam weld was then made between the sleeve and the nickel tube. The resultant joint is helium leak tight and quite strong. The nickel tubing extension of the Cb-1Zr was needed in order that a good seal be made on the cesium reservoir after the cesium was loaded into the capsule. A schematic diagram of the capsule is shown in Figure 16.

The cesium (nominally 99.99% pure and obtained originally for use in the thermionic diode work) was supplied in a glass ampoule (0.20 gm). The cesium was transferred into the capsule by first affixing a copper tube to the end of the nickel tube and placing the ampoule in the copper tube. The tube was then attached to a high-vacuum system and the array was wrapped (except for the area immediately around the Cs ampoule) with heating tape and heated to 150-160°C under vacuum until the pressure in the system dropped into the low 10^{-6} torr (1.33×10^{-4} N/m^2) range (24-hour heating period). When the heating tape was removed and the system was allowed to cool, the pressure dropped about a decade. A pack of dry ice was then

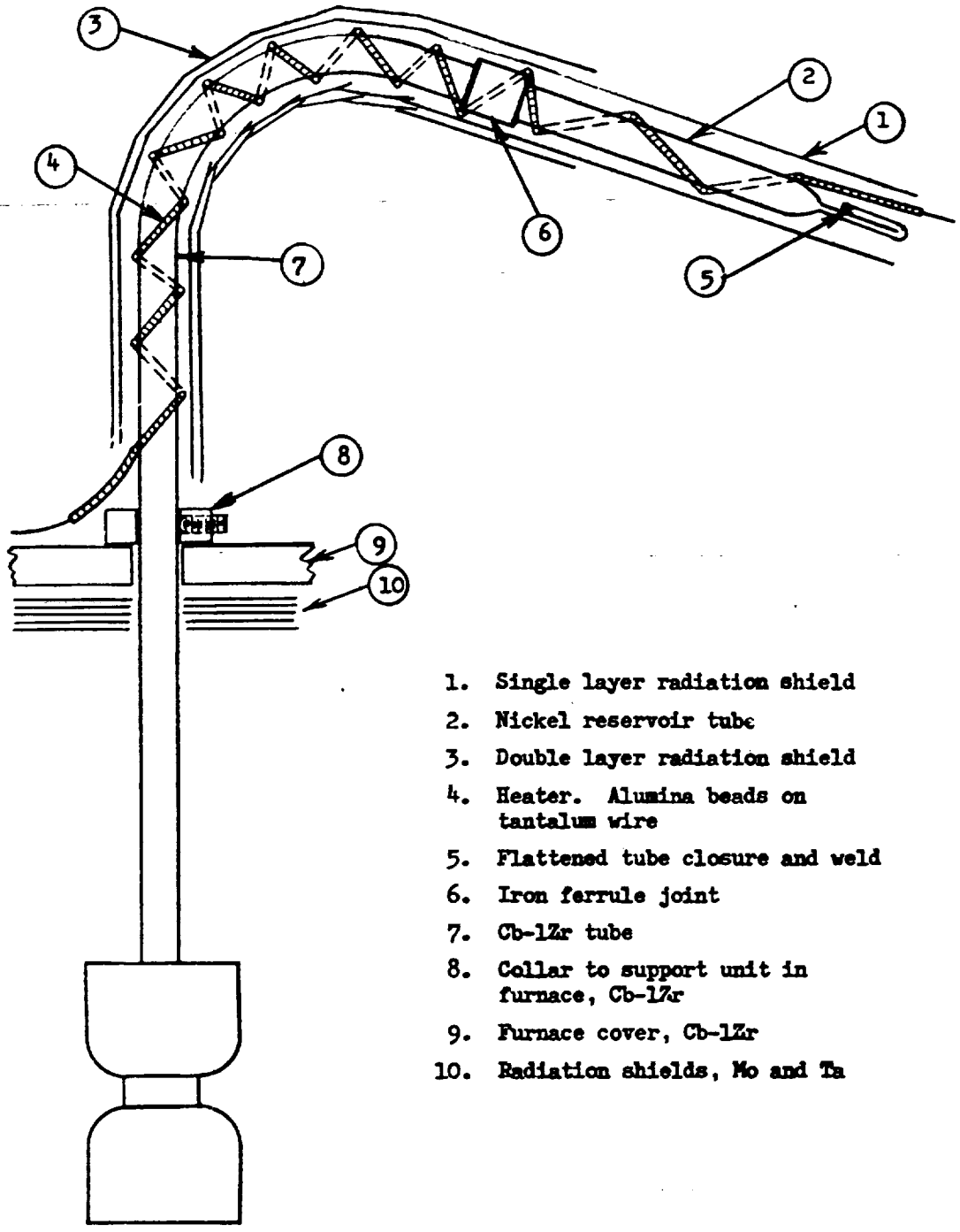

1. Single layer radiation shield
2. Nickel reservoir tube
3. Double layer radiation shield
4. Heater. Alumina beads on tantalum wire
5. Flattened tube closure and weld
6. Iron ferrule joint
7. Cb-1Zr tube
8. Collar to support unit in furnace, Cb-1Zr
9. Furnace cover, Cb-1Zr
10. Radiation shields, Mo and Ta

Figure 16. Schematic Diagram, Cesium Vapor Capsule

placed around the Cb-1Zr tube as a condenser for the Cs-vapor, and then the Cs ampoule was broken by crushing inside the copper tubing. The application of heat to the copper tubing and along the nickel tubing caused the cesium to move toward the dry ice-cooled region. By maintaining the copper and the nickel tubing at 230°C for a half-hour, the cesium was given ample time to diffuse to the cold region and to be trapped there. Then the nickel tube was pinched closed at one point, and pinched off about 1/2-inch (1.27 cm) farther away. The first pinch closure was then held while the nickel was welded closed to complete the loading procedure.

The nickel tubing was then bent about 120° to provide a short reservoir region for the cesium to collect in when the capsule is heated. The reservoir region and the tubing leading to the capsule were fitted with a heater, which was wound so that the reservoir region at the end of the nickel tube was the coldest point in the assembly. The heater was made by stringing alumina insulation beads on a length of tantalum wire. Insulation was provided by wrapping the heater with two layers of tantalum foil. By controlling the reservoir temperature to 338°C, the cesium vapor pressure was maintained at the desired 5 torr.

PHASE II SAMPLES

The samples used in the Phase II studies were bulb-type capsules, and button samples. The capsules are shown in Figure 118 of Appendix XV, and the button samples consist of one-inch (2.54 cm) lengths of 0.25 inch (0.635 cm) diameter Cb-1Zr rod, to the end of which an alumina button, 0.25 inch (0.635 cm) in diameter and 0.125 inch (0.318 cm) high is brazed. The best braze system as determined from the Phase I study was used in preparing the first set of bulb samples.

The seal joint as shown in Figure 118 consists of a 0.50 inch (1.27 cm) OD, 0.10 inch (0.254 cm) wall, ceramic cylinder 0.2 inch (0.508 cm) in length, brazed on each end to a cup-shaped Cb-1Zr section. In order to provide stress equalization across the braze/metal region, a ring of ceramic 0.50 inch (1.27 cm) OD, with an 0.10 inch (0.254 cm) wall, and 0.10 inch (0.254 cm) high is brazed to the inside of the Cb-1Zr sections in alignment with the ceramic section. Four braze regions are thus required, although only two of them are required to be vacuum tight.

One capsule was fabricated using Braze No. 6W, with the previously determined braze conditions of 1870°C for one minute, followed by the nominal 100°C/minute cooling rate. It was helium leak-checked and was found to be tight. Then, five additional seal samples were prepared under the same conditions. However, when they were leak-checked a few days after fabrication all of these seals showed leaks.

In an attempt to identify the location of the leaks, a pressurizing jig was made and the seals were exposed to internal helium pressure while submerged in acetone. No leaks were found at pressures below 25 psig, but all of the seals showed the slow formation of bubbles at 35-40 psig. The leaks were clearly in the braze region, rather than through the ceramic.

Further examination revealed that there were several small radial cracks in the braze metal, and that some of them extended as much as 80% of the way across the braze surface. It was therefore concluded that although this braze (V-2Ti) showed very good wetting and adherence to the alumina, its reactivity was such that too much alumina was dissolving. The dissolution of Al_2O_3 in the braze would not only cause the solution of aluminum in the vanadium-base alloy, but would also introduce oxygen into the braze. The final product of this solution is a braze that apparently cannot withstand the cooling cycle from 1870°C to room temperature.

Because the No. 6W braze was not producing helium leak-tight joints, the decision was made to make a series of tests of alternate braze systems to determine if modifications in technique or braze compositions might prove to be a solution of the problem. Four tests were made: (1) separate foils of V and Ti; (2) a foil of V with TiH_2 as a source of a small amount of Ti; (3) pure V; and (4) the eutectic 65V-35Cb alloy (Braze No. 8).

TABLE XI

BUTTON SAMPLE BRAZE TEST MATRIX: SEPARATE-LAYER GETTER TESTS

No.	Braze	Time sec.	Temp. °C	Shear* lb	Comment
1	V + Ti/W**	60	1890	340	Reaction evident; rough, pebbly braze and ceramic surfaces
2	V + Ti/W**	60	1890	440	Reaction evident; rough, pebbly braze and ceramic surfaces
3	V + Ti/Mo***	60	1890	505	Reaction evident; rough, pebbly braze and ceramic surfaces
4	V + Ti/Mo***	60	1890	-	Metallographic examination: Ceramic markedly discolored, several well-defined layers evident.
5	V + TiH_2/W****	60	1870	410	Reaction evident, rough, pebbly braze and ceramic surfaces
6	V + TiH_2/W****	60	1870	-	Not examined
7	V + TiH_2/Mo*****	60	1870	450	Reaction evident; rough, pebbly braze and ceramic surfaces
8	V + TiH_2/Mo*****	60	1870	75	Reaction evident; rough surfaces, break at metal/braze interface

* Shear values in psi are 20.4 times the values shown.

** 5 mil V foil + 0.5 mil Ti foil with 2 micron W barrier.

*** 5 mil V foil + 0.5 mil Ti foil with 4 micron Mo barrier.

**** 5 mil V foil + 0.1-0.2 mil Ti equivalent TiH_2 with 2 micron W barrier.

***** 5 mil V foil + 0.1-0.2 mil Ti equivalent TiH_2 with 4 micron Mo barrier.

TABLE XII

BUTTON SAMPLE BRAZE TEST MATRIX: NO-GETTER TESTS

No.	Braze	Time sec.	Temp. °C	Shear* lb	Comment
1	pure V/W**	60	1870	110	Some reaction, some blisters in braze and corresponding depressions in ceramic, no cracks
2	pure V/W**	60	1870	245	Some reaction, some blisters in braze and corresponding depressions in ceramic, no cracks.
3	pure V/W**	60	1860	360	Some reaction, few blisters in braze, no cracks.
4	pure V/W**	60	1860	-	Not examined.
5	pure V/W**	60	1850	315	Some reaction, melting and/or wetting incomplete.
6	pure V/W**	60	1850	-	Not examined.
7	65V-35Cb/W**	60	1840	300	Some reaction, smooth break, no cracks.
8	65V-35Cb/W**	60	1840	505	Some reaction, smooth break, no cracks.

* Shear values in psi are 20.4 times the values shown.

** 5 mil metal foils with 4 micron W barrier.

TABLE XIII

VANADIUM BRAZE SEAL FABRICATION SUMMARY

No.	Date Prepared (1971)	Leak Checked (1971)	Comment	Date Leak Rate Measured	Rate Std cc air/sec*
11	5-15	5-14	Good	6-3	$< 2 \times 10^{-10}$
12	5-18	5-19	Leaked		
13	5-19	5-19	Good	6-3	$< 2 \times 10^{-10}$
14	5-20	5-20	Good	6-3	$< 2 \times 10^{-10}$
15	5-21	5-21	Good	6-3	$< 2 \times 10^{-10}$
16	5-24	5-24	Good	6-3	$< 2 \times 10^{-10}$
17	5-25	5-25	Leaked		
18	5-27	5-27	Good	6-3	$< 2 \times 10^{-10}$
19**	6-1	6-1	Good	6-3	$< 2 \times 10^{-10}$
20***	6-3	6-3	Leaked		

* Minimum detectable leak rate is 2×10^{-10} std cc air/sec.

** No. 17 was rebrazed as No. 19.

*** No. 12 was rebrazed as No. 20.

Pure titanium was rolled between tantalum strips to a nominal 0.5 mil thickness and used with a 5 mil vanadium foil in tests with both tungsten and molybdenum barriers. The titanium hydride was ground under hexane in a mortar to form a thin wash which was then brushed on the surface of the barrier on the alumina. The data and observations for these eight samples are shown in Table XI. The samples were strong, but the braze surfaces were rather rough and had a pebbly appearance. However, there was no clear indication that they might not be suitable.

The tests of the un-gettered systems are summarized in Table XII. Here, it was reasoned that the reaction of the braze and the Al_2O_3 should be less than that seen previously. In order to further retard or regulate the extent of the reaction, the decision was made to use a thicker tungsten layer on the Al_2O_3. This decision was arrived at primarily because it had been found that both the 0.2-0.25 micron tungsten and the 3/4-1 micron molybdenum barrier layers had completely dissolved in all of the Phase I tests. The use of a thicker layer would leave some barrier material at the Al_2O_3 surface, or, at the least, would minimize the time during which the braze could freely attack the alumina. The chosen barrier thickness was 3-4 microns of tungsten. Table XII shows that the optimum braze temperature for pure vanadium is 1860°C, and that for the eutectic alloy is 1840°C.

Based upon a comparison of the results of the series of tests summarized in Tables XI and XII, capsule specimens were prepared using the pure vanadium braze. In all, eight capsules were prepared. Six of the eight were leak-tight. The two that leaked were re-brazed, and one of them was then leak-tight. Table XIII summarizes the brazing and leak-check history of the capsules during preparation. The final brazing operation consisted of punching the vanadium rings from nominal 0.005 inch sheet as pieces 0.5 inch (1.27 cm) OD, and 0.3 inch (0.76 cm) ID, and lightly spot-welding them to the Cb-1Zr cups using tantalum electrodes. Then the cups with the attached braze and the 4-micron thick evaporated tungsten-coated alumina rings were assembled in the brazing jig on the clean bench (Figure 10) using gloves. The detailed drawings of the jig parts are shown in Appendix XIV.

The brazing set-up is prepared by inserting a four-inch length of 0.1875 inch (0.476 cm) tungsten rod in the Cb-1Zr alloy base. The first spacer is then slipped over the rod so that the 0.025 inch (0.0635 cm) high shoulder is uppermost. The first alumina ring 0.100 inch high (0.254 cm) is positioned on the shoulder with the metallized surface facing upward. Then the first Cb-1Zr cup with its attached braze rings is placed with its opening facing downward over the alumina and outside of the positioning collar on the spacer. Then the second alumina ring 0.200 inch (0.508 cm) high with both ends metallized is placed on the cup and steadied in position by four 0.030 inch (0.076 cm) tantalum wires whose ends are inserted into the #65 drill holes in the base. The wires are bent so that they just touch the ceramic, but do not apply a force to it.

The second Cb-1Zr cup with its braze rings is placed in the jig with its open end facing upward. Next, the third alumina ring 0.100 inch (0.254 cm) high is put in position with its metallized surface facing downward.

The final operation is the insertion of the second spacer, which is slipped downward on the tungsten rod so that its shoulder fits inside the alumina ring to position it firmly in the jig. Then the jig and the parts are ready for the brazing operation.

The brazing heat cycle consists of heating the jig assembly in about 20 minutes to 1800±10°C and holding it for five minutes to allow it to equilibrate in temperature. Then the heating power is regulated by hand to effect the braze at 1860°C for 60 seconds. The seal is then cooled at about 100°C per minute to 1600°C, at which temperature it is soaked for one hour. It is then cooled to 1400°C and held for an hour, and then to 1200°C for an hour. After the 1200°C soak, the system is cooled in steps at 50-75° per minute to 300-400°C, at which time the heater power is turned off and the seal and jig are allowed to cool for a minimum of four hours and to approach room temperature. The seals are then removed and helium leak-checked.

EVALUATIONS OF THERMAL SHOCK AND THERMAL CYCLING TESTS

All of the brazed samples were subjected to a thermal shock treatment upon being cooled from the brazing temperature to room temperature, although the cooling rate chosen for the final brazing process was considerably lower than that originally selected (which was 100°C/min, maximum). The sample's ability to withstand the cooling regimen imposed was measured by the initial value of the leak rates for each specimen, although if a given sample did leak, it was not necessarily caused by the cooling process. Leaks found during the first helium leak check could arise either from thermal shock or from a failure to form a good joint during brazing. Table XIII shows the first leak-rate measurements made on the samples. Six of them proved to be leak tight within the capability of the Veeco MS-9 Leak Detector, and one showed a measurable leak.

Two of the six leak-tight samples, No. 11 and No. 13, were subjected to the thermal cycling test sequence described on page 53. A typical thermal cycle time-temperature trace is shown in Figure 15. Table XIV shows the leak-rate data obtained from Samples No. 11 and No. 13. The values are seen to lie in the 10^{-9} to 10^{-10} std cc air/sec range, with no persistent trend. The variations observed from test to test are not considered significant, because the background readings were found to vary in the same direction and nominally in the same amount. In no case were the readings of sufficient magnitude relative to the background uncertainties to warrant a belief that the samples were leaking. This belief was corroborated by the helium leak-check measurements made by testing the units directly in the port of the Veeco MS-9 helium leak detector after they were removed from the vacuum system and manifold. Both samples were leak-tight to a value of $< 2 \times 10^{-10}$ std cc air/sec, the limit of sensitivity of the test unit.

TABLE XIV

THERMAL CYCLING TEST DATA

Test Condition / Date	Test Temp. °C	Test Pressure* psia	Leak Rate Sample No. 11 Std cc air/sec**	Test Temp. °C	Test Pressure* psia	Leak Rate Sample No. 13 Std cc air/sec**
Before Cycle No. 1	81	5	2×10^{-10}	90	5	1×10^{-9}
6-10-71	32	20	3×10^{-10}	70	20	1×10^{-9}
	29	25	8×10^{-10}	30	25	1×10^{-9}
Cycle No. 1	1200	5	2×10^{-10}	1200	5	2×10^{-10}
6-10-71	1200	20	2×10^{-10}	1200	20	1×10^{-9}
	1200	25	2×10^{-10}	1200	25	2×10^{-10}
After Cycle No. 1 6-10-71	22	20	2×10^{-10}	22	20	3×10^{-10}
Cycle No. 4	1200	5	2×10^{-10}	1200	5	2×10^{-10}
6-11-71	1200	20	2×10^{-10}	1200	20	2×10^{-10}
	1200	25	2×10^{-10}	1200	25	2×10^{-10}
After Cycle No. 7 6-14-71	25	20	2×10^{-10}	25	20	2×10^{-10}
Cycle No. 16	1200	5	2×10^{-10}	1200	5	2×10^{-10}
6-15-71	1200	20	2×10^{-10}	1200	20	2×10^{-10}
	1200	25	2×10^{-10}	1200	25	2×10^{-10}
After Cycle No. 16	275	5	1×10^{-9}	220	5	2×10^{-10}
6-15-71	250	20	4×10^{-9}	210	20	2×10^{-10}
	230	25	2×10^{-9}	200	25	2×10^{-10}
Before Cycle No. 64	25	5	8×10^{-10}	25	5	1.1×10^{-9}
6-23-71	25	20	8×10^{-10}	25	20	1.1×10^{-9}
	25	25	8×10^{-10}	25	25	1.1×10^{-9}
Cycle No. 64	1201	5	1.1×10^{-9}	1201	5	1.1×10^{-9}
6-23-71	1201	20	1.1×10^{-9}	1201	20	1.1×10^{-9}
	1201	25	1.1×10^{-9}	1201	25	1.1×10^{-9}
After Cycle No. 64 6-23-71	150	25	5×10^{-10}	150	25	5×10^{-10}

* Pressure equivalences: 5 psia = 3.45×10^{4} N/m^2; 20 psia = 1.38×10^{5} N/m^2; 25 psia = 1.72×10^{5} N/m^2.

** The minimum detectable leak is 2×10^{-10} Std cc air/sec for the Veeco MS-9 leak detector instrument used.

EVALUATIONS OF PHASE II AGING TESTS

Tests. — The Phase II aging tests involve the exposure of capsule and button samples to 800°C, 1000°C and 1200°C for 1000 and 5000 hours. One capsule and eight button samples were to be exposed at each temperature. The capsules were to be removed after 1000 hours, helium leak checked and returned to the aging furnace system to complete an additional 4000 hours of exposure. Four of the button samples were to be removed after 1000 hours of exposure and the remaining four after the 5000-hour total exposure time. Two of the button samples were to be tested in shear, a third was to be examined metallographically, and the fourth was a spare. In addition, because samples No. 11 and No. 13 survived the thermal cycling tests, they were used as additional samples in the 1200°C and the 1000°C aging tests, respectively. Sample No. 18, which showed an initial non-zero leak rate was also included in the test series by being aged at room temperature. Sample No. 15, the cesium vapor capsule, was exposed in the 1200°C furnace. Table XV shows the aging samples tested, the conditions of their exposures, their post-exposure examinations, and the percent of theoretical density of the Al_2O_3 buttons used in the various metallurgical and shear test samples.

Shear Test Results. — As is indicated in Table XV, two button samples from each aging exposure condition were tested in shear. The data are shown in Appendix XVI. All of the samples, except those exposed for 5000 hours at 1200°C showed shear values equivalent to the as-brazed samples. The reduction in strength to less than one-quarter of the room temperature value as is exhibited by these 5000-hour aged samples is interpreted as an aging effect.

Metallographic and Microhardness Test Results. — The data obtained from the "Met" samples indicated in Table XV are summarized in Appendix XVII, in which micrographs and microhardness profiles are shown. In addition, micrographs of the brazes of those capsules which had failed during the test sequence are shown in Appendix XVII.

Characteristically, the vanadium braze is seen to be very active in dissolving large amounts of the Cb-1Zr alloy, so that the final braze compositions involve an estimated 50% niobium (columbium), as did Brazes 4W, 6W, and 10M (Figures 114, 115, and 116; Appendix XIII). Because of the strong dissolution effect, and because of the tendency to produce a final braze composition containing a nominal 50% Cb(Nb)-50% V, one might expect to find less attack of the Cb-1Zr (Nb-1Zr) alloy from Braze #8, which is initially 65% V with 35% Cb (Nb). In this system, then, less columbium (niobium) is required to bring the braze melt up to the observed nominal 50% Cb (Nb) composition.

A second feature of concern in this braze system (Cb-1Zr/V/W/Al_2O_3) is the strong tendency for the braze to develop voids under aging conditions.

TABLE XV

POSITION AND SCHEDULE OF SAMPLES IN AGING TESTS

Vacuum System	Furnace Temp. °C	Capsules	Button Samples	
			Remove at 1000 hr	Remove at 5000 hr
1	1200	11*	21-1 (97)** Met	21-2 (97)** Met
		14	34-1 (96) Spare	34-2 (96) Spare
		15***	36-2 (95) Shear	34-3 (96) Shear
			36-3 (95) Shear	36-4 (95) Shear
1	1000	13*	21-3 (97) Met	21-4 (97) Met
		16	35-1 (96) Spare	35-2 (96) Shear
			37-1 (95) Shear	35-3 (96) Spare
			37-2 (95) Shear	37-3 (95) Shear
2	800	19	37-4 (95) Met	34-4 (97) Met
			38-1 (95) Spare	35-4 (96) Shear
			38-2 (95) Shear	36-1 (96) Shear
			38-4 (94) Shear	38-3 (95) Spare
2	R.T.	18		

* Previously exposed to 64 thermal cycles to 1200°C

** Values in parentheses are the % of theoretical density values of the Al_2O_3 buttons.

*** Cesium vapor capsule

Even in the 1000-hour samples, voids are seen to be developing on the grain boundaries, and they enlarge as aging proceeds. In time, the individual voids tend to merge and to develop lines of voids, which ultimately would lead to failure.

If these voids are formed as a consequence of the net diffusion of vanadium from the braze toward the Cb-1Zr alloy being greater than the diffusion of the niobium (columbium) in the alloy back into the braze, then they will inexorably form as the braze joints age. Their rates of formation will depend, of course, on the diffusion coefficients of V and Nb (Cb) in the particular alloy compositions. In these systems, diffusion gradients will be present, and the atoms will move. However, the use of thinner braze foil should be beneficial in reducing the formation of voids. The thinner braze will develop a higher concentration of Nb (Cb) during the brazing step, during which the Nb dissolves in the molten vanadium. But the amount of the dissolved niobium (columbium) is contained in less vanadium, so that the final concentration and concentration gradient of the vanadium will be less for a thin braze foil. With a lower gradient, there should be less tendency for vanadium to diffuse, and for voids to form.

Electrical Resistivity Test Results. — The electrical resistance of the bulbs was measured at room temperature with a voltage of 500 v. using a megohm meter. Capsules #11, #13, #14, and #19 showed readings of 700 000 megohms, and Capsule #16 showed a reading of 600 000 megohms. The difference is not significant, and the capsules show no indication of post-test room temperature electrical break-down.

Aging Capsule Test Results. — Seven capsules were exposed to a 5000-hour aging test under high vacuum. Those samples exposed in Vacuum System #1 were tested under a vacuum of 2 to 3 x 10^{-8} torr (2.67 to 4.0 x 10^{-6} N/m^2), but the samples exposed in Vacuum System #2 were tested under a vacuum level asymptote of 3 x 10^{-7} torr (4.0 x 10^{-5} N/m^2).

The principal performance test of the aging study was a vacuum leak rate test of the capsules, using the helium leak detector. The leak rates of the capsule samples were measured several times during the course of the work. These data are presented in Appendix XVII, and are summarized in graphical form in Figures 17, 18, and 19.

As is shown in the figures, capsule samples #19 (at 800°C), #13 and #16 (at 1000°C) and #14 (at 1200°C) survived the 5000-hour aging test sequence with no detectable loss of vacuum integrity. However, capsule samples #11 and #15 (at 1200°C) developed leaks at some time after the 1000 hours check point of the aging cycle; and capsule sample #18, whose leak developed less than 200 hours after brazing, showed a progressively worsening leak during high vacuum aging to 5000 hours at room temperature.

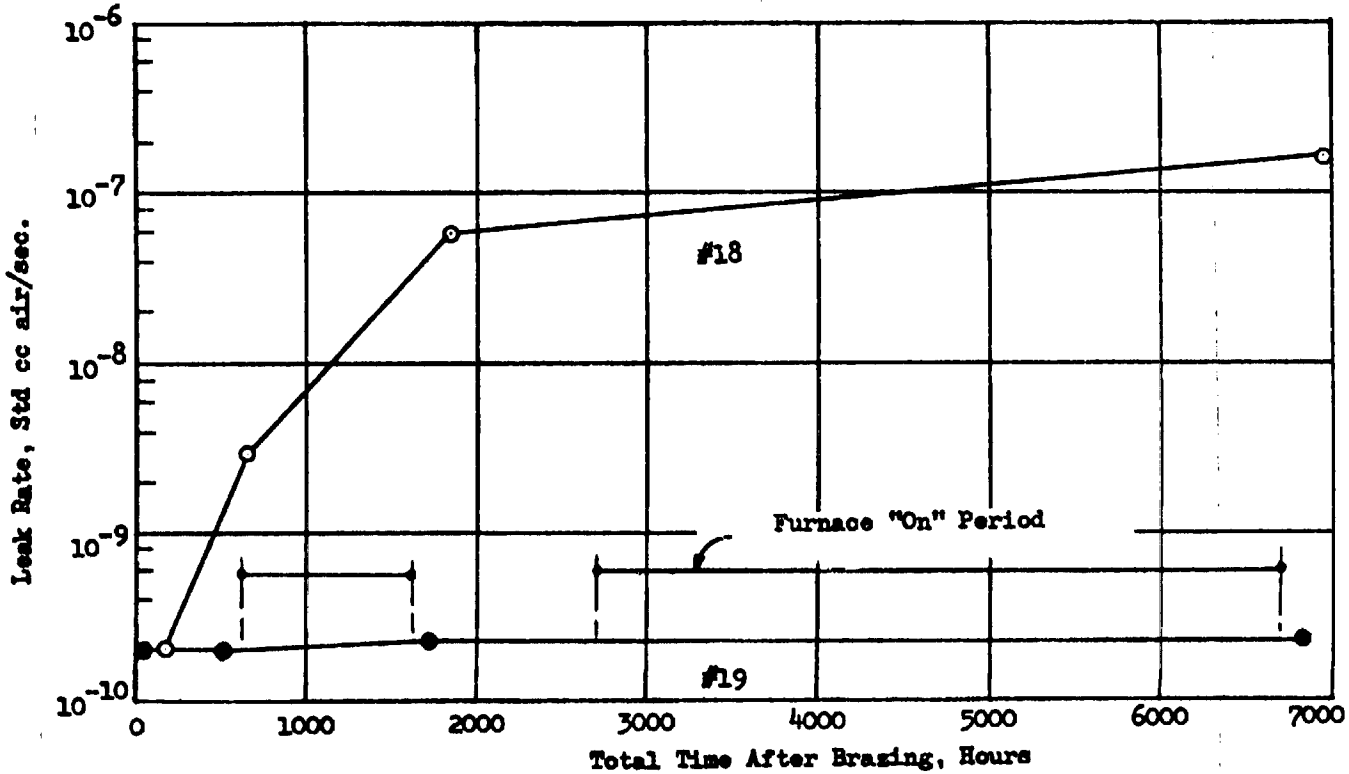

Figure 17. Leak Rate History Chart. Capsule Sample #19 Exposed at 2×10^{-7} Torr (2.67×10^{-5} N/m^2) at 800° C, and Sample #18 Exposed at 2×10^{-7} Torr (2.67×10^{-5} N/m^2) at Room Temperature

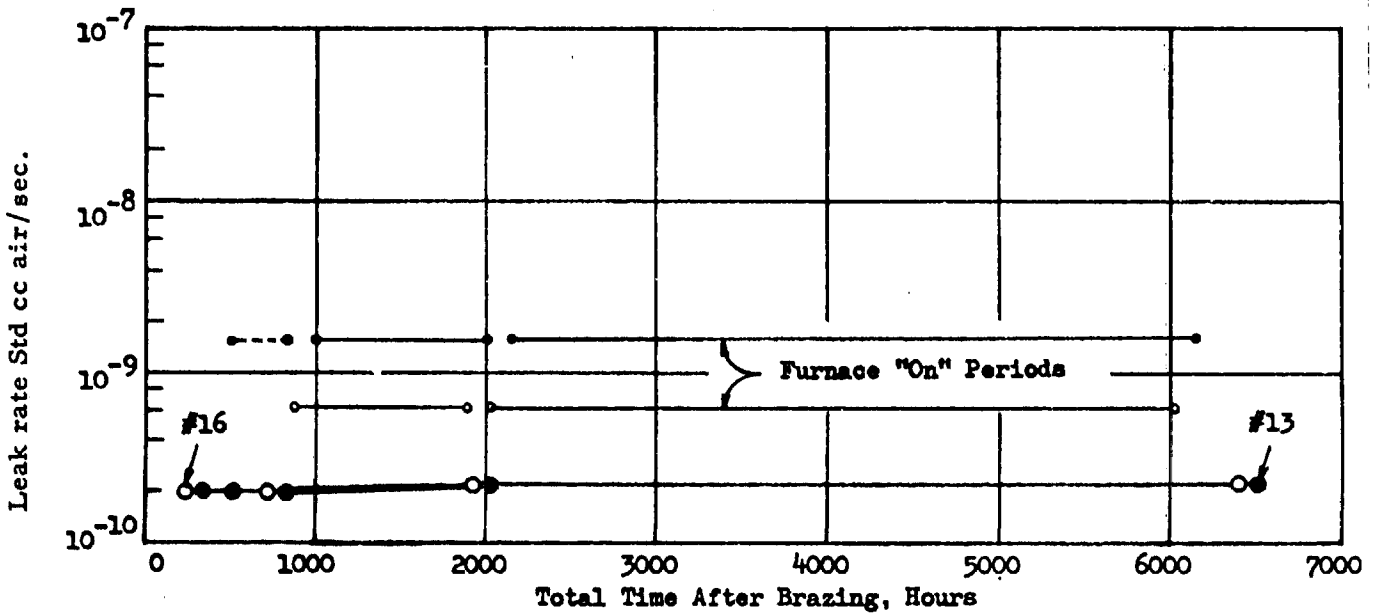

Figure 18. Leak Rate History Chart. Capsule Sample #13 Exposed to 64 Thermal Cycles to 1200°C, and then Exposed at 2 x 10^{-8} Torr (2.67 x 10^{-6} N/m^2) at 1000°C, and Capsule Sample #16 Exposed to 2 x 10^{-8} Torr (2.67 x 10^{-6} N/m^2) at 1000°C

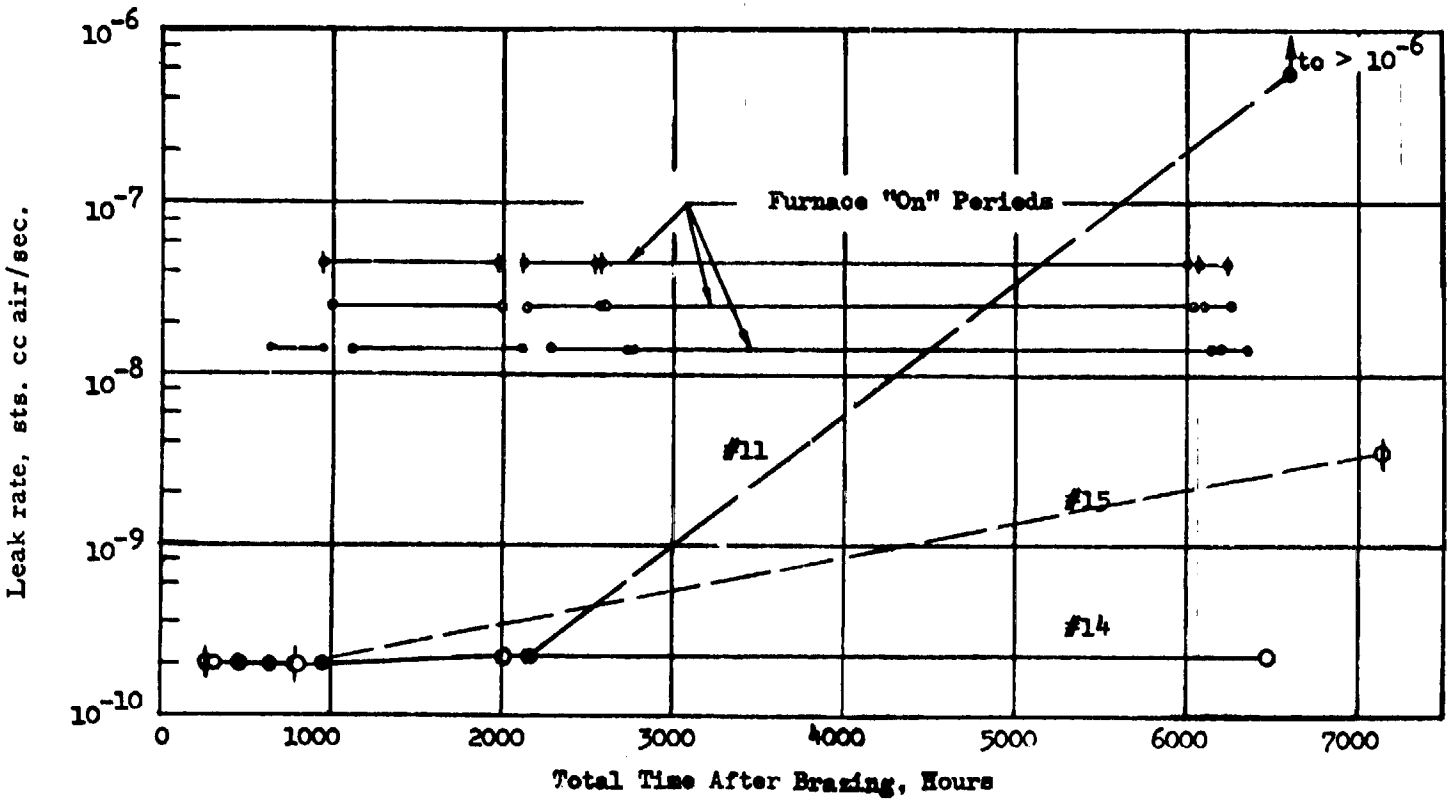

Figure 19. Leak Rate History Chart. Capsule Sample #11 Exposed to 64 Thermal Cycles to 1200°C, and then Exposed at 2 x 10^{-8} Torr (2.67 x 10^{-6} N/m^2) at 1200°C, Capsule #14 Exposed to 2 x 10^{-8} Torr (2.67 x 10^{-6} N/m^2) at 1200°C, and Capsule #15 Exposed to 2 x 10^{-8} Torr (2.67 x 10^{-6} N/m^2) at 1200°C with an Internal Cesium Vapor Pressure of 5 Torr (6.65 x 10^2 N/m^2)

Cesium Vapor Capsule Test Results. — Capsule #15 was used in the cesium vapor aging test. It was fitted with a cesium reservoir as described above and shown in Figure 16, and then exposed in Furnace #1, Vacuum Chamber #1, for 5000 hours at 1200°C. The reservoir temperature was held at 348°C at which temperature the vapor pressure of cesium is 5 torr (6.67×10^2 N/m^2). The capsule was removed from its furnace after 1000 hours of exposure at 1200°C and visually examined. No evidence of failure or degradation was observed and the capsule was returned to the furnace to undergo the remaining 4000 hours at temperature.

When the capsule was removed from the furnace, several dark areas were observed on the top of the capsule. These are shown in Figure 20. The capsule was opened after undergoing a heating and cooling sequence designed to transfer the cesium vapor to the cesium reservoir. With the cesium presumably in the reservoir, the nickel tube was then pinched off near the (nickel)-(Cb-1Zr) joint. This was done to seal the cesium in the reservoir and to permit opening the capsule to air. The opening was done using a file on the thin-walled Cb-1Zr tube. A file was used to permit the sound of the air rushing into the capsule to be heard. However, no in-rush of air was detected.

The cesium reservoir was opened in an argon glove box in an attempt to recover the metallic cesium as a final proof of the presence of cesium vapor in the capsule. No cesium or cesium compound was found in the reservoir. Therefore, the evidence indicated that the capsule had lost its charge of cesium, presumably as a result of a leak in the capsule.

The general leak-check of Capsule #15 revealed a leak that was so large that it could not be measured on the leak check instrument (a Veeco MS-9 helium leak detector). A gas bubble test of the capsule showed that there were major leaks associated with each of the discolored areas in the cap (Figure 20). Examination under a low power microscope of the underside of the cap showed the presence of cracks beneath each of the discolored areas.

An x-ray fluorescence examination of the discolored areas of the capsule cover was performed. No elements other than columbium (niobium) and zirconium were detected.

When it was found that the capsule cover was responsible for the gross leaking of Capsule #15, both the cover and the bottom were removed and the seal was subjected to another helium leak check. A small leak was found, with a leak rate of 36×10^{-10} std cc air/sec, the value reported for the seal in Appendix XVII.

Figure 126 in Appendix XVII shows photomicrographs of the braze area of Capsule #15. Sample A shows the inner end of the braze. This area was exposed to the cesium vapor for as long as it was present within the capsule. It is believed that the cracks in the capsule top developed after the first 1000 hours of the aging period, because there was no indication

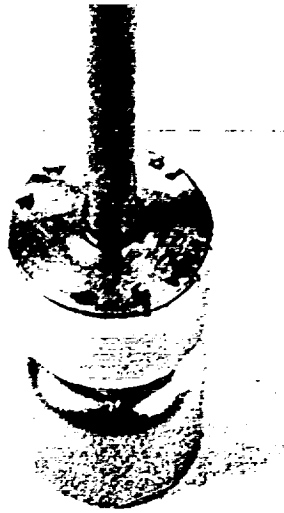

Figure 20. Capsule #15. Top of Capsule after the 5000-hour Aging Test Exposure at 1200°C.

of the discolored regions on the end cap when the capsule was examined after the first 1000 hours. Therefore, the inner surface of the capsule was presumably exposed to cesium vapor for more than 1000 hours. The edge of the braze is rounded, but there is no serious evidence of attack of the exposed Al_2O_3 braze joint area. The corner of the Al_2O_3 is bevelled, with, at most, a three-mil (0.076 mm) loss of Al_2O_3 at the braze. However, the exposed surface does not have a corroded appearance, and one might consider that there was an original defect in the Al_2O_3, such that during brazing the corner cracked away. Some misalignment of the two Al_2O_3 parts is evident, and as a consequence of that, there may have been a lateral force on the corner of the alumina.

The interface regions show, at most, a one mil (0.0254 mm) effect, with no obviously serious chemical attack. The rounding of the end of the braze is believed to be the result of having a liquid layer present at the left side of the photomicrograph of Sample A during the braze period, and the dissolution of the Cb-1Zr and the flowing away of the braze mixture at brazing temperature. It is believed that no attack of either the Al_2O_3 or the V/Cb-1Zr braze can be attributed to the presence of cesium vapor.

Phase II Test Results, (Overall Evaluation). – The foregoing sections have described the test results of the Phase II studies. The best-appearing braze from the Phase I study, Braze System #6W (Cb-1Zr/V-2Ti/W/Al_2O_3), was found to form a strong braze, but the reactivity of the braze melt toward the alumina was so great that the brazes tended to crack and to not be vacuum tight. This behavior was attributed to the reactivity of the titanium in the braze, and, in a sense, was an extension of the observations made in the Phase I work that cerium, zirconium and hafnium appeared to impart excessive chemical reactivity to the brazes; and to produce braze joints in which a physically weak reaction zone formed between the braze and the alumina. In those studies, the titanium additive proved to be significantly superior to the others, with the result that Braze System #6W was the best of those examined.

However, the finding that the V-2Ti braze did not form vacuum-tight joints in the 0.5 inch (1.27 cm) size, prompted the search for a reduced-chemical-activity braze material. Two candidates were found, pure vanadium, and the minimum-melting point vanadium-columbium (vanadium-niobium) alloy 65V-35Cb (65V-35Nb). The brazing temperatures were 1860°C and 1850°C, respectively. Both brazes showed promise; but the pure vanadium system, using a heavy tungsten deposit on the alumina, appeared slightly superior.

As one would expect, the characteristics of the ungettered vanadium brazes were quite similar to those of V-2Ti and V-2Hf. A large amount of the Cb-1Zr (Nb-1Zr) alloy was dissolved, and in many cases the final "braze" thickness was 50% or more greater than that of the braze metal wafer used. Also, the fluidity of the braze alloy was such that it flowed around, and some final brazes were thinner than the original wafer.

The "braze" usually showed a marked epitaxy, with the grains extending from the base Cb-1Zr (Nb-1Zr) alloy to the alumina surface. In some cases, the grain dimensions normal to the alumina were as much as 10 mils (0.254 mm) long and as much as 5 mils (0.127 mm) wide. Good adherence to the alumina was a characteristic of this braze, even without the presence of a Group III or IV element. The vanadium melt, being rather pure at the outset, has a strong tendency to react with and to dissolve any oxide because of the affinity of vanadium for oxygen in dilute solution. This tendency is present in all pure metals, and it is not possible to melt any of the Group III, IV, V or VI elements in contact with any oxide without obtaining some reaction and transferring oxygen from the massive oxide into the metal to form a dilute solution.

In the present systems, there is the possibility of a second factor affecting the reaction with the alumina. That is, the dissolution of some of the Cb-1Zr (Nb-1Zr) by the vanadium brings a low concentration of zirconium into the braze melt. Some time is required for this dissolution and mixing so that the zirconium effect is much less than that from a braze which contains zirconium. However, it must be recognized as a source of active metal, even when the braze is pure vanadium.

The dissolution of Cb-1Zr (Nb-1Zr) and of alumina by the vanadium produces a final molten "braze" material which is really a V-Cb (V-Nb) alloy containing small amounts of zirconium, aluminum, and oxygen. Both the alloying effect and the introduction of oxygen into the braze tend to produce a hardening effect. As a consequence, the final braze melt compositions are significantly harder than is the base Cb-1Zr (Nb-1Zr) alloy, and fall in the 300-400 DPH unit range.

Another aspect of the microhardness profile behavior of these vanadium brazes is the evidence of interdiffusion at the braze/alloy interface. The microhardness traces of the as-brazed samples and of the 800°C aged samples generally show a thinner transition region between the 350± 50 DPH hardness region of the braze and the 75 ± 5 DPH hardness level of the alloy. However, in the 1000°C and the 1200°C aged samples, this transition region is much larger, and can be several mils in thickness.

This evidence of the interdiffusion of the braze and the base alloy components supports the belief that the voids seen in the aged samples are related to the transfer and the net loss of vanadium from the braze by diffusion. This is perhaps the most serious problem observed in these aging tests. The voids develop on grain boundaries, and in one case at least, were found to have become aligned in a continuous string parallel to the alumina interface. In all of the 5000-hour aged samples there was a significantly large incidence of large void formation. Obviously, the extension of the aging period beyond the 5000 hours would permit the enlargement of the voids, and their joining to ultimately produce a crack and/or a vacuum leak path. In one sense, it should not be surprising that such a phenomenon occurs in these systems, because of their rather high temperature service. Using the rule-of-thumb Tamman-temperature

generalization that diffusional processes become very rapid at temperatures in excess of one-half of the absolute melting point, one can infer that all of the test temperatures are within that high-diffusion rate range. For example, 800°C is (100)(800 + 273)/(1860 + 273) or 50.4% of the melting point of the braze; 1000°C is (100)(1000 + 273)/(1860 + 273) or 59.7% of the melting point of the braze; and 1200°C is (100)(1200 + 273)/(1860 + 273) or 69% of the melting point of the braze. Therefore, significant movement of material along diffusion gradients must be expected, and accepted, in these systems.

The inevitable dissolution of alumina by the braze with the corresponding increase in the oxygen content of the braze raises a question regarding the need for extreme purity in the braze alloy. If the final composition will contain several hundred ppm of oxygen, perhaps there is no need for incurring the expense of obtaining zone-refined braze metal with minimum levels of oxygen. As long as it is possible to roll the vanadium into the necessary <5 mil (<0.127 mm) thickness, its oxygen impurity level may not be critical.

The vacuum integrity results for the capsule samples show that four of the six capsules that were subjected to the 5000-hour aging tests survived to the extent that they did not lose their vacuum integrity. The two which did show vacuum leaks after 5000 hours' exposure were sound at the 1000-hour test period. Further, Capsule #11, which showed a large leak after 5000 hours at 1200°C, had been thermal cycled 64 times to 1200°C prior to its 1200°C aging exposure. It very clearly had the most severe exposure of all. Capsule #15, the other sample that showed a leak, began its test history as a cesium-vapor test capsule, but presumably lost its cesium after the 1000-hour examination period due to the development of cracks in its metal cap. There was also a small leak in the braze joint, however, and its microstructure showed distinct evidence that it was degrading. However, it was exposed to the second most severe test conditions, as was Capsule #14, which did not fail after its 5000-hour, 1200°C aging test. The thermal-cycled and 5000-hour aged Capsule #13 and the 5000-hour aged Capsule #16 both survived the 1000°C exposure; as did Capsule #19, which was tested at 800°C. Therefore, these vacuum integrity tests, which show leaks to have developed in the most severely-exposed samples, confirm the observations made on the aged button samples. The more severe test exposures lead to the formation of voids, and to the ultimate loss of vacuum integrity.

A further observation of Capsule #18, which showed a vacuum leak as of four weeks after it was brazed, was that under vacuum aging at room temperature, the capsule's leak rate continued to worsen. This suggests that there may be an aging effect even at room temperature, although a single sample is hardly sufficient to base a firm conclusion on.

In summary, then, it appears that the unalloyed vanadium braze system as developed and used in these tests is capable of use in a vacuum containment application at temperatures to 1200°C for times in excess of 1000 hours. At 1000°C and at lower temperatures, the vanadium braze seals are capable of surviving a 5000-hour aging period. Use at 1000°C for longer times is unproven.

CONCLUSIONS AND RECOMMENDATIONS

Twenty-eight ceramic-to-metal braze seal systems for 800°C, 1000°C, and 1200°C service have been examined in detail. Evaluations were made of the structure, the bonding and the aging behavior to 5000 hours. The system (Cb-1Zr/V/W/Al_2O_3) in the form of a one-half inch diameter seal was found to withstand a 5000-hour, 1000°C aging test, a 5000-hour, 800°C aging test, and at least a 1000-hour, 1200°C aging test with no loss of vacuum integrity.

The brazes, all of which had brazing temperatures in the 1750-1950°C temperature range, characteristically dissolved large amounts of the metal alloy Cb-1Zr (Nb-1Zr) with the result that the final braze joint composition contained from thirty to fifty weight percent columbium (niobium), regardless of the starting composition of the braze foil. Early tests indicated that the presence of one or two percent of an active metal in a vanadium or vanadium-columbium (vanadium-niobium) alloy braze enhanced the braze's ability to wet the alumina ceramic, but subsequent studies showed that these additive elements were not necessary for good wetting and adherence. The chemical activity of vanadium or of the vanadium-columbium alloy is adequate, and strong bonds are formed with either of these braze metals.

In addition to dissolving large amounts of the metal member, the vanadium and vanadium alloy brazes also dissolve Al_2O_3 in an amount sufficient to yield a final "braze" composition containing 1-4 weight percent aluminum. Presumably, the oxygen which was originally associated with the aluminum also dissolves in the braze, and hardens it. Therefore, one should minimize the time during which the braze is molten and should provide annealing temperature holds during the cool-down period to minimize the development of residual stresses in the braze joint.

The test temperatures are relatively high, such that diffusion of the base alloy and the braze components is a major factor in the aging process. After 1000 hours' exposure, voids are found along grain boundaries in the vanadium-rich braze region, and after 5000 hours' exposure the voids have increased in number and enlarged and show a tendency to join along the grain boundaries. This appears to be the principal service-life limiting characteristic of the vanadium braze. Service life periods of 5000 hours have been demonstrated at 1000°C and at 800°C, but at 1200°C, the target temperature of this study, the demonstrated service life lies between 1000 and 5000 hours. None of the brazes showed promise for the desired ultimate goal of three to five year space-power use at these temperatures.

In order to increase the service life of this braze system, it will be necessary to inhibit the diffusion of the vanadium so that void formation is delayed. One method of doing this is to decrease the concentration gradient of vanadium from the braze to the base alloy by using columbium (niobium) as a diluent in the braze. Alternately, a longer braze-time (perhaps 90

seconds) might be used, unless the dissolution of the alumina then becomes too great and too much oxygen is dissolved in the final braze melt. As is noted above, there is a balance to be achieved here in obtaining enough, but not too much, attack of the alumina.

This program's ultimate goal was "to provide long life (3-5 years), high temperature (1200°C), alkali metal resistant, thermal shock resistant, leak-tight, and neutron irradiation resistant seals suitable for application in in-pile or out-of-pile nuclear thermionic power systems." It has not accomplished that purpose in that the relatively few capsule tests performed have indicated only an assured 1000 hours satisfactory service at the target temperature of 1200°C. However, there is a strong indication that the service life of the braze system in the one-half inch size could be extended to at least 5000 hours at 1200°C. The further demonstration of this performance will require additional studies of the brazing process and an approach which leads to a reduction in the rate of formation of voids. In the proof testing of any improved system, a statistically significant number of capsules must be prepared and tested. A further demonstration of a successful 1200°C braze would involve an examination of braze joints larger than one-half inch (1.27 cm) in diameter. A final test which also must be a part of any further development study of the vanadium braze (or any seal) is the examination of the electrical resistance of the braze joint while aging under a steady dc potential difference at temperature.

While this program has made significant progress toward the development of a 1000°C seal which has promise of long life, it seems unlikely that the unalloyed vanadium braze seal can be developed to be suitable for long-term service at 1200°C. The problems to be overcome include the control of the brazing conditions, which must be very carefully regulated, and the inhibition of the diffusion effects, which are very deleterious at high temperatures. However, the development of a truly successful seal capable of attaining the ultimate life-span goal of 3-5 years, even at 1000°C, will require additional development and demonstration work.

APPENDIX I. INTERNATIONAL SYSTEM OF UNITS

In keeping with the desire of the scientific community to establish and use a standardized system of units, this report has been prepared using the usual English and/or metric system units as the primary values reported, with the International System Units (SI) as secondary units. The SI units and equivalents used in computing the secondary units are those quoted in NASA SP-7013 (Ref. 15), which reports the values agreed upon by the Eleventh General Conference on Weights and Measures, which met in October, 1960.

The units and the conversion factors used in this report are listed in the following Table XVI.

TABLE XVI

UNITS AND CONVERSION FACTORS

Primary Unit	SI Unit	Equivalences
foot, ft	meter, m	1 ft = 3.048×10^{-1} m
gallon per minute, gpm	cubic meter per second, m^3/s	1 gpm = 6.309×10^{-5} m^3/s
hour, hr	second, s	1 hr = 3.60×10^{3} s
inch, in.	centimeter, cm	1 in. = 2.54 cm
inch, in.	meter, m	1 in. = 2.54×10^{-2} m
inch, in.	millimeter, mm	1 in. = 25.4 mm
liters per second ℓ/s	cubic meters per second, m^3/s	1 ℓ/s = 1.00×10^{-3} m^3/s
mils	millimeter, mm	1 mil = 2.54×10^{-2} mm
mils	meter, m	1 mil = 2.54×10^{-5} m
pound (force) lbf	newton, N	1 lbf = 4.448 N
pound per square inch, psi	newtons per square meter, N/m^2	1 psi = 6.895 N/m^2
torr	newtons per square meter, N/m^2	1 torr = 1.333×10^{2} N/m^2

APPENDIX II. MATERIALS

This appendix gives the details of the composition and the fabrication of the materials used in the program.

Alumina Ceramics. — The ceramic material used in this program was high-purity, low-silica alumina (99.99%). The specifications for the alumina bodies were that they be 99.9+% pure, with a maximum of 50 ppm SiO_2, and that the bodies have less than five percent porosity. The parts were of three types: button samples (1/4-inch (0.635 cm) diameter x 1/8-inch (0.318 cm) high, right circular cylinders); modulus of rupture rods (0.20 inch (0.508 cm) diameter x 1-inch (2.54 cm) long cylinders); and cylindrical seal specimens in two sizes: 0.5 inch (1.27 cm) O.D. x 0.10 inch (0.254 cm) wall x 0.20 inch (0.508 cm) high rings, and 0.5 inch (1.27 cm)O.D. x 0.10 inch (0.254 cm) wall x 0.10 inch (0.254 cm) high rings.

In addition, some larger diameter cylindrical seal specimens were obtained using the same starting materials and preparative techniques. These were procured in the event that tests of larger diameter bulb samples were desired. These cylindrical specimens were of four sizes: (1) 1.5 inch (3.81 cm) O.D. x 0.10 inch (0.254 cm) wall x 0.20 inch (0.508 cm) high rings, (2) 1.5 inch (3.81 cm) O.D. x 0.10 inch (0.254 cm) wall x 0.10 inch (0.254 cm) high rings, (3) 4.0 inch (10.16 cm) O.D. x 0.10 inch (0.254 cm) wall x 0.20 inch (0.508 cm) high rings and (4) 4.0 inch (10.16 cm) O.D. x 0.10 inch (0.254 cm) wall x 0.10 inch (2.54 cm) high rings. Figure 21 shows these parts in the as-received condition. In general, the surfaces of the parts were discolored, but much of the color was removed by heating in vacuum to 1800°C for an hour.

The analysis of the raw material used in the preparation of the alumina parts is shown in Table XVII, together with the analyses of finished parts. The critical impurity element silicon is seen to be well within tolerance at < 20 ppm Si (< 43 ppm SiO_2). This analysis is substantiated by the Atomics International Analytical Chemistry Unit, which found 50 ± 5 ppm SiO_2 in the as-delivered product. Table XVII also shows the purity computation outlined in Appendix IV of Contract NAS3-11840, and it is seen that the total of the 16 impurities is <107.6 ppm as oxides, which yields a nominal purity by difference of 99.99% Al_2O_3.

The densities of the alumina materials were measured using their dimensions and weights. It was found that all of the ring specimens of all sizes and all of the 20% sampling of the rod samples showed densities well in excess of the required 95% of theoretical. However, about 60% of the button samples were found to have densities at or below 93% of theoretical. Accordingly, a request was made for the replacement of the low-density parts. About 30% of the replacement button parts were also found to have low densities. However, since a significant excess of material was delivered, an adequate number of on-specification Al_2O_3 buttons was available for the test program.

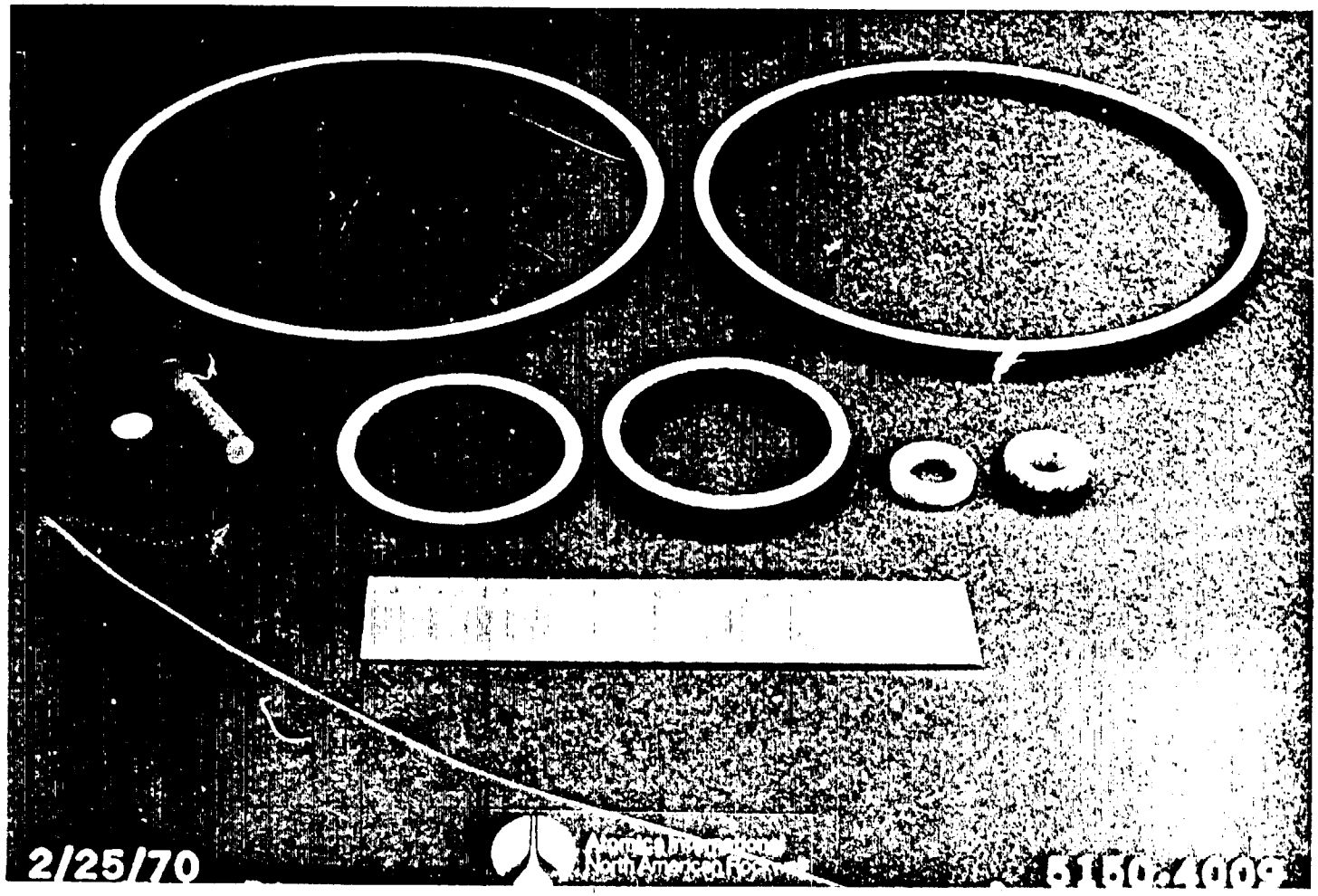

Figure 21. Alumina Ceramic Parts

TABLE XVII

ANALYSES OF ALUMINA CERAMICS*

Impurity Element	Starting Powder Material** ppm as element	Button Sample*** ppm as element	Rod Sample*** ppm as element	Ring Sample*** 0.5" (1.27 cm) ppm as element	Ring Sample*** 1.5" (3.81 cm) ppm as element	Product Average ppm as element	Product Average**** ppm as oxide
B	< 3	< 3	< 3	< 3	< 3	< 3	< 9.5
Ca	< 1	†	< 1	< 1	(20)†	< 1	< 1.4
Cd		< 4	< 4	< 4	< 4	< 4	< 4.6
Co	4.5						
Cr	< 3	< 3	< 3	< 3	< 3	< 3	< 4.4
Cu	< 1	< 1	< 1	< 1	< 1	< 1	< 1.3
Fe	< 3	< 3	< 3	< 3	< 3	< 5	< 7.2
Ga	2.5	< 2	< 2	< 2	< 2	< 2	< 2.7
Mg	< 1	< 1	< 1	< 1	< 1	< 1	< 1.6
Mn	< 1	< 1	< 1	< 1	< 1	< 1	< 1.4
Mo	< 3	< 3	< 3	< 3	< 3	< 3	< 4.5
Ni	< 3	< 3	< 3	< 3	< 3	< 3	< 3.8
Pb	< 1	< 1	< 1	< 1	< 1	< 1	< 1.1
Si	< 20	< 20††	< 20	< 20	< 20	< 20	< 43
Ti	< 10	< 10	< 10	< 10	< 10	< 10	< 16.7
V	< 3	< 3	< 3	< 3	< 3	< 3	< 4.4
						TOTAL	< 107.6

By difference, the alumina is 99.989 or 99.99% pure

* Prepared by Atomergic Chemetals, Co., 584 Mineola Ave., Carle Place, L.I., N.Y. 11514.

** Analysis by Atomergic Chemetals Co., Sample No. C 2813. Analysis reported Sept. 10, 1969.

*** Analysis by Lucius Pitkin, Inc., 50 Hudson St., New York, N.Y. 10013, dated Sept. 4, 1969; Report No. 672655-659.

**** Impurity calculations as oxide, as per Appendix IV of the NAS3-11840 Contract.

† Sample contaminated in handling

†† An analysis of the as-received material was made at Atomics International using the SPEX Co. 6-9s Al_2O_3 as the standard reference sample. The result showed 23 ± 2.5 ppm Si (50 ± 5 ppm SiO_2).

Beryllia Ceramics. — In addition to the larger sized alumina ceramic rings, a selection of beryllia sample parts was obtained for possible use in the program. The specifications for the beryllia bodies were that they be 99.9+% pure, with a maximum of 75 ppm SiO_2, and that the bodies have less than five percent porosity. The parts were of the same types and sizes as the alumina parts described above. Figure 22 shows these parts in the as-received condition. The surfaces are seen to be very clean, and require no further treatment (other than a final solvent cleaning step) prior to use.

The analyses of the beryllia materials is shown in Table XVIII. The analyses were only made for critical impurity elements and for those which might be expected to be subject to pick-up in handling. The last column shows the 15 impurities calculated as oxides, for which a total impurity concentration of < 218.4 ppm is found. Thus, the nominal beryllia product purity, as measured by difference, becomes 99.98% BeO.

The densities of the beryllia materials were measured using their dimensions and weights. It was found that all of the parts delivered showed densities in excess of the required 95% of theoretical.

Ceramic-to-Metal Graded Seals. — Ten nominal one-inch (2.54 cm) diameter ceramic-to-metal graded seals were provided by the National Aeronautics and Space Administration, Lewis Research Center, for possible use on the program. However, due to budget restrictions, these samples were not used in the test program. The seals are shown in Figure 23, and consist of two end-pieces of niobium (columbium) formed in the shape of a shallow flat-ended cup. The ends of two of these cups are separated by a graded mixture of niobium and alumina powders, which are pressed and sintered in place as indicated in Figure 24.

Braze Alloys. — Thirteen braze alloys were originally specified for testing in the program. These alloys were to be compounded and rolled to a nominal 0.005 inch (0.127 mm) thick foil, with a foil width of at least one inch (2.54 cm). High purity starting materials were specified, with minimum purities of 99.9% being called out. In addition, the starting alloys were to be triple-pass zone refined, preferably in an electron-beam zone refiner. Alloying was to be done by double arc remelting under conditions such that the purities of the final alloy ingots were not poorer than those of the starting material. The original list included compositions that had not previously been formulated, and whose ductilities were unknown. Therefore, it is not too surprising that some difficulties were experienced in the preparation of some of these braze foils. The original list of braze compositions is shown in Table XIX. In the first series of attempts to prepare these alloy foils only six of the thirteen were found to be fabricable in the required size. The remainder were too hard to roll. Subsequent work by the supplier resulted in the successful fabrication of #6 (98V-2Ti) and #7 (90V-10Mo).

Two of the remaining brazes were fabricated in the Atomics International laboratory. The first of these, Alloy #1, was modified to the 99Pt-1Ce composition by mixing equal parts of the hard 98Pt-2Ce alloy with pure platinum

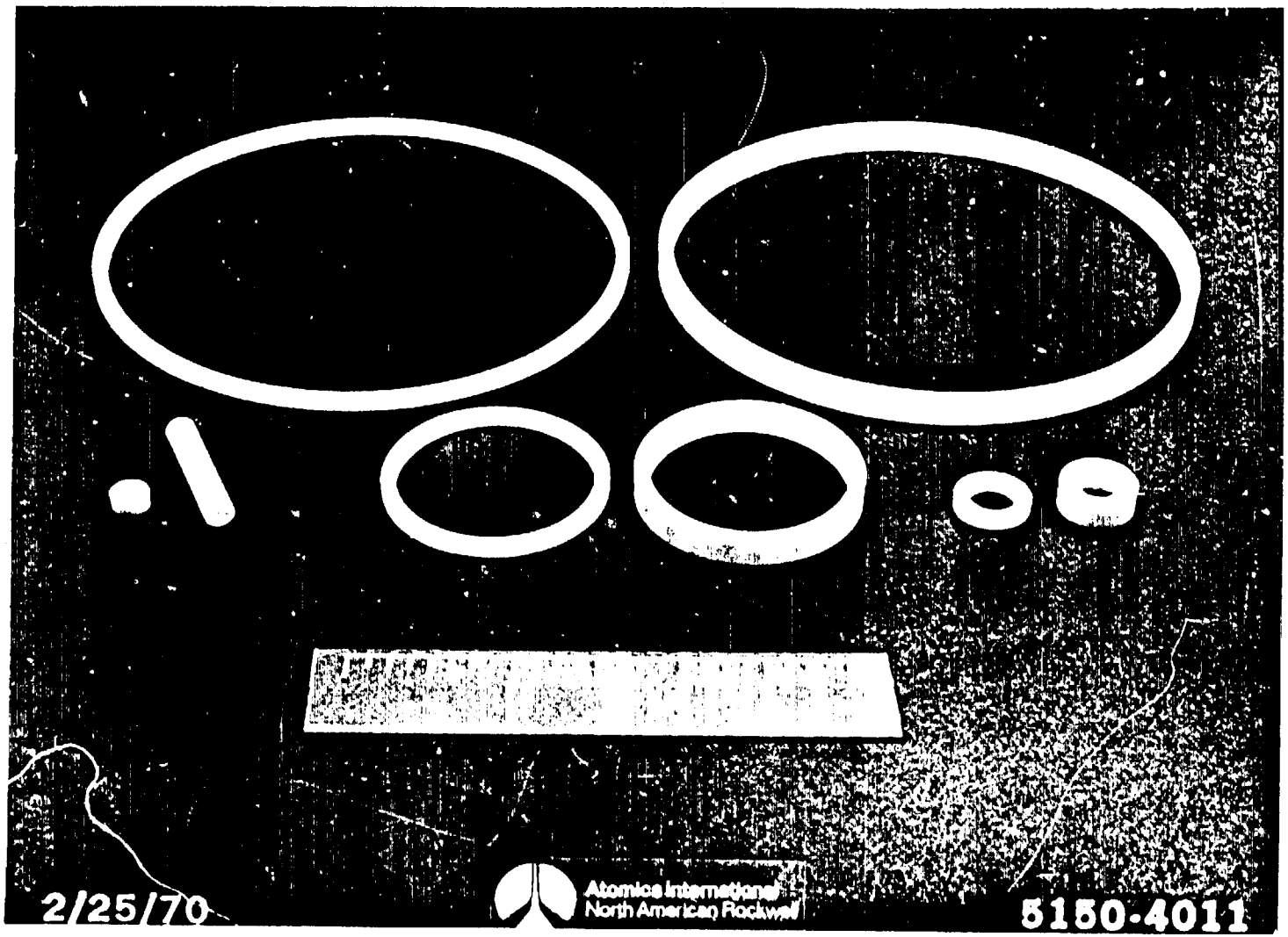

Figure 22. Beryllia Ceramic Parts

TABLE XVIII

ANALYSES OF BERYLLIA CERAMICS*

Impurity Element	Starting Materials				Green Parts ppm as element	Finished Parts			Product Average ppm as element	Product Average*** ppm as oxide
	Typ.**	44-18	44-44	43-10		55-17-1	55-31-1	55-31-3		
	ppm as element					ppm as element				
Al	10	28	9	10	10	20	10	10	13	24.6
B	< 1								< 1	< 3.2
Ca	< 10								< 10	< 14.
Cd	< 1								< 1	< 1.2
Co	< 1								< 1	< 1.3
Cr	< 2								< 2	< 3
Cu	< 2	8	2	ND	ND	ND	ND	ND	< 2	< 2.5
Fe	8	18	9	10	10	60	20	10	30	43.
Mg	10	28	5	ND	20	40	20	20	27	43.3
Mn	< 2								< 2	< 2.8
Mo	< 3								< 3	< 4.5
Ni	< 3								< 3	< 3.8
Pb	< 2								< 2	< 2.2
Si	10	20	8	40	20	40	30	20	30	64.
Ti	< 2	ND	ND	ND	-	ND	10	ND	3	5.0
									TOTAL	< 218.4
By difference, the beryllia is nominally 99.98% pure										

* Prepared by the National Beryllia Corporation, Greenwood Ave., Haskell, N.J. 07420.

** Typical analyses of Brush A-1188 High Purity BeO used as starting material.

*** Impurity calculations as oxide, as per Appendix IV of the NAS3-11840 contract. Typical analyses used in the absence of more definitive data in computing the expected oxide impurity level.

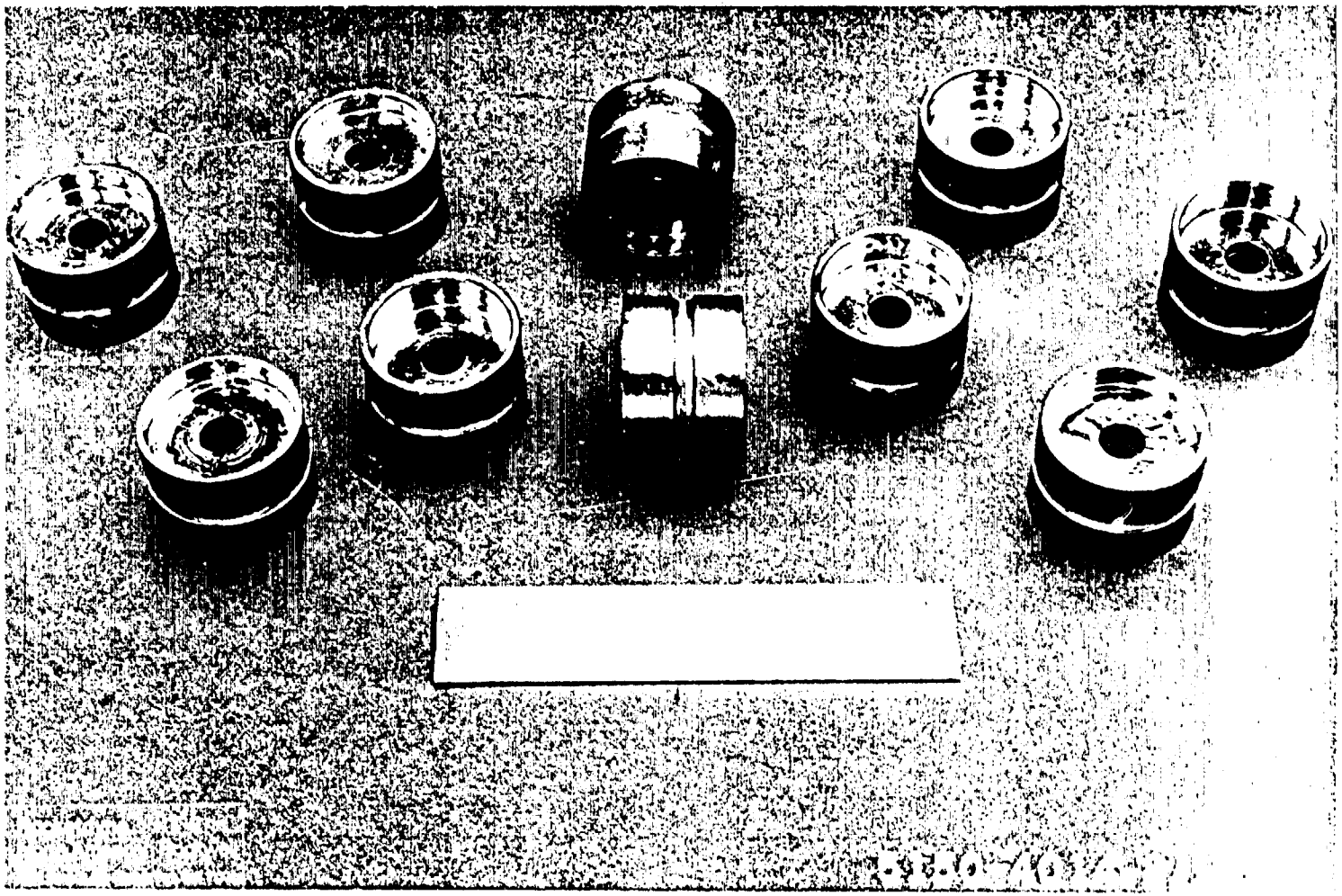

Figure 23. Graded Seals

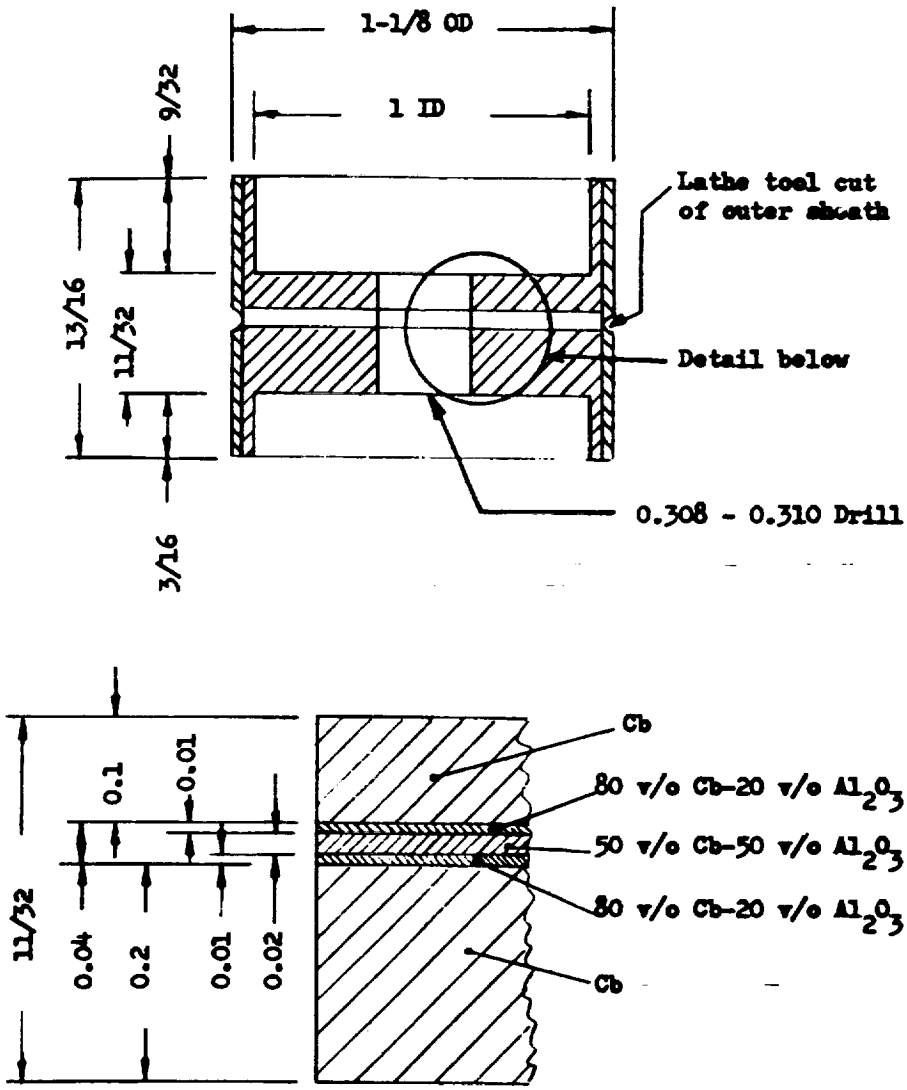

Figure 24. Graded Seals, Details

TABLE XIX

BRAZE ALLOYS, ORIGINAL SELECTIONS

1.	98 Pt - 2 Ce	8.	65V - 35 Cb*
2.	98 Pt - 2 Hf*	9.	64V - 34 Cb - 2 Zr
3.	98 V - 2 Ce*	10.	64V - 34 Cb - 2 Ti*
4.	98 V - 2 Hf*	11.	60 Zr - 25 V - 15 Cb
5.	99 V - 1 Zr*	12.	49 Cb - 36 Zr - 15 V
6.	98 V - 2 Ti*	13.	59 Re - 40 V - 1 Zr
7.	90 V - 10 Mo*		

* These brazes were prepared in foil form by Materials Research Corp., Orangeburg, New York.

and remelting. The resulting braze was found to be readily rolled. The second braze to be formulated in the AI laboratory was #9 (64V-34Cb-2Zr). This alloy was found to be more difficult to handle, but by the judicious use of intermediate anneals, the arc melt ingot was rolled.

The remaining three alloys, #11 (60Zr-25V-15Cb), #12 (49Cb-36Zr-15 and #13 (59Re-40V-1Zr) proved to be intractable. Because of this, and because of the rather good behavior of two of the other brazes when used with Al_2O_3 and Cb-1Zr, substitutions of the braze materials were made with the new brazes being used with Al_2O_3 and T-111 in an effort to obtain a good sea in the T-111 system. The brazes, with their ceramic and refractory alloy combinations as actually tested in Phase I are called out in Table XX. Braz #13A (90V-8Mo-2Zr) was formulated and fabricated in the AI laboratory. It was rolled with some difficulty. As is shown in Table XX, there were eight brazes tested with Cb-1Zr alloy. Figure 25 shows the braze alloys used in the Phase I program.

The pure vanadium braze was used in the Phase II program as is described below. It was rolled from zone-refined vanadium rod into 5-mil foil in the AI laboratory.

The chemical analyses of the brazes are shown in Table XXI. The metallic components are seen to fall reasonably close to the nominal compositions. The only element which showed a significant difference in its final vs. its initial amount is cerium. This change is not unexpected, because its volatility is relatively high; but although an allowance was made for the expected evaporation loss, the losses experienced were greater than those expected.

Refractory Metal Alloys. — Two refractory metal alloys were used in the program: Cb-1Zr and T-111 (Ta-8W-2Hf). The shapes purchased were: T-111 alloy in 1/4-inch (0.635 cm) rods; and Cb-1Zr in 1/4-inch (0.635 cm) rods, 0.020-inch (0.051 cm) sheet, and 0.030-inch (0.076 cm) sheet. The purchase specifications for Cb-1Zr are shown in Table XXII, together with the analyses of the various materials received. As is shown in the table, the rod stock is well within tolerance on all impurities except for the first shipment, Heat No. 520225-Cb-1Zr, which showed 175 ppm Hf instead of the desired < 100 ppm Hf. Because hafnium is a refractory metal and behaves very much like zirconium, its presence, even at the 175 ppm level, is not deleterious. In contrast, silicon, which is a notorious glass former if oxygen is present, is found to be very low at < 50 ppm Si as compared to the allowable level of < 200 ppm. Molybdenum is also seen to be quite low, as are all of the interstitials. The sheet stock was certified by the supplier to be within the limits of the purchase specification.

Table XXIII shows the purchase specifications for the T-111 alloy, and the analysis of the rod stock received. This material was well within specification on all of the listed impurity elements.

TABLE XX

CERAMIC-TO-METAL SEAL BRAZE SYSTEMS

System No.	Nominal Braze Composition	Phase I Ceramic	Phase I Alloy
1 A	99 Pt - 1 Ce	Al_2O_3	Cb-1Zr
2	98 Pt - 2 Hf	Al_2O_3	Cb-1Zr
3	98 V - 2 Ce	Al_2O_3	Cb-1Zr
4	98 V - 2 Hf	Al_2O_3	Cb-1Zr
5	99 V - 1 Zr	Al_2O_3	Cb-1Zr
6	98 V - 2 Ti	Al_2O_3	Cb-1Zr
7	90 V - 10 Mo	Al_2O_3	T-111
8	65 V - 35 Cb	Al_2O_3	T-111
9	64 V - 34 Cb - 2 Zr	Al_2O_3	Cb-1Zr
10	64 V - 34 Cb - 2 Ti	Al_2O_3	Cb-1Zr
11 A	98 V - 2 Hf	Al_2O_3	T-111
12 A	64 V - 34 Co - 2 Zr	Al_2O_3	T-111
13 A	90 V - 8 Mo - 2 Zr	Al_2O_3	T-111

TABLE XXI

CHEMICAL ANALYSES OF BRAZES

No.	Nominal Composition	Major Constituent Analysis, w/o	Interstitial Analyses*, w/o		
			Carbon	Oxygen	Nitrogen
1	98Pt - 2Ce	1.32Ce*	0.040	0.028	< 0.005
2	98Pt - 2Hf	2.14 Hf*	0.030	0.055	< 0.005
3	98V - 2Ce	1.28 Ce*	0.046	0.006	< 0.005
4	98V - 2Hf	1.86 Hf*	0.040	0.057	< 0.005
5	99V - 1Zr	1.35 Zr*	0.044	0.049	< 0.005
6	98V - 2Ti	1.94 Ti*	0.049	0.042**	< 0.005
7	90V - 10Mo	9.43 Mo*	0.034	0.048	< 0.005
8	65V - 35Cb	31.1 Cb*	0.045	0.048	< 0.005
9	64V - 34Cb - 2Zr	35.6 Cb, 1.9 Zr*	0.049	0.085**	< 0.005
10	64V - 34Cb - 2Ti	34.8 w/o Cb, 2.1 Ti*	0.047	0.040	< 0.005
11	60Zr - 25V - 15Cb	25.5 V, 14.8 Cb*	0.045	0.102	< 0.005
12	49Cb - 36Zr - 15V	36.4 Zr, 14.8 V*	0.049	0.040	< 0.005
13	59Re - 40V - 1Zr	38.9 V, 1.0 Zr*	0.045	0.045	< 0.005
1A	99Pt - 1Ce	0.6 Ce**	(0.040)	0.022	(< 0.005)
11A	98V - 2Hf	1.86 Hf*	0.040	0.057	< 0.005
12A	64V - 34Cb - 2Zr	35.6 Cb, 1.9 Zr*	0.049	0.077**	< 0.005
13A	90V - 8Mo - 2Zr	9.2 Mo, 1.9 Zr**	(0.034)	0.095**	(< 0.005)
14	Pure V	99.98V	0.006	0.011	< 0.001

* Analysis by manufacturer, Materials Research Corporation

**Analysis by Atomics International

TABLE XXII

CHEMICAL ANALYSES OF Cb-1Zr ALLOY*

Impurity Element	Purchase** Spec. ppm	Rod Stock*** ppm	Rod Stock**** ppm	Rod Stock***** ppm
Cb Zr	98.5 (w/o) 0.8-1.2 (w/o)	Bal 0.82-1.2 (w/o)	Bal. 1.1-1.15 (w/o)	Bal. 1.11-1.15 (w/o)
C O H N	< 100 < 300 < 10 < 100	< 30 75 4.5 28	< 40 185 7 66	< 10 87 5 44
Ta Mo W Si	< 1000 < 1000 < 300 < 200	560 < 20 238 < 50	695 < 20 250 < 50	< 300 < 20 < 300 < 20
Hf Ti Fe V	< 100 < 100 < 50 < 50	175 < 40 < 50 < 20	< 80 < 40 < 50 < 20	< 100 < 10 < 20 < 50
Co Pb Mn	< 20 < 20 < 20	< 10 < 20 < 20	< 10 < 20 < 20	< 20 < 20 < 20
Ni RE	< 20 100	< 20 -	< 20 -	< 20 < 10 (Yb)

* Alloy obtained from Wah Chang Albany Corp., PO Box 460, Albany, Oregon 97321.

** Sheet stock certified by supplier to conform with this specification.

*** Heat No. 520225-Cb-1Zr (June 23, 1969).

**** Heat No. 530033-Cb-1Zr (June 23, 1969).

***** Heat No. 520228-Cb-1Zr (March 18, 1970).

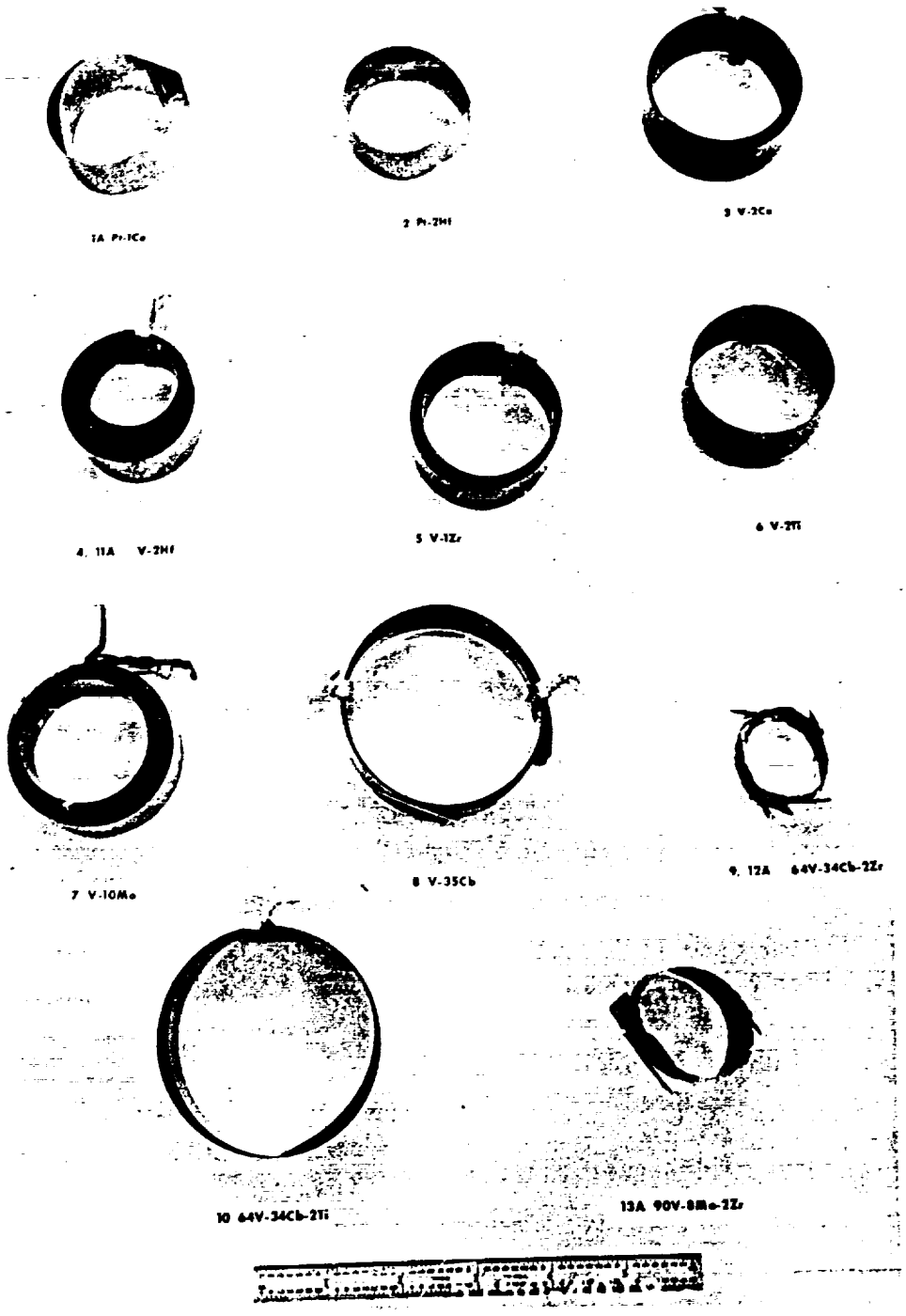

Figure 25. Braze Alloys

TABLE XXIII

CHEMICAL ANALYSES OF T-111 ALLOY (Ta-8W-2Hf)

(Ta-8W-2Hf)

Impurity Element	Purchase Spec. ppm	Rod Stock** ppm
W	7.0-9.0 (w/o)	8.4 (w/o)
Hf	1.8-2.4 (w/o)	1.9 (w/o)
C	< 50	40
N	< 50	10
O	< 100	50-60
H	< 10	2.0
Cb	< 1000	405-455
Mo	< 200	< 10
Ni	< 50	< 10
Co	< 50	< 5
Fe	< 50	< 20
V	< 20	< 10
Al		< 10
Si		< 20
Ti		< 20

* Alloy obtained from Wah Chang Albany Corp., PO Box 460, Albany, Oregon 97321. Analyses provided by supplier.

**Heat No. 650061-T-111-Ta. (May 26, 1969).

APPENDIX III. GENERAL EQUIPMENT

The general laboratory equipment items used in the program are described below.

Furnaces and Power Supplies. — The specifications for furnaces to be used on this program called for the use of refractory split tube elements and prohibited the use of insulators of any type within the heater zone. Accordingly, inquiries were sent to furnace manufacturers for the construction of four furnaces to be built with the following characteristics: (a) minimum temperature capability 1800°C, (b) 5000 hours (1.8×10^7 s) minimum life at 1400°C, (c) tungsten mesh heating element of split tube design five inches (12.7 cm) diameter by ten inches (25.4 cm) long, (d) five radiation shields, the two inner ones being tantalum, the three outer ones being molybdenum, (e) water-cooled copper shell, and (f) 18 KVA power supply (transformer) with 208/220 VAC or 440/480 VAC input matched to heater element load impedance. In addition, bids were requested on a silicon-controlled rectifier and an automatic temperature control system.

Figure 26 shows one of the furnaces and its heating element.* The temperature control instrumentation** included four 24 KVA-480 Vac SCR's, four Current Limiter Units, four Meter Box Assemblies with current transformers and temperature controllers, and a Line Spike Suppressor.

Electrical Power Feed-Throughs. — The electrical power feed-throughs* used are shaped lengths of 3/4-inch (1.91 cm) copper tubing, inside of which 1/4-inch (0.635 cm) copper tubing is inserted nearly to the end. The outer tube is insulated from its flange mounting by a ceramic-to-metal seal. Cooling is effected by flowing about 1 gpm (6.31×10^{-5} m^3/s) of water through the system. Figure 27 shows a pair of the feed-throughs. Figure 28 shows one of the vacuum systems with the electrical feed-throughs in place, and Figure 29 shows the second vacuum system.

Vacuum Chambers. — The vacuum chambers which house the aging test furnaces*** are nominally 30 inches (76 cm) in diameter, and 30 inches (76 cm) high. They are fitted with Curvac flanges*** and metal gaskets in all access ports. There are two systems, each uses a turbomolecular pump for roughing, and a 1200 ℓ/sec (1.2 m^3/s) ion pump*** for the attainment of high vacuum. When cold, these systems operate at $< 1 \times 10^{-8}$ torr (1.33×10^{-6} N/m^2) as measured on a nude ionization gauge. The chambers are shown in Figures 28 and 29.

Clean Bench. — The clean bench on which the braze assembly is carried out is a six-foot (1.83 m) Edgegard Hood unit manufactured by Baker Instruments, Inc. It is shown in Figure 30.

---

* The supplier of the furnaces, step-down transformers, and electrical power feed-throughs was Richard D. Brew and Company, Inc.

** Obtained from Loyola Industries, Inc.

*** Manufactured by Ultek Division, Perkin-Elmer Corp.

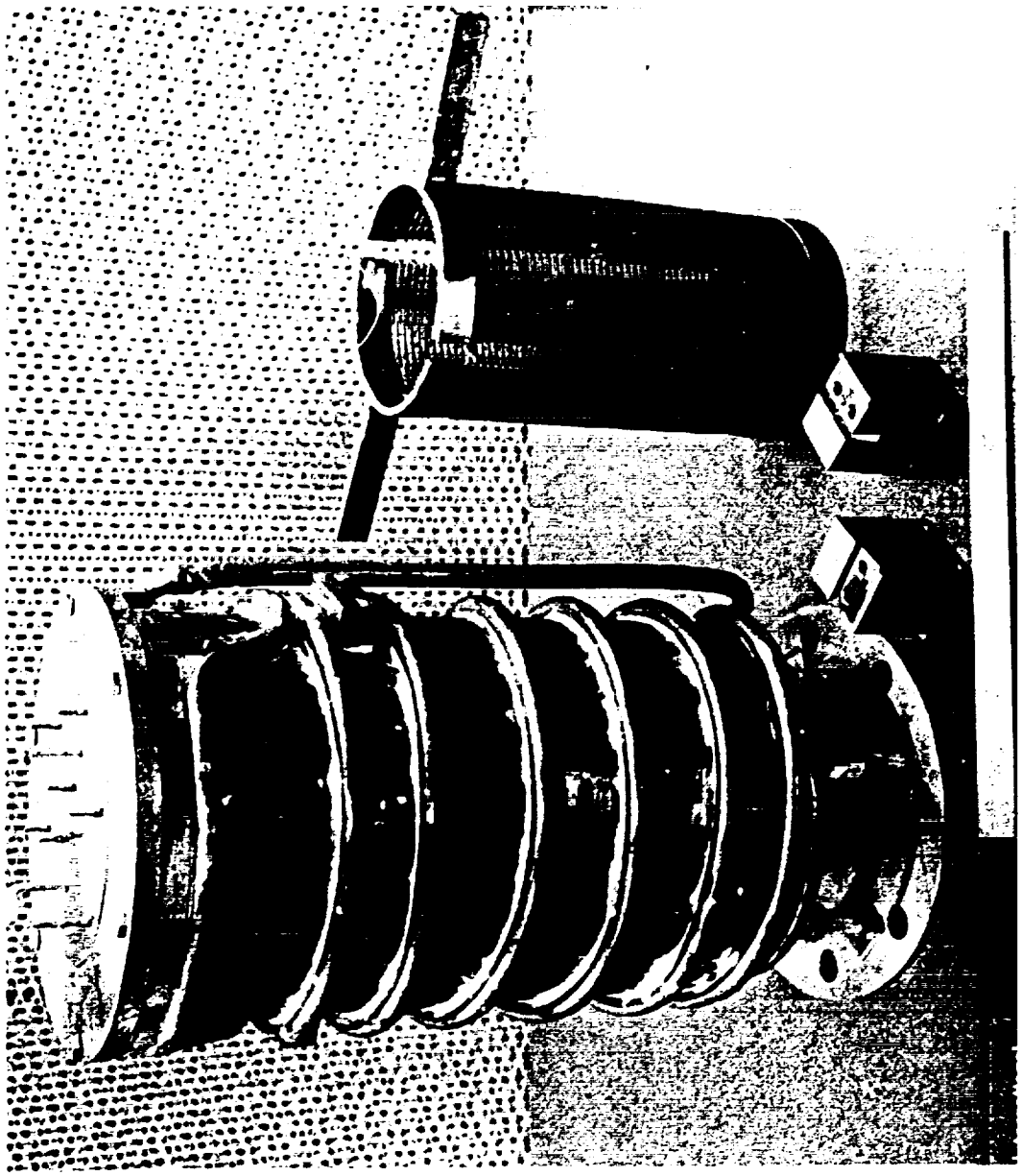

Figure 26. Furnace and Heating Element

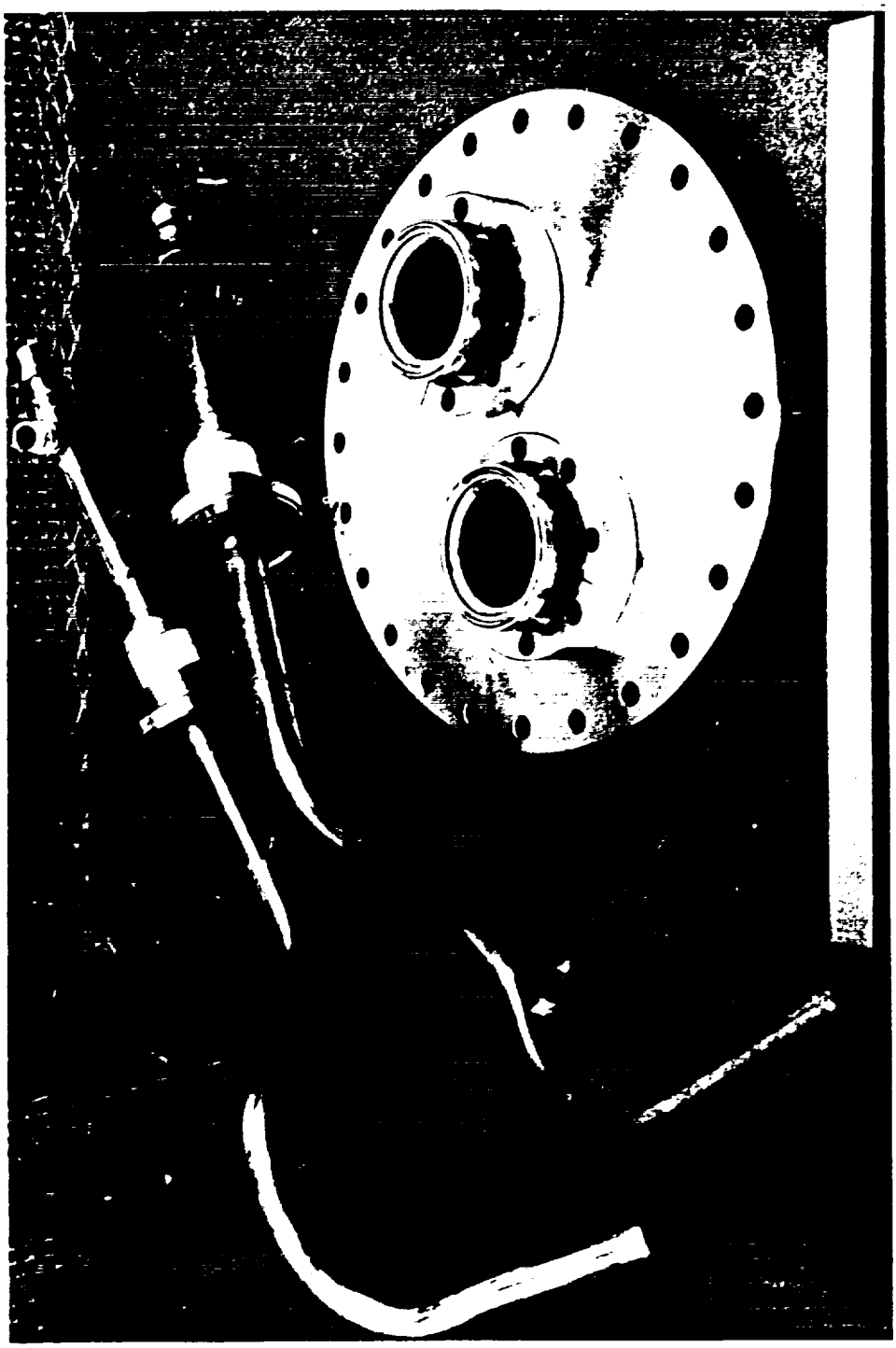

Figure 27. Electrical Feed-Through

Figure 28. Vacuum System I

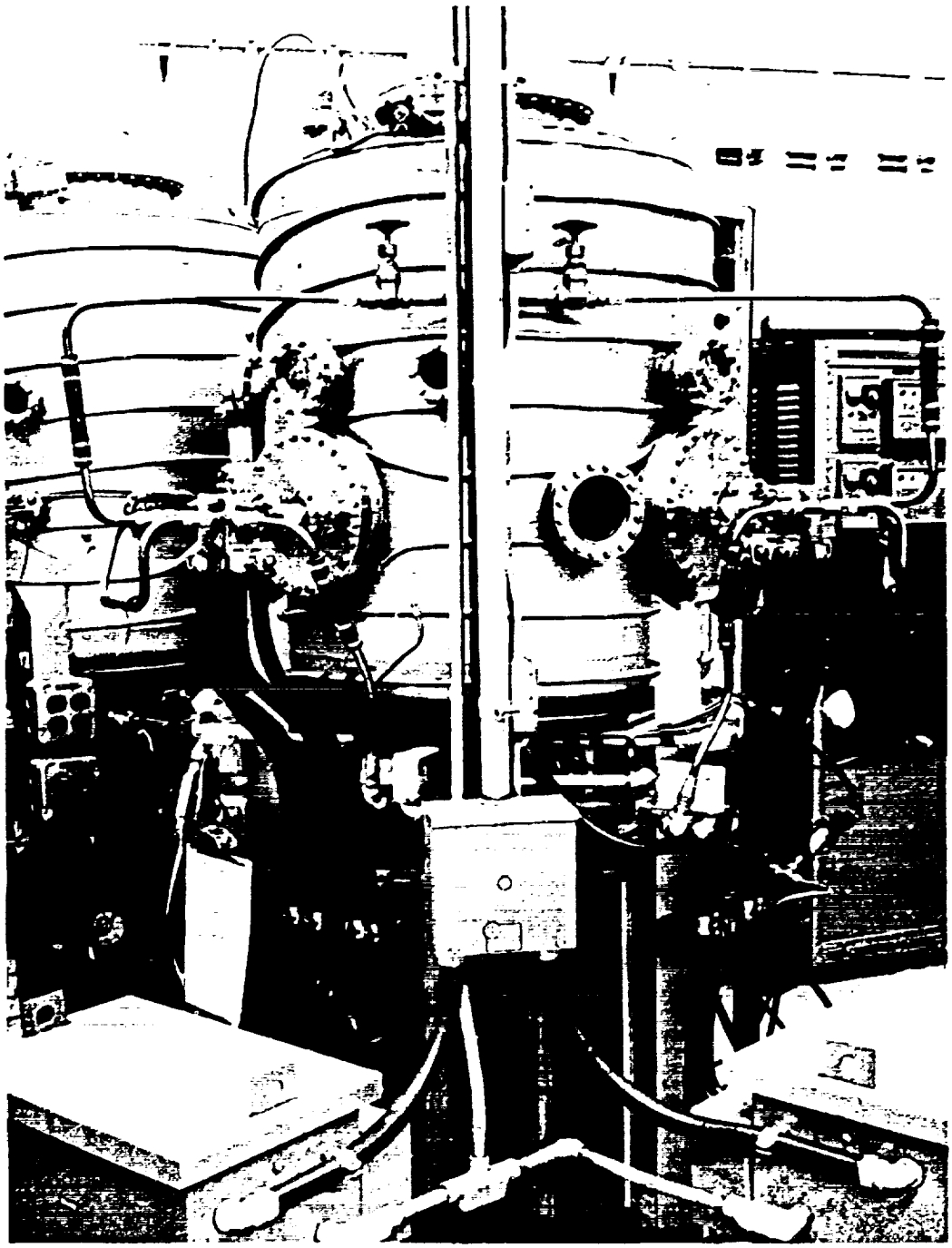

Figure 29. Vacuum System II

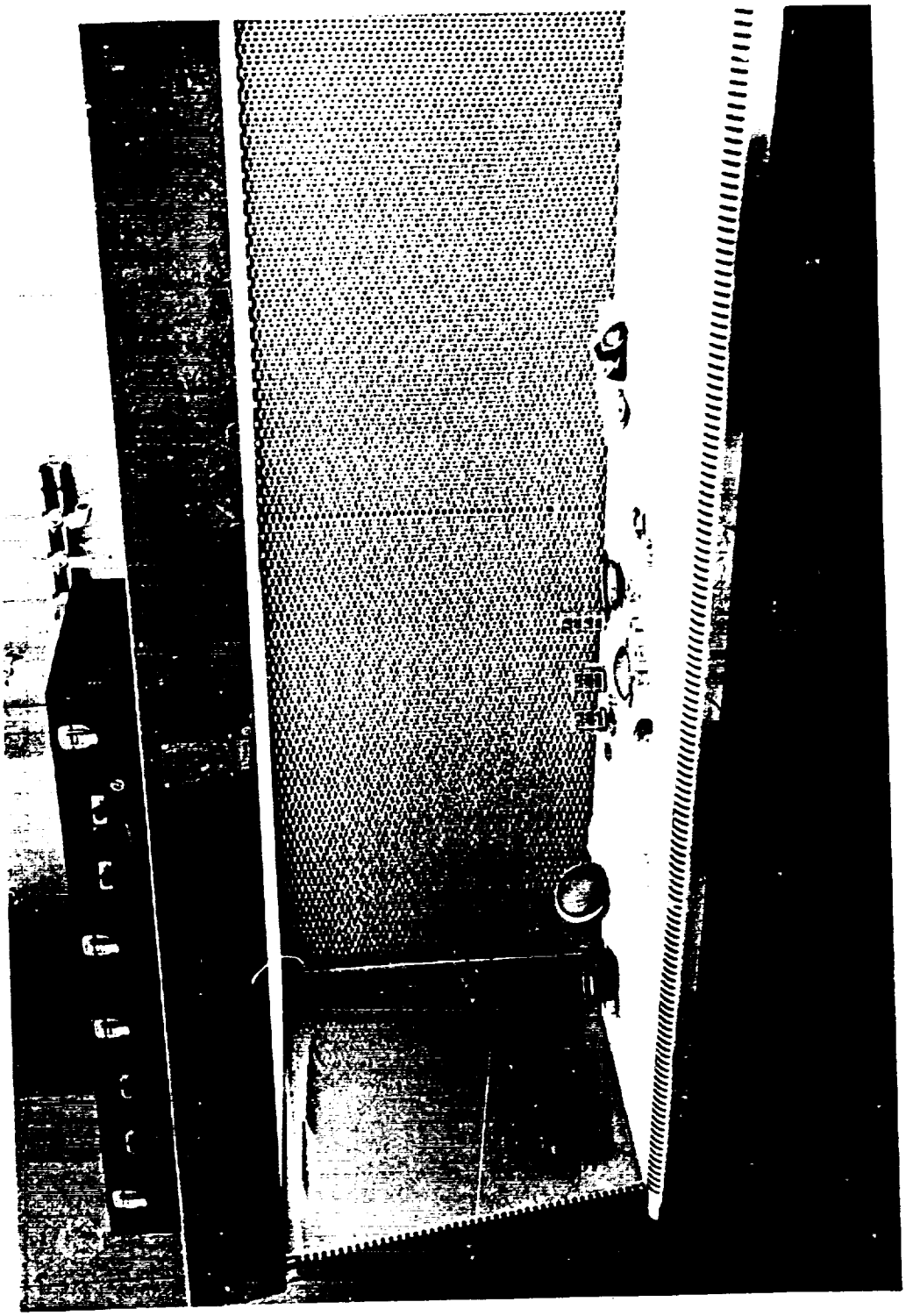

Figure 30 Clean Bench

Brazing Furnace. — The brazing furnace is a commercial unit manufactured by National Research Corporation, and is fitted with a liquid N_2 cold-trapped oil diffusion pump vacuum system. The heating element is a horizontally mounted tantalum strip formed into a 4-1/2 inch (11.4 cm) diameter circle, and powered by a step-down transformer, with a manual 23.5 KVA auto transformer control. This unit is shown in Figure 31.

Figure 31. Brazing Furnace

APPENDIX IV

BRAZING JIG, BUTTON SAMPLE

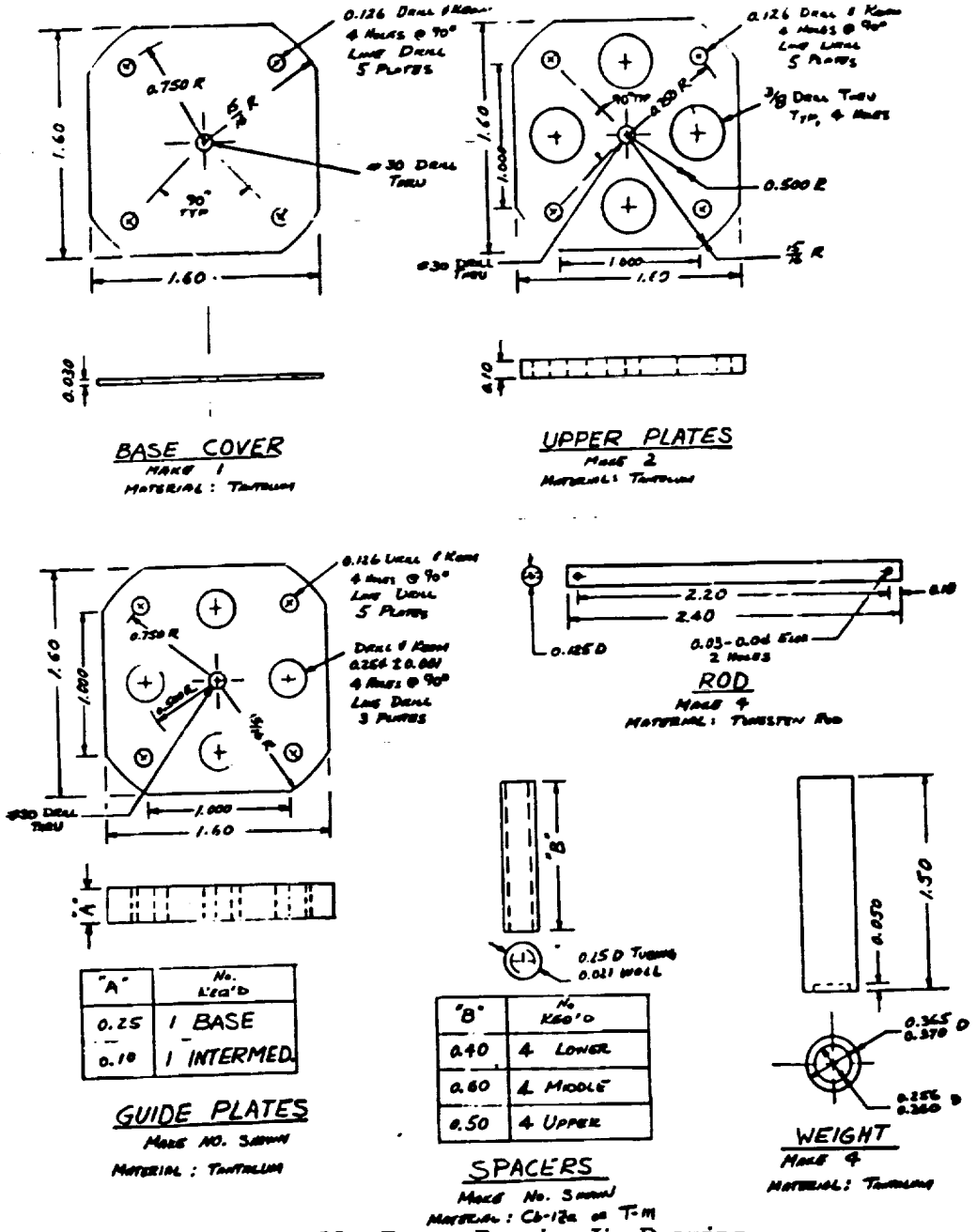

Figure 32. Button Brazing Jig Drawing

APPENDIX V

BRAZING JIG, MOR SAMPLES

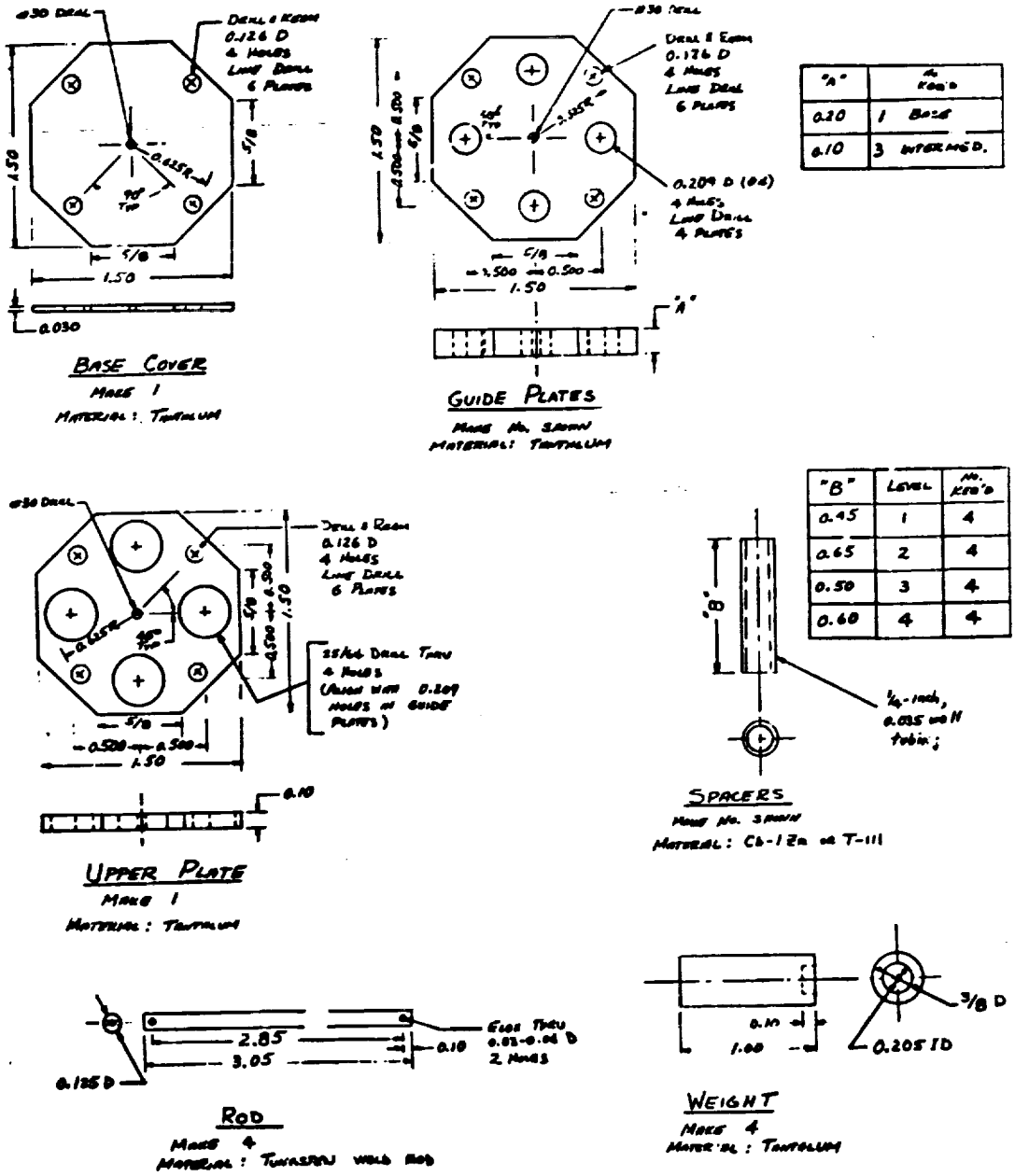

Figure 33. MOR Brazing Jig Drawing

APPENDIX VI. ULTRASONIC TECHNIQUE EVALUATION

Because the scan-trace analysis technique for evaluating braze joints proved to be unsatisfactory when applied to the small diameter samples used in this program, an alternate technique described as a comparative echo-display analysis method (or photographic evaluation technique) was devised and used. The bases for each of these analysis techniques are given in the text (p. 11 ff). The two methods have been compared using shear-strength data from the test specimens. These data are given in Tables XXV to XXVII in Appendix X.

The increase in the usefulness of the photographic evaluation technique over the previously used scan-trace evaluations is shown by comparing the data given in Figures 34 and 35. Figure 34 shows the plot of the shear breaking strengths plotted against the ultrasonic test interpretations in terms of G, GF, F, FP, and P designations for the samples measured by the scan-trace technique, and Figure 35 shows the corresponding plot for the samples evaluated by the photographic method. These sca. er diagrams, as such graphs are designated, clearly show the superiority of the correlation coefficient for the data of Figure 35 over that of Figure 34. Although there is a distinct range of breaking strengths under the G and GF ultrasonic test evaluations in Figure 35, there were no high shear values found for the P and FP groups. This is in contrast to the data of Figure 34, in which the majority of samples were classified P, even though many of them later showed high shear strengths.

An alternate approach to the evaluation of the photographic or comparative echo-display analysis method involves the calculation of the average shear breaking force values for each of the letter-designation groups (Ref. 16). These values, with their average deviations from the average, are, (in psi): G, 9138 (2860); GF, 8494 (2060); F, 4827 (1140); FP, 1923 (760); and P, 1610 (900). These average values, when plotted against a "cumulative percent of samples in the group" abscissa scale show the rather typical population "S" curve characteristics. This is not unexpected for data such as these -- i.e., for the measurement of a single parameter (shear strength) in a group of (ten) different (but fundamentally similar) kinds of brazes.

Perhaps the most significant finding of this analysis is that the data divide more naturally into three groups, (G + GF), F, and (FP + P). However, because of the differences in the kinds of brazes, further analysis of these particular data is not warranted. One can conclude that the comparative echo display analysis is superior to the scan-trace method for this application.

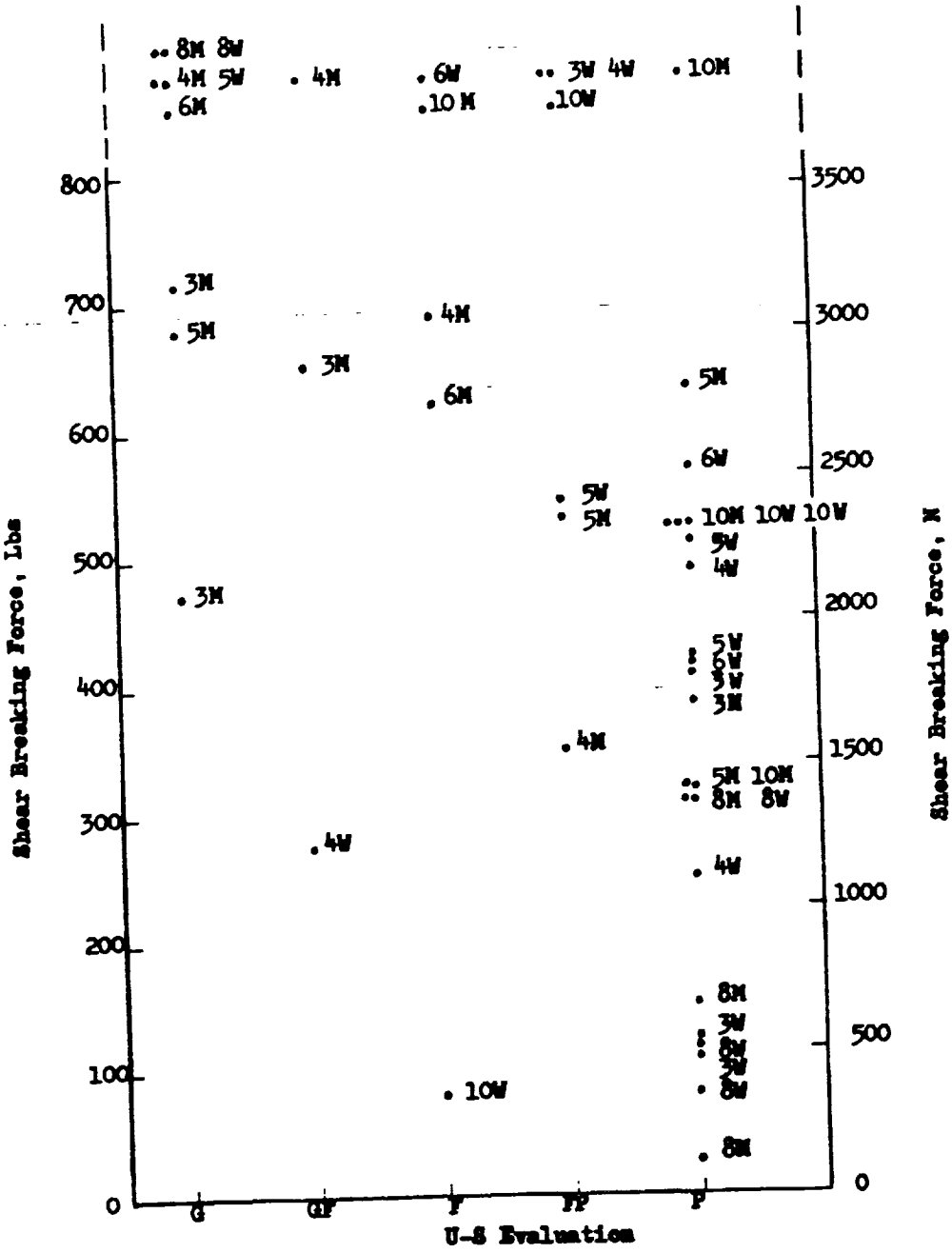

Figure 34. Scatter-Plot of Scan-Trace U-S Evaluations and Shear Break Values.

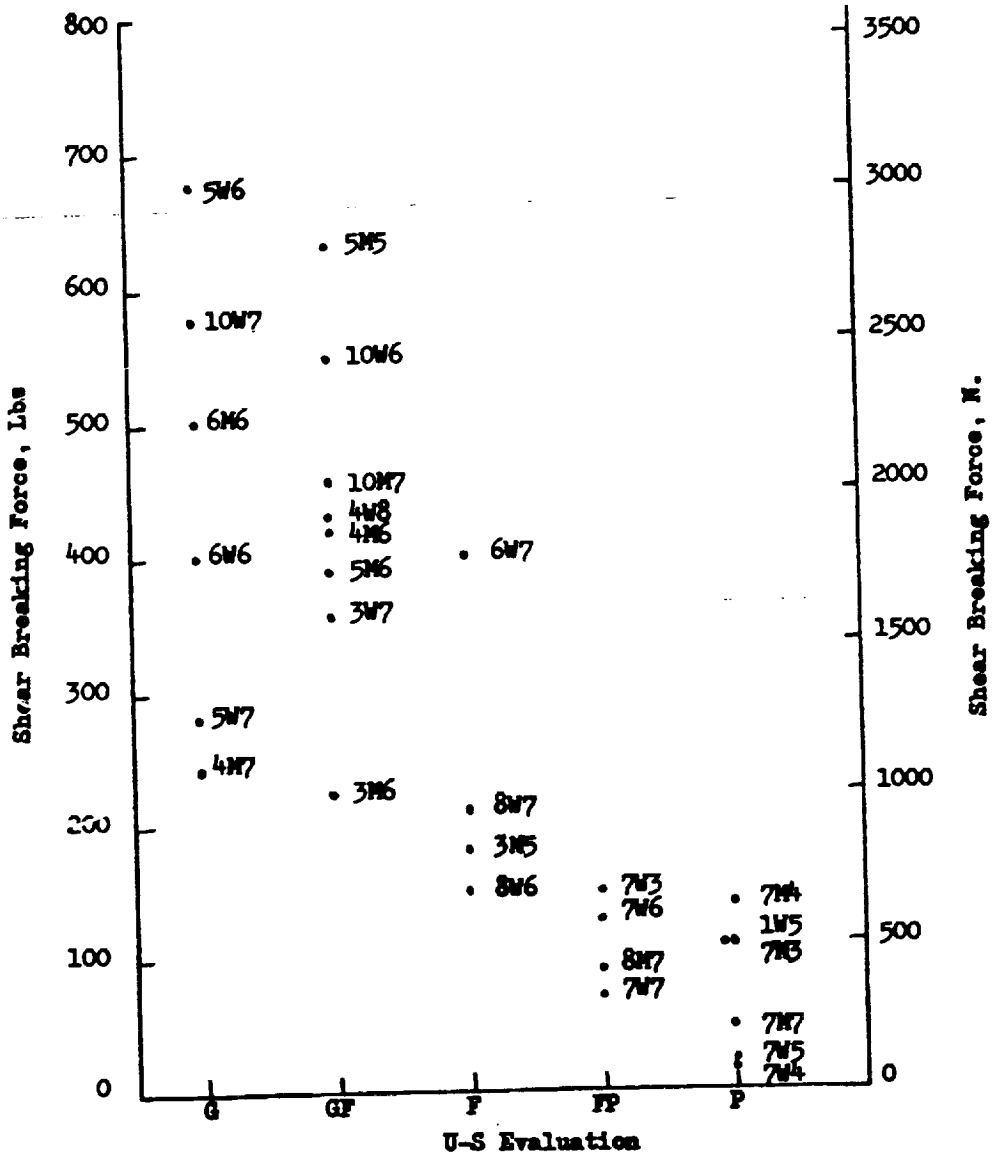

Figure 35. Scatter-Plot of Photographic U-S Evaluations and Shear Break Values

APPENDIX VII

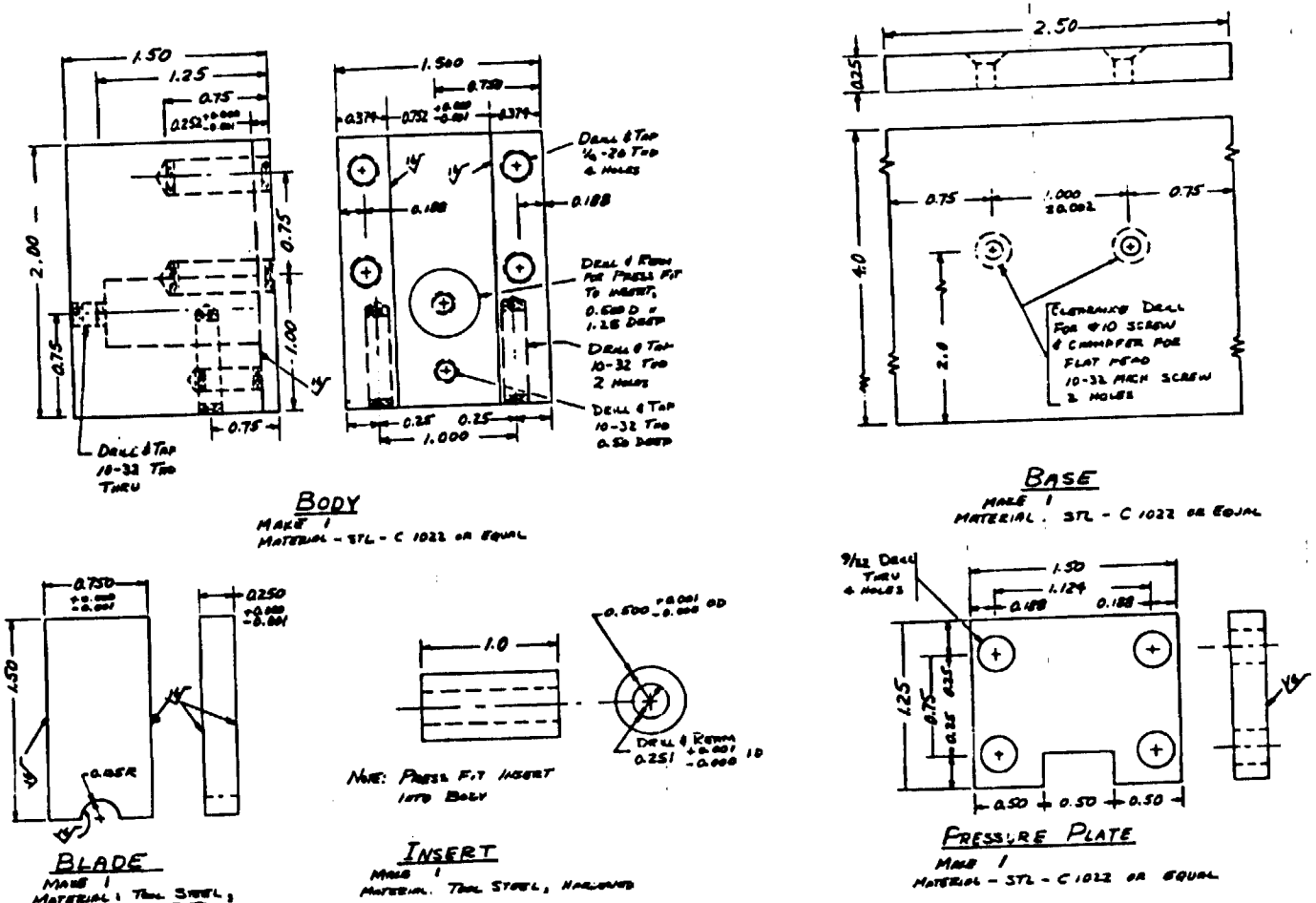

Figure 36. Shear Test Jig Drawing

APPENDIX VIII

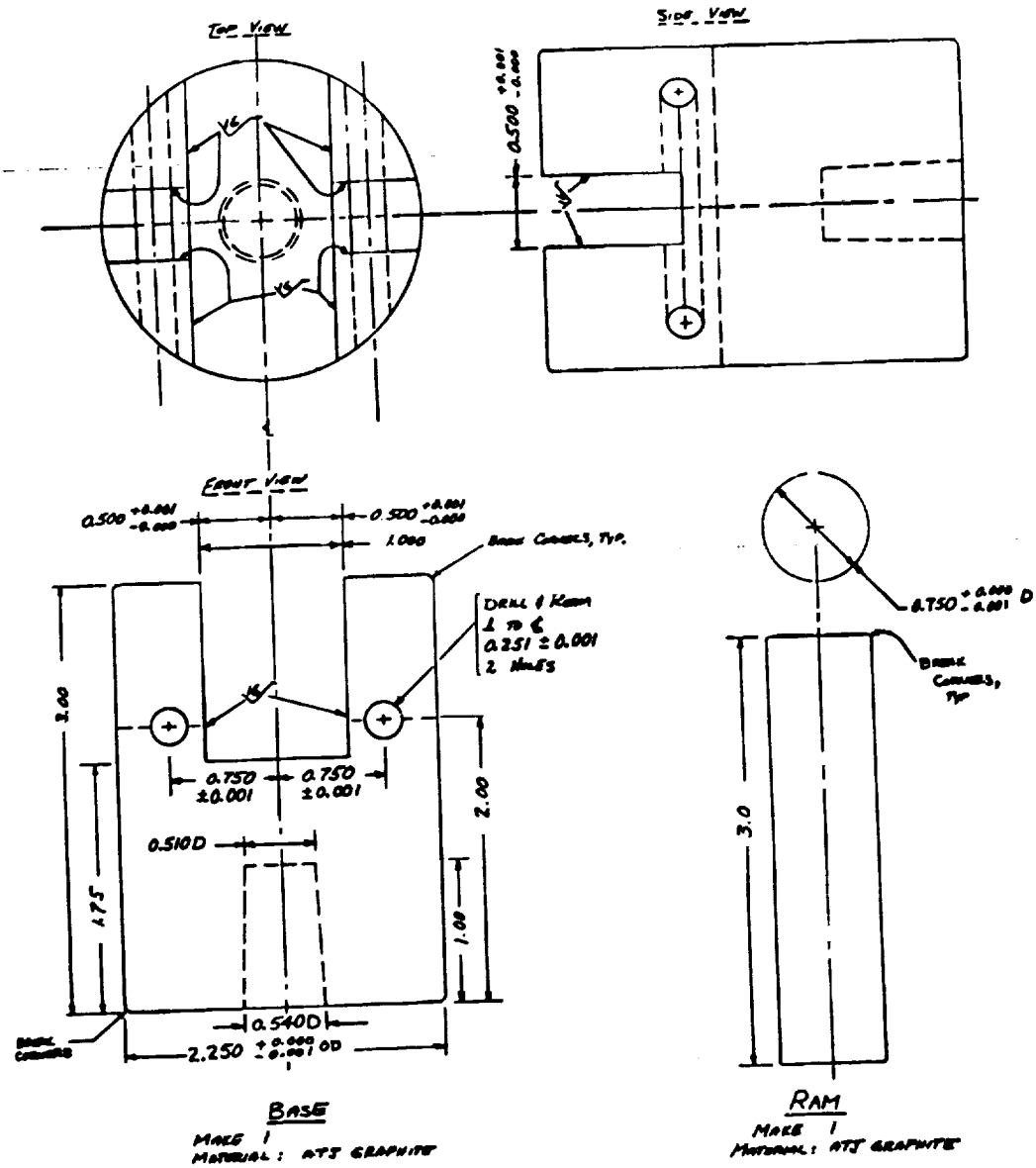

Figure 37. MOR Test Jig Drawing, Part 1

APPENDIX VIII

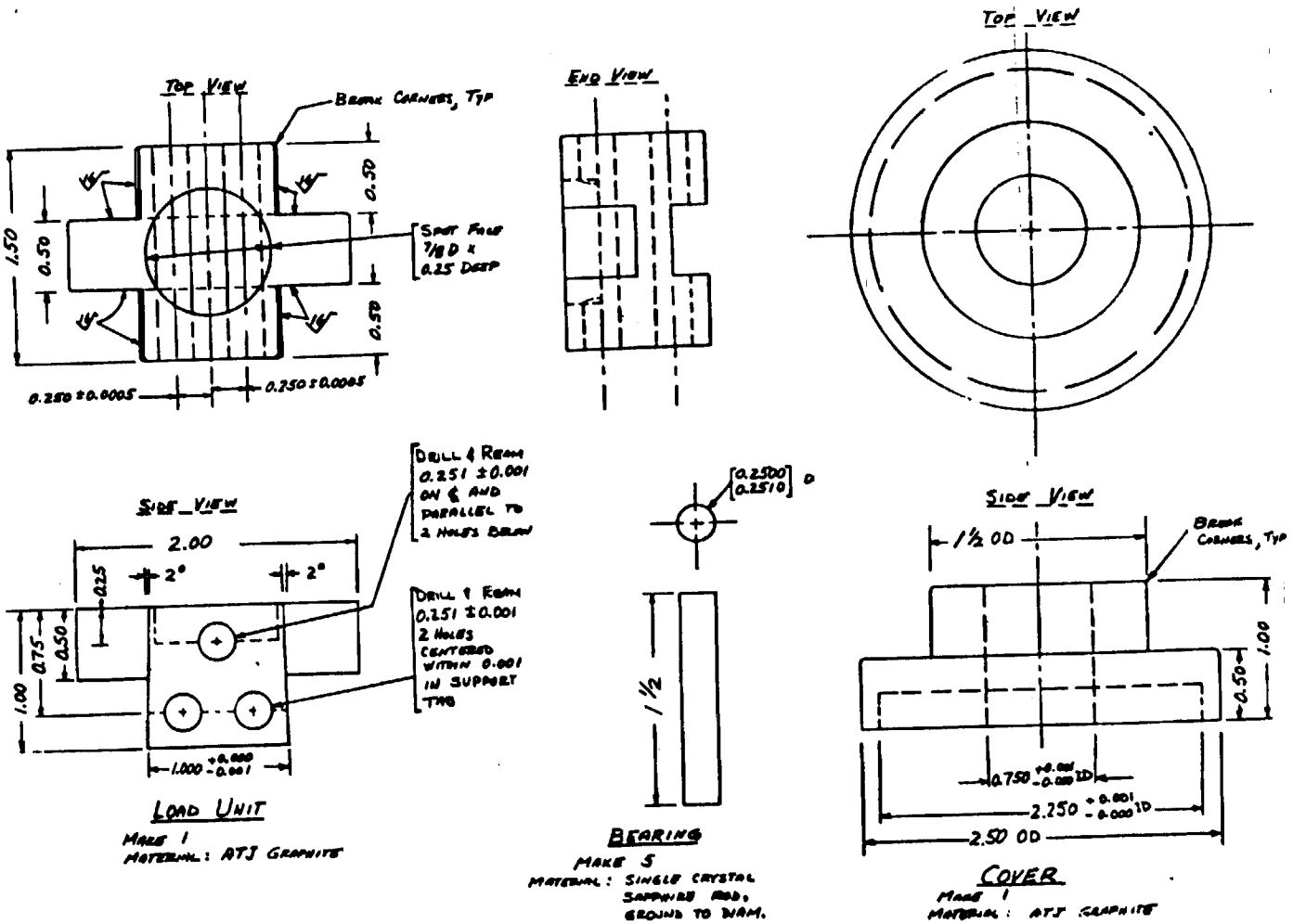

Figure 38. MOR Test Jig Drawing, Part II

APPENDIX IX. ELECTRON MICROPROBE DATA ANALYSIS

The electron microprobe x-ray analyzer used to examine the specimens is an Applied Research Laboratories, Inc., Model EMX. The unit at Atomics International contains a 0-50 kev high voltage power supply, an electron beam scanning system, and three crystal spectrometers. In electron microprobe analysis, a finely focused ($\sim$ 1-2 microns in diameter) beam of high energy electrons strikes the surface of the specimen being analyzed. This causes the specimen to emit x-rays characteristic of the elements present in the surface volume under excitation. The x-rays from the specimen are sorted by crystals and sent to x-ray detectors, where they are converted to electrical pulses. The pulses are then either counted (typewriter printout) or converted to a D.C. signal and displayed (x - y recorder, oscilloscope). The ratio of counts obtained for a given element in the specimen to the counts obtained from a standard of that element (e.g., the pure element) provides an approximation of the concentration (in weight percent) of that element in the specimen. More accurate results are obtained by applying corrections to the specimen data to take into account items like background, dead time, mass absorption, fluorescence, and atomic number effects.

Schematically, five steps were involved in arriving at the concentration profile data:

1. Obtaining N_i' [observed counts for each element examined in the specimen, as well as from the standards (pure elements)].
2. Subtracting instrument errors and background, yielding N_i.
3. Ratioing $N_{i\ spec}$ to $N_{i\ std}$ for each element. The result is called the K_i value, but can also be referred to as the relative intensity or apparent concentration.
4. Converting from apparent concentration (K_i) to true concentration (C_i, in weight percent) via application of conversion formulae.
5. Normalizing the results.

The conditions of analysis for obtaining data for the elements Nb, V, and Al in the specimens were as follows: the electron beam voltage was 30 kev, the specimen current was 0.028 microamperes on pure Nb, the electron beam was $\sim$ 1-2 microns, the counting interval was 10 seconds, and the distance between datum points was 4-1/2 microns. Data for V-$K\alpha_1$, (2.503 Å) were taken on Spectrometer #1, Nb-$L\alpha_1$ (5.725 Å) on Spectrometer #2, and Al-$K\alpha_1$ (8.338 Å) on Spectrometer #3. Each specimen was examined on a path perpendicular to the metal-ceramic interface beginning in the Al_2O_3 or Cb-1Zr and continuing to the Cb-1Zr or Al_2O_3.

The procedure used for converting K values to C values is that known as the Ziebold-Ogilvie or Z-O method (Ref. 17). Ziebold and Ogilvie showed that for a wide variety of binary alloys, a valid relationship between K_1 and C_1 is

given by,

$$\frac{1-K_1}{K_1} = a_{12}\frac{1-C_1}{C_1} \qquad (13)$$

where

K_1 is the apparent concentration of element 1 in element 2

C_1 is the true concentration (weight percent) of element 1

a_{12} is the conversion parameter for element 1 in element 2.

Because there is only one parameter (a_{12}) to be determined, only one calibration standard is required for a binary system. For a ternary system, the conversion parameter for element 1 in a mixture of element 2 and element 3 is given by the expression.

$$\bar{a}_{123} = \frac{a_{12}C_2 + a_{13}C_3}{C_2 + C_3}. \qquad (14)$$

One can see that the value of $\bar{a}_{123}$ as evaluated from Equation 14 will be a function of the ternary alloy composition, and that the experimental evaluation of ternary conversion parameters could be very time-consuming. However, Ziebold and Ogilvie developed a binary parameter estimation expression, which can be evaluated and used in Equation 14 to determine the ternary conversion parameters. The expression is,

$$a_{12} = 0.95 \left(\frac{\sigma + X^1_2}{\sigma + X^1_1}\right)\left(\frac{Z_1}{Z_2}\right)^{0.28} \qquad (15)$$

where

$\sigma = 1820\ (30/\text{Kev})^2$

Kev = accelerating voltage of the electron beam in kilovolts,

$X^1_2 = (\mu/\rho)^1_2 \csc\theta$

$(\mu/\rho)^1_2$ = mass absorption coefficient for line 1 in element 2

θ = spectrometer take-off angle (52-1/2° in the present instrument)

Z = atomic number.

Equation 15 applies to systems in which there is no strong fluorescence. The present systems do not show fluorescence interferences, so Equation 15 can be used to estimate the binary coefficients and to develop a table of values of ternary coefficients. These values can be checked by evaluating the ternary values from one or more ternary specimens of known composition using the ternary expressions equivalent to Equation 13,

$$\frac{1-K_1}{K_1} = a_{123}\,\frac{1-C_1}{C_1}, \tag{16}$$

$$\frac{1-K_2}{K_2} = a_{213}\,\frac{1-C_2}{C_2}, \tag{17}$$

$$\frac{1-K_3}{K_3} = a_{312}\,\frac{1-C_3}{C_3}. \tag{18}$$

The estimates of the ternary a-values for V, Nb, and Ti were compared against experimental values obtained from the #10 braze (64V-34Nb-2Ti). For the estimates of the a-values for aluminum, Equations 14 and 15 were evaluated for the low-aluminum, low-titanium, low-zirconium region of the V-Nb-Ti-Zr-Al system. These calculated values were compared against experimental a-values obtained from a standard sample prepared by adding Al to equal parts of 98V-2Ti and Cb-1Zr. The analysis of the standard was 46.8V-47.2Nb-4.6Al-0.95Ti-0.45Zr.

The values of a for the systems examined in the microprobe were plotted against alloy composition and the experimental values of a_{123}, etc., were used to modify the curves such that the final results were normalized to a total percent concentration value of 99%. The final normalized a-value results based on the data from the standards showed both the V and Nb to be within a 2% relative error of the assumed composition. Over the range of compositions reported in the braze reaction regions, it is estimated that the V and Nb data are accurate to ± 2 w/o absolute. The corrected Al reading on the standard was found to be low by about 5% relative. This information shows that no large errors are involved in the reported results for Al concentrations in the braze reaction regions near the Al_2O_3 interface. An additional standard (e.g., 18V-80Nb-1Zr-1Al) would be needed to determine relative accuracies for Al in the braze reaction regions near the Cb-1Zr. Here the relative accuracies would be expected to be poorer because of the very low Al concentrations.

APPENDIX X. PHASE I BRAZING TEST DATA SUMMARY

A total of 189 button braze screening tests were made on the thirteen braze systems. All of the brazes were formed as 0.004-0.005" (0.102-0.127 mm) thick foil, although two of them, #9 (64V-34Cb-2Zr) and #13A (90V-8Mo-2Zr) were formed with some difficulty, as is indicated on Figure 25. Each of the 189 tests was evaluated on six bases: (1) Braze Visual, which described the external appearance of the joint; (2) Ultrasonic, which describes the evaluation of this test on the G, GF, F, FP, and P scale; (3) Ceramic Visual, which describes the color in the ceramic at the braze break surface; (4) Shear, which is the shear failure load; (5) Break, which describes the location of the break along the ceramic-braze-alloy unit; and (6) Braze, which describes the appearance of the fracture surface of the braze. Further definitions of these terms and the symbols used in describing them are shown in Table XXIV, which also serves as a code reference for the symbols used in Tables XXV through XXXVIII. Tables XXV through XXXVIII show the results of these evaluations for each of the braze systems.

Table XXV shows the data for Braze System 1A, Pt-1Ce vs. Cb-1Zr. The ultrasonic evaluations are generally poor, and the brazes were characterized by significant amounts of braze alloy having flowed out of the joint region and run down the metal member. Apparently the braze metal dissolves the Cb-1Zr alloy to form a large amount of fluid, which does not remain in the braze region. The shear strengths of the joints are not particularly high, and pores were observed to have formed in the braze joint in several samples.

Table XXVI shows the data for Braze System 2, Pt-2Hf vs. Cb-1Zr. The ultrasonic observations are FP at best, with one exception. This braze shows about as great a tendency to dissolve the Cb-1Zr alloy as does Braze 1A. The C-MA samples showed several good shear values, indicating that sound brazes are obtainable under a variety of time and temperature conditions. However, several of the C-WA braze samples were broken in our attempts to remove the rundown braze material and could not be tested in shear. The brazes themselves appeared to be brittle, as evidenced by the fractures within the brazes (B/B) as opposed to being at the braze-ceramic interface (B/C), and the presence of the many cracked and crumbled braze fracture regions.

Indications of the vacuum integrities of the as-brazed joints C-MA-9 and C-MA-10 were obtained by drilling a 1/16-inch hole along the center-line of the metal member to the braze interface in each sample. The brazes were then examined by using a helium mass spectrometer, and by surrounding the periphery of the braze with a small plastic bag which was filled with helium. Neither of the samples showed any evidence of a leak.

Table XXVII shows the data for Braze System 3, V-2Ce vs. Cb-1Zr. The braze material appeared to remain in place, and to produce good appearing bonds. The C-MA series also showed good ultrasonic test results, but the C-WA series was poor. The C-MA shear test data corroborated the U - S data in that high shear values were obtained, but except for C-WA-1,

TABLE XXIV*

Braze Evaluation Factor Codes - Screening Tests

Metal Surf

Describes the metal alloy, the surface coating material and the ceramic material: C represents Cb-1Zr alloy, T represents T-111 alloy, M represents a molybdenum coating, W represents a tungsten coating, A represents an alumina ceramic, and B represents a beryllia ceramic.

Braze Visual

Describes the external appearance of the braze joint. G implies no rundown of the braze, and a good fillet around the joint; RD describes the condition in which the braze has obviously run out of the joint and downward along the metal member; XRD describes an excessive rundown condition; Dp describes one drop showing out of the joint, 2 Dp describes two drops showing, C indicates the ceramic has cracks; NM describes a not-melted condition; O describes a joint in which the button is offset from the metal rod; and F denotes the presence of an unmelted braze fin in the braze region.

U-S

Ultrasonic data are classified in five groups. G, good; GF, good to fair; F, fair; FP, fair to poor; and P, poor. The asterisk indicates evaluations made using the photographic technique.

Ceram Visual

Describes the color of the ceramic at the braze break surface. All colors are rather faint, at their strongest, but the intensity of color (for those elements which form colored species) is a rough indication of the amount of interaction and the amount of diffusion into the ceramic.

Shear

This is the shear failure load. In the early tests a 1000 lb load cell was used, and some samples appeared to be stronger than 1000 lb. After reducing their loads from 950-1000 lb, they were reloaded and all failed in the mid-range. Because of the uncertainty of the actual breaking strength, their values are reported as > XXX. The second load cell used was a 5000 lb cell, but, after its installation, no samples exceeded 1000 lb to failure. The shear strength in psi can

*This table is the code listing for the entries in Tables XXV through XXXVIII.

evaluated by multiplying the load in lbs by 20.4 in^{-2}, the reciprocal of the area of a 1/4-inch rod.

Break

This column describes the location of the break. The position is indicated by the slash. In some cases a break was observed in more than one location. For example, the symbol B/C/C indicates the break to be partly at the braze-ceramic interface and partly in the ceramic itself.

Braze

This column describes the appearance of the fracture surface of the braze. X denotes the presence of carcks, †denotes a crumbled braze, p indicates the presence of pores, t indicates the braze appears thin, and O indicates an intact (uncracked) braze surface.

TABLE XXV

BRAZE TEST SUMMARY - SYSTEM NO. 1A

Braze	Metal Surf.	No.	Temp. °C	Time sec	Braze Visual	U-S	Ceram Visual	Shear‡ lb	Shear N/m^2	Break	Braze
1A Pt - 1Ce	C-MA	1	1720	30	XRD	FP	Yellow	150	2.1×10^7	B/C	0
		2	1710	30	G	P	Yellow	220	3.1×10^7	B/C	P
		3	1700	30	G	F	Yellow	-	-	B/C	P
		4	1690	120	XRD	P*	Yellow	510	7.2×10^7	M/B	†
		5	1740	120	XRD	-	-	-	-	-	-
1A Pt - 1Ce	C-WA	1	1720	30	XRD	P	Yellow	-	-	B/C	P
		2	1710	30	RD	P	Yellow	410	5.8×10^7	B/B/C/C	X†
		3	1700	30	XRD	P	Yellow	170	2.4×10^7	B/C	P
		4	1690	120	XRD	P*	Yellow	400	5.6×10^7	B/C	†
		5	1740	120	2 Dp	P*	Yellow	110	1.55×10^7	B/C	0

‡For the test sample, the shear stress in psi is 20.4 times the shear load in lb.

TABLE XXVI

BRAZE TEST SUMMARY - SYSTEM NO. 2

Braze	Metal Surf.	No.	Temp. °C	Time sec	Braze Visual	U-S	Ceram Visual	Shear‡ lb	Shear N/m^2	Break	Braze
2. Pt - 2Hf	C-MA	1	1680	30	NM	-	-	-	-	-	-
		2	1700	30	NM	-	-	-	-	-	-
		3	1735	30	XRD	P	White	960	1.35×10^8	M/B/C	†
		4	1720	30	Dp	FP	White	-	-	B/C	†
		5	1710	30	RD	FP	White	680	9.6×10^7	M/B/C	X
		6	1700	30	XRD	FP	White	360	5.1×10^7	M/B	†
		7	1690	120	RD	FP*	White	810	1.14×10^8	M/B/B	-
		8	1740	120	Dp	P*	White	590	8.3×10^8	M/B/B	-
		9	1740	30	XRD0	FP*	White	340	4.8×10^8	M/B	†
		10	1740	30	XRD0	FP*	White	200	2.8×10^8	M/B/C	†
2. Pt - 2Hf	C-WA	1	1680	30	NM	-	-	-	-	-	-
		2	1700	30	NM	-	-	-	-	-	-
		3	1735	30	XRD	P	White	-	-	M/B	0
		4	1720	30	XRD	P	White	80	1.1×10^7	B/C	t
		5	1710	30	XRD	-	-	-	-	-	t
		6	1700	30	XRD	G	-	-	-	-	t
		7	1690	120	NM	-	-	-	-	-	-
		8	1740	120	Dp	P*	White	690	9.7×10^7	B/C/C	X

‡For the test sample, the shear stress in psi is 20.4 times the shear load in lb.

TABLE XXVII

BRAZE TEST SUMMARY - SYSTEM NO. 3

Braze	Metal Surf.	No.	Temp. °C	Time sec	Braze Visual	U-S	Ceram Visual	Shear‡ lb	Shear N/m^2	Break	Braze
3. V - 2Ce	C-MA	1	1869	30	G	G	Yellow	480	6.9×10^7	-	X
		2	1853	120	G	G	Yellow	710	1.9×10^8	B/C	X
		3	1853	30	XRD	GF	Yellow	660	9.3×10^7	B/C	bt
		4	1843	120	G	P	Yellow	380	5.3×10^7	B/C	bXt
		5	1870	120	G	F*	Yellow	180	2.5×10^7	B/C/C	p
		6	1885	30	RDO	GF*	Yellow	230	3.2×10^7	B/C	t
		7	1855	120	G	GF*	Yel-Grn	160	2.2×10^7	B/C	bp
		8	1855	120	Dp	P*	Yellow	60	8.5×10^6	B/C/C	bpX
		9	1855	120	O	F*	Yellow	540	7.6×10^7	B/C/C	p
		10	1855	120	O	F*	-	-	-	-	-
3. V - 2Ce	C-WA	1	1869	30	G	FP	Yellow	>950	$>1.33 \times 10^8$	B/C	X
		2	1830	120	NM	-	-	-	-	-	-
		3	1842	120	G	P	Yellow	410	5.8×10^7	B/C/C	t
		4	1854	30	G	P	Yellow	140	2.0×10^7	B/C	bX
		5	1854	120	Dp	-	Yellow	120	1.7×10^7	B/C	bX
		6	1870	120	2Dp	P*	Yellow	300	4.2×10^7	B/C	bt
		7	1885	30	-	GF*	Yellow	360	5.1×10^7	B/C	t

‡For the test sample, the shear stress in psi is 20.4 times the shear load in lb.

the shear values of the C-WA samples were lower. In all cases, the post-shear test examination of the braze showed cracks and a crumbled appearance.

Table XXVIII shows the data for Braze System 4, V-2Hf vs. Cb-1Zr. This braze tended to remain in place in the joint, but the joint quality as measured by U - S ranged from good to poor. Several anomalies appeared in the correspondence between the U - S and the shear test data. C-MA-1, rated G, showed only a 410 lb (1820 N) shear break; but C-MA-3, rated F, showed a 690 lb (3070 N) shear break while C-WA-1, rated FP, showed a > 1000 lb (> 4448 N) shear strength. Sample C-WA-2, rated GF, shows an apparently low value of > 280 lb (> 1245 N), but this is discounted in view of a known error in the shear test procedure -- the cross head was being brought down to the shear test unit at a "fast" rate which was ten times the standard rate of 0.05 inches/minute (0.0212 mm/s), but the head was not stopped soon enough. The break was executed during stopping, and the value recorded happened to be 280 lb.

Table XXIX shows the data for Braze System 5, V-1Zr vs. Cb-1Zr. In general, this braze tended to run out of the joints, although the amount of material leaving the joint was only one drop. The ultrasonic tests made with the scan-trace technique suggest a rather poor behavior, but the shear strengths are quite adequate. In addition, a vacuum integrity test of Sample C-WA-8 showed no leak.

Table XXX shows the data for Braze Systems 6, V-2Ti vs. Cb-1Zr. A variety of joints were produced, ranging in appearance from good to run-down. The U - S data are mixed, with several G ratings and also several P ratings. However, the shear test data are generally favorable.

Table XXXI shows the data for Braze 7, V-10Mo vs. T-111. It has been tested over quite a range of temperatures and neither the molybdenum-nor the tungsten-coated samples show promise. The minimum braze temperature is quite high, 1945°C, just about 100°C below the melting point of the Al_2O_3. The braze does not appear to wet the Al_2O_3 nor to bond well to it, hence the "0" designation for the braze appearance after the shear break. Further, the close scrutiny of the ceramic under a low-power (15X) microscope does show the presence of radial cracks in some of the buttons. It is thought that there are two problems with this braze. One is its very high melting point, which may subject the Al_2O_3 to severe thermal shock upon cooling, and the other is the lack of sufficient chemical reactivity. Although vanadium itself has some tendency to react with Al_2O_3, the presence of the Mo tends to decrease the tendency, so that good bonding is not achieved with this braze alloy.

Table XXXII shows the data for Braze 8, 65V-35Cb vs. T-111. As is shown in the table, it was inadvertently used in two trials each with the Cb-1Zr alloy, and showed rather good shear values, both with the molybdenum- and the tungsten-coated Al_2O_3. The T-111 results are all much poorer, and there is an indication that the braze did not readily wet the ceramic. The wetting of the Al_2O_3 in the C-MA and C-WA tests is ascribed to the dissolution

TABLE XXVIII

BRAZE TEST SUMMARY - SYSTEM NO. 4

Braze	Metal Surf.	No.	Temp. °C	Time sec	Braze Visual	U-S	Ceram Visual	Shear‡ lb	Shear N/m^2	Break	Braze
4. V - 2Hf	C-MA	1	1869	30	2Dp	G	Blue-Grn	410	5.8×10^7	-	-
		2	1869	120	2Dp	GF	Sea Grn	940	1.32×10^8	B/C/C	X
		3	1853	120	G	F	Pale Grn	690	9.7×10^7	B/C/C	X
		4	1853	30	Dp	G	White	880	1.24×10^8	B/C/C	X
		5	1843	120	G	FP	White	340	4.8×10^7	B/C/C	†
		6	1870	120	O	GF*	Green	430	6.0×10^7	B/C	†
		7	1885	30	G	G*	Green	240	3.4×10^7	B/C	†
		8	1860	60	G	GF*	Green	500	7.0×10^7	B/C/C	p
4. V - 2Hf	C-WA	1	1869	30	2Dp	FP	-	>1000	$>1.4 \times 10^8$	C/C	X
		2	1869	120	XRD	GF	Pale Grn	> 280	$>3.9 \times 10^7$	B/C	0
		3	1830	120	NM	-	-	-	-	-	-
		4	1842	120	F	P	White	250	3.5×10^7	B/C/C	pt
		5	1854	30	G	P	Pale Grn	480	6.8×10^7	B/C/C	†
		6	1854	120	2Dp	-	Pale Grn	420	5.9×10^7	B/C/C	0
		7	1870	120	Dp	GF*	Green	670	9.4×10^7	B/C	X†
		8	1885	30	-	GF*	Green	440	6.2×10^7	B/C	0
		9	1870	60	Dp	GF*	Green	-	-	B/C	0

‡For the test sample, the shear stress in psi is 20.4 times the shear load in lb.

TABLE XXIX

BRAZE TEST SUMMARY - SYSTEM NO. 5

Braze	Metal Surf.	No.	Temp. °C	Time sec	Braze Visual	U-S	Ceram Visual	Shear‡ lb	Shear N/m^2	Break	Braze
5. V - 1 Zr	C-MA	1	1869	30	Dp	FP	Pale Grn	525	7.4×10^7	B/C	X
		2	1853	120	Dp	G	Sea Grn	680	9.6×10^7	B/C	†
		3	1853	30	G	P	White	640	9.0×10^7	B/C	†
		4	1843	120	Dp	P	White	320	4.5×10^7	B/C	X†
		5	1870	120	O	GF*	Green	640	9.0×10^7	B/C	0
		6	1885	30	RDO	GF*	Pale Grn	390	5.5×10^7	B/C	X
		7	1860	60	3DpO	G*	White	220	3.1×10^7	B/C	0
5. V - 1Zr	C-WA	1	1869	30	Dp	GF	Green	>1000	$>1.4 \times 10^8$	C/C	X
		2	1830	120	NM	-	-	-	-	-	-
		3	1842	120	Dp	P	White	510	7.2×10^7	B/C	X
		4	1854	30	Dp	P	Pale Grn	430	6.0×10^7	B/C	X
		5	1854	120	Dp	FP	Sea Grn	530	7.5×10^7	B/C/C	X
		6	1870	120	Dp	G*	Green	670	9.4×10^7	B/C/C	†
		7	1885	30	-	G*	Green	280	3.9×10^7	B/C/C	0
		8	1870	60	G	G*	Green	-	-	B/C	0

‡For the test sample, the shear stress in psi is 20.4 times the shear load in lb.

TABLE XXX

BRAZE TEST SUMMARY - SYSTEM NO. 6

Braze	Metal Surf.	No.	Temp. °C	Time sec	Braze Visual	U-S	Ceram Visual	Shear‡ lb	Shear N/m^2	Break	Braze
6. V - 2Ti	C-MA	1	1869	30	Dp	FP	-	-	-	C/C	X
		2	1853	120	XRD	F	Grey	630	8.9×10^7	B/C/C	X
		3	1853	30	G	G	Grey-Brn	820	1.15×10^8	B/C/C	X†
		4	1843	120	O	P	-	-	-	-	-
		5	1870	120	RD	P*	-	200	2.8×10^7	C/C	-
		6	1885	30	DpO	G*	Grey	500	7.0×10^7	B/C/C	X†
		7	1860	60	XRD	GF*	Grey	580	8.2×10^7	B/C/C	0
6. V - 2Ti	C-WA	1	1869	30	2Dp	F	Grey	>1000	$>1.4 \times 10^8$	B/C/C	X
		2	1830	120	NM	-	-	-	-	-	-
		3	1842	120	Dp	P	Grey-Brn	560	7.9×10^7	B/C/C	†
		4	1854	30	Dp	P	Grey	420	5.9×10^7	B/C/C	0
		5	1854	120	G	-	Grey	380	5.3×10^7	B/C	X
		6	1870	120	RD	G*	Grey	400	5.6×10^7	B/C/C	0
		7	1885	30	-	F*	Grey	400	5.6×10^7	B/C/C	†
		8	1870	60	XRD	G*	Grey	460	6.5×10^7	B/C	X

‡For the test sample, the shear stress in psi is 20.4 times the shear load in lb.

TABLE XXXI

BRAZE TEST SUMMARY - SYSTEM NO. 7

Braze	Metal Surf.	No.	Temp. °C	Time sec	Braze Visual	U-S	Ceram Visual	Shear‡ Lb	Shear N/m^2	Break	Braze
7. V - 10Mo	T-MA	1	1850	30	NM	-	-	-	-	-	-
		2	1885	30	NM	-	-	-	-	-	-
		3	1945	30	-	P*	Blue-Grn	110	1.55×10^7	B/C	0
		4	1945	120	C	P*	Blue-Grn	140	2.0×10^7	B/C	0
		5	1980	30	-	-	White	-	-	B/C	0
		6	1960	30	C	FP*	Blue-Grn	30	4.2×10^6	B/C	0
		7	1960	120	C	P*	Blue-Grn	50	7.0×10^6	B/C	0
7. V - 10Mo	T-WA	1	1850	30	NM	-	-	-	-	-	-
		2	1885	30	NM	-	-	-	-	-	-
		3	1945	30	-	FP*	Blue-Grn	150	2.1×10^7	B/C	0
		4	1945	120	C	P*	Blue-Grn	20	2.8×10^6	B/C	0
		5	1980	30	-	P*	White	30	4.3×10^6	B/C	0
		6	1960	30	C	FP*	Blue-Grn	130	1.8×10^7	B/C	0
		7	1960	120	C	FP*	Blue-Grn	80	1.1×10^7	B/C	0

‡For the test sample, the shear stress in psi is 20.4 times the shear load in lb.

TABLE XXXII

BRAZE TEST SUMMARY - SYSTEM NO. 8

Braze	Metal Surf.	No.	Temp. °C	Time sec	Braze Visual	U-S	Ceram Visual	Shear‡ lb	Shear N/m^2	Break	Braze
8. 65V-35Cb	C-MA	1	1820	30	NM	-	-	-	-	-	-
	C-MA	2	1870	30	G	G	Blue-Grn	930	1.3×10^8	B/C	X
	T-MA	3	1869	120	G	P	Blue-Grn	310	4.4×10^7	B/C	0
	T-MA	4	1853	120	G	P	Blue-Grn	160	2.2×10^7	B/C	p
	T-MA	5	1869	30	RD	P	Blue-Grn	30	4.2×10^6	B/C	0
	T-MA	6	1870	300	O	-	Blue-Grn	80	1.1×10^7	B/C	0
	T-MA	7	1885	120	Dp	FP*	Blue-Grn	100	1.4×10^7	B/C	0
8. 65V-35Cb	C-WA	1	1820	30	NM	-	-	-	-	-	-
	C-WA	2	1870	30	G	FP	Pale Grn	>1000	1.4×10^8	B/C	X
	T-WA	3	1869	120	Dp	P	Blue-Grn	310	4.4×10^7	B/C	0
	T-WA	4	1853	120	G	P	Grn Edge	130	1.8×10^7	B/C	t
	T-WA	5	1869	30	G	P	Blue-Grn	80	1.1×10^7	B/C	0
	T-WA	6	1870	300	G	F*	Blue-Grn	150	2.1×10^7	B/C	0
	T-WA	7	1885	120	Dp	F*	Blue-Grn	210	3.0×10^7	B/C	0

‡For the test sample, the shear stress in psi is 20.4 times the shear load in lb.

of some Cb-1Zr, whose Zr then participated in the bonding. The amount of dissolution of the T-111 alloy is small so that, although the hafnium present in the T-111 presumably could act as a reactive wetting agent as does the zirconium in Cb-1Zr, the amount of hafnium available is apparently too small to be effective. As a consequence of the poor bonding, the U - S evaluations are generally poor, and the shear strengths of the T-MA and T-WA samples are low.

Table XXXIII shows the data for Braze 9, 64V-34Cb-2Zr vs. Cb-1Zr. In general, the braze performs well on the button samples, although typically a drop of braze does come out of the braze region. The U - S evaluations are quite good, as are the shear values. A vacuum integrity test on Sample C-MA-6 showed no leak.

Table XXXIV shows the data for Braze System 10, 64V-34Cb-2Ti vs. Cb-1Zr. This braze is a modification of Braze 8 with a 2% addition of Ti which was used to act as a wetting agent. Its performance is markedly better than that of Braze 8, although the reason for greater success may be that Braze 10 is used with Cb-1Zr alloy, and all of the brazes tested with T-111 have shown poor performance. In this braze system, both the molybdenum- and the tungsten-coated samples show some very good shear behavior but the tungsten-coated samples appear superior. In this system there was the presence of a fin in many of the braze joints. This appeared to be the result of border-line melting of the braze, with possibly a thin film of surface oxidation remaining on the braze from the rolling process. The U - S examinations are, at best, fair; but many of the samples showed shear strengths of > 500 lb (> 2224 N).

Table XXXV shows the data for Braze System 11A, 98V-2Hf vs. T-111. Nine attempts to form a braze with this system were made. The melting point of the braze was found to be above 1855°C in this system. The ceramic buttons were found to have radial cracks in the samples in which the braze did melt. The U - S measurement showed G and F evaluations, although only modest strengths were found. Both samples, T-MA-3 and T-WA-3, were tested for their vacuum integrity and proved to have tight joints, even though the ceramic was cracked at their surfaces. Typical peripheral cracks in the Al_2O_3 ceramic are shown in Figures 39 and 40. Such a braze is designated with a "C" notation in the Braze Visual column in Tables XXV through XXXVIII.

Table XXXVI shows the data for Braze System 12A, 64V-34Cb-2Zr vs. T-111. Nine tests were made. The four T-MA samples all showed rather good-appearing joints, although the ceramic buttons all showed radial peripheral cracks. The five T-WA samples all showed that a drop of braze had flowed out of the joint, and the presence of radial cracks in the ceramic buttons. All joints show GF or G in the ultrasonic examinations. The shear strengths are low to moderate values.

TABLE XXXIII

BRAZE TEST SUMMARY - SYSTEM NO. 9

Braze	Metal Surf.	No.	Temp. °C	Time sec	Braze Visual	U-S	Ceram Visual	Shear‡ lb	Shear N/m^2	Break	Braze
9. 64V-34Cb-2Zr	C-MA	1	1855	120	G	G*	Pale Grn	530	7.5×10^7	B/C	X
		2	1870	120	2DpO	GF*	Green	300	4.2×10^7	B/C	X
		3	1870	30	G	GF*	Green	760	1.07×10^8	B/C	†
		4	1885	30	Dp	G*	Green	640	9.0×10^7	B/C	0
		5	1840	120	Dp	GF*	Green	240	3.4×10^7	B/C	0
		6	1870	60	2DpO	G*	Green	320	4.5×10^7	B/C	0
9. 64V-34Cb-2Zr	C-WA	1	1855	120	DpO	GF*	Pale Grn	260	3.6×10^7	B/C	Xp
		2	1870	120	2DpO	GF*	Green	300	4.2×10^7	B/C	Xp
		3	1870	30	G	FP*	Green	880	1.24×10^7	B/C/C	†
		4	1885	30	Dp	GF*	Green	560	7.9×10^7	B/C	†
		5	1840	120	2Dp	G*	Green	770	1.08×10^8	B/C	†
		6	1870	60	XRD	G*	Green	660	9.3×10^7	B/C	0

‡For the test sample, the shear stress in psi is 20.4 times the shear load in lb.

TABLE XXXIV

BRAZE TEST SUMMARY - SYSTEM NO. 10

Braze	Metal Surf.	No.	Temp. °C	Time sec	Braze Visual	U-S	Ceram Visual	Shear‡ lb	Shear N/m^2	Break	Braze
10. 64V-34Cb-2Ti	C-MA	1	1820	30	NM	-	-	-	-	-	-
		2	1870	30	G	P	Brown	900	1.27×10^8	B/C/C	X
		3	1853	120	FO	F	Buff	970	1.36×10^8	B/C/C	X
		4	1853	300	FO	P	Pale Rose	320	4.5×10^7	B/C	t
		5	1860	120	F	P	Pale Rose	520	7.3×10^7	B/C	Xp
		6	1870	300	OFRD	GF*	Rose	550	7.7×10^7	B/C/C	Xp
		7	1885	120	Dp	GF*	Tan	460	6.5×10^7	B/C	X
		8	1855	120	Dp	G*	Grey	760	1.07×10^8	B/C/C	†
		9	1855	120	DpOF	G*	Grey	660	9.3×10^7	B/C/C	p
		10	1855	120	FO	GF*	-	-	-	-	-
		11	1855	120	G	GF*	Grey	590	8.3×10^7	B/C/C	†
		12	1860	60	2Dp	GF*	Grey	340	4.8×10^7	B/C/C	0
10. 64V-34Cb-2Ti	C-WA	1	1820	30	NM	-	-	-	-	-	-
		2	1870	30	F	FP	Tan	>910	$>1.28 \times 10^8$	C/C	X
		3	1853	120	F	F	-	80	1.1×10^7	B/M	0
		4	1853	300	F	P	Rose	520	7.3×10^7	B/C/C	†
		5	1860	120	F	P	Rose	520	7.3×10^7	B/C/C	Xp
		6	1870	300	RDFO	GF*	Tan	550	7.7×10^7	B/C	0
		7	1885	120	RDF	G*	Tan	570	8.0×10^7	B/C/C	X
		8	1870	60	Dp	GF*	Grey	410	5.8×10^7	B/C	†

‡For the test sample, the shear stress in psi is 20.4 times the shear load in lb.

TABLE XXXV

BRAZE TEST SUMMARY - SYSTEM NO. 11A

Braze	Metal Surf.	No.	Temp. °C	Time sec	Braze Visual	U-S	Ceram Visual	Shear‡ lb	Shear* N/m^2	Break	Braze
11A. V - 2Hf	T-MA	1	1855	30	NM	P*	-	20	2.8×10^6	M/B	-
		2	1855	120	NM	P*	White	-	-	M/B	-
		3	1870	30	GC	G*	Green	180	2.5×10^7	B/C	0
		4	1885	30	RDC	G*	Green	120	1.7×10^7	B/C	0
11A. V - 2Hf	T-WA	1	1855	30	NM	P*	-	-	-	M/B	-
		2	1855	120	NM	P*	White	-	-	M/B	-
		3	1870	30	GC	F*	Green	240	3.4×10^7	B/C	0
		4	1885	30	GC	GF*	Green	250	3.5×10^7	B/C	0
		5	1885	30	GC						

‡For the test samples, the shear stress in psi is 20.4 times the shear load in lb.

Figure 39. Peripheral Crack in the Ceramic in an Alumina-to-T-111 Alloy Braze, 5X

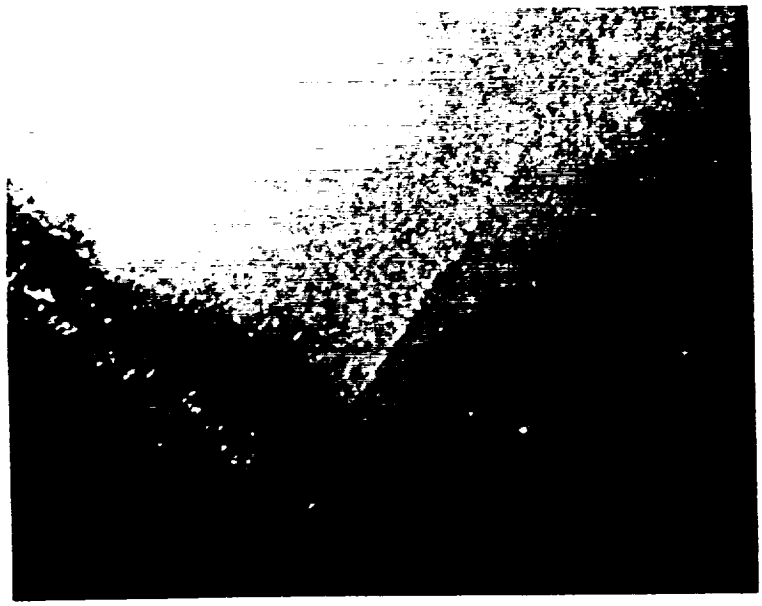

Figure 40 Peripheral Crack in the Ceramic in an Alumina-to-T-111 Alloy Braze, 50X

TABLE XXXVI

BRAZE TEST SUMMARY - SYSTEM NO. 12A

Braze	Metal Surf.	No.	Temp. °C	Time sec	Braze Visual	U-S	Ceram Visual	Shear‡ lb	Shear N/m^2	Break	Braze
12A. 64V-34Cb-2Zr	T-MA	1	1855	30	GC	GF*	Grey	310	4.4×10^7	B/C/C	0
		2	1855	120	GC	GF*	31 Grn	140	2.0×10^7	B/C/C	0
		3	1870	30	GC	F*	Green	-	-	B/C	0
		4	1885	30	DpC	G*	Bl Grn	240	3.4×10^7	B/C	0
12A. 64V-34Cb-2Zr	T-WA	1	1855	30	DpOC	GF*	Grey Grn	200	2.8×10^7	B/C	0
		2	1855	120	DpC	GF*	Green	100	1.4×10^7	B/C/C	0
		3	1870	30	DpC	GF*	Grey Grn	340	4.8×10^7	B/C	0
		4	1885	30	2DpC	FP*	Bl Grn	180	2.5×10^7	B/C/C	0
		5	1870	30	GC	-	Green	220	3.1×10^7	B/C	0

‡For the test sample, the shear stress in psi is 20.4 times the shear load in lb.

Table XXXVII shows the data for Braze System 13A, 90V-8Mo-2Zr vs. T-111. Seven tests were made, and all showed cracked ceramic buttons and braze melting points just below 1940°C, about 75°C above the melting points of the vanadium-base brazes.

Table XXXVIII shows the data obtained in a brief study designed to further investigate the formation of a braze bond to T-111 alloy. Ten attempts were made to bond to Al_2O_3. The most significant finding from these brazes is that the alumina cracked in eight of them. The bonding to the ceramic was greater than was observed for Brazes 7 and 8. This is attributed to the action of the Zr and the Ti in these brazes. The greater incidence of cracking is thought to be in part due to the better adherence of the brazes, coupled with the difference in thermal expansion between the T-111 and the Al_2O_3. This difference amounts to 0.30 percent at 1800°C. If the system cools elastically from this temperature, the maximum stress in a one-inch (2.54 cm) diameter alumina section becomes 50,000 psi (3.45 x $10^8 N/m^2$) tension. For an Al_2O_3 : Cb-1Zr system, the expansion difference is 0.06 percent. This itself results in a lower stress by a factor of five. A further reduction is caused by the lower modulus of elasticity of the Cb-1Zr, so that the maximum stress in a one-inch (2.54 cm) diameter alumina section in the Al_2O_3 : Cb-1Zr joint becomes only 5700 psi (3.93 x $10^7 N/m^2$) tension. These stress values are based upon the assumption that there is no ductility in the braze layer, so that it is very unlikely that these stresses would ever actually be achieved. However, the potential for the development of rather high shear stresses in Al_2O_3 : braze : T-111 systems is present.

The last three entries in Table XXXVII show the results of tests of three gettered brazes in joining T-111 alloy to BeO buttons. These tests were prompted by the high prevalence of cracking in the Al_2O_3 buttons when they are joined to T-111 alloy. In the T-111 : BeO System, the expansion difference is much less than that in the T-111 : Al_2O_3 system. None of these show promise.

Table XXXIX was prepared as a summary of the data from Tables XXV through XXXVII in which the braze tests are listed in the descending order of breaking strength. The ultrasonic evaluations for these brazes are also shown. Braze attempts which did not yield a breaking strength have been omitted. Further reduction and evaluation of these data is described in the text, p. 25 ff.

TABLE XXXVII

BRAZE TEST SUMMARY - SYSTEM NO. 13A

Braze	Metal Surf.	No.	Temp. °C	Time sec	Braze Visual	U-S	Ceram Visual	Shear‡ lb	Shear N/m^2	Break	Braze
13A. 90V-8Mo-2Zr	T-MA	1	1940	30	C	G*	Bl Grn	230	3.2×10^7	B/C	0
		2	1950	30	GC	G*	Bl Grn	290	4.1×10^7	B/C/C	0
		3	1960	30	C	GF*	Bl Grn	260	3.7×10^7	B/C/C	0
13A. 90V-8Mo-2Zr	T-WA	1	1940	30	GC	F*	Bl Grn	100	1.4×10^7	B/C/C	0
		2	1950	30	C	F*	Bl Grn	200	2.8×10^7	B/C/C	0
		3	1960	30	C	GF*	Bl Grn	240	3.4×10^7	B/C	0
		4	1950	30	GC	-	Bl Grn	120	1.7×10^7	B/C	0

‡For the test sample, the shear stress in psi is 20.4 times the shear load in lb.

TABLE XXXVIII

BRAZE TEST SUMMARY - MISCELLANEOUS T-111 SYSTEMS

Braze	Metal Surf.	No.	Temp. °C	Time sec	Braze Visual	U-S	Ceram Visual	Shear‡ lb	Break	Braze
V-1Zr	T-MA	1	1885	120	C	GF*	Bl Grn	90	B/C	-
		2	1870	120	DpC	GF*	Bl Grn	120	B/C	0
		3	1885	30	DpC	GF*	Green	160	B/C	0
V-1Zr	T-WA	1	1885	120	C	GF*	Bl Grn	260	B/C	-
		2	1870	120	C	GF*	-	-	-	-
		3	1885	30	DpC	GF*	Green	160	B/C	0
64V-34Cb-2Ti	T-MA	1	1885	120	FC	F*	Grey	420	B/C/C	Xp
		2	1870	120	XRDC	G*	Grey	300	B/C	0
64V-34Cb-2Ti	T-WA	1	1885	120	F	F*	Grey	400	B/C/C	p
		2	1870	120	DpC	GF*	Grey	380	B/C/C	0
64V-34Cb-2Zr	T-WB	1	1870	30	DpFC	-	Grey	50	B/C/C	0
V-2Hf	T-WB	1	1885	30	NMC	-	White	180	M/B/C	0
90V-8Mo-2Zr	T-WB	1	1950	30	-	-	Grey	140	B/C/C	0

‡For the test sample, the shear stress in psi is 20.4 times the shear load in lb.

TABLE XXXIX

SCREENING TEST STRENGTH AND

ULTRASONIC EVALUATION SUMMARY

Braze	Sample	Strength (lb)	Strength N	U-S	Braze	Sample	Strength (lb)	Strength N	U-S
1A	C-MA-4	510	2260	P*	4	C-MA-2	940	4180	GF
1A	C-MA-2	220	977	P	4	C-MA-4	880	3910	G
1A	C-MA-1	150	667	FP	4	C-MA-3	690	3070	F
1A	C-WA-2	410	1820	P	4	C-MA-8	500	2220	GF*
1A	C-WA-4	400	1780	P*	4	C-MA-6	430	1910	GF*
1A	C-WA-3	170	755	P	4	C-MA-1	410	1820	G
1A	C-WA-5	110	480	P*	4	C-MA-5	340	1510	FP
					4	C-MA-7	240	1070	G*
2	C-MA-3	960	4260	P	4	C-WA-1	> 1000	> 4450	FP
2	C-MA-7	810	3600	FP*	4	C-WA-7	670	2980	GF*
2	C-MA-5	680	3020	FP	4	C-WA-5	480	2130	G
2	C-MA-8	590	2620	P*	4	C-WA-8	440	1950	GF*
2	C-MA-6	360	1600	FP	4	C-WA-6	420	1870	-
2	C-MA-9	340	1510	FP	4	C-WA-2	> 280	> 1280	GF
2	C-MA-10	200	890	FP*	4	C-WA-4	250	1110	P
2	C-WA-8	690	3070	P*	5	C-MA-2	680	3020	G
2	C-WA-4	80	358	P	5	C-MA-3	640	2840	P
3	C-MA-2	710	3160	G	5	C-MA-5	640	2840	GF*
3	C-MA-3	660	2930	GF	5	C-MA-1	525	2330	FP
3	C-MA-9	540	2400	F*	5	C-MA-6	390	1730	GF*
3	C-MA-1	480	2140	G	5	C-MA-4	320	1420	P
3	C-MA-4	380	1690	P	5	C-MA-7	220	978	G*
3	C-MA-6	230	1020	GF*	5	C-WA-1	> 1000	> 4450	GF
3	C-MA-5	180	800	F*	5	C-WA-6	670	2980	G*
3	C-MA-8	60	267	P*	5	C-WA-5	530	2360	FP
3	C-WA-1	> 950	> 4220	FP	5	C-WA-3	510	2250	P
3	C-WA-3	410	1820	P	5	C-WA-4	430	1910	P
3	C-WA-7	360	1600	GF*	5	C-WA-7	280	1240	G*
3	C-WA-6	300	1330	P*					
3	C-WA-4	140	622	P					
3	C-WA-5	120	533	-					

TABLE XXXIX (Cont.)

SCREENING TEST STRENGTH AND

ULTRASONIC EVALUATION SUMMARY

Braze	Sample	Strength (lb)	Strength N	U-S	Braze	Sample	Strength (lb)	Strength N	U-S
6	C-MA-3	820	3640	G	9	C-MA-3	760	3380	GF*
6	C-MA-2	630	2800	F	9	C-MA-4	640	2840	G*
6	C-MA-7	580	2580	GF*	9	C-MA-1	530	2360	G*
6	C-MA-6	500	2220	G*	9	C-MA-6	320	1420	G*
6	C-MA-5	200	890	P	9	C-MA-2	300	1330	GF*
6	C-WA-1	> 1000	> 4450	F	9	C-MA-5	240	1070	GF*
6	C-WA-3	560	2490	P	9	C-WA-3	880	3910	FP*
6	C-WA-8	460	2040	G*	9	C-WA-5	770	3420	G*
6	C-WA-4	420	1870	P	9	C-WA-6	660	2930	G*
6	C-WA-6	400	1780	G*	9	C-WA-4	560	2490	GF*
6	C-WA-7	400	1780	F*	9	C-WA-2	300	1330	GF*
6	C-WA-5	380	1690	-	9	C-WA-1	260	1155	GF*
7	T-MA-4	140	622	P*	10	C-MA-3	970	4310	F
7	T-MA-3	110	488	P*	10	C-MA-2	900	4000	P
7	T-MA-7	50	222	P*	10	C-MA-8	760	3380	G*
7	T-MA-6	30	133	FP*	10	C-MA-9	660	2940	G*
7	T-WA-3	150	667	FP*	10	C-MA-11	590	2620	GF*
7	T-WA-6	130	578	FP*	10	C-MA-6	550	2440	GF*
7	T-WA-7	80	356	FP*	10	C-MA-5	520	2310	P
7	T-WA-5	30	133	P*	10	C-MA-7	460	2040	GF*
7	T-WA-4	20	89	P*	10	C-MA-12	340	1510	GF*
8	T-MA-3	310	1380	P	10	C-MA-4	320	1420	P
8	T-MA-4	160	711	P	10	C-WA-2	> 910	> 4040	FP
8	T-MA-7	100	445	FP*	10	C-WA-7	570	2540	G*
8	T-MA-6	80	356	-	10	C-WA-6	550	2440	GF*
8	T-MA-5	30	133	P	10	C-WA-5	520	2310	P
8	T-WA-3	310	138	P	10	C-WA-4	520	2310	P
8	T-WA-7	210	934	F*	10	C-WA-8	410	1820	GF*
8	T-WA-6	150	667	F*	10	C-WA-3	80	356	F
8	T-WA-4	130	578	P	11A	T-MA-3	180	800	G*
8	T-WA-5	80	356	P	11A	T-MA-4	120	533	G*

TABLE XXXIX (Cont.)

SCREENING TEST STRENGTH AND

ULTRASONIC EVALUATION SUMMARY

Braze	Sample	Strength lb	Strength N	U-S	Braze	Sample	Strength lb	Strength N	U-S
11A	T-MA-1	20	89	P*	5	T-MA-3	160	712	GF*
11A	T-WA-4	250	1110	GF*	5	T-MA-2	120	533	GF*
11A	T-WA-3	240	1070	F*	5	T-MA-1	90	400	GF*
12A	T-MA-1	310	1380	GF*	5	T-WA-1	260	1115	GF*
12A	T-MA-4	240	1070	G*	5	T-WA-3	160	712	GF*
12A	T-MA-2	140	622	GF*	10	T-MA-1	420	1870	F*
12A	T-WA-3	340	1510	GF*	10	T-MA-2	300	1330	G*
12A	T-WA-1	200	890	GF*	10	T-WA-1	400	1780	F*
12A	T-WA-4	180	800	FP*	10	T-WA-2	380	1690	GF*
12A	T-WA-2	100	445	GF*					
13A	T-MA-2	290	1290	G*					
13A	T-MA-3	260	1115	GF*					
13A	T-MA-1	230	1020	G*					
13A	T-WA-3	240	1070	GF*					
13A	T-WA-2	200	890	F*					
13A	T-WA-1	100	445	F*					

APPENDIX XI. MOR TEST DATA SUMMARY

The MOR test results are listed in Tables XL and XLI and are shown in graphical form in Figure 12. Eight samples of each braze system were tested, with duplicates at each of four test conditions. Although two data points for each test condition is really too few from which to draw firm quantitative conclusions, the pattern of MOR values as demonstrated by the group of eight test results for each braze system is indicative of the behavior of the braze system. In particular, trends in the temperature and aging effects can be determined. It is interesting to note in Table XL that the 1200°C test MOR values are in many cases higher than those measured at room temperature. This is not unexpected, because it has been found in studies of ceramic materials that the presence of adsorbed moisture on the ceramic surface tends to reduce the apparent tensile (MOR) strength. Another factor of concern in the measurement of ceramic strength by a MOR test is the surface finish and/or the presence of microcracks in the surface. Such factors contribute to the variation in measured MOR test data, so that such data for ceramic systems usually show a significant variation.

TABLE XL

MOR DATA (ENGLISH UNITS)

Braze No.	Composition	MOR, psi			
		As-Brazed Broken at RT	As-Brazed Broken at 1200°C	Aged 100 hr at 1200°C Broken at RT	Aged 1000 hr at 1200°C Broken at RT
2M	PT-2Hf	7640	4450, 7330	3820, 8270	4450, 9550
3M	V-2Ce	7330, 8270	*10820, 7950	8590, 10820	* 8590, 2230
4M	V-2Hf	9860, ** 5090	** - , ** 9860	* 9860, **6360	5720, **8270
4W	V-2Hf	** 5410, 5410	** 8910, 12730	**11460, 10190	5410, 5720
5W	V-1Zr	* 12100, 5090	* - 12420	* 7330, 8910	1910, 4450
6W	V-2Ti	* 9860, ** 7000	9550, 8270	* 11460, *11780	6040, 9550
9M	64V-34Cb-2Zr	9550, 12420	12100, * 14000	8590, 13380	5720, 9550
9W	64V-34Cb-2Zr	* 1910, 10190	**19750, 11140	11780, *11460	4770, 5410
10M	64V-34Cb-2Ti	**11780, > 5720	16240, ** -	**10190, * 6360	11140, **5090
10W	64V-34Cb-2Ti	** 6360, * 12730	** 4770, 7330	* 11140, *14640	6680, * 7330

* Breaks occurred at least partly in the ceramic

**Breaks occurred in the ceramic away from the braze region.

TABLE XLI

MOR DATA (SI UNITS)

Braze No.	Composition	MOR, N/m^2							
		As-Brazed Broken at RT x 10^{-6}		As-Brazed Broken at 1200°C x 10^{-6}		Aged 3.6 x 10^5 s at 1200°C Broken at RT, x 10^{-6}		Aged 3.6 x 10^6 s at 1200°C, Broken at RT, x 10^{-6}	
2M	Pt-2Hf	52.6	-	30.4	50.6	26.3	57.0	30.4	65.9
3M	V-2Ce	50.5	57.0	* 74.6	57.0	59.2	74.6	59.2	15.4
4M	V-2Hf	68.0	**35.1	** -	**68.0	* 68.0	** 43.9	37.4	**57.0
4W	V-2Hf	**37.4	37.4	** 61.5	87.9	**79.0	70.2	37.4	39.4
5W	V-1Zr	* 83.5	35.1	* -	85.8	* 50.5	61.5	13.2	30.7
6W	V-2Ti	* 68.0	**48.4	65.9	57.0	* 79.0	* 81.1	41.6	65.8
9M	64V-34Cb-2Zr	65.8	85.6	83.5	* 99.6	59.2	92.2	32.9	37.4
9W	64V-34Cb-2Zr	* 13.2	70.2	**136.2	76.9	81.2	* 79.0	32.9	37.4
10M	64V-34Cb-2Ti	**81.1	> 39.4	112.0	** -	**70.2	* 43.9	76.8	**35.1
10W	64V-34Cb-2Ti	**43.9	* 87.8	** 32.9	50.5	* 76.9	* 101.0	46.1	* 50.5

* Breaks occurred at least partly in ceramic

**Breaks occurred in the ceramic away from the braze region.

APPENDIX XII. METALLOGRAPHIC, MICROHARDNESS, AND ELECTRON MICROPROBE DATA SUMMARY

The analyses of the Phase I tests involved the evaluation and comparison of metallographic, microhardness, and electron microprobe data. Most of these data are given in this Appendix, but the more quantitative concentration profile measurements are in Appendix XIII.

The metallographic, microhardness, and electron microprobe measurements are made on the same sample, and in order to best illustrate the relationship of the metallographic record and the microhardness profile, both are aligned on the same figure. The 10-hour (3.6×10^4s) samples are labelled "A"; the 100-hour (3.6×10^5s) samples are labelled "B"; the 500-hour (1.8×10^6s) samples are labelled "C"; and the 1000-hour (3.6×10^6s samples are labelled "D". Because many of the electron microprobe line profiles are quite similar, all of the separate traces have not been shown. However, for each system, a listing showing the figure numbers of the actual profiles or of an equivalent line profile is provided on the figure showing the micrograph and the microhardness profile of each of the forty samples tested.

In general, the examinations of the data in the following figures shows that the braze alloys dissolved rather large amounts of the Cb-1Zr alloy, so that in every case the final "braze" composition had Nb(Cb) as a major constituent. Because of this dissolution, niobium (columbium) concentration gradients were produced within the braze region during the brazing period. It is quite probable that the two greatest factors in determining the observed concentration gradients of the components was the extent of the solution of Cb-1Zr alloy during the brazing operation, and the extent of mixing within the liquid braze. Other features of the brazes which are indicated in the following are the braze thickness, the tendency of the braze to react with the Al_2O_3 to form a noticeable reaction-product layer at the surface, the DPH hardness levels and the type of hardness profile, and the general character of the braze.

Braze System 2M (Cb-1Zr/Pt-2Hf/Mo/Al_2O_3). An examination of Figure 41, the micrographic and the microhardness data for Braze System 2M, shows the braze region to be about 2 mils (0.0508 mm) thick in the 10-hour (3.6×10^4s) aged A sample, and that it has a two-phase structure. A rather thin, less than 0.1 mil (0.00254 mm) reaction zone appears at the Al_2O_3 surface. This zone is believed to consist of a mixture of oxides, because of its behavior in the electron microprobe. Zirconium oxide has been found to exhibit a fluorescence when traversed by the microprobe beam. Such a fluorescence was noted in this sample, although it was rather faint compared to the responses seen in some of the other samples.

The 100 gm DPH hardness value found in this Pt-2Hf braze layer is about 650, while that in the Cb-1Zr alloy is about 75, and that in the Al_2O_3 is more than 1000. This braze is a discrete layer and appears as a different phase than that of the Cb-1Zr alloy. This is different from the behavior of the vanadium-containing brazes, whose grains tend to be continuous with those in the Cb-1Zr alloy. The braze layer is also shown in the Back-Scattered

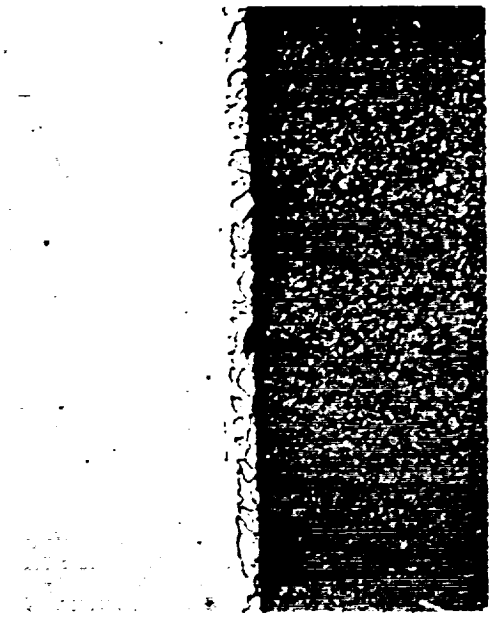

A. Micrograph, 100X

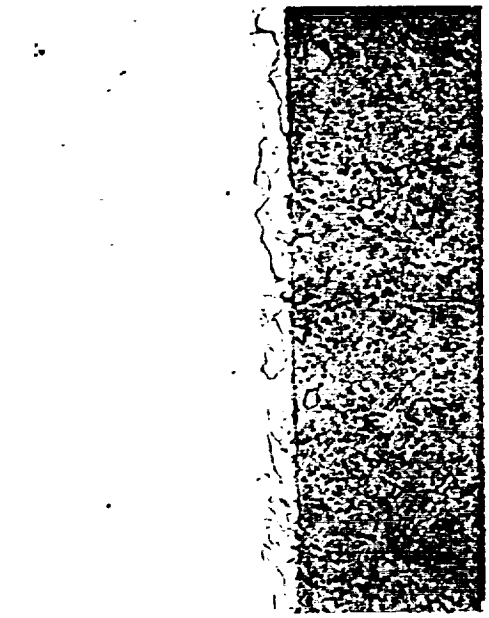

B. Micrograph, 100X

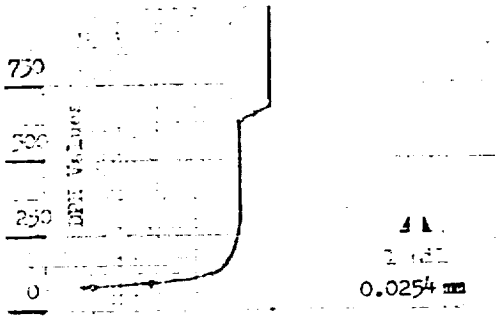

A. Microhardness Profile

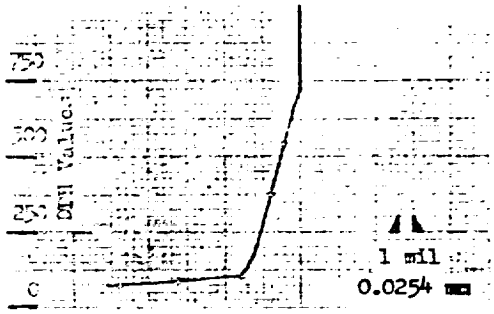

B. Microhardness Profile

Pt:	Figure 44
Hf:	Figure 43
Cb(Nb):	Figure 44
Zr:	Figure 45
Mo:	Figure 45
Al:	Figures 43, 44, 45.

A. Electron Microprobe Line Profile Summary

Pt:	Figure 46
Hf:	Similar to Figure 45
Cb(Nb):	Figure 46
Zr:	Similar to Figure 45
Mo:	Similar to Figure 45
Al:	Figure 46

B. Electron Microprobe Line Profile Summary.

Figure 41. Braze Analysis Data: Braze System 2M (Cb-1Zr/Pt-2Hf/Mo/Al_2O_3) brazed at 1720°C for 60 s. Sample A aged for 10 hrs (3.6×10^4s) at 1200°C; Sample B aged for 100 hrs (3.6×10^5s) at 1200°C.

C. Micrograph, 100X

D. Micrograph, 100X

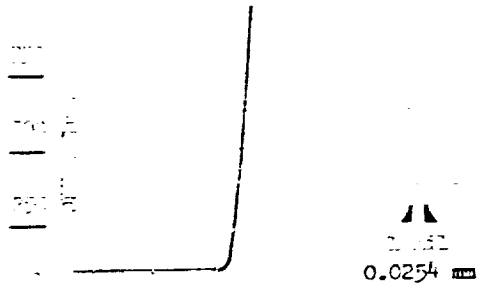

C. Microhardness Profile

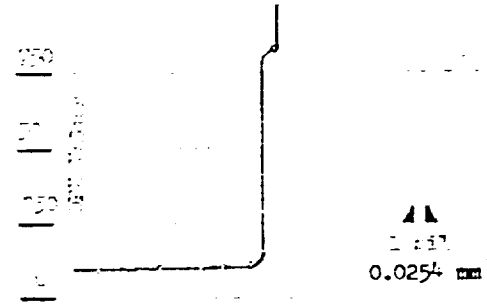

D. Microhardness Profile

Pt:	Figure 47
Hf:	Similar to Figure 43
Cb(Nb):	Figure 47
Zr:	Similar to Figure 45
Mo:	Similar to Figure 45
Al:	Figure 47

C. Electron Microprobe Line Profile Summary

Pt:	Figure 48
Hf:	Similar to Figure 43
Cb(Nb):	Figure 48
Zr:	Similar to Figure 45
Mo:	Similar to Figure 45
Al:	Figure 48

D. Electron Microprobe Line Profile Summary.

Figure 42. Braze Analysis Data: Braze System 2M (Cb-1Zr/Pt-2Hf/Mo/Al_2O_3) brazed at 1720°C for 60s. Sample C aged for 500 hrs (1.8×10^6s) at 1200°C. Sample D aged for 1000 hours (3.6×10^6s) at 1200°C.

Electron Image photograph in Figure 43. In addition, the two-phase structure of a high-platinum (light area) and a low-platinum phase (intermediate darkness area is also clearly shown. The niobium area-scan photograph of Figure 43 shows the expected high amount of niobium (columbium) in the Cb-1Zr alloy region, as evidenced by the nearly white area and the lower amount of niobium (columbium) in the braze. The rather sharp demarcation between the refractory alloy and the braze metal is also demonstrated in that photograph.

The electron microprobe line profiles for the A sample are shown in Figures 43, 44, and 45. The two-phase nature of the braze region is shown in the Nb(Cb) and the Pt profiles of Figure 44. The presence of two levels of Nb and of Pt, plus the correspondence in the braze region of the higher Nb level with the lower Pt level, and the correspondence of the lower Nb level with the higher Pt level is unmistakable evidence of the presence of two distinct Nb-Pt phases.

The presence of such large amounts of Nb(Cb) in the braze is the result of a rather massive dissolution of the Cb-1Zr alloy by the molten braze. Thus, shortly after melting, the braze consists not only of the platinum and its 2% hafnium, but also of considerable amounts of niobium (columbium) and its 1% zirconium from the alloy.

The line profiles of Hf (Figure 43) and of Zr (Figure 45) show concentrations of these elements at the Al_2O_3-braze interface. This is presumed to be the result of chemical action of these Group IV metals with Al_2O_3 with the production of hafnium and zirconium oxides which remain near the interface in the thin reaction zone. The aluminum metal which is freed by the reaction is seen to have dissolved in the braze and to appear at a relatively uniform concentration through the braze. It is also of interest to note that the presence of the high local concentrations of Zr and Hf are also reflected in the existence of a dip in the profiles of the Nb and Pt near the interface.

The molybdenum coating originally put on the Al_2O_3 is seen to have been nominally uniformly dissolved in the braze, as shown by the rather level Mo profile in Figure 45.

The B photomicrograph of Figure 41 shows the braze layer in the 100-hour (3.6×10^5s) aged sample to be about 3 mils (0.0762 mm) thick, and to show the same two-phase character as does the A sample. The reaction zone thickness is barely discernible. The hardness of the braze, however, shows a gradual gradation from the base Cb-1Zr alloy DPH value of 75 to about 650 at the braze-Al_2O_3 interface. Again, there is a sharp demarcation between the Cb-1Zr alloy and the braze. The back-scattered electron image (not shown) was very similar to that of Figure 43, and clearly shows the two phases in the braze.

Figure 46 shows the electron microprobe line profiles for Nb(Cb) and Pt in the B sample. Again, two distinct phases are indicated, as well as a substantial amount of dissolution of the Cb-1Zr alloy. The Hf and Zr line

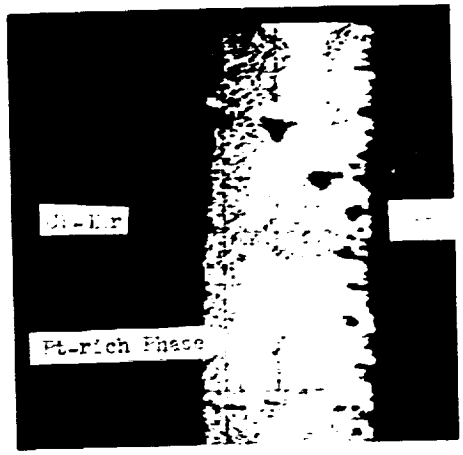

Sample A. Aged 10 hours at 1200°C
Back-Scattered Electron Image, 400X

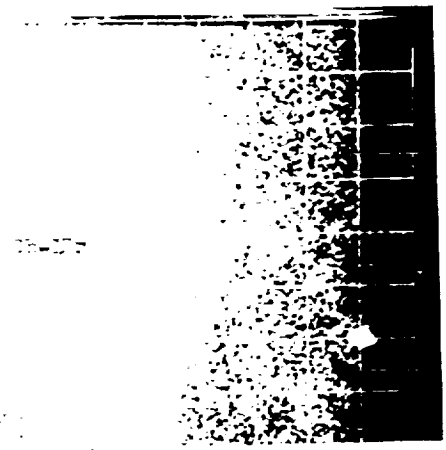

Sample A. Aged 10 hours at 1200°C
Area-Scan for Niobium, 400X

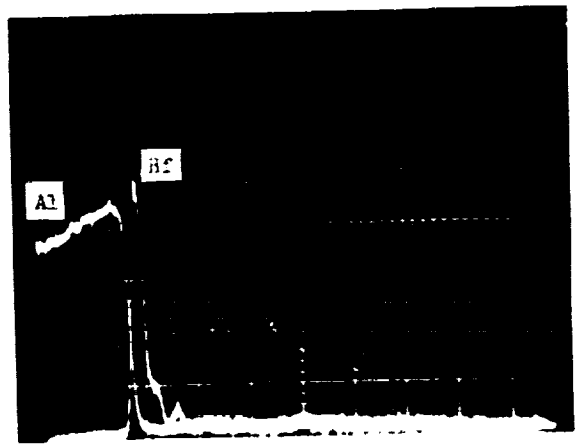

Sample A. Aged 10 hours at 1200°C
Line Profiles, Al and Hf, 800X

Figure 43. Braze Analysis Data: Braze System 2M (Cb-1Zr/Pt-2Hf/Mo/Al_2O_3) brazed at 1720°C for 1 minute.

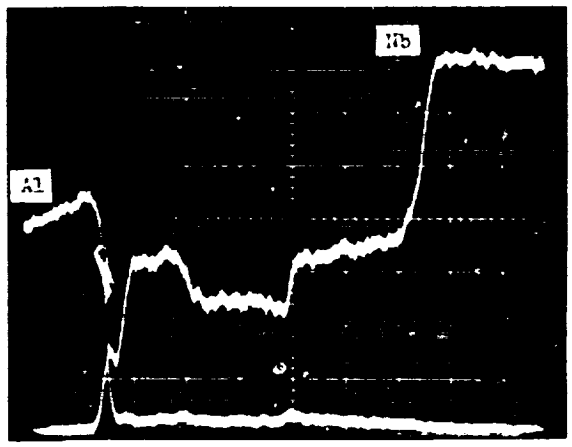

Sample A. Aged 10 hours at 1200°C
Line Profiles, Al and Nb, 800X

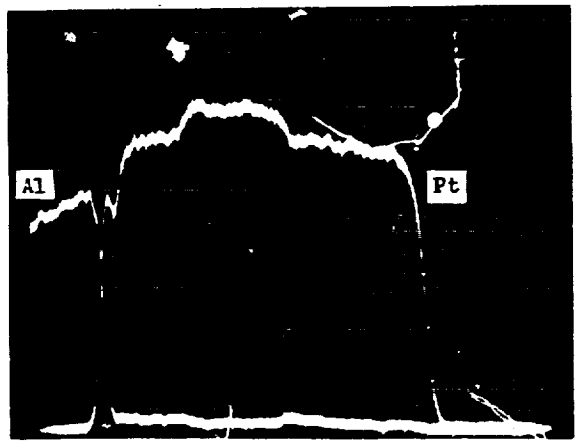

Sample A. Aged 10 hours at 1200°C
Line Profiles, Al and Pt, 800X

Figure 44. Braze Analysis Data: Braze System 2M (Cb-1Zr/Pt-2Hf/Mo/Al_2O_3) brazed at 1720° C for 1 minute.

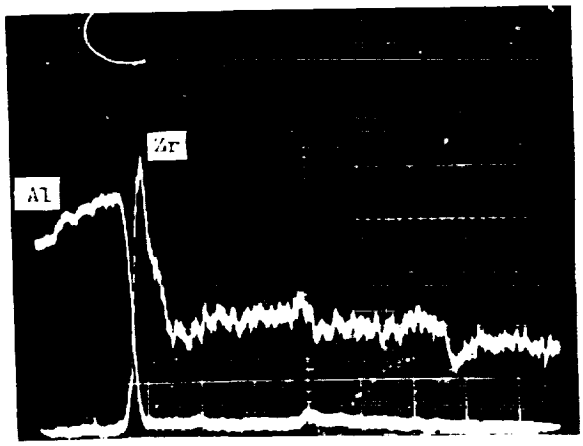

Sample A. Aged 10 hours at 1200°C
Line Profiles, Al and Zr, 800X

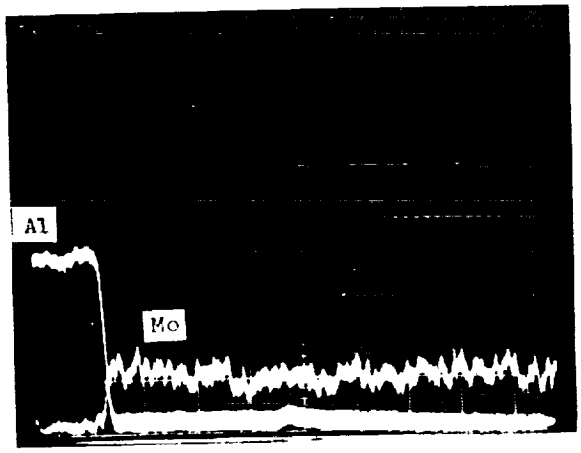

Sample A. Aged 10 hours at 1200°C
Line Profiles, Al and Mo, 800X

Figure 45. Braze Analysis Data: Braze System 2M (Cb-1Zr/Pt-2Hf/Mo/Al_2O_3) brazed at 1720°C for 1 minute.

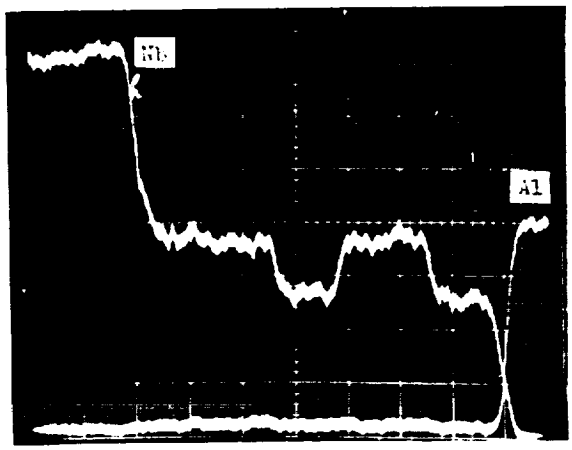

Sample B. Aged 100 hours at 1200°C
Line Profiles, Al and Nb, 800X

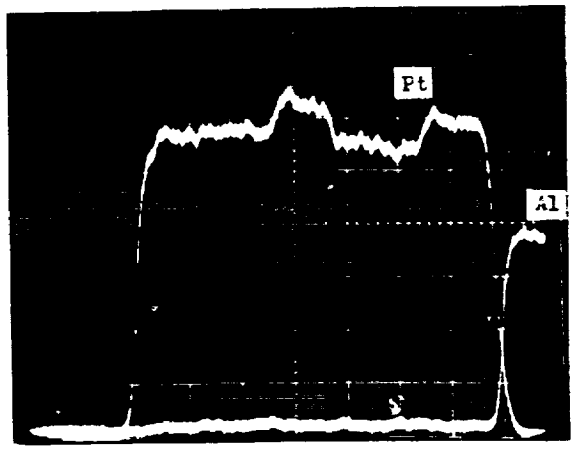

Sample B. Aged 100 hours at 1200°C
Line Profiles, Al and Pt, 800X

Figure 46. Braze Analysis Data: Braze System 2M (Cb-1Zr/Pt-2Hf/Mo/Al_2O_3) brazed at 1720° C for 1 minute.

profiles are similar to those shown in Figures 43 and 45, respectively. However, the corresponding dip in the Nb and Pt line profiles was not observed. The molybdenum line profile was identical to that shown in Figure 45.

The C photomicrograph of Figure 42 shows a very thin braze region, and the microhardness profile corroborates that observation. The reaction zone is very thin. The shadow seen along the braze region is caused by the sloping character of the braze as it slopes downward from the hard Al_2O_3 to the soft Cb-1Zr alloy. The incident light is reflected to the side, and the region appears dark. The nominal braze thickness is only about 2.5 mils (0.0635 mm) thick. The hardness grades sharply from the rather typical DPH value of 75 in the Cb-1Zr to a value of nearly 1000 about one mil (0.0254 mm) from the Al_2O_3 interface. The width of the braze is also shown in Figure 47, which shows the electron microprobe line profiles of Nb and Pt in the C or 500-hour (1.8×10^6s) aged sample. The shapes of these profiles are again typical of the other 2M brazes and show the presence of two phases. Electronics interference was present in the electron microprobe and these traces are more jagged than most.

Again, the Hf, Zr, and Mo traces are not shown, but are similar to those shown in Figures 43, and 45.

The D photomicrograph shown in Figure 42 shows a thin braze layer, as does the corresponding microhardness profile. The braze thickness is about 1.5 mils (0.038 mm). The braze is seen to conform rather well to imperfections in the Al_2O_3 surface. In this photomicrograph, there is a suggestion of the development of an incipient intergranular crack in the Al_2O_3. This may be the result of aging, but it seems that is is more likely to be caused by the character of the Al_2O_3 body. The Al_2O_3 grains are very large. This is atypical. None of the other D samples have such large grains, so it is believed that this sample had the large grains at the outset. Perhaps because such material is weak, and because there was a good bond to the braze, the expansion forces were the cause of the crack.

The DPH hardness value in the braze very near the Al_2O_3 interface is 825, while that in the Cb-1Zr is, as usual, 75-80.

Figure 48 shows the presence of three rather distinct Pt-Nb phases in the D samples and a dip in the Pt and Nb traces at the Al_2O_3 interface. This corresponds to the presence of Hf and Zr concentrations in the interface, similar to those shown in Figures 43 , and 45 although the reaction zone is very thin. The molybdenum, originally deposited on the Al_2O_3 surface, dissolved and was found to be rather uniformly distributed in the braze.

In summary, this 2M braze typically is seen to dissolve significant amounts of Cb-1Zr, and to form Cb-Pt phases of at least three different compositions. The Hf in the braze and the Zr from the dissolved Cb-1Zr alloy become concentrated at the Al_2O_3-braze interface, presumably as a result of reaction with the Al_2O_3. The thickness of the final braze is smaller

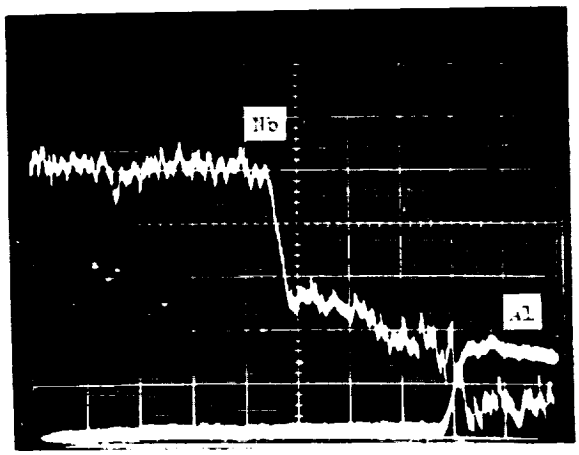

Sample C. Aged 500 hours at 1200°C
Line Profiles, Al and Nb, 800X

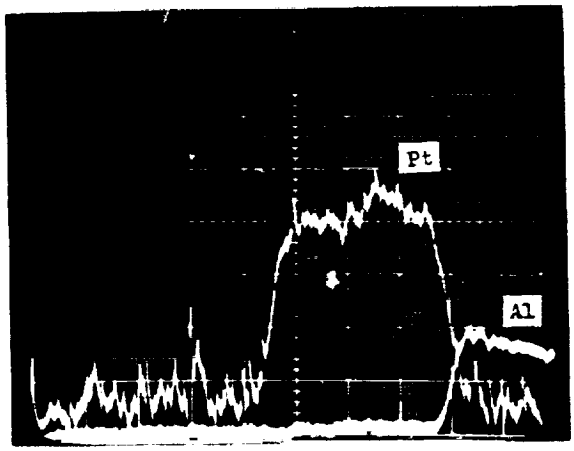

Sample C. Aged 500 hours at 1200°C
Line Profiles, Al and Pt, 800X

Figure 47. Braze Analysis Data: Braze System 2M (Cb-1Zr/Pt-2Hf/Mo/Al_2O_3) brazed at 1720° C for 1 minute.

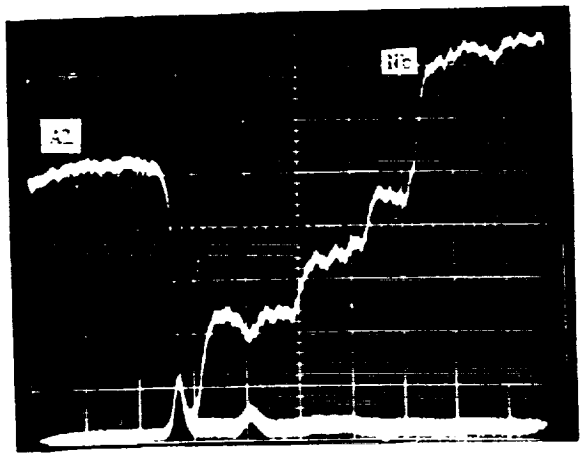

Sample D. Aged 1000 hours at 1200°C
Line Profiles, Al and Nb, 800X

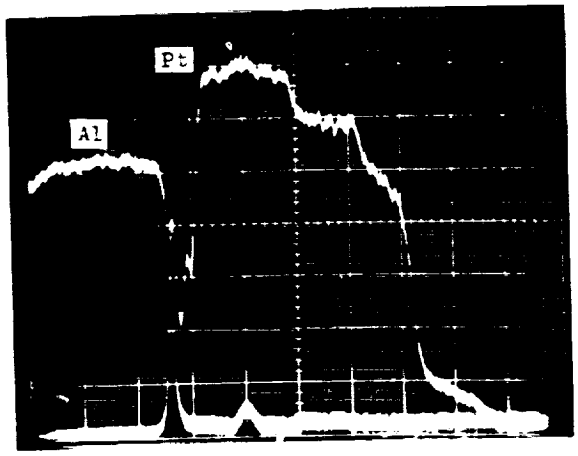

Sample D. Aged 1000 hours at 1200°C
Line Profiles, Al and Pt, 800X

Figure 48. Braze Analysis Data: Braze System 2M (Cb-1Zr/Pt-2Hf/Mo/Al_2O_3) brazed at 1720° C for 1 minute.

than that of the original braze wafer, and drops of braze alloy are frequently found to have run out of the braze region. This would account for the reduced braze thickness, although it is not a particularly desirable characteristic for the braze to have.

Although a comparison of the Al_2O_3 grain sizes in the A, B, C, and D sample sequence of Braze System 2M suggests that a grain-growth factor might be active in these systems, an examination of Al_2O_3 specimens from other braze systems shows that the present sequence is more likely to be the result of an accidental choice of the Al_2O_3 buttons used.

Braze System 3M (Cb-1Zr/V-2Ce/Mo/Al_2O_3). An examination of Figure 49, the data for Braze System 3M, shows the braze region to be about 7 mils (0.178 mm) thick in the 10-hour (3.6×10^4s) aged A sample. Although the braze layer is well defined in this sample, there is evidence of an epitaxy in the braze, suggesting that as the molten braze cooled, it tended to freeze out on the existing crystals in the Cb-1Zr alloy surface, and to continue the grains into the braze. Some of them extend to the surface of the Al_2O_3. The shadow along the Cb-1Zr-braze juncture is caused by a sloping region in which there is an elevation change between the soft Cb-1Zr and the harder braze. At the other side of the braze, a reaction zone about 0.5 mil (0.0127 mm) wide is seen.

The 100 gm DPH hardness value of the braze is about 300-325 with a distinct gradient, while that of the Cb-1Zr alloy is about 75.

Figure 51 shows the electron microprobe back-scattered electron image for the A sample. Careful examination of the photograph shows the diminution in the intensity of the lightness as one moves through the braze from the Cb-1Zr interface to the Al_2O_3 interface. This is also shown in the line profile for Nb(Cb) in Figure 51. The line profile for the other major component of the final braze region, vanadium, is shown in Figure 53. This profile is also seen to be quite regular, with a smooth concentration gradient in the V trace as it approaches the Cb-1Zr alloy.

Figure 52 shows the electron microprobe line profiles for Ce and for Zr. There is a very slight indication that a cerium concentration occurs at the Al_2O_3 interface, but one cannot be certain that the last little peak is not an artifact of the electronics of the microprobe. Certainly, there is no indicataion that there was any concentration of Zr at the Al_2O_3 interface. This is in distinct contrast to the electron microprobe findings in the 2M braze system.

The braze layer in the 100-hour (3.6×10^5s) aged B sample shown in Figure 49 is quite wide, and the demarcation between the braze and the Cb-1Zr is less pronounced, although the braze thickness is about 8 mils (0.203 mm). The braze DPH hardness is nominally 300 units, and that of the Cb-1Zr alloy is, again, 75 units. A rather level microhardness profile is found, with only a slight hardness increase at the Al_2O_3-braze interface.

A. Micrograph, 100X

B. Micrograph, 100X

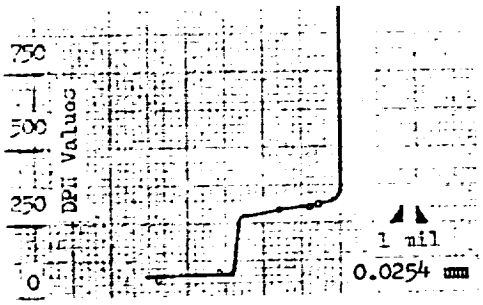

A. Microhardness Profile

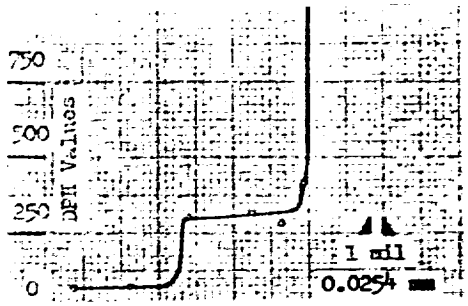

B. Microhardness Profile

V:	Figure 53
Ce:	Figure 52
Cb(Nb):	Figure 51
Zr:	Figure 52
Mo:	Similar to Figure 45
Al:	Figures 51, 52, 53

A. Electron Microprobe Line Profile Summary

V:	Figure 54
Ce:	Figure 53
Cb(Nb):	Figure 51
Zr:	Similar to Figure 52
Mo:	Similar to Figure 45
Al:	Figures 53, 54

B. Electron Microprobe Line Profile Summary

Figure 49. Braze Analysis Data: Braze System 3M (Cb-1Zr/V-2Ce/Mo/Al_2O_3) brazed at 1860°C for 60 s. Sample A aged for 10 hrs (3.6×10^4s) at 1200°C; Sample B aged for 100 hrs (3.6×10^5s) at 1200°C.

C. Micrograph, 100X

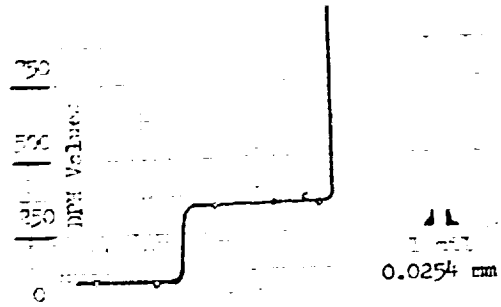

C. Microhardness Profile

V:	Similar to Figure 53
Ce:	Similar to Figure 52
Cb(Nb):	Similar to Figure 51
Zr:	Similar to Figure 52
Mo:	Figure 54
Al:	Figure 54

C. Electron Microprobe Line Profile Summary

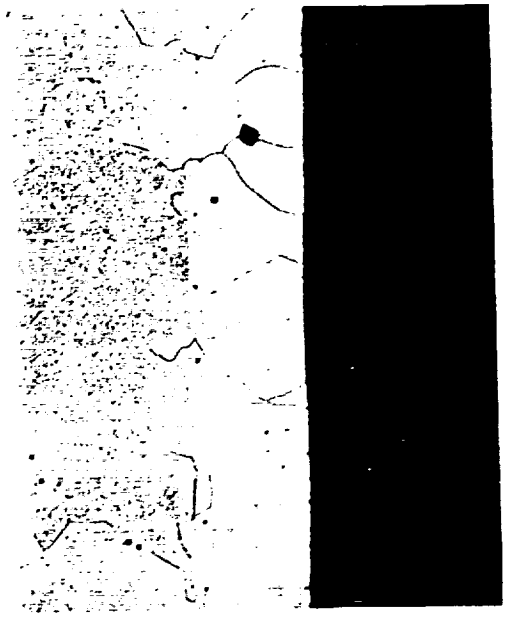

D. Micrograph, 100X

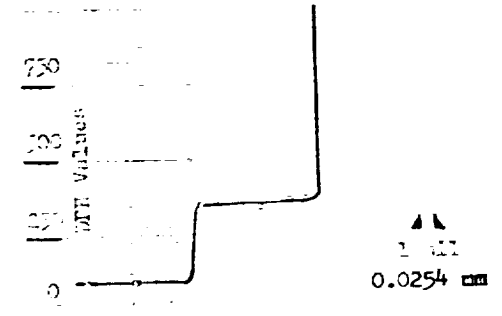

D. Microhardness Profile

V:	Figure 55
Ce:	Similar to Figure 52
Cb(Nb):	Figure 55
Zr:	Figure 56
Mo:	Similar to Figures 45, 54
Al:	Figures 55, 56

D. Electron Microprobe Line Profile Summary

Figure 50. Braze Analysis Data: Braze System 3M (Cb-1Zr/V-2Ce/Mo/Al_2O_3) brazed at 1860°C for 60 s. Sample C aged for 500 hrs (1.8×10^6 s) at 1200°C; Sample D aged for 1000 hrs (3.6×10^6 s) at 1200°C.

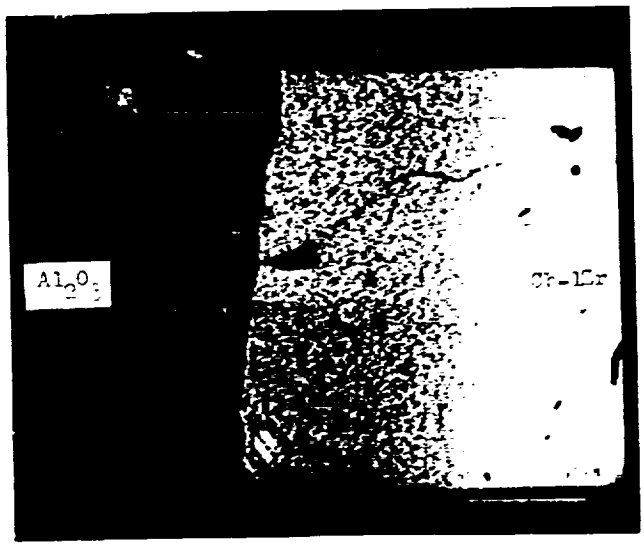

Sample A. Aged 10 hours at 1200°C
Back-Scattered Electron Image, 400X

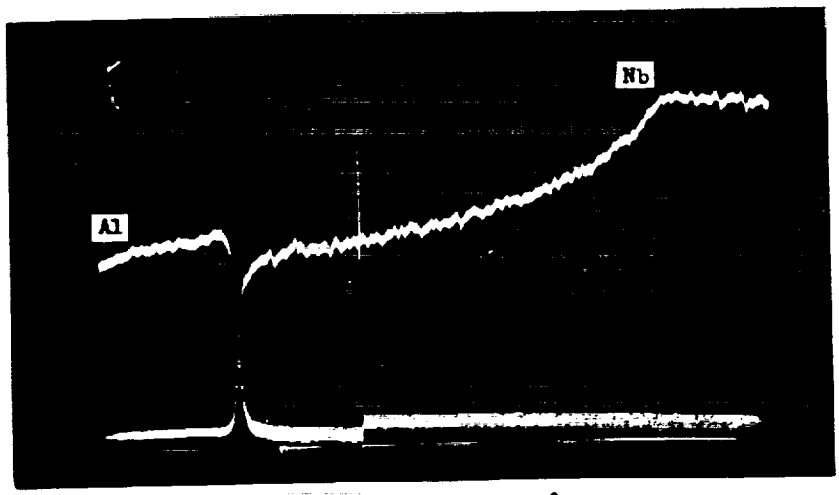

Sample A. Aged 10 hours at 1200°C
Line Profiles, Al and Nb, 800X

Figure 51. Braze Analysis Data: Braze System 3M (Cb-1Zr/V-2Ce/Mo/Al_2O_3) brazed at 1860°C for 1 minute.

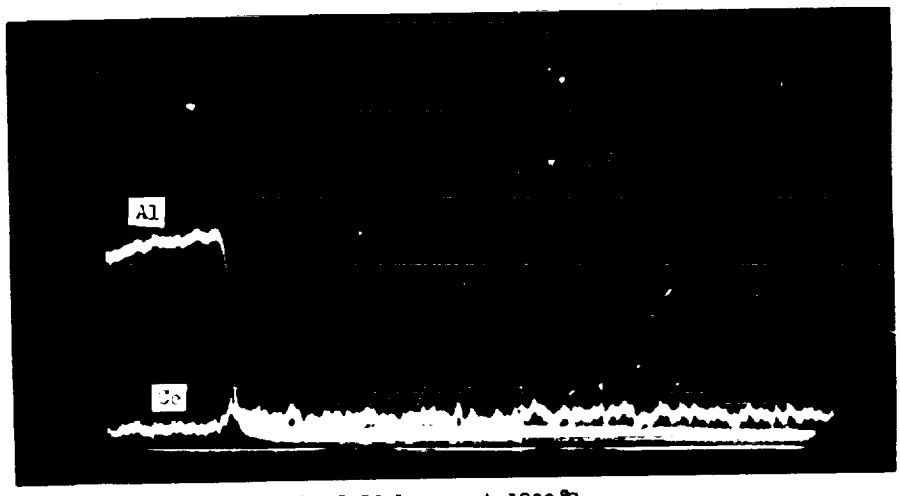

Sample A. Aged 10 hours at 1200°C
Line Profiles, Al and Ce, 800X

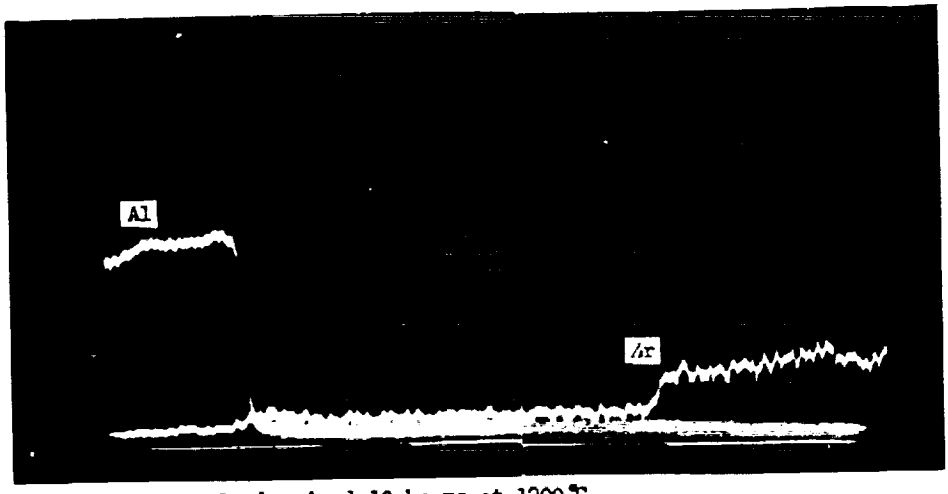

Sample A. Aged 10 hours at 1200°C
Line Profiles, Al and Zr, 800X

Figure 52. Braze Analysis Data: Braze System 3M (Cb-1Zr/V-2Ce/Mo/Al_2O_3) brazed at 1860°C for 1 minute.

Figure 53 shows the electron microprobe line profile for Ce in the B sample. A distinct concentration of Ce at the Al_2O_3 interface is shown, with a rather uniformly low concentration level throughout the remainder of the braze region. Figure 54 shows the V line profile for the B sample. The concentration is seen to be quite uniform near the Al_2O_3 interface, and the rather typical gradient in the vicinity of the Cb-1Zr interface is shown. The central region of the braze was not examined, because of the large braze thickness.

Figure 50 shows the micrograph and the microhardness profile of the 500-hour (1.8×10^6s) C sample of Braze System 3M. The braze region is 10 mils (0.254 mm) thick, and several large crystals are seen to cross the Cb-1Zr vs braze interface in an epitaxial growth pattern.

A reaction zone about 0.5 mils (0.0127 mm) thick is seen at the Al_2O_3 interface, although there is no indication of a strong concentration of Ce or Zr at the interface from the electron microprobe data.

Figure 54 shows the Mo line profile to be rather uniform through the thickness of the braze. Similarly the V and Nb(Cb) concentration profiles are typically smooth and similar to those shown in Figures 53 and 51, respectively The Ce profile resembles that shown in Figure 52, with only a very slight tendency to concentrate at the Al_2O_3 interface.

Figure 50 shows the micrograph and the microhardness profile of the 1000-hour (3.6×10^6s) D sample of Braze System 3M. The braze region is about 8 mils (0.203 mm) thick. Again, epitaxy in the braze and Cb-1Zr alloy grains is clearly shown. An irregular appearing reaction zone ranging from 0.2 to more than 1 mil (0.0051 to 0.0254 mm) appears at the Al_2O_3 surface.

Figure 55 shows the electron microprobe line profiles at the braze-Al_2O_3 interface and at the braze-Cb-1Zr interface of Nb(Cb) and of V. Thes are rather regular in character and show smooth gradients over the braze thickness. The back-scattered electron image shown in Figure 56 confirms the niobium (columbium) gradient seen in the line profile of Figure 55.

Figure 56 also shows the Zr line profile of the D sample of System 3M. In the braze region, the Zr trace is rather uniform, and shows no tendency to concetrate at the Al_2O_3 interface. However, there is an apparent anomaly in the body of the Al_2O_3, which shows a region of high Zr concentration matched by a decreased Al concentration. This is attributed to the fact that the braze metal sometimes penetrates into pores in the Al_2O_3. Such a penetration is shown in Figure 49 (B), and a similar penetration is believed to be the cause of the present phenomenon.

In summary, the 3M braze is seen to dissolve rather large amounts of Cb-1Zr, but in contrast to the 2M braze alloy, the 3M brazes tend to remain in the joint. Upon freezing, the braze tends to crystallize beginning at the Cb-1Zr surface, and to grow on the existing crystal surfaces, so that a gros

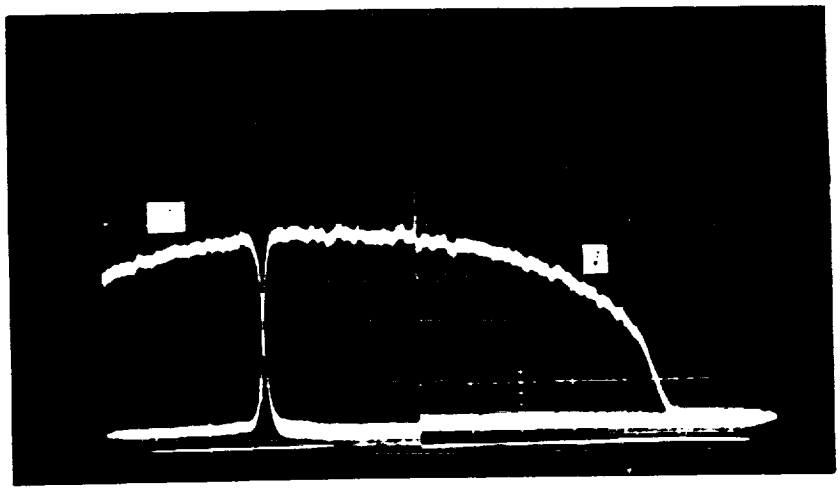

Sample A. Aged 10 hours at 1200°C
Line Profiles, Al and V, 300X

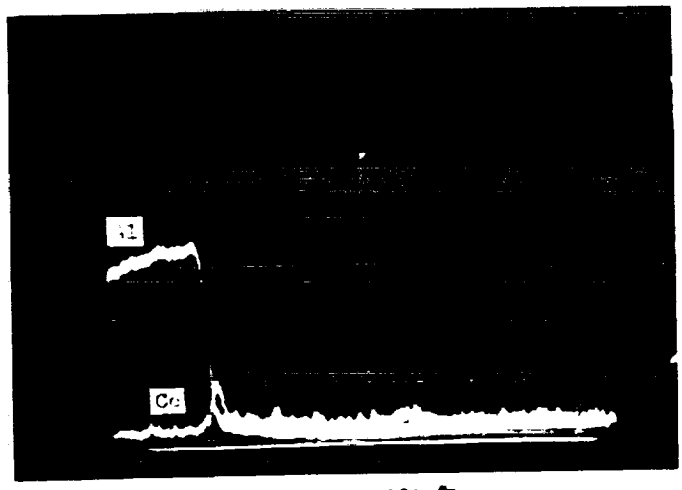

Sample B. Aged 100 hours at 1200°C
Line Profiles, Al and Ce, 300X

Figure 53. Braze Analysis Data: Braze System 3M (Cb-1Zr/V-2Ce/Mo/Al_2O_3) brazed at 1860° C for 1 minute.

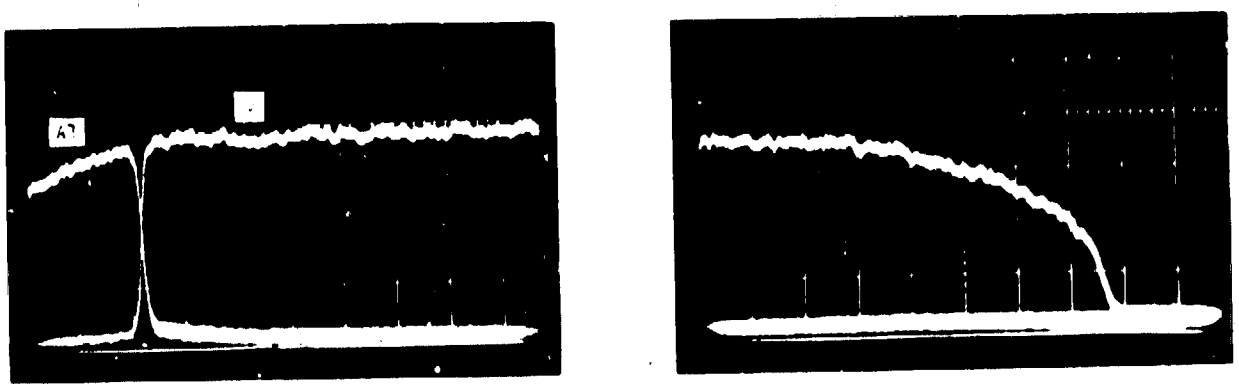

Sample B. Aged 100 hours at 1200°C
Line Profiles, Al and V, 800X

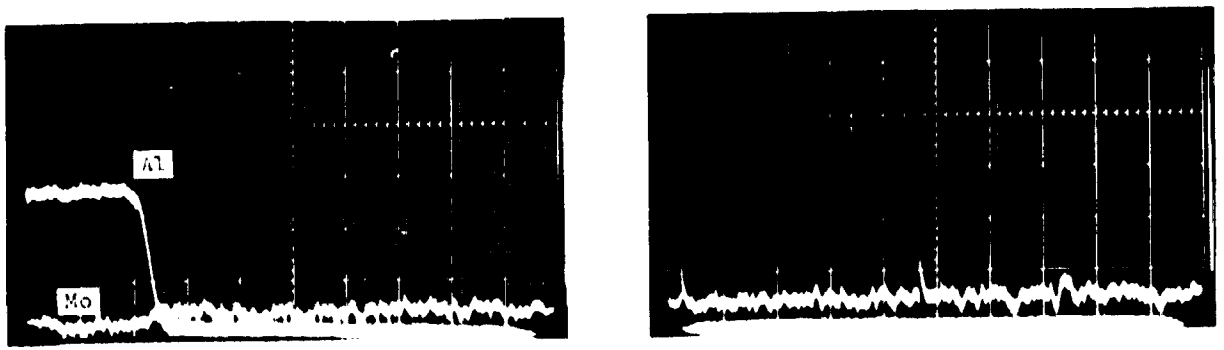

Sample C. Aged 500 hours at 1200°C

Figure 54. Braze Analysis Data: Braze System 3M (Cb-1Zr/V-2Ce/Mo/Al_2O_3) brazed at 1860°C for 1 minute.

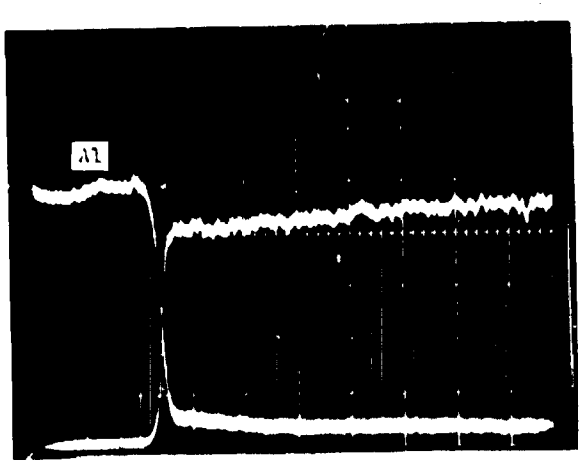

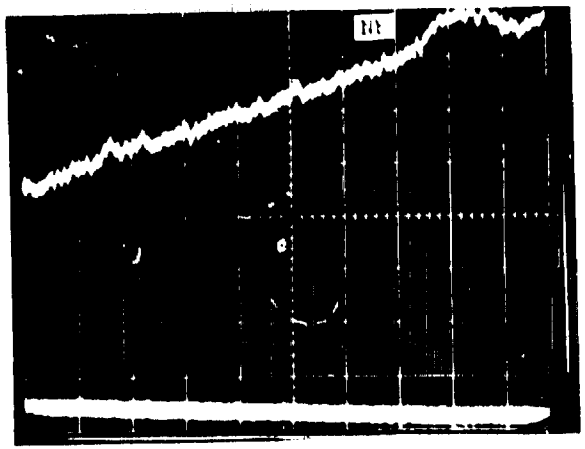

Sample D. Aged 1000 hours at 1200°C
Line Profiles, Al and Nb, 800X

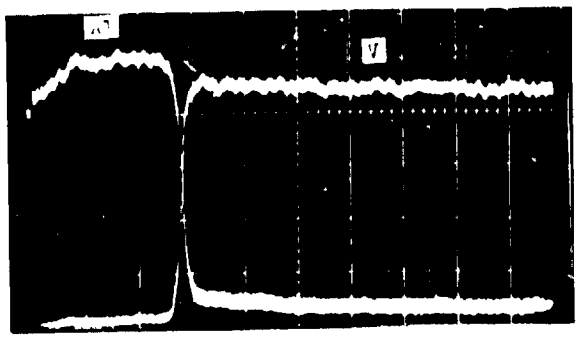

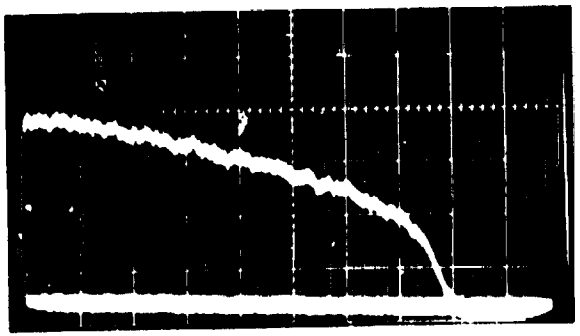

Sample D. Aged 1000 hours at 1200°C
Line Profiles, Al and V, 800X

Figure 55. Braze Analysis Data: Braze System 3M (Cb-1Zr/V-Ce/Mo/Al_2O_3) brazed at 1860° C for 1 minute.

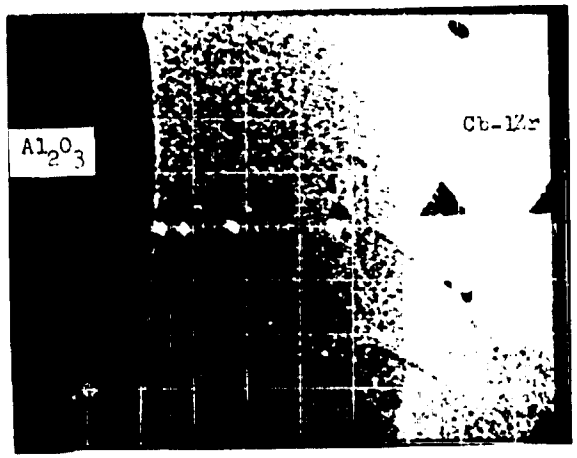

Sample D. Aged 1000 hours at 1200°C
Back-Scattered Electron Image, 400X

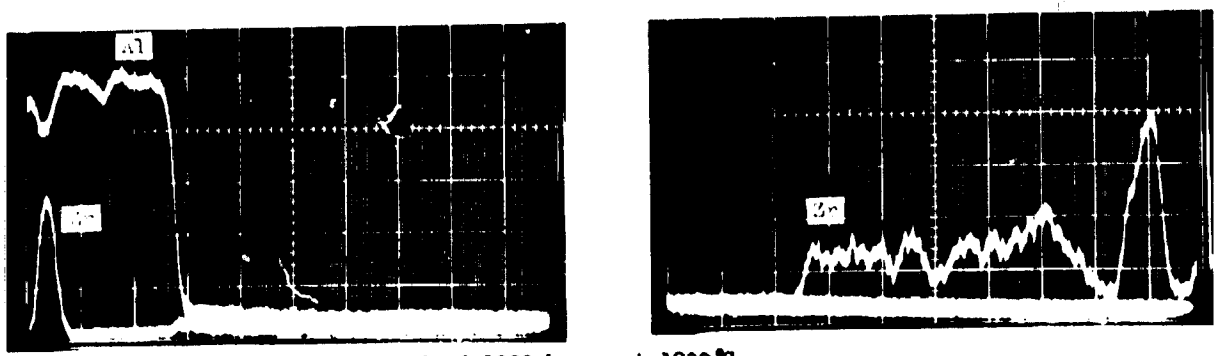

Sample D. Aged 1000 hours at 1200°C
Line Profiles, Al and Zr, 800X

Figure 56. Braze Analysis Data: Braze System 3M (Cb-1Zr/V-2Ce/Mo/Al_2O_3) brazed at 1860°C for 1 minute.

A. Micrograph, 100X

B. Micrograph, 100X

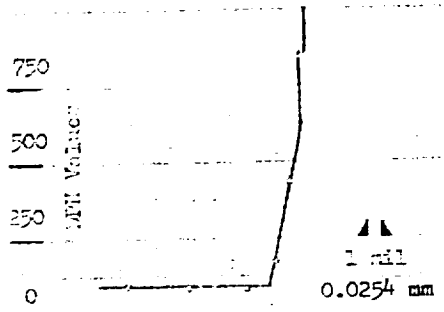

A. Microhardness Profile

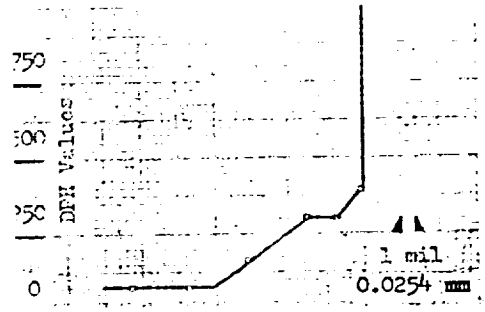

B. Microhardness Profile

V:	Similar to Figure 53
Hf:	Figure 59
Cb(Nb):	Similar to Figure 51
Zr:	Figure 59
Mo:	Similar to Figures 45, 54
Al:	Figure 59

A. Electron Microprobe Line Profile Summary.

V:	Figure 60
Hf:	Similar to Figure 59
Cb(Nb):	Figure 60
Zr:	Similar to Figure 59
Mo:	Similar to Figures 45, 54
Al:	Figure 60

B. Electron Microprobe Line Profile Summary

Figure 57. Braze Analysis Data: Braze System 4M (Cb-1Zr/V-2Hf/Mo/Al_2O_3) brazed at 1860° C for 60 s. Sample A aged for 10 hrs (3.6×10^4 s) at 1200° C; Sample B aged for 100 hrs (3.6×10^5 s) at 1200° C.

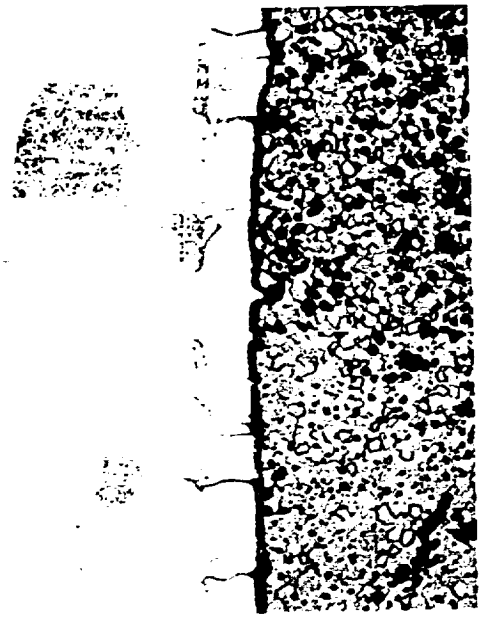

C. Micrograph, 100X

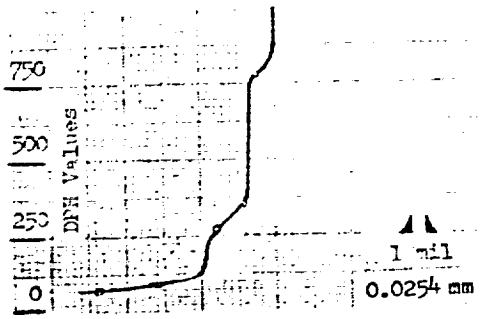

C. Microhardness Profile

V:	Similar to Figure 55
Hf:	Figure 61
Cb(Nb):	Similar to Figure 55
Zr:	Figure 61
Mo:	Similar to Figures 45, 54
Al:	Figure 61

C. Electron Microprobe Line Profile Summary.

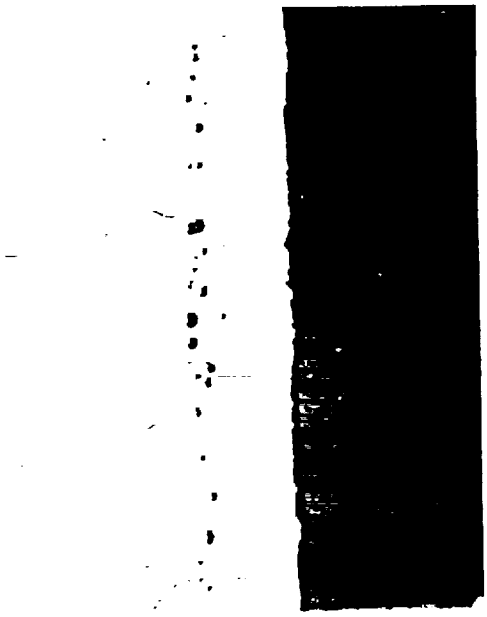

D. Micrograph, 100X

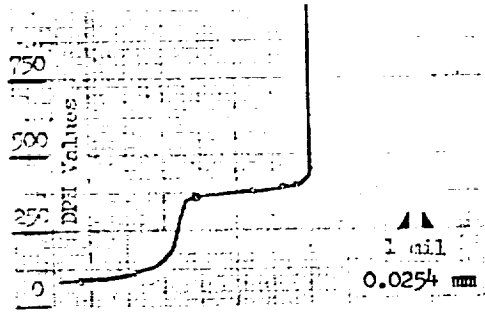

D. Microhardness Profile

V:	Similar to Figure 55
Hf:	Figure 62
Cb(Nb):	Similar to Figure 55
Zr:	Similar to Figure 59
Mo:	Similar to Figures 45, 54
Al:	Figure 62

D. Electron Microprobe Line Profile Summary.

Figure 58. Braze Analysis Data: Braze System 4M (Cb-1Zr/V-2Hf/Mo/Al_2O_3) brazed at 1860°C for 60 s. Sample C aged for 500 hrs (1.8×10^6s) at 1200°C; Sample D aged for 1000 hrs (3.6×10^6s) at 1200°C.

epitaxial growth occurs. Some of the crystals extend across the full thickness of the braze.

The tendency of the reactive elements Ce and Zr, which are dissolved in the braze to react with the Al_2O_3, is not pronounced, although some reaction was observed in the 10-hour (3.6×10^4s) and the 500-hour (1.8×10^6s) C samples.

Braze System 4M (Cb-1Zr/V-2Hf/Mo/Al_2O_3): An examination of Figure 57, the data for Braze System 4M shows the braze region to be about 2.0 mils (0.051 mm) thick in the 10-hour (3.6×10^4s) aged A sample. The reaction layer which appears dark in the micrograph is nominally 0.5 mil (0.0127 mm) thick at the braze-alumina interface. Its 100 gm DPH hardness is 850, but that in the braze layer ranges sharply downward from about 500 to the 75-80 value characteristic of the Cb-1Zr alloy. Epitaxial growth of crystals in the Cb-1Zr alloy into the braze region is observed.

Figure 59 shows the electron microprobe back-scattered electron image for the A sample of Braze System 4M. A significant concentration of Nb(Cb) is seen in the braze region, with the customary gradient from the Cb-1Zr alloy to the Al_2O_3 interface. The hardness indents verify the profile shown in Figure 57. Line profiles of Zr and Hf are also shown in Figure 59, with the positive indication that these elements reacted strongly with the Al_2O_3 in the region of the reaction zone. The presence of appreciable amounts of Zr and Hf at the interface is also shown by the step-like break in the Al line profile in the same location. The presence of such a large amount of zirconium in the braze verifies the fact the braze is a good solvent for the Cb-1Zr alloy. The Nb(Cb) and the V profiles are smooth and normal and are equivalent to those shown in Figures 51 and 53, respectively.

The braze layer in the 100-hour (3.6×10^5s) aged B sample is about 10 mils (0.254 mm) thick and a very thin reaction zone is seen at the Al_2O_3 surface. The DPH hardness of the braze layer ranges from about 400 near the Al_2O_3 to 75 in the Cb-1Zr alloy. Again, Sample B clearly shows epitaxy in the braze layer.

Figure 60 shows the Nb(Cb) and V line profiles for the B sample of Braze 4M. The curves are quite regular except for the small rather level regions in the Al_2O_3-braze interface region. These are caused by the presence of Zr and Hf, whose profiles are similar to those shown in Figure 59 . The Mo line profile (not shown) shows this element to be uniformly distributed in the braze.

The braze layer in the 500-hour (1.8×10^6s) aged C sample is at least 5 mils (0.127 mm) thick, and may be as much as 8 mils (0.203 mm) thick as is shown in Figure 58. Marked epitaxy is shown. The dark band at the Al_2O_3 interface partially obscures a thin, 0.1 mil (0.0025 mm) thick reaction zone. The shadow is caused by a sloping region between two different elevations on the polished sample. The DPH hardness profile shows a rather high value of 775 about 1 mil (0.0254 mm) from the Al_2O_3 interface, and then a rather sudden drop to 350, followed by a gradual decrease to 75-80, the usual value found in the base Cb-1Zr alloy.

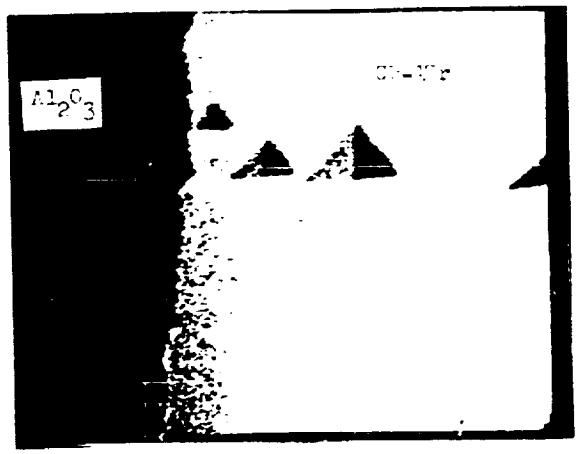

Sample A. Aged 10 hours at 1200°C
Back-Scattered Electron Image, 400X

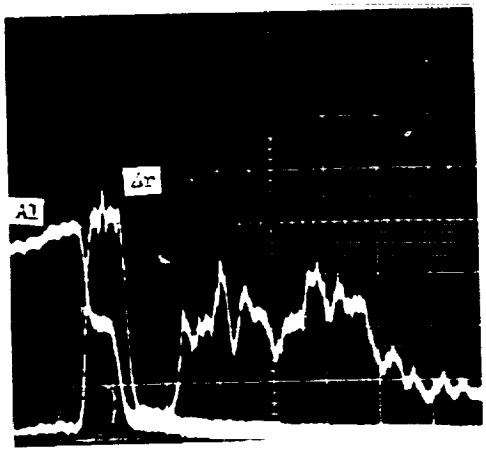

Sample A. Aged 10 hours at 1200°C
Line Profiles, Al and Zr, 800X

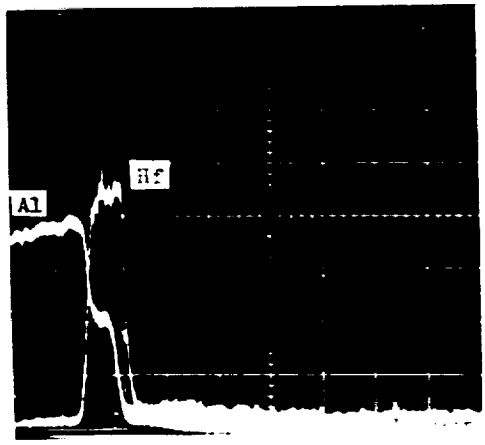

Sample A. Aged 10 hours at 1200°C
Line Profiles, Al and Hf, 800X

Figure 59. Braze Analysis Data. Braze System 4M (Cb-1Zr/V-2Hf/Mo/Al_2O_3) brazed at 1860°C for 1 minute.

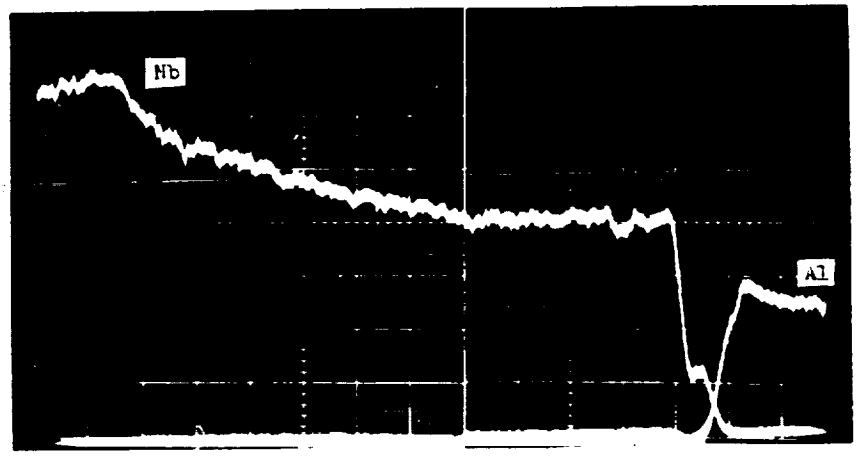

Sample B. Aged 100 hours at 1200°C
Line Profiles, Al and Nb, 800X

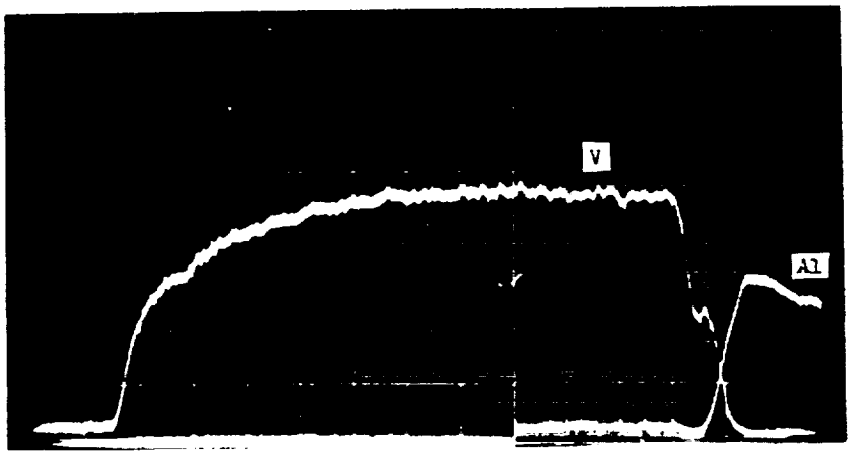

Sample B. Aged 100 hours at 1200°C
Line Profiles, Al and V, 800X

Figure 60. Braze Analysis Data. Braze System 4M (Cb-1Zr/V-2Hf/Mo/Al_2O_3) brazed at 1860°C for 1 minute.

Figure 61 shows the electron microprobe line profiles for Zr and for Hf in this C sample. These traces differ from those of the A and B samples in that no evidence of an interaction of these elements with Al_2O_3 is seen. The rather jagged appearance of the Zr trace in the Cb-1Zr alloy region is attributed to noise in the microprobe electronics, although the concentration level of Zr is higher there than it is in the braze. The Nb and V line profiles are quite regular, and show no perturbations in the interface region. This is a confirmation of the absence of a concentration of Zr or Hf at that location. The Nb and V traces are thus similar to those shown in Figure 55.

The braze layer in the 1000-hour (3.6×10^6s) aged D sample of Braze System 4M is seen in Figure 58 to be 8 mils (0.203 mm) thick. A reaction layer about 0.4 mils (0.01 mm) thick appears at the Al_2O_3 surface. The dark spots at the Cb-1Zr-braze juncture are pits. Their source is not known, but they may be etching artifacts if there were particles at the original surface, or they might have begun as voids at the surface. Marked epitaxy is shown, and the DPH hardness profile is rather level in the braze, ranging from 350 to 400 across the 10 mil (0.254 mm) thickness.

Figure 62 shows the wide braze region and the presence of Nb(Cb) in the braze. The line profile of Hf in the braze shows a small but distinct peak at the interface, and a rather uniform and low level in the remainder of the sample. The Zr profile also shows a peaking at the interface, similar to that of Figure 59. However, the Nb and V profiles did not show the effects of the Zr and the Hf in the braze region, and are similar to the profiles shown in Figure 55 rather than those of Figure 60.

In summary, the 4M braze appears to have a variable character. In some cases a hard interface layer is found, while in other cases, there is none. Some of the brazes are quite thick, but the A braze is only about 2 mils (0.051 mm) thick. The hardness at the interface may be associated with the presence of high Zr and Hf at that location, with the presumption that a reaction with Al_2O_3 has occurred to form Zr and Hf oxides in the reaction zone. However, there is a lack of consistency in this hypothesis, too, in that the C sample, which showed no Zr and Hf concentration at the surface, did show a high DPH hardness value near the interface, while the D sample, in which there was a marked Zr and Hf concentration effect, showed a rather level DPH profile through the braze.

Braze System 4W (Cb-1Zr/V-2Hf/W/Al_2O_3): An examination of Figure 63, the data for Braze System 4W shows the braze thickness to be about 5 mils (0.127 mm) in the 10-hour (3.6×10^4s) aged A sample. The dark band at the Cb-1Zr-braze juncture is a polishing artifact, coupled with 100X microscopy. Under 500X or 750X magnification, there is no band. A reaction zone 0.3 mils (0.008 mm) wide appears at the Al_2O_3 surface.

The hardness profile of the braze is shown to have a very slight slope, with the one point measured at a DPH value of 660 being neglected. This was done on the basis of the indents shown in the Back-Scattered Electron Image of Figure 65, which photograph shows the last indent to not be entirely in the

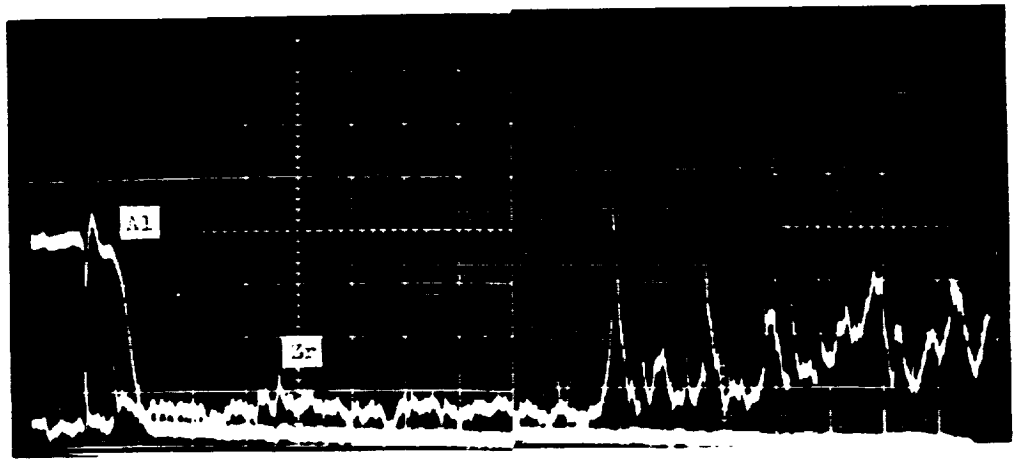

Sample C. Aged 500 hours at 1200°C
Line Profiles, Al and Zr, 800X

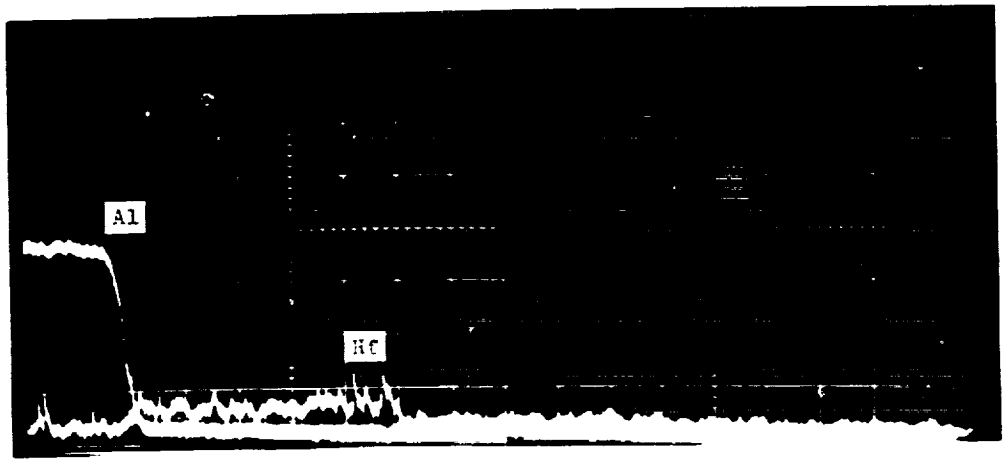

Sample C. Aged 500 hours at 1200°C
Line Profiles, Al and Hf, 800X

Figure 61. Braze Analysis Data. Braze System 4M (Cb-1Zr/V-2Hf/Mo/Al_2O_3) brazed at 1860°C for 1 minute.

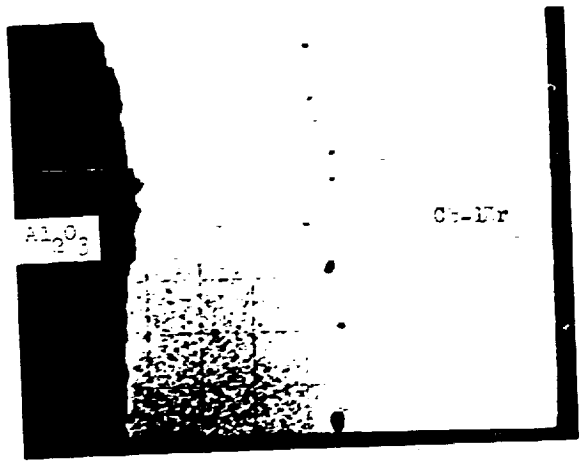

Sample D. Aged 1000 hours at 1200°C
Back-Scattered Electron Image, 200X

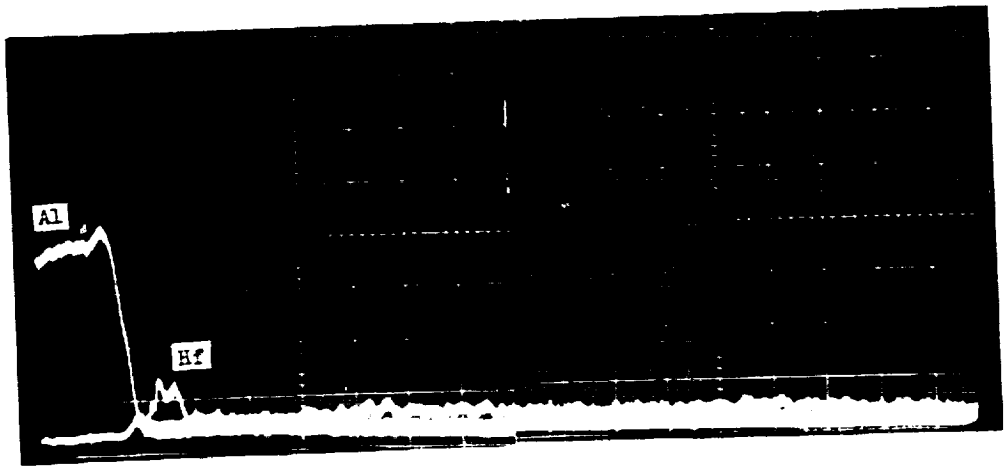

Sample D. Aged 1000 hours at 1200°C
Line Profiles, Al and Hf, 800X

Figure 62. Braze Analysis Data. Braze System 4M (Cb-1Zr/V-2Hf/Mo/Al_2O_3) brazed at 1860°C for 1 minute.

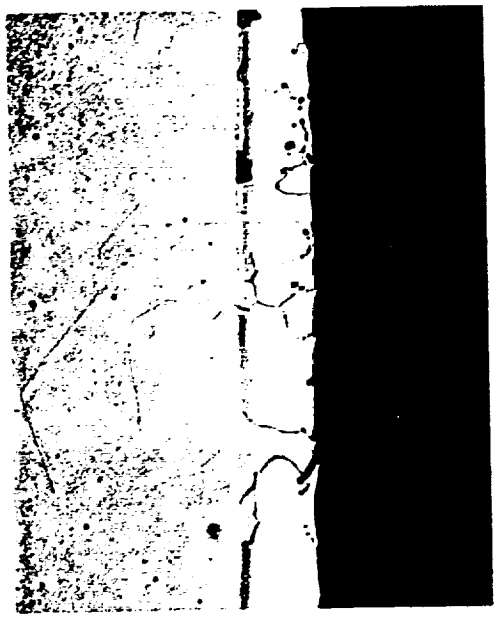

A. Micrograph, 100X

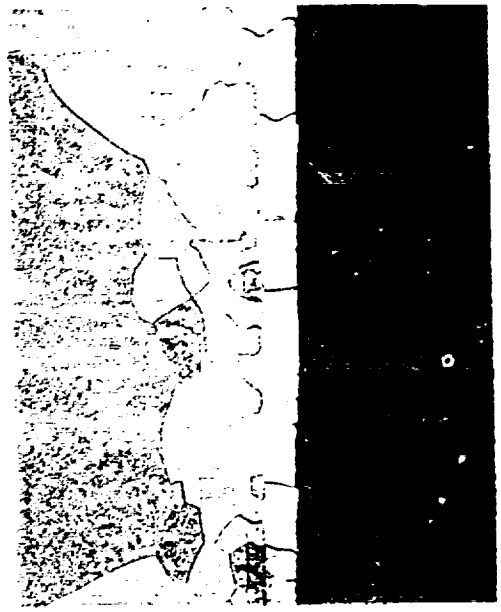

B. Micrograph, 100X

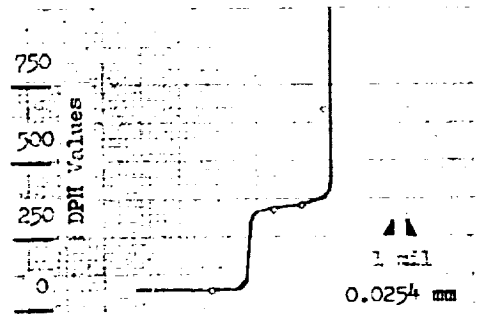

A. Microhardness Profile

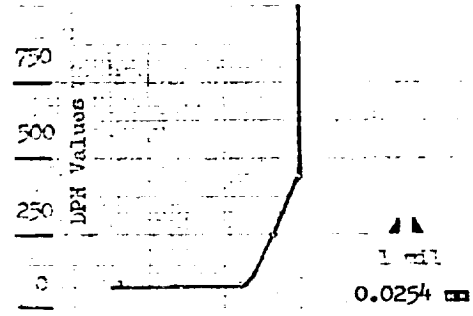

B. Microhardness Profile

V:	Figure 66
Hf:	Similar to Figure 61
Cb(Nb):	Figure 66
Zr:	Similar to Figure 52
W:	Figure 65
Al:	Figures 65, 66

A. Electron Microprobe Line Profile Summary.

V:	Figure 68
Hf:	Figure 67
Cb(Nb):	Figure 68
Zr:	Similar to Figure 52
W:	Similar to Figure 65
Al:	Figures 67, 68

B. Electron Microprobe Line Profile Summary.

Figure 63. Braze Analysis Data. Braze System 4W (Cb-1Zr/V-2Hf/W/Al_2O_3) brazed at 1870°C for 60 s. Sample A aged for 10 hrs (3.6×10^4 s) at 1200°C; Sample B aged for 100 hrs (3.6×10^5 s) at 1200°C.

C. Micrograph, 100X

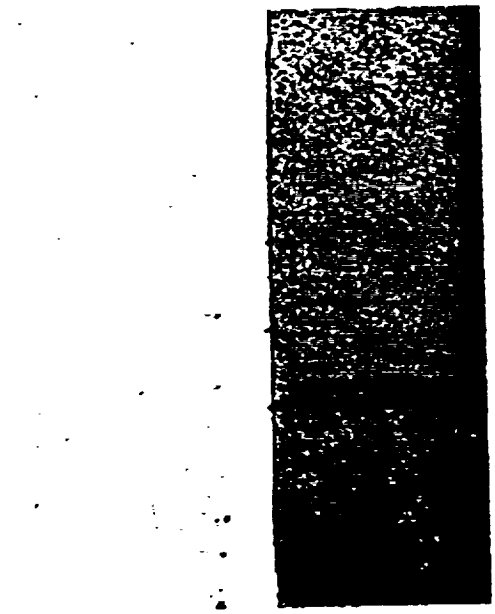

D. Micrograph, 100X

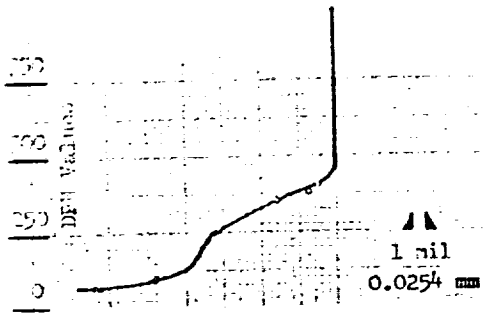

C. Microhardness Profile

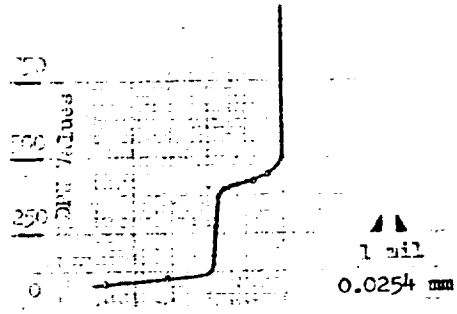

D. Microhardness Profile

V:	Figure 69
Hf:	Similar to Figure 67
Cb(Nb):	Figure 69
Zr:	Figure 70
W:	Similar to Figure 65
Al:	Figures 69, 70

C. Electron Microprobe Line Profile Summary.

V:	Figure 71
Hf:	Similar to Figure 67
Cb(Nb):	Figure 71
Zr:	Similar to Figure 52
W:	Similar to Figure 65
Al:	Figure 71

D. Electron Microprobe Line Profile Summary.

Figure 64. Braze Analysis Data: Braze System 4W (Cb-1Zr/V-2Hf/W/Al_2O_3) brazed at 1870° C for 60s. Sample C aged for 500 hrs (1.8×10^6s) at 1200° C; Sample D aged for 1000 hrs (3.6×10^6s) at 1200° C.

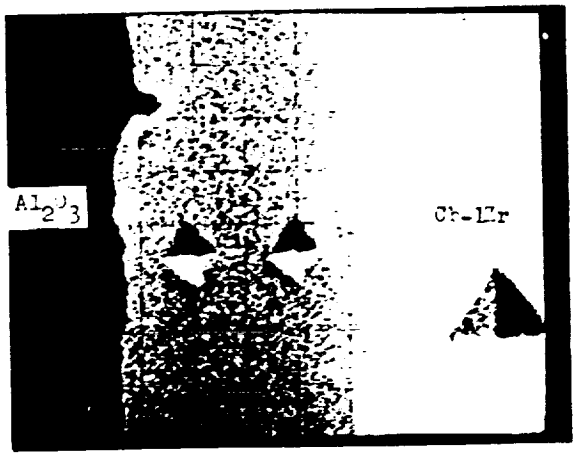

Sample A. Aged 10 hours at 1200°C
Back-Scattered Electron Image, 400X

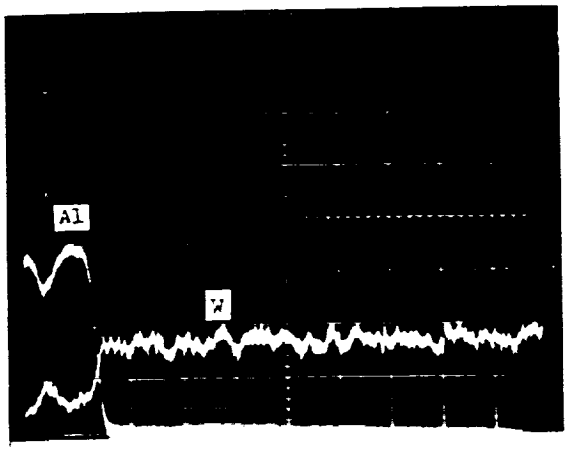

Sample A. Aged 10 hours at 1200°C
Line Profiles, Al and W, 800X

Figure 65. Braze Analysis Data: Braze System 4W (Cb-1Zr/V-2Hf/W/Al_2O_3) brazed at 1870°C for 1 minute.

braze. Because the Al_2O_3 is harder than the braze, such a hardness reading will be high. The DPH values in the braze range from 340 to 375.

Figure 65 also shows the line profile for tungsten. In this braze system, a tungsten barrier was evaporation deposited on the Al_2O_3. However, the braze appears to have dissolved the tungsten and it appears rather uniformly distributed in the braze thickness. Figure 66 shows the line profiles for Nb(Cb) and V in the A sample of Braze System 4W. Both profiles are seen to be smooth, with no anomalies. The profiles of Hf and Zr are not shown, but there was no concentration of these elements at the Al_2O_3 interface, and their profiles appear quite similar to those shown in Figures 61 and 52, respectively.

The braze layer in the 100-hour (3.6×10^5 s) aged Sample B (Figure 63) is about 3.5 mils (0.0888 mm) thick, and shows a definite structuring at the nominal braze–Cb-1Zr juncture. A layer about 1 mil (0.0254 mm) thick is in evidence there. The hardness profile through the braze is essentially linear from about 425 near the Al_2O_3 to 75 at the Cb-1Zr. Thus there is no indication of a hardness effect of the metal interface layer.

Figure 67 shows the Back-Scattered Electron Image, and the demonstration that there is Nb(Cb) distributed through the braze region. Figure 67 also shows the Hf line profile, which is seen to be rather uniform over the braze thickness with no indication of any concentration at the Al_2O_3 interface. Figure 68 shows the line profiles for Nb(Cb) and V, and they, too, are seen to be quite smooth and regular. The Zr and the W profiles are not shown, but ar quite smooth and are similar to those shown in Figures 52 and 65, respectively.

The braze layer shown for the 500-hour (1.8×10^6 s) aged C sample in Figure 64 is about 10 mils (0.254 mm) thick, and has a gradually increasing DPH hardness profile from the 75 typical of Cb-1Zr alloy to 400 near the Al_2O_3. Epitaxial growth of the braze on the Cb-1Zr is evident. Figure 69 shows the Nb(Cb) and V line profiles, which are generally smooth except for a dip at the mid-point. At the corresponding point, the Zr profile shows a peak in Figure 70. The specific cause for this anomaly is that the scan trace moved across a grain boundary at that point, and there was a higher concentration of Zr in the boundary region than in the adjacent crystallites. The Hf and the W profiles were quite regular and uniform.

The braze layer of the 1000-hour (3.6×10^6 s) aged D sample is shown in Figure 64. It is about 5 mils (0.127 mm) thick and shows a rather uniform DPH hardness value of 400-420 across its entire thickness. Epitaxy is also evident, as is a rather thin reaction zone at the Al_2O_3 surface.

The Back-Scattered Electron Image is shown in Figure 70 and the V and Nb(Cb) electron microprobe line profiles for Sample D are shown in Figure 71. The distribution of Nb(Cb) is similar to that in the other samples of Braze System 4W. The V trace shows a discontinuity, which is not a real phenomenon but is the result of a change in the electronics of the micro-

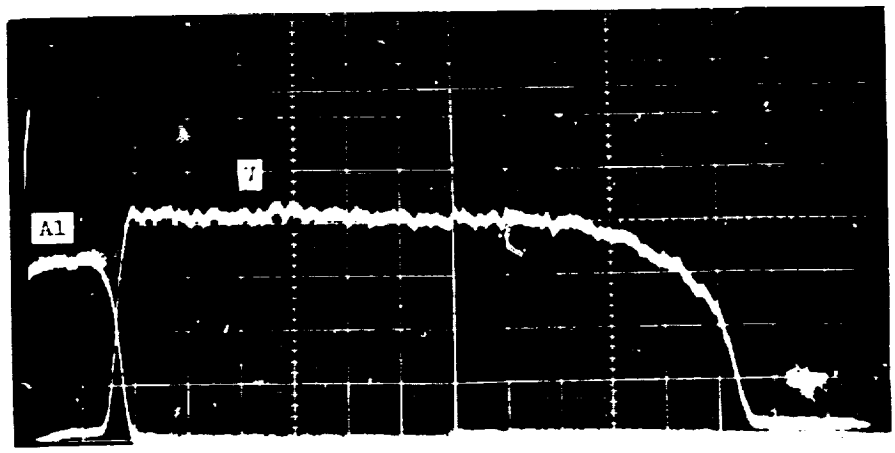

Sample A. Aged 10 hours at 1200°C
Line Profiles, Al and V, 300X

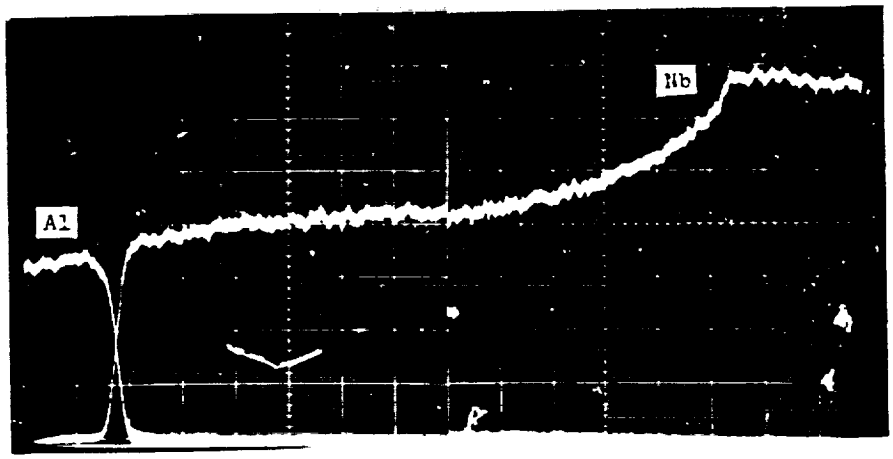

Sample A. Aged 10 hours at 1200°C
Line Profiles, Al and Nb, 300X

Figure 66. Braze Analysis Data: Braze System 4W (Cb-1Zr/V-2Hf/W/Al_2O_3) brazed at 1870° C for 1 minute.

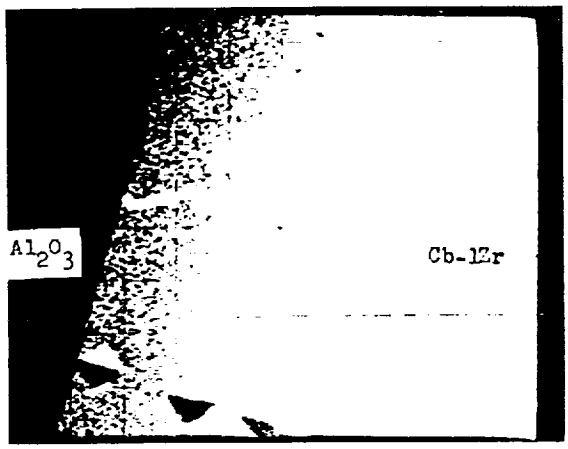

Sample B. Aged 100 hours at 1200°C
Back-Scattered Electron Image, 400X

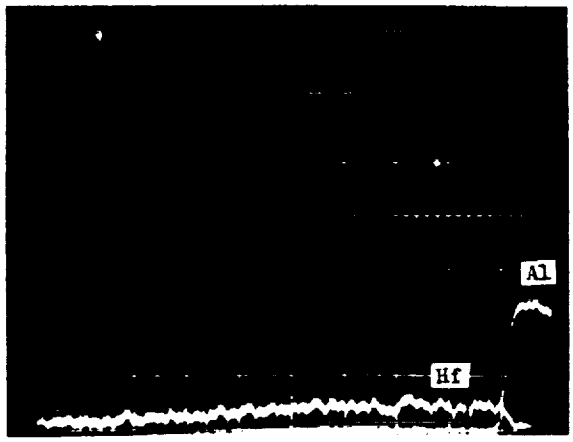

Sample B. Aged 100 hours at 1200°C
Line Profiles, Al and Hf, 800X

Figure 67. Braze Analysis Data: Braze System 4W ($Cb-1Zr/V-2Hf/W/Al_2O_3$) brazed at 1870° C for 1 minute.

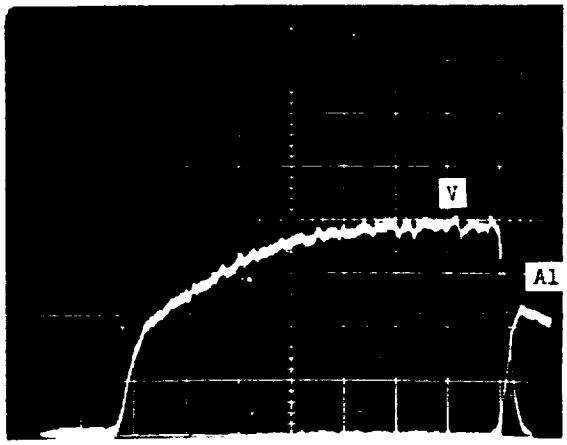

Sample B. Aged 100 hours at 1200°C
Line Profiles, Al and V, 800X

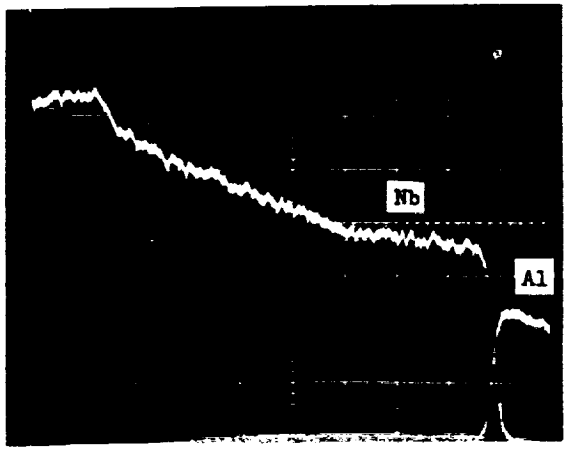

Sample B. Aged 100 hours at 1200°C
Line Profiles, Al and Nb, 800X

Figure 68. Braze Analysis Data: Braze System 4W (Cb-1Zr/V-2Hf/W/Al_2O_3) brazed at 1870°C for 1 minute.

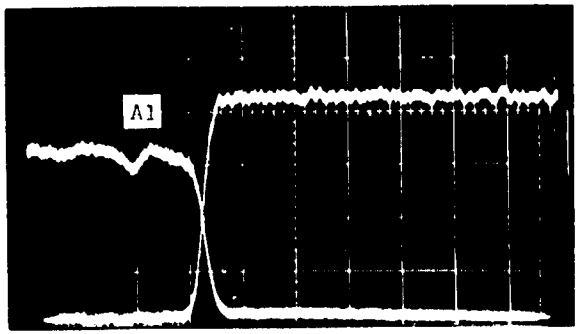

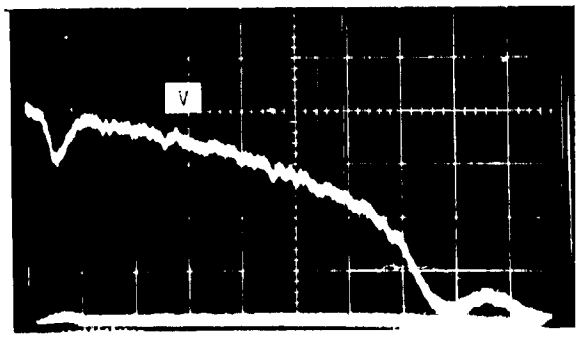

Sample C. Aged 500 hours at 1200°C
Line Profiles, Al and V, 800X

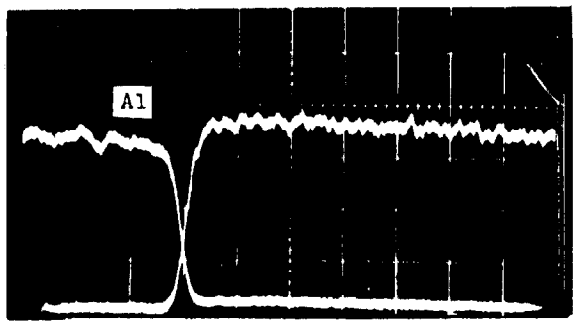

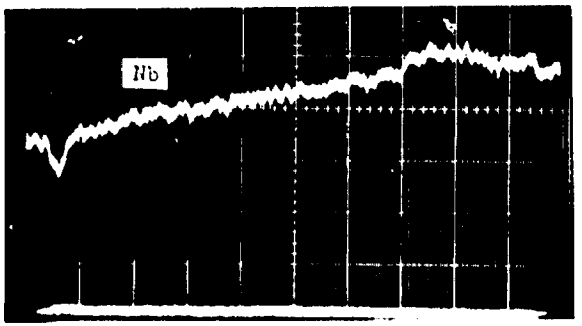

Sample C. Aged 500 hours at 1200°C
Line Profiles, Al and Nb, 800X

Figure 69. Braze Analysis Data. Braze System 4W (Cb-1Zr/V-2Hf/W/Al_2O_3) brazed at 1860°C for 1 minute.

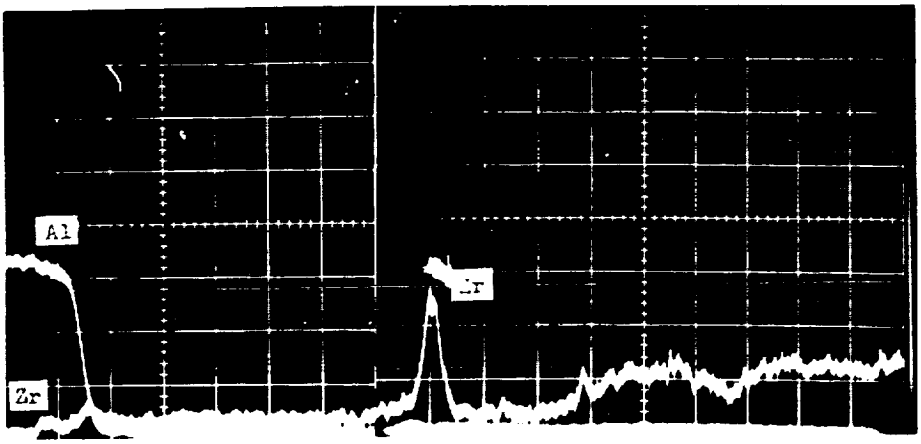

Sample C. Aged 500 hours at 1200°C
Line Profiles, Al and Zr, 800X

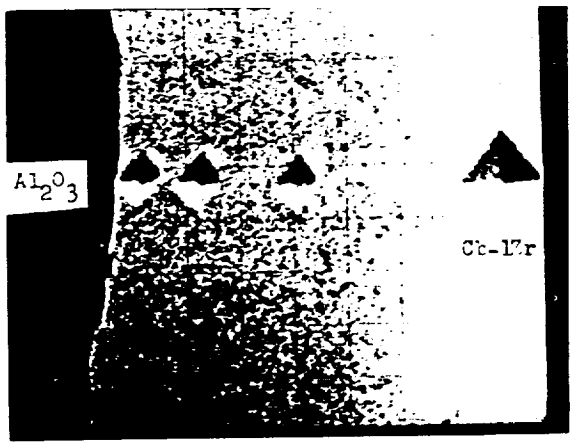

Sample D. Aged 1000 hours at 1200°C
Back-Scattered Electron Image, 400X

Figure 70. Braze Analysis Data. Braze System 4W ($Cb-1Zr/V-2Hf/W/Al_2O_3$) brazed at 1860°C for 1 minute.

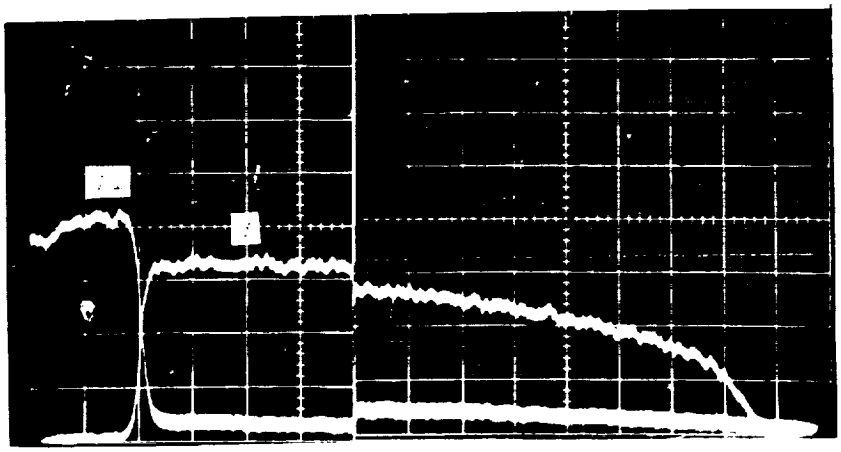

Sample D. Aged 1000 hours at 1200°C
Line Profiles, Al and V, 800X

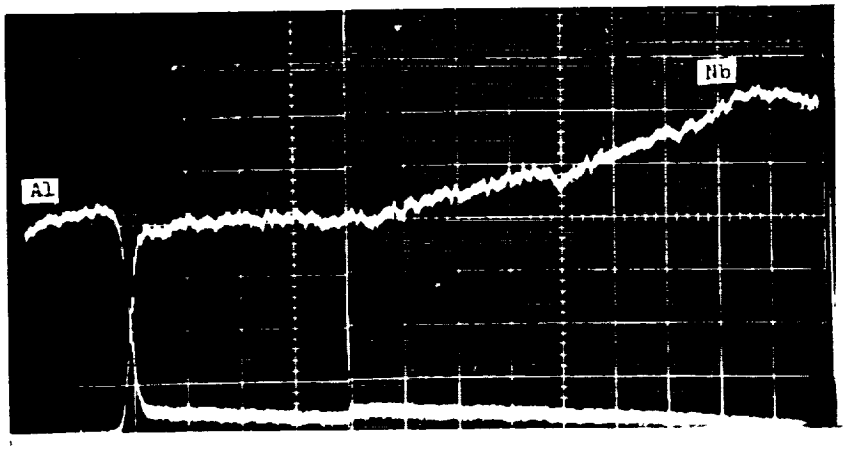

Sample D. Aged 1000 hours at 1200°C
Line Profiles, Al and Nb, 800X

Figure 71. Braze Analysis Data. Braze System 4W (Cb-1Zr/V-2Hf/W/Al_2O_3) brazed at 1870°C for 1 minute.

probe between the tracing of the Al_2O_3 interface region and tracing the Cb-1Zr-braze interface region. When the two photographs were cut and joined, the base levels of the traces were found to be different.

The Zr, Hf, and W line profiles are all quite uniform and closely resemble those shown in Figures 52, 67, and 65, respectively.

In summary, the Braze System 4W samples are characterized by having moderately wide to very wide braze joints, with generally uniform hardness profiles showing DPH values in the 300-400 range. No tendency for the segragation of the Group IV elements at the Al_2O_3 was seen, and the braze-Al_2O_3 interface regions were all good-appearing. The V-2Hf braze is a good solvent for Cb-1Zr alloy and major amounts of Nb(Cb) are found in the braze joint.

Braze System 5W (Cb-1Zr/V-1Zr/W/Al_2O_3): An examination of Figure 72, the data for Braze System 5W, shows the braze thickness of the 10-hour (3.6×10^4s) aged A sample to be about 5 mils (0.127 mm) thick. An interaction layer appears in the A sample, and it is about 0.7 mils (0.0178 mm) thick. The hardness values of the braze metal itself are uniform (300 units, 100gm DPH) with a sharp drop to about 75 in the Cb-1Zr alloy.

Figure 74 shows the electron microprobe Back-Scattered Electron Image and demonstrates the presence of Nb(Cb) in the braze region. The Zr line profile of the same figure shows a rather uniform distribution of Zr, on which is superimposed a double peak. These peaks appear as anomalies, because neither the Nb(Cb) nor the V line profiles show a corresponding dip. The Nb(Cb) and V line profiles are quite normal and are similar to those shown in Figure 66. The W profile is also quite smooth and resembles that shown in Figure 65.

The braze layer in the 100-hour (3.6×10^5s) aged B sample of Figure 72 is about 10 mil (0.254 mm) thick. There is no interface reaction region at the Al_2O_3 surface. Although a demarcation line appears at the braze-Cb-1Zr juncture, epitaxy is evident, and the braze DPH hardness value is about 320 units, with the usual value of 75 in the Cb-1Zr.

Figure 75 shows the Nb(Cb) and the V line profiles to be rather smooth, although there is a dip in the Nb(Cb) trace near its center. There is a suggestion of a corresponding dip in the V trace, but it is much less evident, and might be discounted if it were not for the Nb(Cb) trace. However, a peak also occurs on the Zr profile, so the phenomenon is considered real, and is attributed to crossing a grain boundary along the line of traverse. The W trace is similar to that shown in Figure 65.

The braze layer in the 500-hour (1.8×10^6s) Sample C is shown in Figure 73 and is seen to be about 5 mils (0.127 mm) wide. A thin reaction zone of about 0.2 mils (0.0051 mm) is also seen, but the difference in

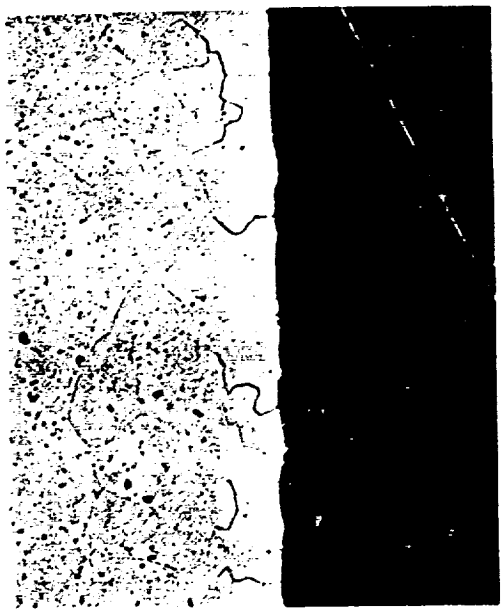

A. Micrograph, 100X

B. Micrograph, 100X

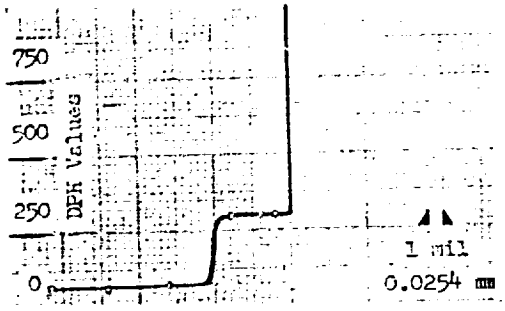

A. Microhardness Profile

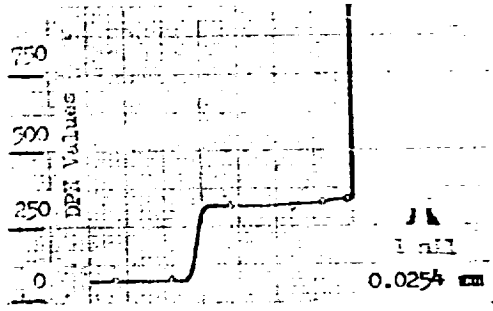

B. Microhardness Profile

V:	Similar to Figure 66
Zr:	Figure 74
Cb(Nb):	Similar to Figure 66
W:	Similar to Figure 65
Al:	Figure 74

A. Electron Microprobe Line Profile Summary.

V:	Figure 75
Zr:	Similar to Figure 74
Cb(Nb):	Figure 75
W:	Similar to Figure 65
Al:	Figure 75

B. Electron Microprobe Line Profile Summary.

Figure 72. Braze Analysis Data: Braze System 5W (Cb-1Zr/V-1Zr/W/Al_2O_3) brazed at 1870°C for 60 s. Sample A aged for 10 hrs (3.6×10^4s) at 1200°C; Sample B aged for 100 hrs (3.6×10^5s) at 1200°C.

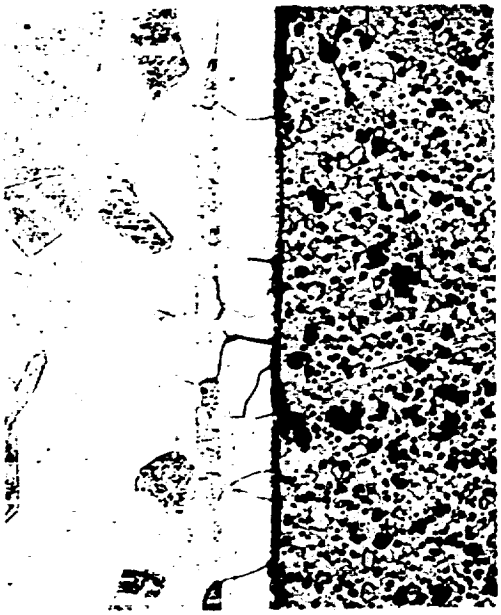

C. Micrograph, 100X

D. Micrograph, 100X

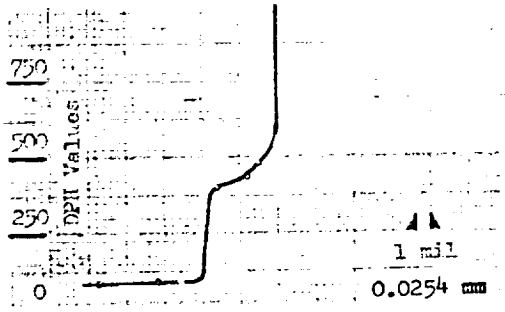

C. Microhardness Profile

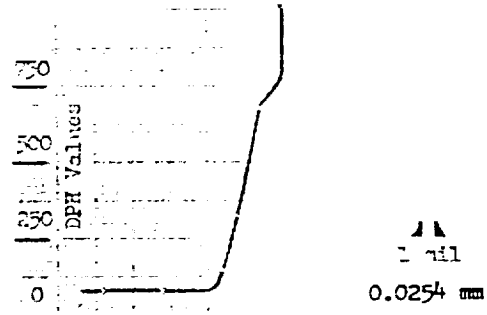

D. Microhardness Profile

V:	Figure 76
Zr:	Figure 76
Cb(Nb):	Similar to Figure 75
W:	Similar to Figure 65
Al:	Figure 76

C. Electron Microprobe Line Profile Summary.

V:	Figure 78
Zr:	Figure 77
Cb(Nb):	Figure 78
W:	Similar to Figure 65
Al:	Figures 77, 78

D. Electron Microprobe Line Profile Summary

Figure 73. Braze Analysis Data: Braze System 5W (Cb-1Zr/V-1Zr/W/Al_2O_3) brazed at 1870°C for 60s. Sample C aged for 500 hrs (1.8×10^6s) at 1200°C; Sample D aged for 1000 hrs (3.6×10^6s) at 1200°C.

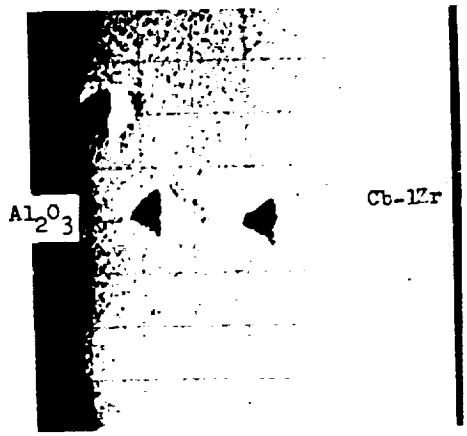

Sample A. Aged 10 hours at 1200°C
Back-Scattered Electron Image, 400X

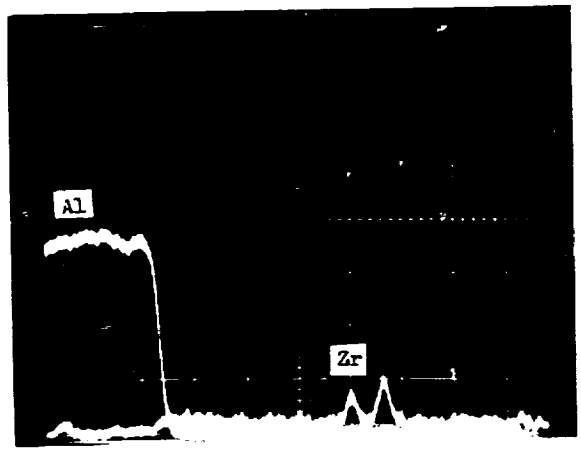

Sample A. Aged 10 hours at 1200°C
Line Profiles, Al and Zr, 800X

Figure 74. Braze Analysis Data: Braze System 5W (Cb-1Zr/V-1Zr/W/Al_2O_3) brazed at 1870°C for 1 minute.

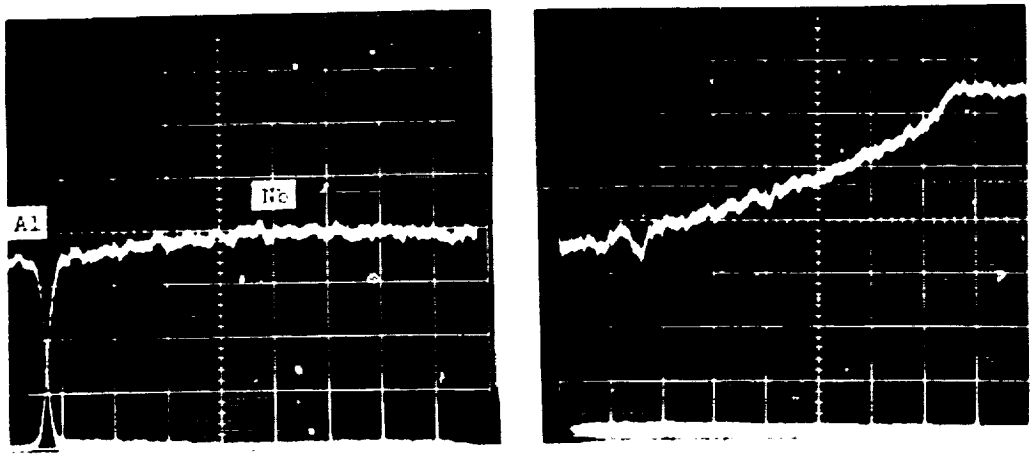

Sample B. Aged 100 hours at 1200°C
Line Profiles, Al and Nb, 800X

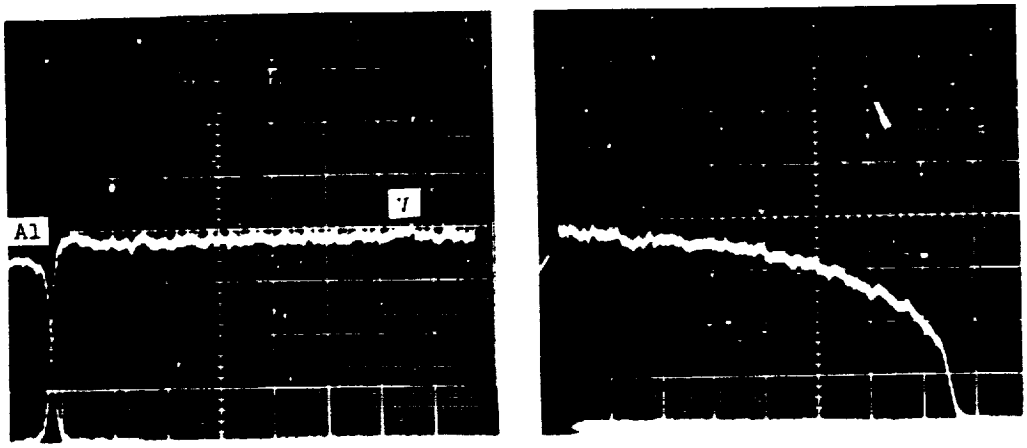

Sample B. Aged 100 hours at 1200°C
Line Profiles, Al and V, 800X

Figure 75. Braze Analysis Data: Braze System 5W (Cb-1Zr/V-1Zr/W/Al_2O_3) brazed at 1870°C for 1 minute.

levels of the Al_2O_3 and the braze makes it difficult to see. An interfacial region at the Cb-1Zr and braze juncture is also seen, although the crystallites continue through this region from the Cb-1Zr on the one side to the braze proper on the other. The hardness profile is seen to rise from a DPH value of 400 to 475 across the braze.

Figure 76 shows the Zr and the V line profiles for this C sample. A Zr peak is shown at the interface, but there is no corresponding perturbation in the V trace. The Nb(Cb) trace is not shown, but it, too, does not show a perturbation corresponding with that of the Zr trace. The Nb(Cb) trace is similar to that shown in Figure 75, and the W trace is similar to that of Figure 65.

The braze layer in the 1000-hour (3.6×10^6s) Sample D is shown in Figure 73. The braze itself is 5 mils (0.127 mm) thick. In addition, a very wide (1-2 mil, 0.0254-0.0508 mm) reaction area is present. In this sample, the etchant has preferentially attacked the reaction zone material and cut a groove in the sample. This groove is also seen in Figure 77, the Back-Scattered Electron Image of this D sample. The groove is more visible at higher magnifications, and the appearance of its depths verifies that it was caused by very active etching, even though the degree of etching on the base braze and Cb-1Zr surfaces is not excessive.

The hardness profile of the braze region is a steep curve which rises from the usual DPH value of 75 for the Cb-1Zr to at least 675 at a point 1.5 mils (0.038 mm) from the Al_2O_3.

Figure 77 also shows the Zr line profile for this D sample. The depression in both the Al and the Zr traces at the interface represents the groove, whose depth interferes with the x-ray optics of the electron microprobe. A low value is typically observed in a line profile that passes over a groove whose depth exceeds a mil (.0254 mm).

Figure 78 shows the Nb(Cb) and V line profiles. A great deal of structure is apparent, although it is not readily explained. The initial groove in the Nb(Cb) and Al traces is present, but it does not appear in the V trace. The presence of a Nb-V-Al phase is suggested by the correspondence of the flat regions in the Nb, V, and Al traces about one scale division (11.3μ) from the interface. Then, just adjacent to that region, the V trace rises abruptly and the Nb and the Al traces fall to lower values. In the next region, the Nb(Cb) and the Al rise, and the V again falls. Finally, the Al returns to its more common low level, the V rises to its normal curve position, and the Nb(Cb) drops slightly to its normal position. Beyond this point, all traces behave normally. The different levels of the Al trace are real, because they appear in both Figures 77 and 78. Therefore, one must conclude that some compound or, at least, some ternary phase of Nb(Cb) with V and Al has formed in this D sample. One possible explanation is that the development of the phase is the consequence of aging and the presence of a larger-than-usual amount of Al. Similar evidence of a ternary phase is seen in Sample 9M, but without further evidence, one cannot be certain as to its cause.

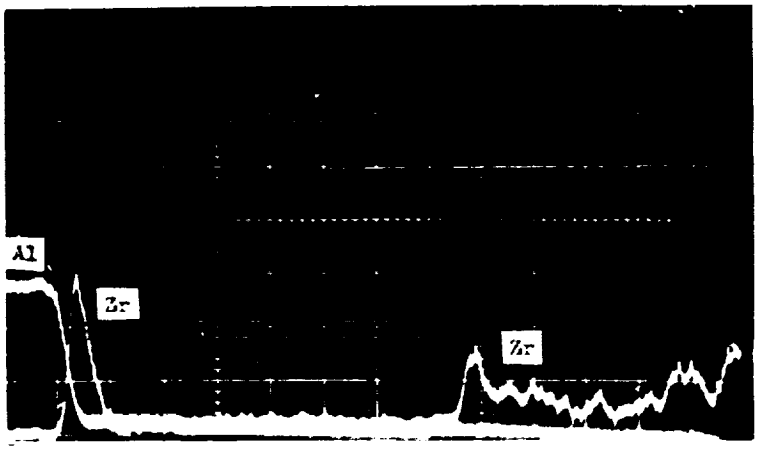

Sample C. Aged 500 hours at 1200°C
Line Profiles, Al and Zr, 800X

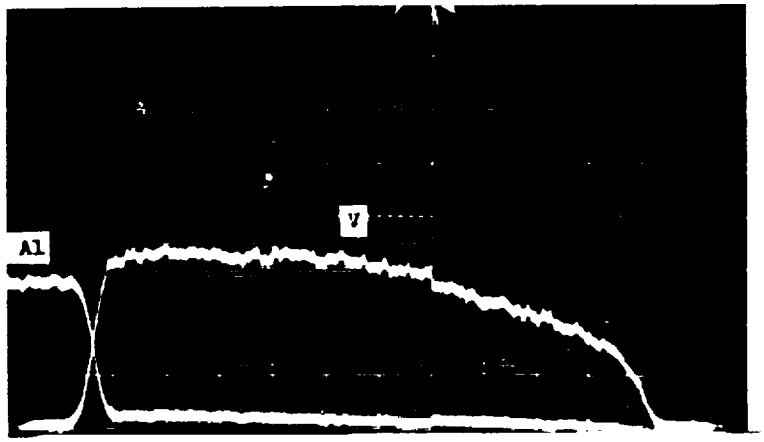

Sample C. Aged 500 hours at 1200°C
Line Profiles, Al and V, 800X

Figure 76. Braze Analysis Data: Braze System 5W ($Cb-1Zr/V-1Zr/W/Al_2O_3$) brazed at 1870° C for 1 minute.

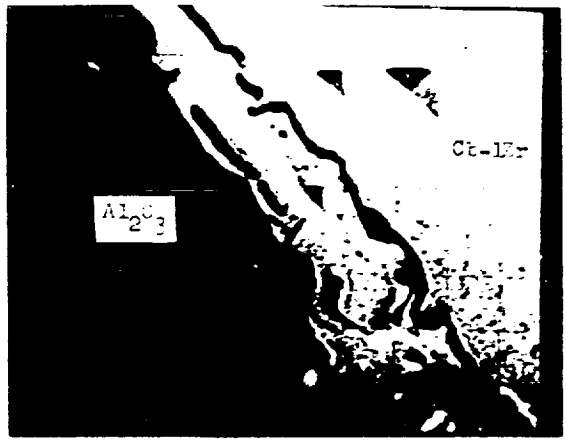

Sample D. Aged 1000 hours at 1200°C
Back-Scattered Electron Image, 400X

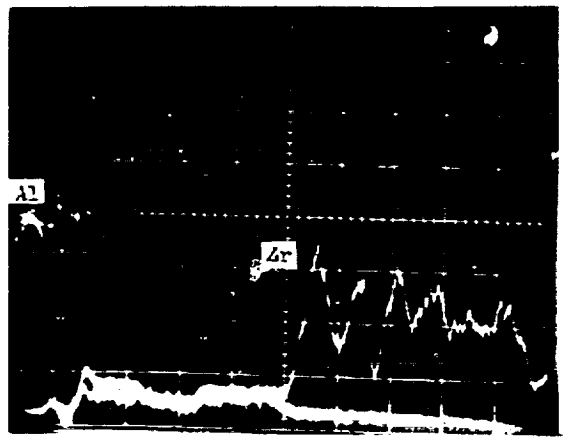

Sample D. Aged 1000 hours at 1200°C
Line Profiles, Al and Zr, 800X

Figure 77. Braze Analysis Data: Braze System 5W (Cb-1Zr/V-1Zr/W/Al_2O_3) brazed at 1870°C for 1 minute.

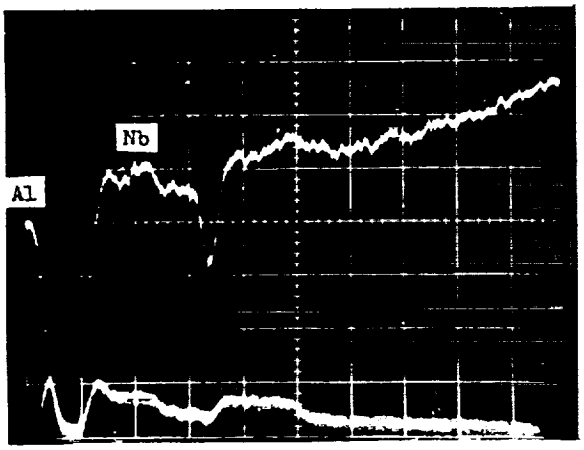

Sample D. Aged 1000 hours at 1200°C
Line Profiles, Al and Nb, 800X

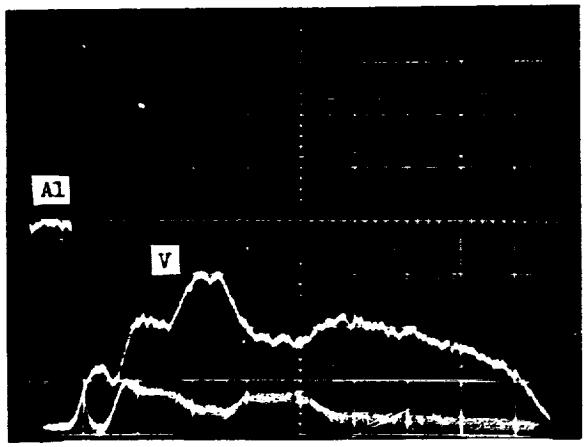

Sample D. Aged 1000 hours at 1200°C
Line Profiles, Al and V, 800X

Figure 78. Braze Analysis Data: Braze System 5W (Cb-1Zr/V-1Zr/W/Al_2O_3) brazed at 1870°C for 1 minute.

In summary, Braze System 5W does not show a really consistent pattern. The A and D samples show rather large interaction regions, but the B and C samples do not. The A and B samples show moderate and level hardness profiles, but C and D samples show a slope. There is an indication of a concentration of Zr at the interface in Sample C, but it does not appear to happen in the other samples. Finally, there is evidence in the D sample of the development of a ternary Nb(Cb)-V-Al phase.

Braze System 6W (Cb-1Zr/V-2Ti/W/Al_2O_3): An examination of Figure 79, which shows data for Braze System 6W shows the thickness of the 10-hour (3.6×10^4s) aged A sample to be 4 mils (0.10 mm). Epitaxy is evident, as is a thin interface reaction layer at the Al_2O_3 surface, and a suggestion of a layer at the Cb-1Zr surface. The DPH hardness values are essentially linear ranging from about 500 near the Al_2O_3 to the characteristic value of 75 in the Cb-1Zr. However, there is some question regarding the accuracy of the highest value, because the Back-Scattered Electron Image of the sample (Figure 81) shows the last indent to be only partly in the braze. Therefore, if there is a correction, it is a downward one. Figure 81 also shows the Ti line profile for Sample A, and it is seen to be rather uniformly distributed in the braze region with no indication of any concentration at the Al_2O_3 interface.

Figure 82 shows the Zr and the W line profiles, and they, too, are seen to be rather flat across the braze thickness. A group of peaks is shown near the braze-Cb-1Zr interface in the Zr profile, but there is no corresponding change in either the Nb(Cb) or the V line profiles shown in Figure 83. The Zr behavior in this region remains an anomaly, but it should be remembered that Zr is shown using a scale factor of 0.2 v/cm (0.2 v/scale div.) while the Al is shown at 5 v/cm (5 v/scale div.) and Nb(Cb) and V are shown at 1 v/cm (1 v/scale div.). Therefore, the nominal 3 scale div. height of the Zr peaks represents a microprobe pickup response corresponding to 0.6 v, while the 4.5 scale div. response for the maximum Al trace represents 22.5 v. Similarly, in Figure 83 the 8.0 scale div. for V represents an 8 volt response, and the 4.5 scale div. record for Nb represents a 4.5 v response. In comparison, therefore, the 0.6 v Zr peaks are not of major import.

The braze layer in the 100-hour (3.6×10^5s) aged B sample of Figure 79 is wedge-shaped, and ranges in thickness from less than 6 mils (0.152 mm) to nearly 7 mils (0.178 mm). Epitaxy is evident. No layer at the Al_2O_3 surface is seen, but the hardness profile (100 gm DPH) is unusual. The Al_2O_3-braze interface is softer than the bulk of the braze, and the lowest value was read rather close to the Al_2O_3. However, all DPH values are in the 250-325 range. The photomicrograph clearly shows the hardness indents. They are also seen in the Back-Scattered Electron Image of Figure 84, which also shows the last indent to be within the braze. Figure 84 shows the Nb(Cb) line profile for Sample B, and Figure 85 shows the V line profile. These are seen to be rather smooth and regular in shape. The Ti, Zr, and W profiles are similar to those shown in Figures 81, 82, and 82, respectively.

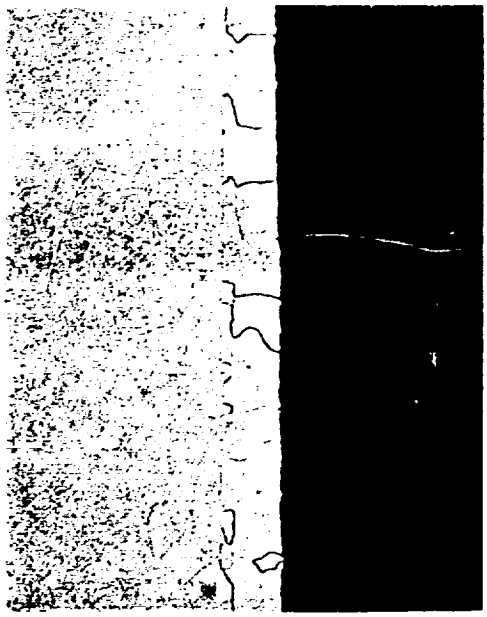

A. Micrograph, 100X

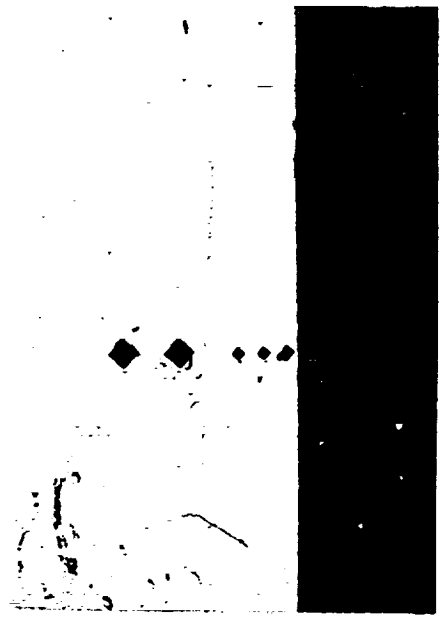

B. Micrograph, 100X

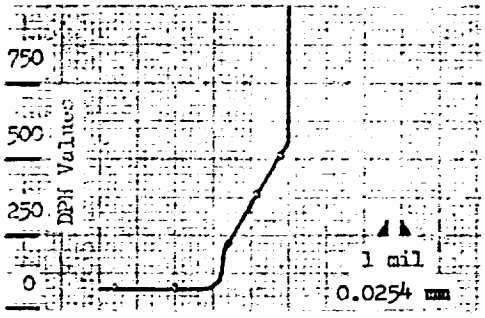

A. Microhardness Profile

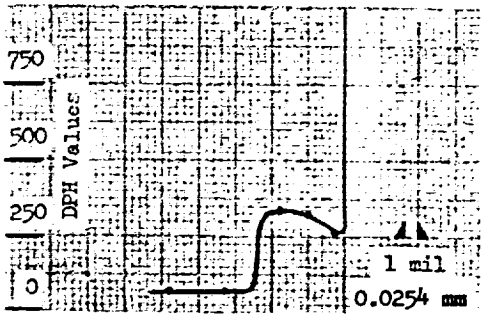

B. Microhardness Profile

V:	Figure 83
Ti:	Figure 81
Cb(Nb):	Figure 83
Zr:	Figure 82
W:	Figure 82
Al:	Figures 81, 82, 83

A. Electron Microprobe Line Profile Summary

V:	Figure 85
Ti:	Similar to Figure 81
Cb(Nb):	Figure 84
Zr:	Similar to Figure 82
W:	Similar to Figure 82
Al:	Figures 84, 85

B. Electron Microprobe Line Profile Summary

Figure 79. Braze Analysis Data: Braze System 6W (Cb-1Zr/V-2Ti/W/Al_2O_3) brazed at 1870°C for 60s. Sample A aged for 10 hrs (3.6×10^4s) at 1200°C; Sample B aged for 100 hrs (3.6×10^5s) at 1200°C.

C. Micrograph, 100X

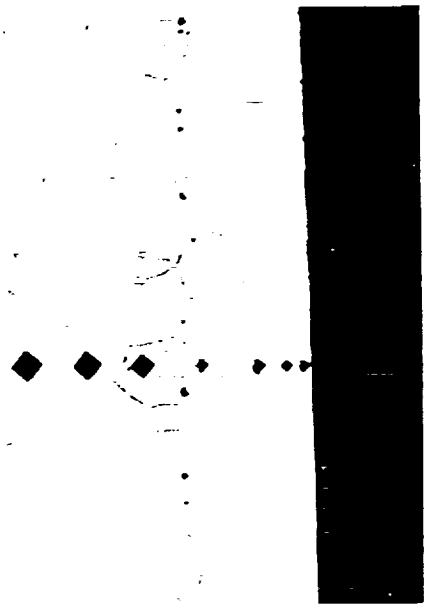

D. Micrograph, 100X

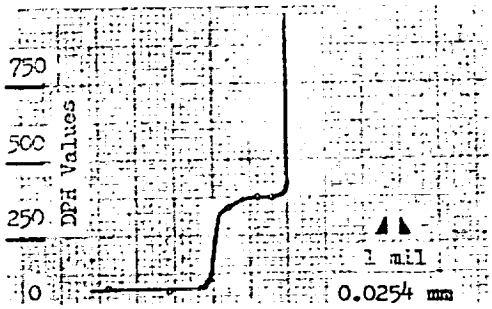

C. Microhardness Profile

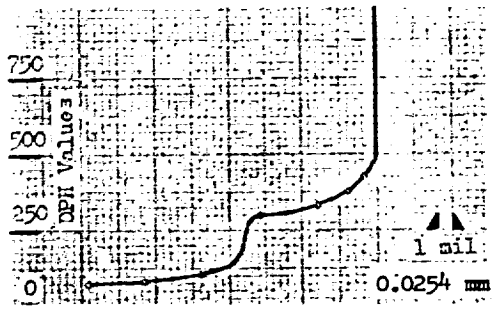

D. Microhardness Profile

V:	Figure 86
Ti:	Similar to Figure 81
Cb(Nb):	Figure 85
Zr:	Similar to Figure 82
W:	Similar to Figure 82
Al:	Figures 85, 86

C. Electron Microprobe Line Profile Summary.

V:	Figure 87
Ti:	Similar to Figure 81
Cb(Nb):	Figure 86
Zr:	Similar to Figure 82
W:	Similar to Figure 82
Al:	Figures 86, 87

D. Electron Microprobe Line Profile Summary.

Figure 80. Braze Analysis Data: Braze System 6W (Cb-1Zr/V-2Ti/W/Al_2O_3) brazed at 1870° C for 60 s. Sample C aged for 500 hrs (1.8×10^6 s) at 1200° C; Sample D aged for 100 hrs (3.6×10^6 s) at 1200° C.

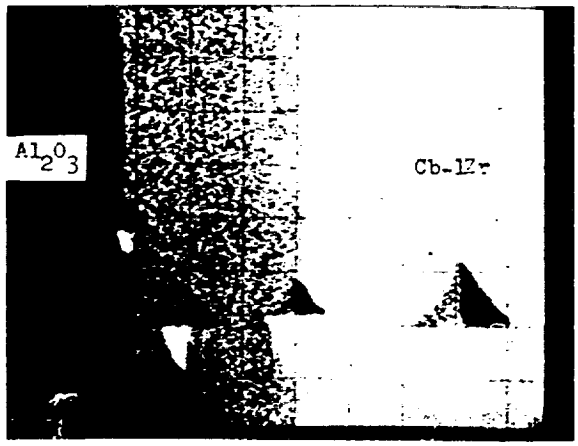

Sample A. Aged 10 hours at 1200°C
Back-Scattered Electron Image, 400X

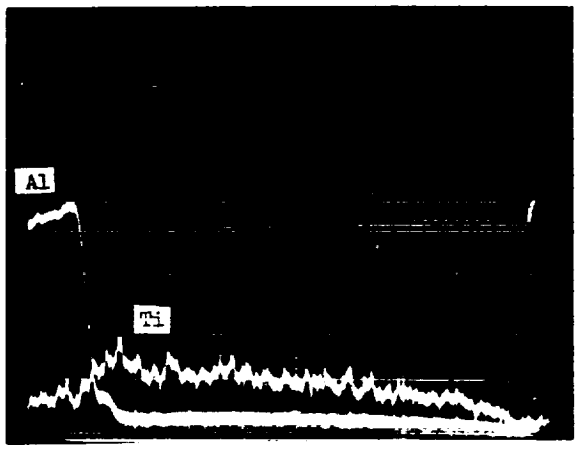

Sample A. Aged 10 hours at 1200°C
Line Profiles, Al and Ti, 800X

Figure 81. Braze Analysis Data: Braze System 6W (Cb-1Zr/V-2Ti/W/Al_2O_3) brazed at 1870°C for 1 minute.

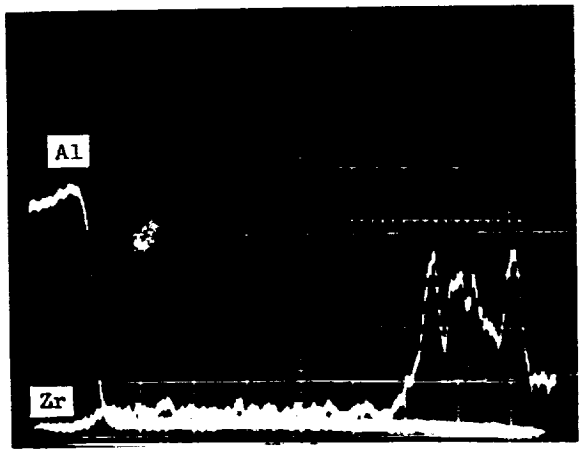

Sample A. Aged 10 hours at 1200°C
Line Profiles, Al and Zr, 800X

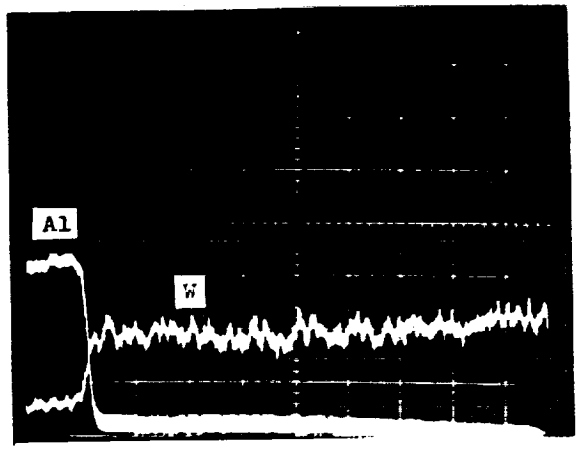

Sample A. Aged 10 hours at 1200°C
Line Profiles, Al and W, 800X

Figure 82. Braze Analysis Data: Braze System 6W (Cb-1Zr/V-2Ti/W/Al_2O_3) brazed at 1870° C for 1 minute.

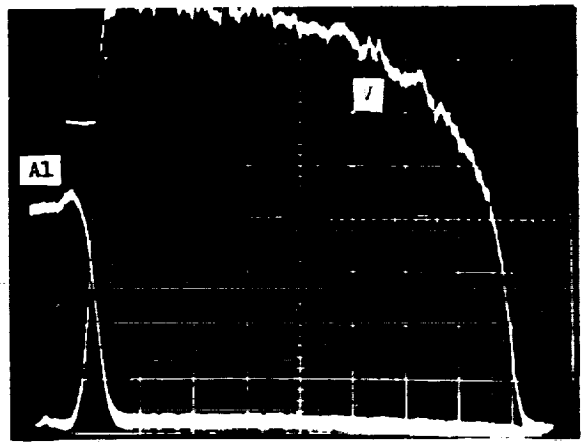

Sample A. Aged 10 hours at 1200°C
Line Profiles, Al and V, 800X

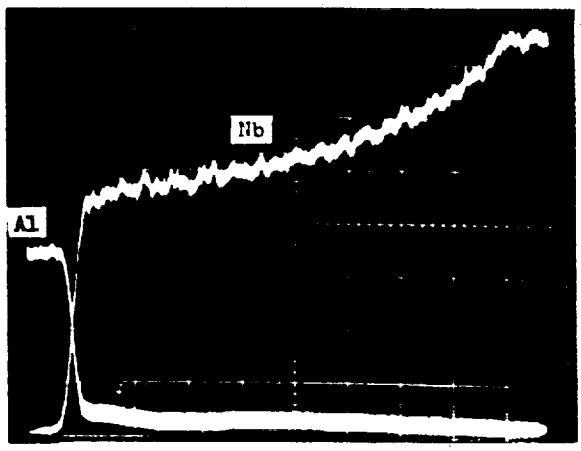

Sample A. Aged 10 hours at 1200°C.
Line Profiles, Al and Nb, 800X

Figure 83. Braze Analysis Data: Braze System 6W (Cb-1Zr/V-2Ti/W/Al_2O_3) brazed at 1870°C for 1 minute

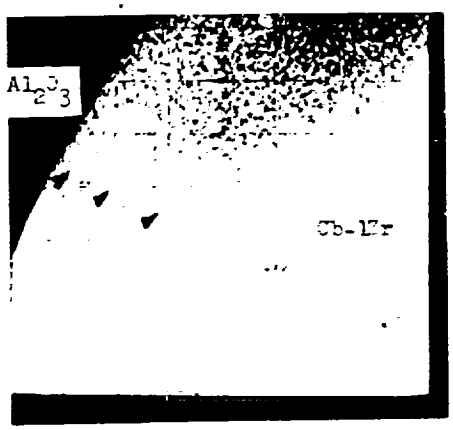

Sample B. Aged 100 hours at 1200°C
Back-Scattered Electron Image, 400X

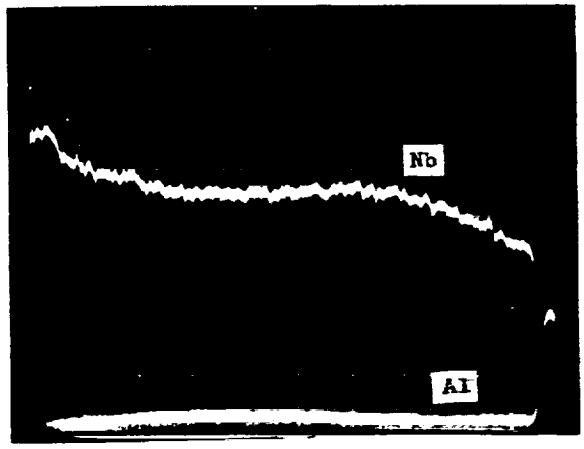

Sample B. Aged 100 hours at 1200°C.
Line Profiles, Al and Nb, 400X

Figure 84. Braze Analysis Data: Braze System 6W (Cb-1Zr/V-2Ti/W/Al_2O_3) brazed at 1870°C for 1 minute

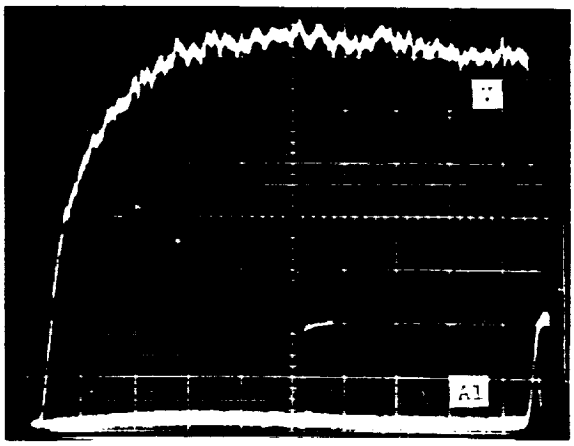

Sample B. Aged 100 hours at 1200°C.
Line Profiles, Al and V, 400X

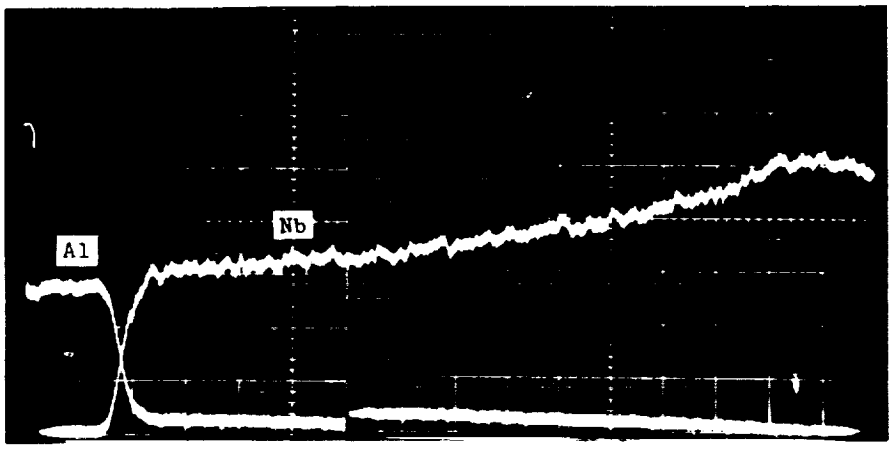

Sample C. Aged 500 hours at 1200°C
Line Profiles, Al and Nb, 800X

Figure 85. Braze Analysis Data: Braze System 6W (Cb-1Zr/V-2Ti/W/Al_2O_3) brazed at 1870° C for 1 minute

The braze layer in the 500-hour (1.8×10^6s) aged C sample is shown in Figure 80. The braze is about 5 mils (0.127 mm) thick and shows some epitaxy, although it is not as pronounced as it is in other specimens. The DPH hardness profile of the braze is rather flat and shows values of 350 to 375. Figure 85 shows the Nb(Cb) line profile and Figure 86 shows the V line profile for this C sample. Both are smooth and regular in shape. The Ti, Zr, and W line profiles are quite uniform, and are similar to those shown in Figures 81, 82, and 82, respectively.

The braze layer in the 1000-hour (3.6×10^6s) aged D samples is shown in Figure 80. The braze is about 9 mils (0.228 mm) thick and is quite coarse grained. An 0.2 mil (0.005 mm) thick reaction zone is present next to the Al_2O_3. The DPH hardness profile rises from the usual value of 75 in the Cb-1Zr to a level of 300, and then the value increases to 425 as the Al_2O_3 interface is approached. The last indent is seen to be within the braze both in Figure 80, and in the Back-Scattered Electron Image shown in Figure 87.

Figure 86 shows the Nb(Cb) line profile of the D sample, and it is seen to be smooth except for one dip at mid-length. The V line shown in Figure 87 is correspondingly smooth, except for a dip in the same location. The Zr trace shows a series of peaks at this location, which correspond to a grain boundary in the sample. The Ti and W line profiles are uniform, and are similar to those shown in Figures 81 and 82, respectively.

In summary, the 6W braze system produces brazes which range from 5 to 10 mils (0.127 to 0.254 mm) in thickness and show small reaction zones. The DPH microhardness values measured within the braze layers are in the range 300 to 425 (if the questionable value in the A sample is discounted). The electron microprobe line profiles are all rather regular and no anomalies appear to be present in the system.

Braze system 9M (Cb-1Zr/64V-34Cb-2Zr/Mo/Al_2O_3): An examination of Figure 88, the data for Braze System 9M shows the thickness of the 10-hour (3.6×10^4s) aged A sample to be about 2 mils (0.0508 mm) including a nominal 0.5 mil (0.0127 mm) reaction zone at the Al_2O_3 interface. Epitaxy is evident. The DPH hardness of the interface layer is 750, that of the mid-region of the braze is 450 and the Cb-1Zr alloy shows 75, as usual.

Figure 90 shows the Back-Scattered Electron Image for the A sample. The presence of Nb in the Braze is evident. No line profiles for this sample are shown because they are all quite normal. The Nb(Cb), Al, and V profiles are similar to those shown in Figure 83. The Zr line profile resembles the one shown in Figure 82, and the Mo profile is represented by those in Figures 45 or 54.

The braze layer in the 100-hour (3.6×10^4s) aged B sample in Figure 88 appears to be about 5 mils (0.127 mm) thick. No interface layer at the Al_2O_3 is present. The grain pattern suggests such a region at the Cb-1Zr-braze juncture, although no indication of a hardness effect is seen. The hardness profile rises from the typical DPH value of 75 in the Cb-1Zr to 425 near the Al_2O_3 interface in a smooth curve.

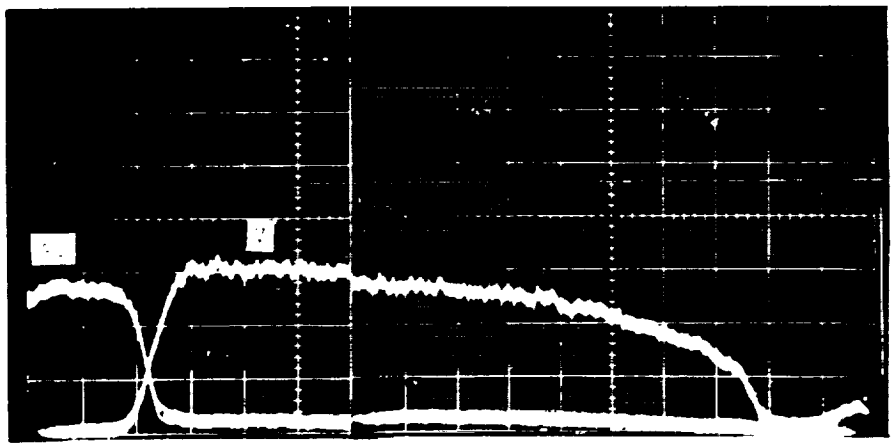

Sample C. Aged 500 hours at 1200°C
Line Profiles, Al and V, 800X

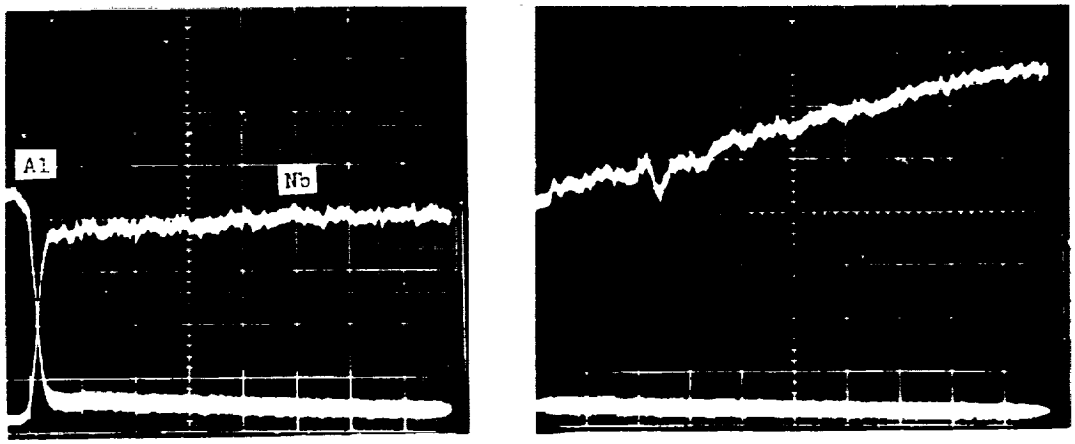

Sample D. Aged 1000 hours at 1200°C
Line Profiles, Al and Nb, 800X

Figure 86. Braze Analysis Data: Braze System 6W ($Cb-1Zr/V-2Ti/W/Al_2O_3$) brazed at 1870° C for 1 minute

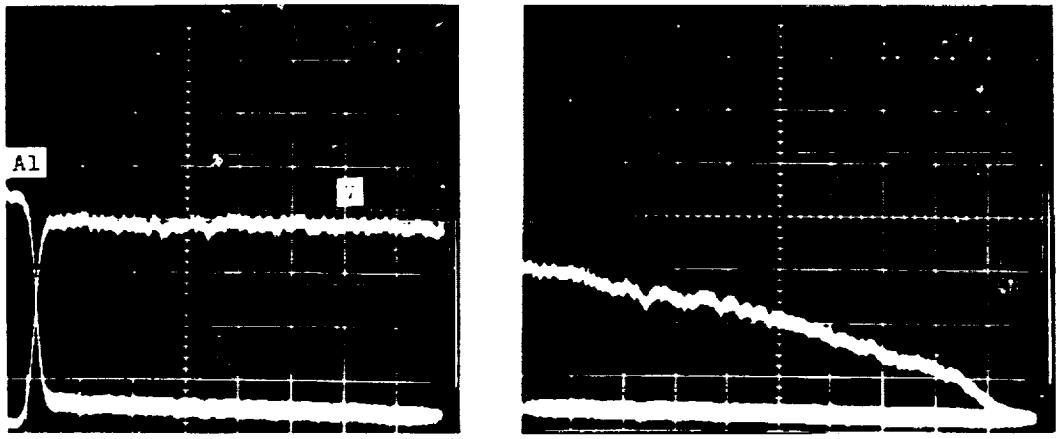

Sample D. Aged 1000 hours at 1200°C
Line Profiles, Al and V, 800X

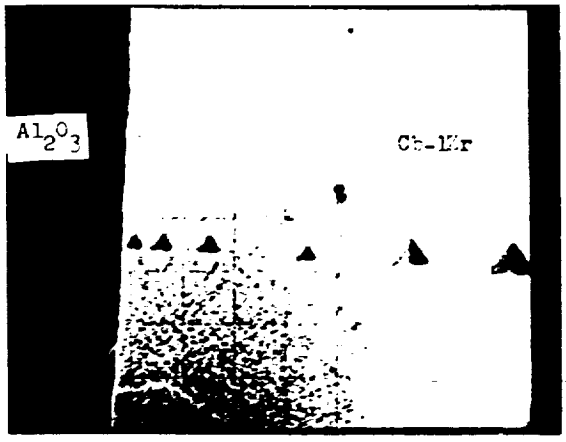

Sample D. Aged 1000 hours at 1200°C
Back-Scattered Electron Image, 200X

Figure 87. Braze Analysis Data: Braze System 6W (Cb-1Zr/V-2Ti/W/Al_2O_3) brazed at 1870°C for ½ minute.

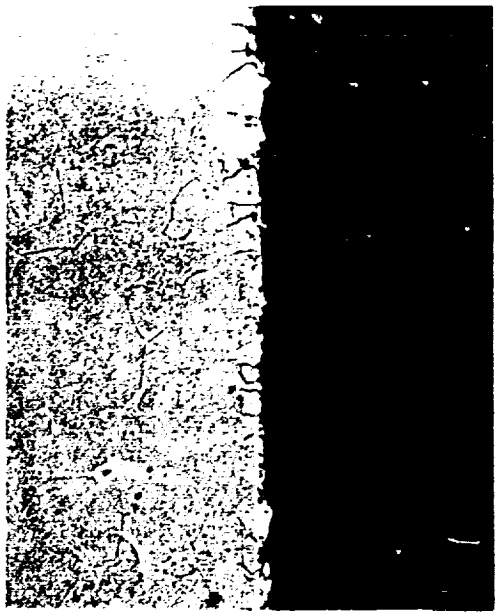

A. Micrograph, 100X

B. Micrograph, 100X

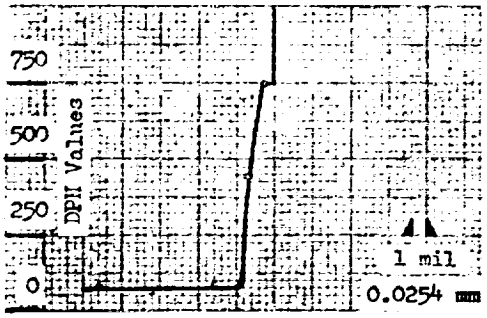

A. Microhardness Profile

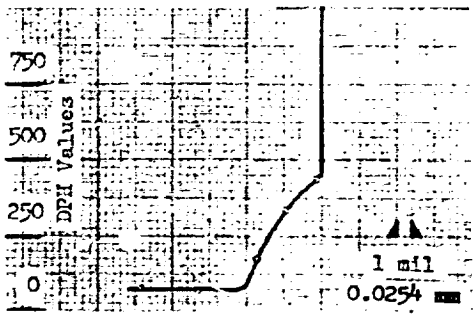

B. Microhardness Profile

V:	Similar to Figure 83
Cb(Nb):	Similar to Figure 83
Zr:	Similar to Figure 82
Mo:	Similar to Figures 45, 54
Al:	Similar to Figure 83

A. Electron Microprobe Line Profile Summary.

V:	Figure 91
Cb(Nb):	Figure 91
Zr:	Figure 90
Mo:	Similar to Figures 45, 54
Al:	Figures 90, 91

B. Electron Microprobe Line Profile Summary

Figure 88. Braze Analysis Data: Braze System 9M (Cb-1Zr/64V-34Cb-2Zr/Mo/Al_2O_3) brazed at 1860° C for 60 s. Sample A aged for 10 hrs (3.6×10^4 s) at 1200° C; Sample B aged for 100 hrs (3.6×10^5 s) at 1200° C.

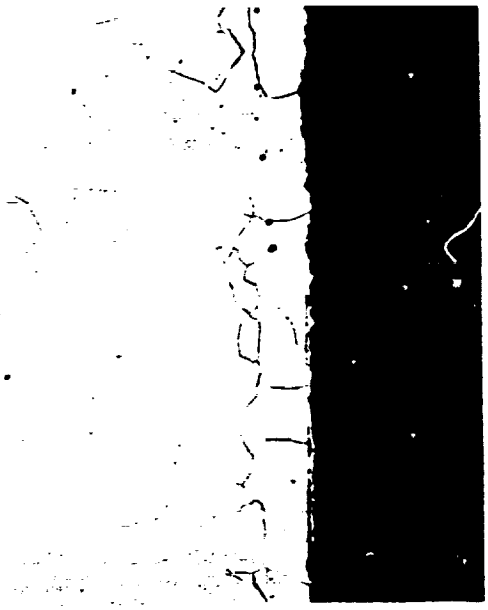

C. Micrograph, 100X

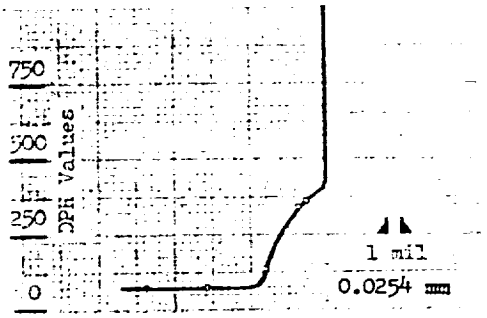

C. Microhardness Profile

V:	Figure 92
Cb(Nb):	Figure 92
Zr:	Similar to Figure 90
Mo:	Similar to Figures 45, 54
Al:	Figure 92

C. Electron Microprobe Line Profile Summary

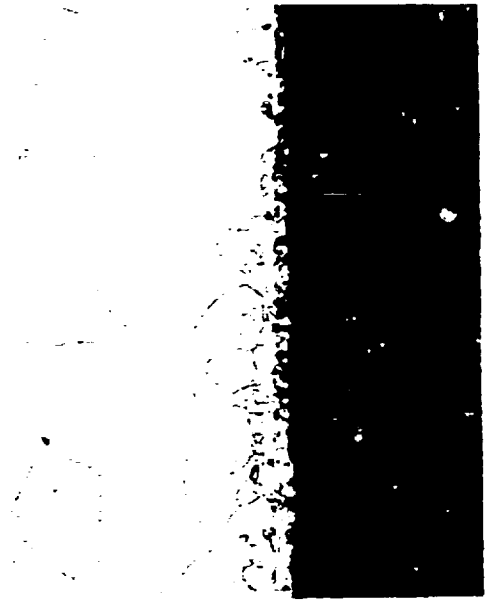

D. Micrograph, 100X

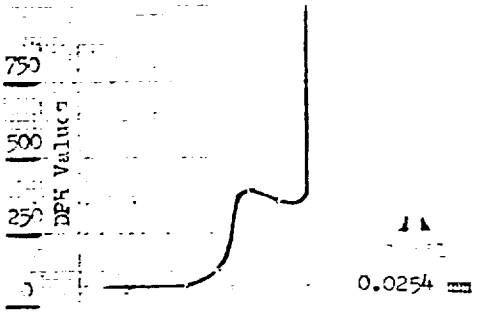

D. Microhardness Profile

V:	Figure 94
Cb(Nb):	Figure 94
Zr:	Figure 93
Mo:	Similar to Figures 45, 54
Al:	Figures 93, 94

D. Electron Microprobe Line Profile Summary.

Figure 89. Braze Analysis Data: Braze System 9M (Cb-1Zr/64V-34Cb-2Zr/Mo/Al_2O_3) brazed at 1860° C for 60 s. Sample C aged for 500 hrs (1.8 x 10^6s) at 1200° C; Sample D aged 1000 hrs (3.6 x 10^6s) at 1200° C.

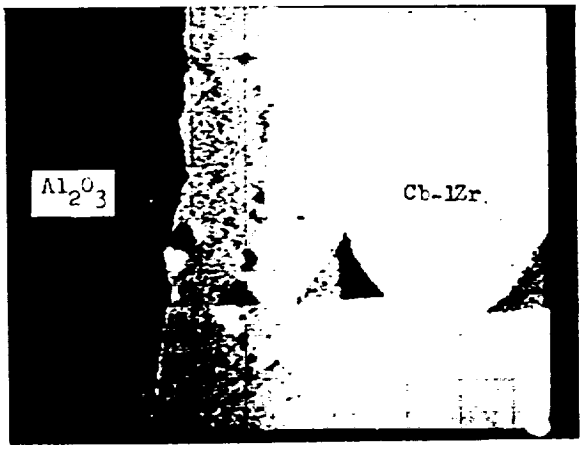

Sample A. Aged 10 hours at 1200°C
Back-Scattered Electron Image, 400X

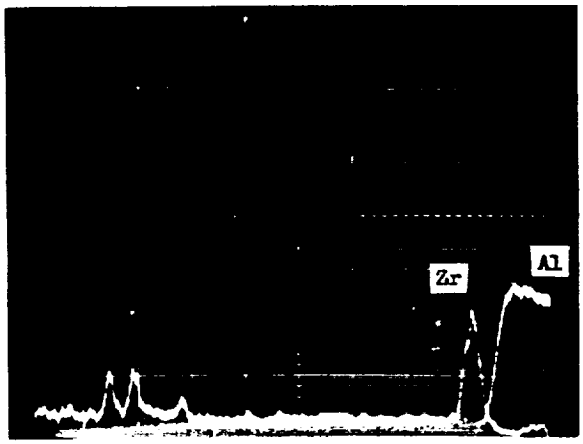

Sample B. Aged 100 hours at 1200°C
Line Profiles, Al and Zr, 800X

Figure 90. Braze Analysis Data: Braze System 9M (Cb-1Zr/64V-34Cb-2Zr/Mo/Al_2O_3) brazed at 1860°C for 1 minute.

Figure 90 shows the Zr line profile for this sample to have a modest peak at the Al_2O_3 interface. In addition, three small peaks appear in the region of the Cb-1Zr-braze interface. Figure 91 shows the Nb(Cb) and line profiles for Sample B. No irregularities are seen in these traces, suggesting that the effect of the Zr peak (0.4 v) is within the noise variations of the Nb(Cb) and the V traces.

The braze layer in the 500-hour (1.8×10^6s) aged C sample is shown in Figure 89. The layer is about 4 mils (0.102 mm) thick with an 0.4 mil (0.0102 mm) thick reaction zone adjacent to the Al_2O_3. Epitaxy is shown. The hardness profile is seen to rise steadily from the DPH value of 75 in the Cb-1Zr to a value of 360 about 1 mil (0.0254 mm) from the interface.

Figure 92 shows the Nb(Cb) and V line profiles for the C samples. Small dips are seen at the interface region, otherwise the traces are smooth and normal. The Zr line profile shows a large peak corresponding to these dips, which confirms the presence of the reaction layer.

The braze layer in the 1000-hour (3.6×10^6s) aged D sample is shown in Figure 89. The braze is about 5 mils (0.127 mm) thick with a 1 mil (0.0254 mm) thick reaction layer at the Al_2O_3 surface. The hardness profile is unusual in that a maximum appears in the middle of the braze region, although its DPH value is only 375. The base Cb-1Zr again shows its characteristic DPH value of 75.

Figure 93 shows the Back-Scattered Electron Image of the D sample. This image is similar to those of other brazes in that the presence of Nb(Cb) is shown throughout the braze. It has an additional feature of several very dark regions, which are probably areas in which reaction products have formed, and which were then more heavily etched than the surrounding areas. Because of this, the scattered electrons from the etch grooves originate from a different level and are out of focus relative to the adjacent areas. These regions thus appear dark.

Figure 93 also shows the Zr line profile for the D sample, and the presence of modest peaks at the mid-width of the braze is observed. More disturbing features, however, are the line profiles of Nb(Cb), V, and Al in this specimen. These are shown in Figure 94. There is a suggestion that a Nb-V-Al phase appears near the Al_2O_3 interface, because there is a distinct rise in the Nb(Cb) trace coupled with a drop in the V trace, and with both levels being about one scale division (nominally 12 microns) wide. At the same location, there is a small, but noticeable, increase in the Al profile height for about the same width. In addition, there is another region at the mid-width of the braze. Here the Nb(Cb) trace is flat at the same level as that at the Al_2O_3 interface, and the V and the Al trace levels are also the same as those at the interface. Thus, this is very strong evidence that the factor producing this set of perturbations in the traces involves the three elements. Zirconium does not appear to be involved, in that there is no peak in the Zr profile at the interface, although one of the two peaks at the mid-

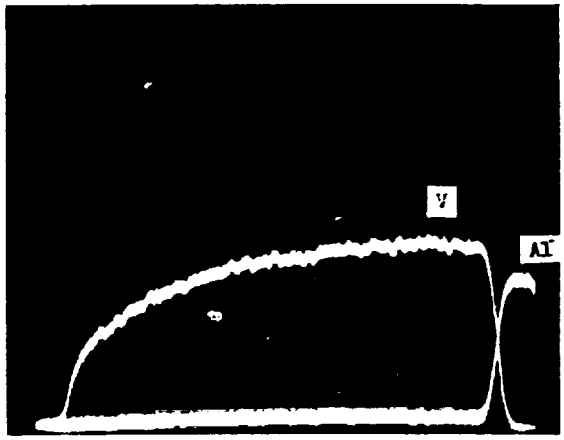

Sample B. Aged 100 hours at 1200°C
Line Profiles, Al and V, 800X

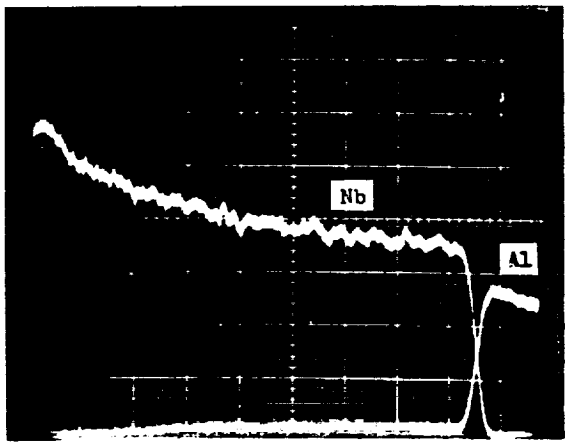

Sample B. Aged 100 hours at 1200°C.
Line Profiles, Al and Nb, 800X

Figure 91. Braze Analysis Data. Braze System 9M (Cb-1Zr/64V-34Cb-2Zr/Mo/Al_2O_3) brazed at 1860°C for 1 minute.

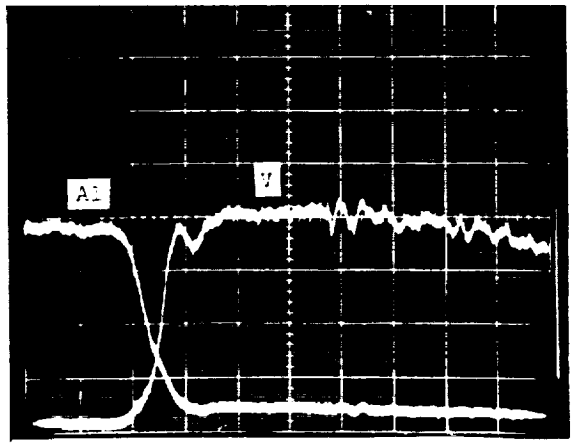

Sample C. Aged 500 hours at 1200°C
Line Profiles, Al and V, 800X

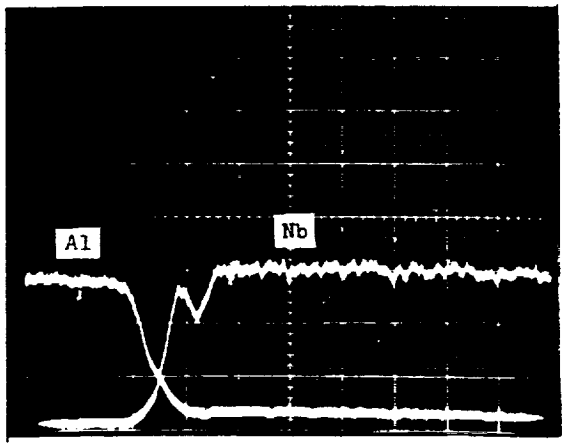

Sample C. Aged 500 hours at 1200°C
Line Profiles, Al and Nb, 800X

Figure 92. Braze Analysis Data. Braze System 9M (Cb-1Zr/64V-34Cb-2Zr/Mo/Al_2O_3) brazed at 1860° C for 1 minute.

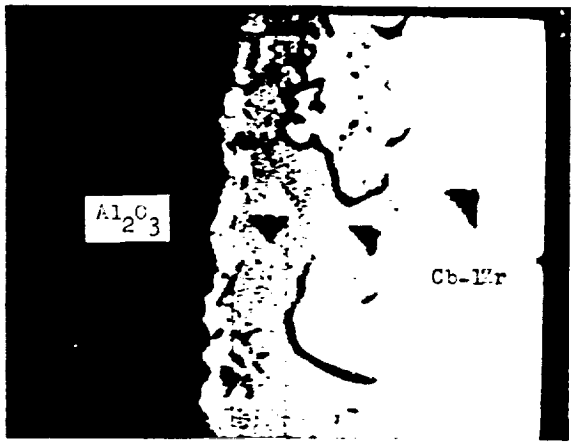

Sample D. Aged 1000 hours at 1200°C
Back-Scattered Electron Image, 400X

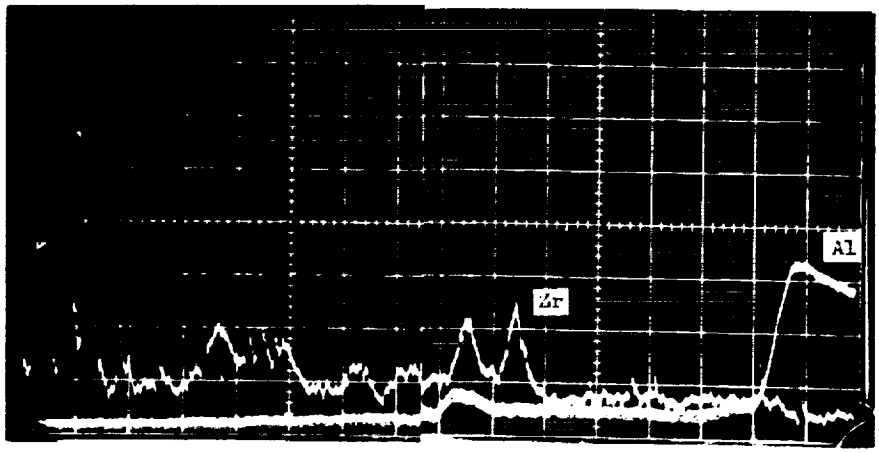

Sample D. Aged 1000 hours at 1200°C
Line Profiles, Al and Zr, 800X

Figure 93. Braze Analysis Data. Braze System 9M (Cb-1Zr/64V-34Cb-2Zr/Mo/Al_2O_3) brazed at 1860°C for 1 minute.

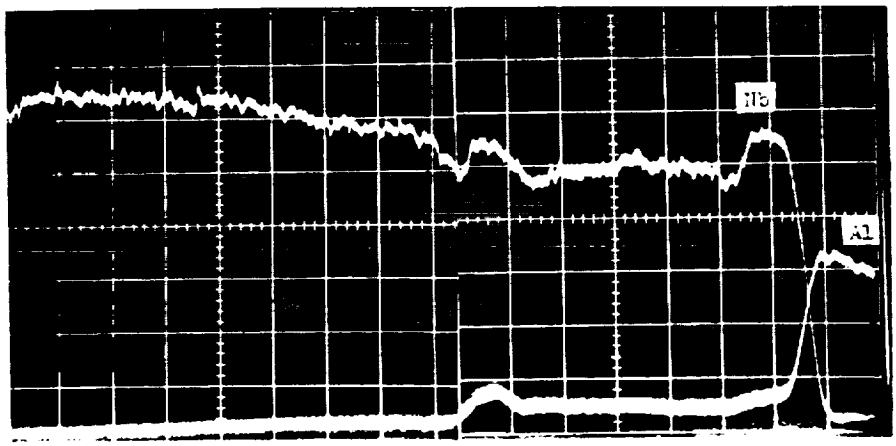

Sample D. Aged 1000 hours at 1200°C
Line Profiles, Al and Nb, 800X

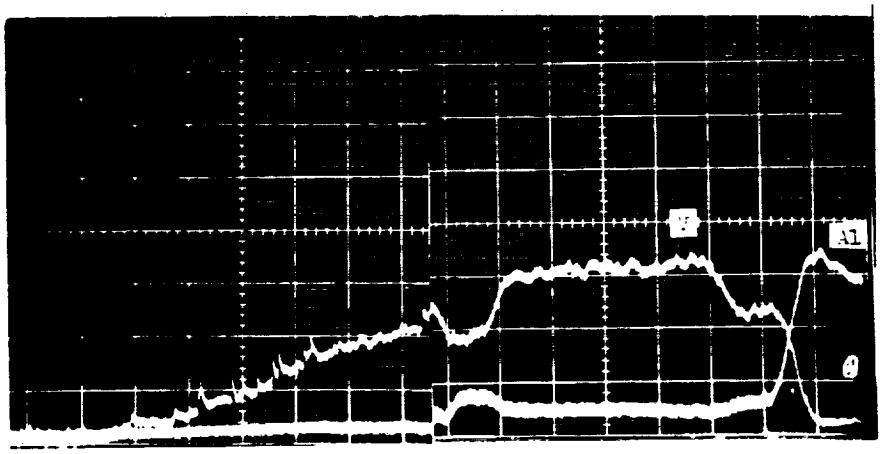

Sample D. Aged 1000 hours at 1200°C
Line Profiles, Al and V, 800X

Figure 94. Braze Analysis Data. Braze System 9M (Cb-1Zr/64V-34Cb-2Zr/Mo/Al_2O_3) brazed at 1860°C for 1 minute.

width does correspond in position with the Nb-V-Al effect. Because the second Zr peak does not correspond with any features of the other profiles, and because the Zr trace seems to be somewhat noisy in any event, it is concluded that Zr is not a factor here.

In summary, the 9M braze system is characterized by the presence of substantial interaction regions, which in the 1000-hour (3.6×10^6s) D sample approach a mil (0.0254 mm) in width. It is not clear whether the D sample's wide reaction zone was the result of the aging treatment, but it is one of the thickest reaction zones seen in any braze system. The DPH hardness values of these brazes are generally below 400, although one value of 750 was found. Epitaxial growth of the braze alloy on the Cb-1Zr grains is common.

Braze System 9W (Cb-1Zr/64V-34Cb-2Zr/W/Al_2O_3): An examination of Figure 95, the data for Braze System 9W, shows the visually discernable braze of the 10-hour (3.6×10^4s) aged A sample to be about 4 mils (0.101 mm) thick. A slight interface layer is evident adjacent to the Al_2O_3. The hardness profile shows the highest value at the Cb-1Zr-braze juncture, and a minimum (except for the Cb-1Zr alloy) of 250 DPH units near the Al_2O_3.

No electron microprobe data are shown for this sample, because all of the traces are quite similar to others which have been shown previously. The Nb(Cb) and V traces are smooth and resemble those shown in Figure 91. The Zr trace shows evidence of a concentration at the interface, and is similar to the trace shown in Figure 90. However, there is no reflection of the presence of the local increase in Zr in the Nb(Cb) or V traces. The W trace is uniform at a low level as indicated by the trace in Figure 82.

The braze layer in the 100-hour (3.6×10^5s) aged B sample of Figure 95 is 6 mils (0.152 mm) thick and shows a gradual decrease in DPH hardness from the Al_2O_3 interface (325) to the edge of the braze (about 250), and then a drop to the 75-80 DPH value of Cb-1Zr alloy. No surface layer is seen at the Al_2O_3. Epitaxy and rather large grains are evident in this braze.

Figure 97 shows the line profile of Zr in the B sample. A concentration of Zr is observed at the Al_2O_3 interface, but the V and Nb(Cb) profiles do not show any compensating effects, and are similar to the profiles of Figure 66. The W trace is uniform across the braze thickness, and is represented by Figure 82.

The braze layer in the 500-hour (1.8×10^6s) aged C sample shown in Figure 96 is about 9 mils (0.229 mm) thick. A very thin interface layer is shown, and the braze DPH hardness values are rather uniform at 300 over the entire braze thickness. Figure 97 shows the Zr profile for the 9W-C braze, and as in the A and B samples, a concentration of Zr appears at the Al_2O_3 surface. Again, as was seen in the B samples, the Nb(Cb) and V traces are normal and do not reflect the presence of Zr at the interface. The W line profile is flat and similar to that shown in Figure 82.

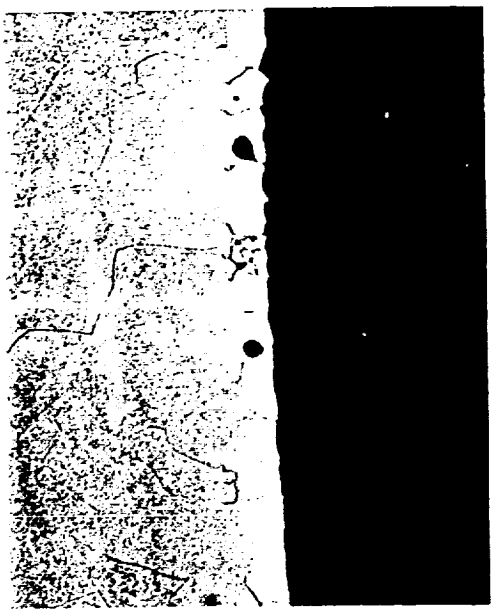

A. Micrograph, 100X

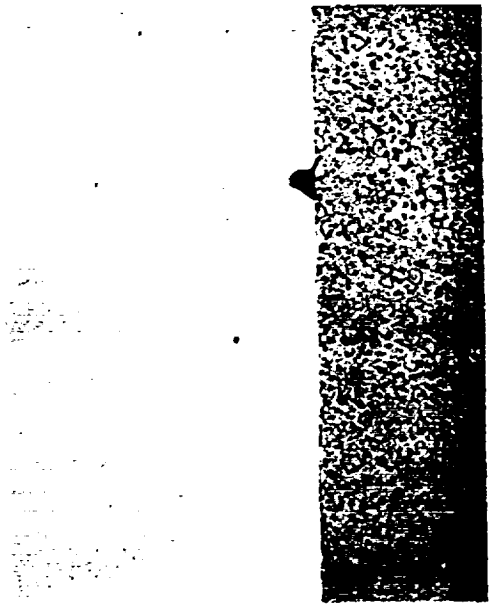

B. Micrograph, 100X

A. Microhardness Profile

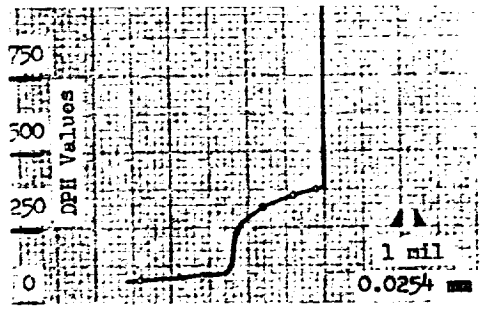

B. Microhardness Profile

V: Similar to Figure 91
Cb(Nb): Similar to Figure 91
Zr: Similar to Figure 90
W: Similar to Figure 82
Al: Similar to Figure 90, 91

A. Electron Microprobe Line Profile Summary.

V: Similar to Figure 66
Cb(Nb): Similar to Figure 66
Zr: Figure 97
W: Similar to Figure 82
Al: Figure 97

B. Electron Microprobe Line Profile Summary.

Figure 95. Braze Analysis Data: Braze System 9W (Cb-1Zr/64V-34Cb-2Zr/Al_2O_3) brazed at 1870°C for 60 s. Sample A aged for 10 hrs (3.6×10^4s) at 1200°C; Sample B aged for 100 hrs (3.6×10^5s) at 1200°C.

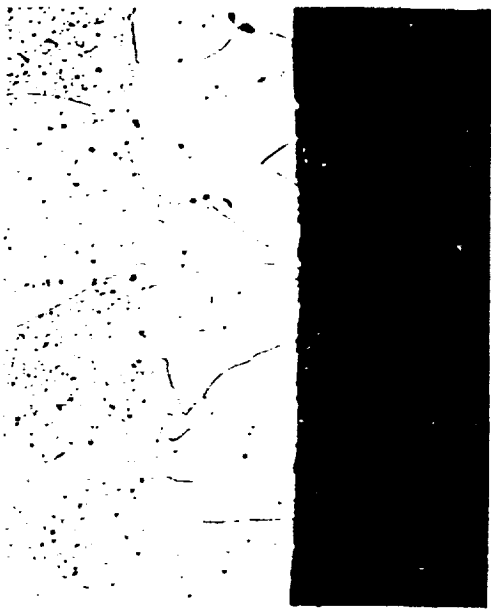

C. Micrograph, 100X

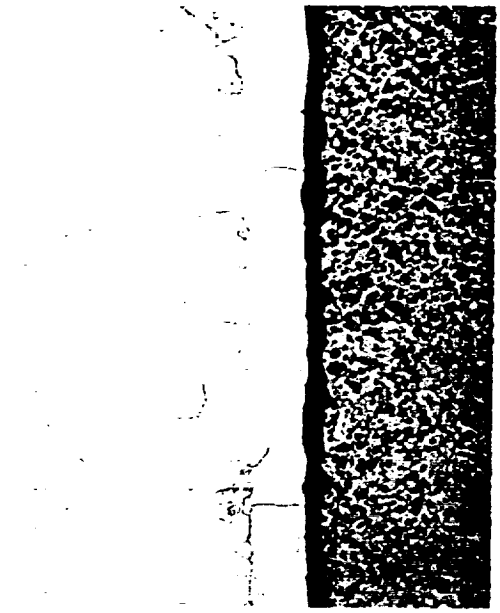

D. Micrograph, 100X

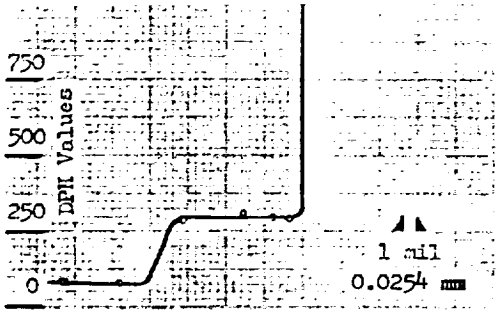

C. Microhardness Profile

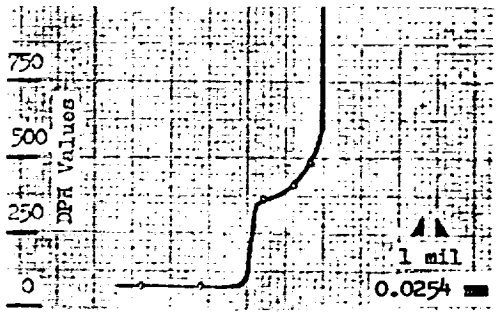

D. Microhardness Profile

V:	Similar to Figure 66
Cb(Nb):	Similar to Figure 66
Zr:	Figure 97
W:	Similar to Figure 82
Al:	Figure 97

C. Electron Microprobe Line Profile Summary

V:	Figure 98
Cb(Nb):	Figure 98
Zr:	Similar to Figure 82
W:	Similar to Figure 82
Al:	Figure 98

D. Electron Microprobe Line Profile Summary

Figure 96. Braze Analysis Data: Braze System 9W (Cb-1Zr/64V-34Cb-2Zr/W/Al_2O_3) brazed at 1870°C for 60s. Sample C aged for 500 hrs (1.8×10^5s) at 1200°C; Sample D aged for 1000 hrs (3.6×10^6s) at 1200°C.

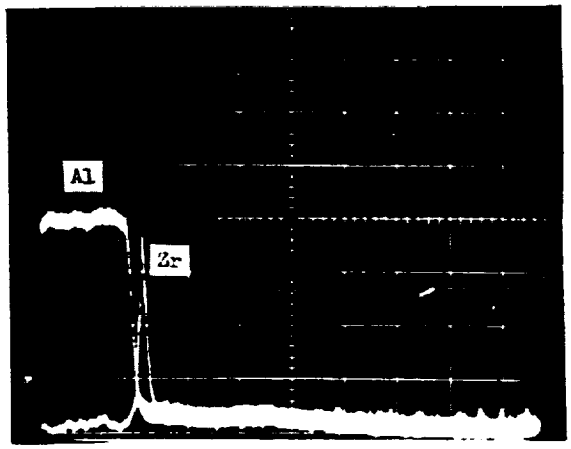

Sample B. Aged 100 hours at 1200°C
Line Profiles, Al and Zr, 800X

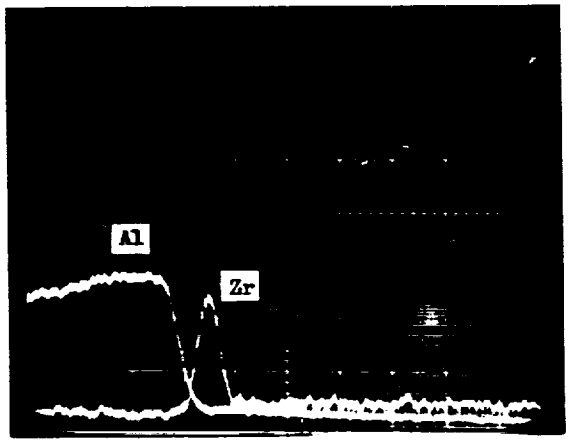

Sample C. Aged 500 hours at 1200°C
Line Profiles, Al and Zr, 800X

Figure 97. Braze Analysis Data: Braze System 9W (Cb-1Zr/64V-34Cb-2Zr/W/Al_2O_3) brazed at 1870°C for 1 minute.

The braze layer in the 1000-hour (3.6×10^6s) aged D sample is shown in Figure 96. The braze is about 4.5 mils (0.115 mm) thick, but there is a reaction layer about 1.5 mil (0.038 mm) wide adjacent to the Al_2O_3. Actually, the dark strip shown in the 100X photomicrograph is a groove, which is thought to have been developed by the etchant. The further proof of the presence of the groove is seen in Figure 98, which shows both the Nb(Cb) and the V line profiles to have large dips in them, as well as corresponding dips in the Al traces, at the Al_2O_3 interface.

A clear demarcation between the braze and the Cb-1Zr is seen in Figure 96, even though the braze solidified epitaxially on the Cb-1Zr. The hardness profile in this D sample shows a rising character as one goes from the usual DPH value of 75 in the Cb-1Zr to 365 in the adjacent braze area. The values continue to rise as the Al_2O_3 is approached and reach 485 near the edge of the braze. The Zr line profile is not shown but it is similar to the one shown in Figure 82, in which no concentration at the Al_2O_3 interface is seen.

In summary, the 9W braze system is characterized by the presence of a zirconium concentration at the Al_2O_3 interface, except that it does not appear in the D sample. The D sample, however, does show a rather wide reaction zone, and the others have only a small zone or essentially none at all. The DPH hardness values are, in general, moderate at 300-375, except for the D sample, whose hardness then approaches 500 near the Al_2O_3 interface. The most plausible reason for the large reaction zone in the D sample appears to be that it is the result of aging. No evidence of a ternary Nb(Cb)-V-Al phase was found in these samples, which one would think should closely parallel the 9M braze behavior.

Braze System 10M (Cb-1Zr/64V-34Cb-2Ti/Mo/Al_2O_3): An examination of Figure 99, the data for Braze System 10M shows the braze layer of the 10-hour (3.6×10^4s) aged A sample to be 7 mils (0.178 mm) thick, and to have a nominal 0.3 mil (0.0076 mm) thick reaction region at the Al_2O_3 surface. The hardness profile slopes downward from a DPH value of 625 near the Al_2O_3 interface to the 75 value of Cb-1Zr. The shadowed line lying along the braze-Cb-1Zr interface region is an artifact of polishing and the 100X magnification. Epitaxial growth is evident across this boundary.

Figure 101 shows the Nb(Cb) and the V line profiles for the A sample. The dips in the Nb(Cb) and the V traces and the concurrent peak in the Al curve is interpreted as being the result of the microprobe's traversing over a tiny (say 5μ) Al_2O_3 particle which became loosened from the Al_2O_3 during brazing, and which then became an occlusion in the braze metal.

The Ti, Zr, and Mo line profiles all show constant levels of these elements across the braze thickness, as is shown in Figures 81, 82, and 45, respectively. Figure 102 shows the Back-Scattered Electron Image of the braze, and demonstrates the presence of much Nb(Cb) in the braze region.

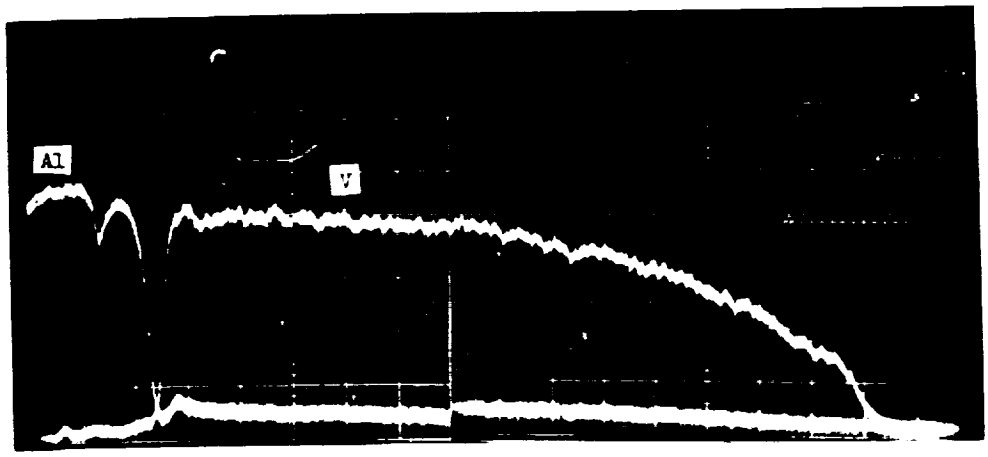

Sample D. Aged 1000 hours at 1200°C
Line Profiles, Al and V, 800X

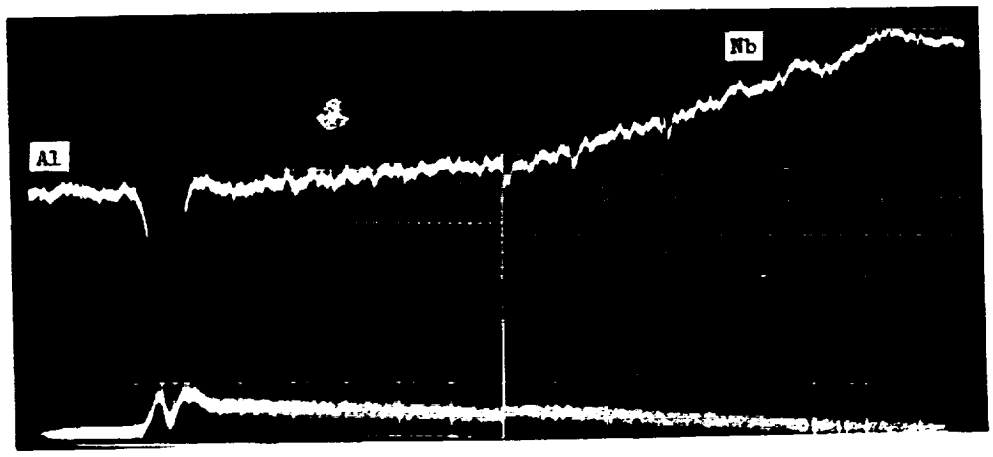

Sample D. Aged 1000 hours at 1200°C
Line Profiles, Al and Nb, 800X

Figure 98. Braze Analysis Data: Braze System 9W (Cb-1Zr/64V-34Cb-2Zr/W/Al_2O_3) brazed at 1870°C for 1 minute

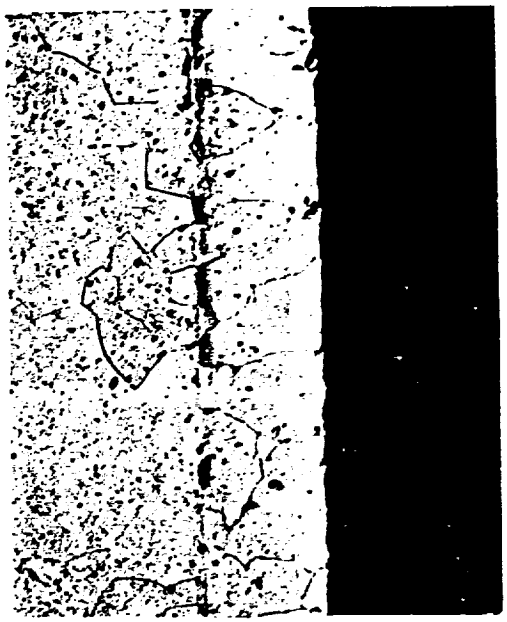

A. Micrograph, 100X

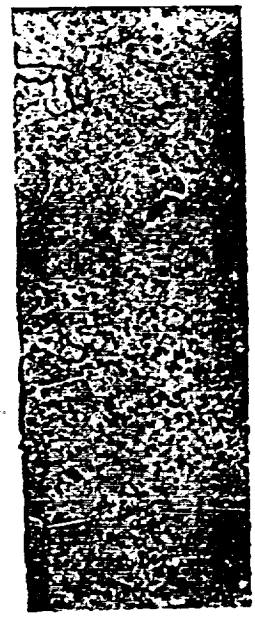

B. Micrograph, 100X

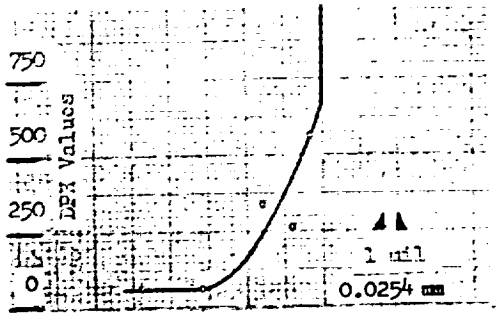

A. Microhardness Profile

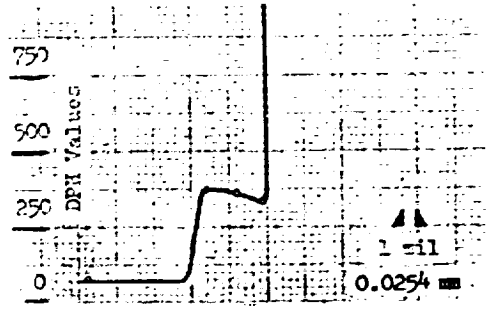

B. Microhardness Profile

V:	Figure 101
Cb(Nb):	Figure 101
Ti:	Similar to Figure 81
Zr:	Similar to Figure 82
Mo:	Similar to Figure 45
Al:	Figure 101

A. Electron Microprobe Line Profile Summary

V:	Figure 103
Cb(Nb):	Figure 103
Ti:	Similar to Figure 81
Zr:	Similar to Figure 82
Mo:	Similar to Figure 45
Al:	Figure 103

B. Electron Microprobe Line Profile Summary

Figure 99. Braze Analysis Data: Braze System 10M (Cb-1Zr/64V-34Cb-2Ti/Mo/Al_2O_3) brazed at 1860°C for 120 s. Sample A aged for 10 hrs (3.6×10^4s) at 1200°C; Sample B aged for 100 hrs (3.6×10^5s) at 1200°C.

C. Micrograph, 100X

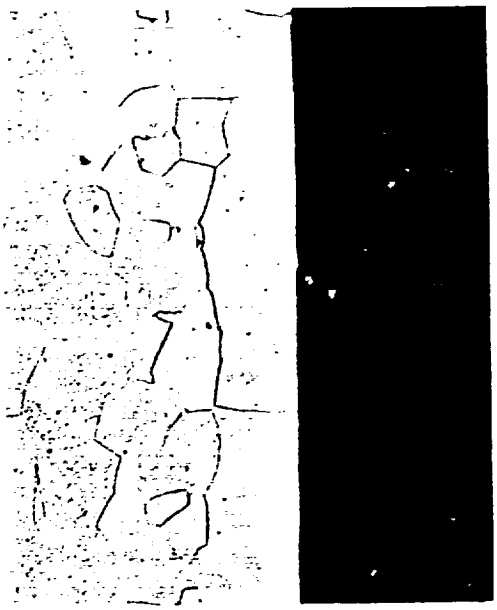

D. Micrograph, 100X

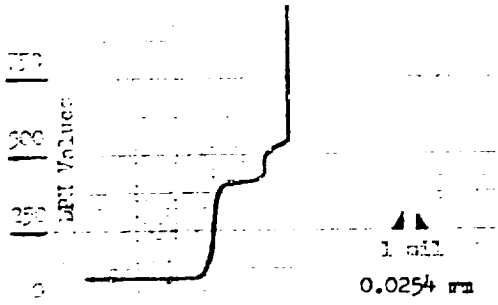

C. Microhardness Profile

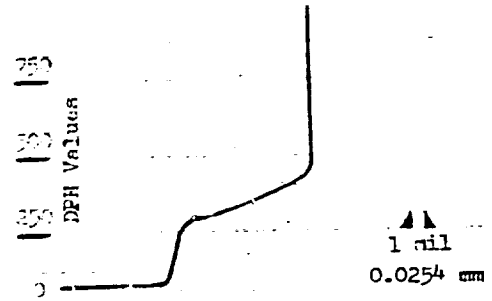

D. Microhardness Profile

V:	Figure 104
Cb(Nb):	Figure 104
Ti:	Figure 105
Zr:	Figure 105
Mo:	Similar to Figure 45
Al:	Figures 104. 105.

C. Electron Microprobe Line Profile Summary

V:	Figure 106
Cb(Nb):	Figure 106
Ti:	Similar to Figure 105
Zr:	Similar to Figure 105
Mo:	Similar to Figure 45
Al:	Figure 106

D. Electron Microprobe Line Profile Summary

Figure 100. Braze Analysis Data: Braze System 10M (Cb-1Zr/64V-34Cb-2Ti/Mo/Al_2O_3) brazed at 1860°C for 120 s. Sample C aged for 500 hrs (1.8×10^6s) at 1200°C; Sample D aged for 1000 hrs (3.6×10^6s) at 1200°C.

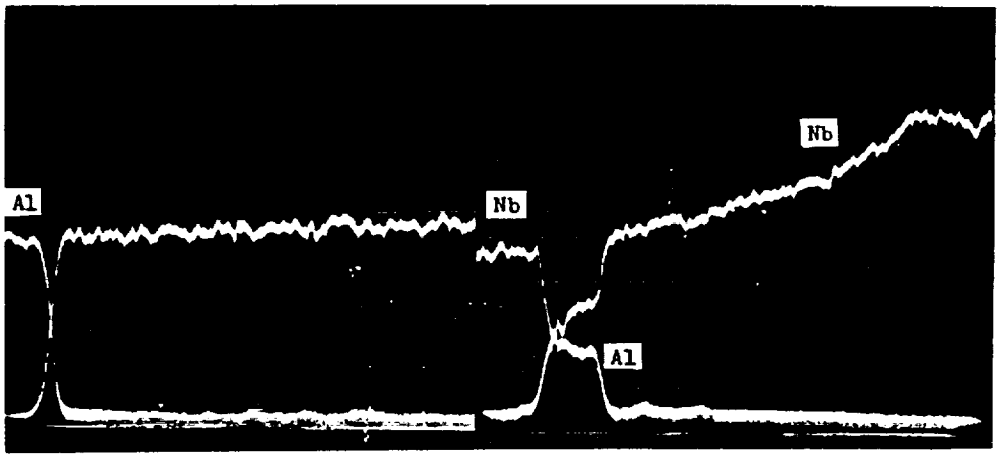

Sample A. Aged 10 hours at 1200°C
Line Profiles, Al and Nb, 800X

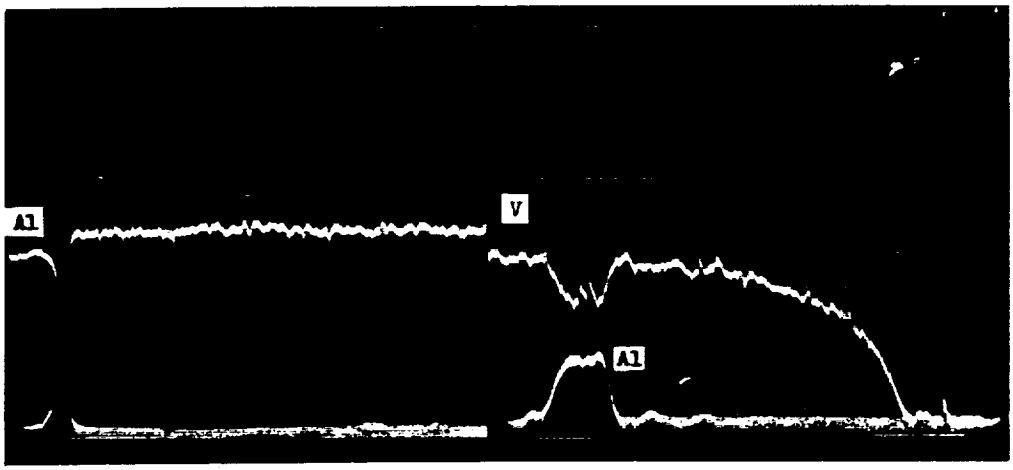

Sample A. Aged 10 hours at 1200°C
Line Profiles, Al and V, 800X

Figure 101. Braze Analysis Data: Braze System 10M (Cb-1Zr/64V-34Cb-2Ti/Mo/Al_2O_3) brazed at 1860° C for 2 minutes.

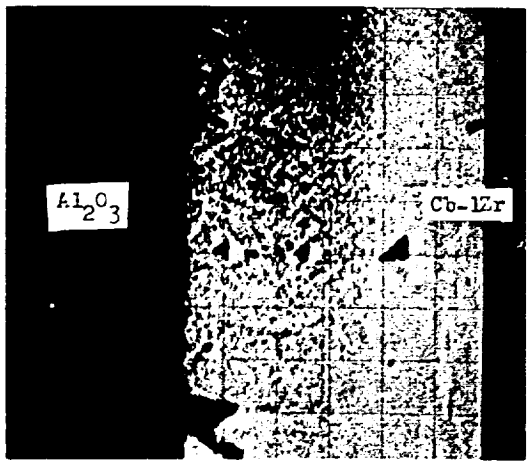

Sample A. Aged 10 hours at 1200°C

Back-Scattered Electron Image, 400X

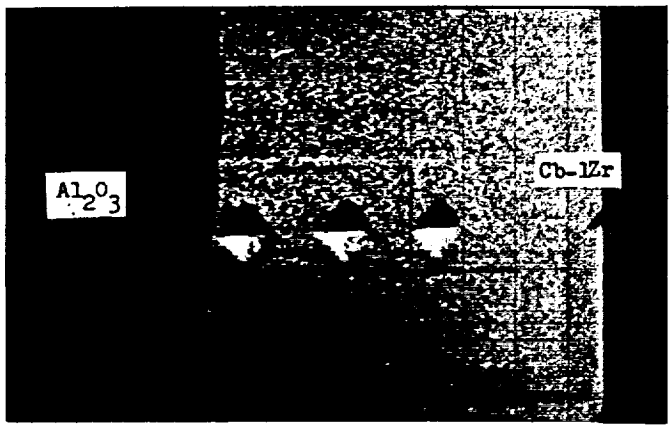

Sample B. Aged 100 hours at 1200°C

Back-Scattered Electron Image, 400X

Figure 102. Braze Analysis Data: Braze System 10M (Cb-1Zr/64V-34Cb-2Ti/Mo/Al_2O_3) brazed at 1860° C for 2 minutes

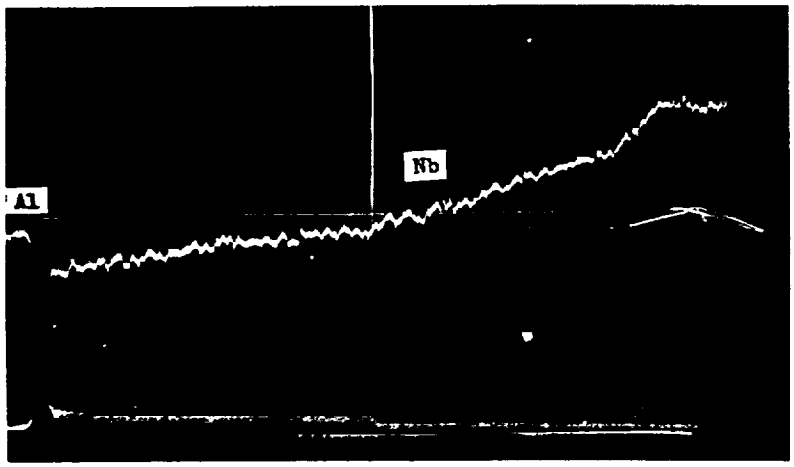

Sample B. Aged 100 hours at 1200°C
Line Profiles, Al and Nb, 800X

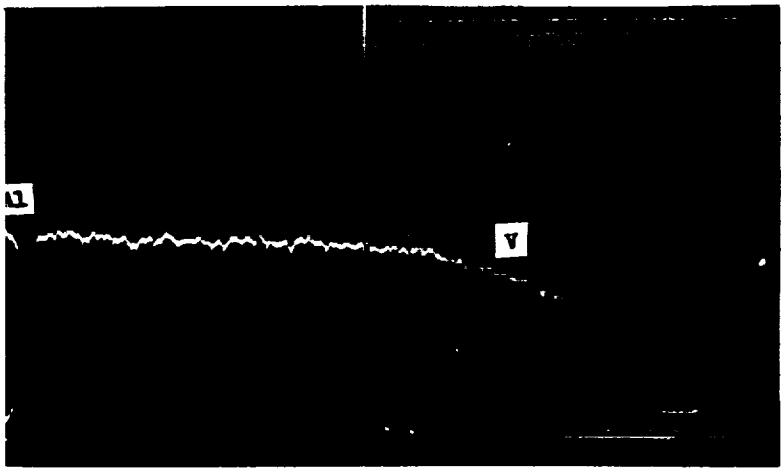

Sample B. Aged 100 hours at 1200°C
Line Profiles, Al and V, 800X

Figure 103. Braze Analysis Data: Braze System 10M (Cb-1Zr/64V-34Cb-2Ti/Mo/Al_2O_3) brazed at 1860°C for 2 minutes

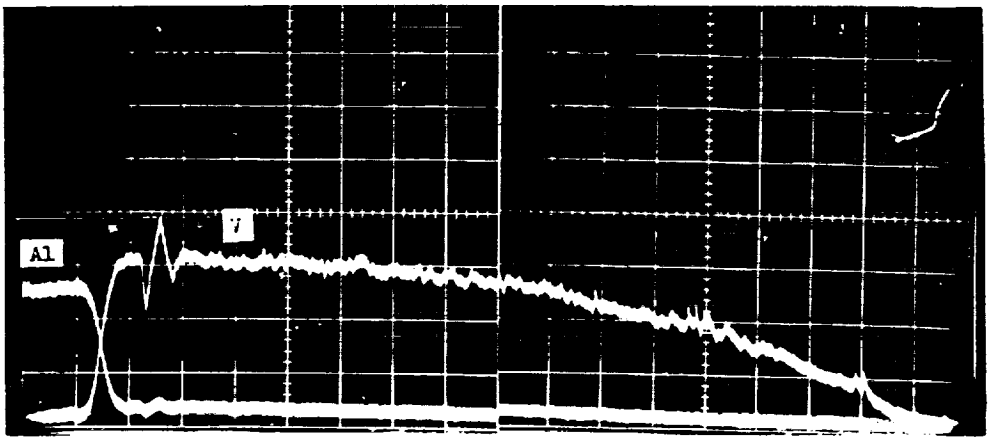

Sample C. Aged 500 hours at 1200°C
Line Profiles, Al and V, 800X

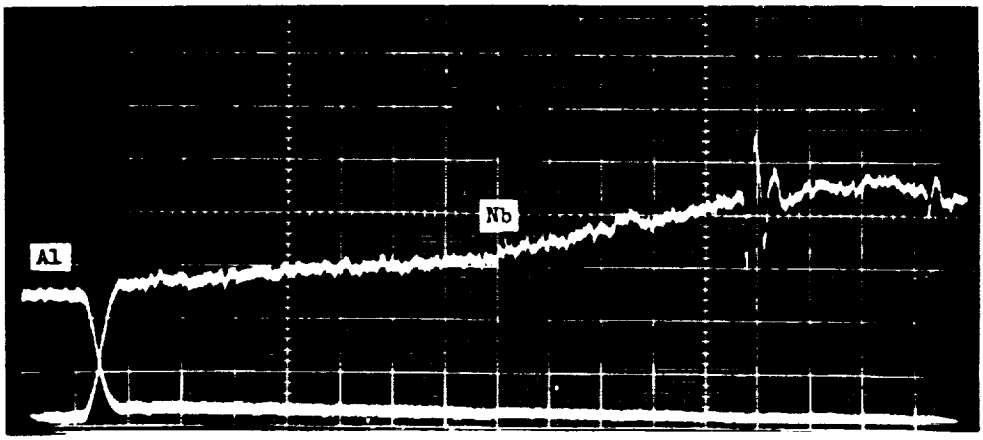

Sample C. Aged 500 hours at 1200°C
Line Profiles. Al and Nb. 800X

Figure 104. Braze Analysis Data: Braze System 10M (Cb-1Zr/64V-34Cb-2Ti/Mo/Al_2O_3) brazed at 1860° C for 2 minutes.

The braze layer in the 100-hour (3.6×10^5 s) aged B sample is about 5 mils (0.127 mm) thick. A slight indication of an interface layer at the Al_2O_3 is present. The hardness profile shows a reversal, although the DPH values are all in the range of 325-375 in the braze. The Cb-1Zr alloy again shows a DPH value of 75.

The Back-Scattered Electron Image for Sample B is shown in Figure 102. The rather uniform sizes of the hardness indents are seen, as is the presence of a large amount of Nb(Cb) in the braze. Figure 103 shows the Nb(Cb) and the V line profiles to be quite smooth and regular. The Ti, Zr, and Mo line profile traces are also quite uniform and regular and resemble those shown in Figures 81, 82, and 45, respectively.

The braze layer in the 500-hour (1.8×10^6 s) aged C sample is shown in Figure 100. The braze is 5 mils (0.127 mm) thick, and the interface layer is about 0.8 mil (0.020 mm) thick. The hardness profile shows generally increasing DPH values from the standard value of 75 in the Cb-1Zr alloy to a value of 510 about one mil (0.0254 mm) from the Al_2O_3. The V and the Nb(Cb) line profiles for the C sample are shown in Figure 104. The traces are generally uniform and smooth except for an unexplained perturbation in each. None of the other element traces has a corresponding perturbation at the same location, so it is concluded that these are spurious.

This view is supported by the fact that there is a perturbation in one of the Al traces in Figure 105, and not in the other, nor are there perturbations in either of the Al traces in Figure 104, so the C sample Al trace perturbation must be spurious. The Zr and the Ti traces in Figure 105 are seen to be rather uniform, with no suggestion of a concentration of these metals at the Al_2O_3 interface.

The braze layer in the 1000-hour (3.6×10^6 s) aged D sample is shown in Figure 100. The braze is seen to be about 8-9 mils (0.203-0.223 mm) thick and to have a wide transition-like zone at the Cb-1Zr-braze interface. Epitaxy is evident in this region. There is also an interface layer, about 0.5 mil (0.0127 mm) in thickness. The hardness profile slopes upward from a DPH value of 75 in the Cb-1Zr to a value of 390 about 1.2 mils (0.030 mm) from the Al_2O_3.

Figure 106 shows the V and Nb(Cb) line profiles for the D sample. They are quite regular and smooth, as are the line profiles for Ti, Zr, and Hf. These are similar to the traces shown in Figure 105, 105, and 45, respectively.

In summary, Braze System 10M is characterized by the presence of a modest-sized interfacial layer at the Al_2O_3 surface, and by a thick braze region. The DPH hardnesses are not all consistent, although the values are below 500. No deleterious effects are observed in the aged Al_2O_3.

Braze System 10W (Cb-1Zr/64V-34Cb-2Ti/W/Al_2O_3): An examination of Figure 107, the data for Braze System 10W, shows the braze layer of the

Sample C. Aged 500 hours at 1200°C
Line Profiles, Al and Zr, 800X

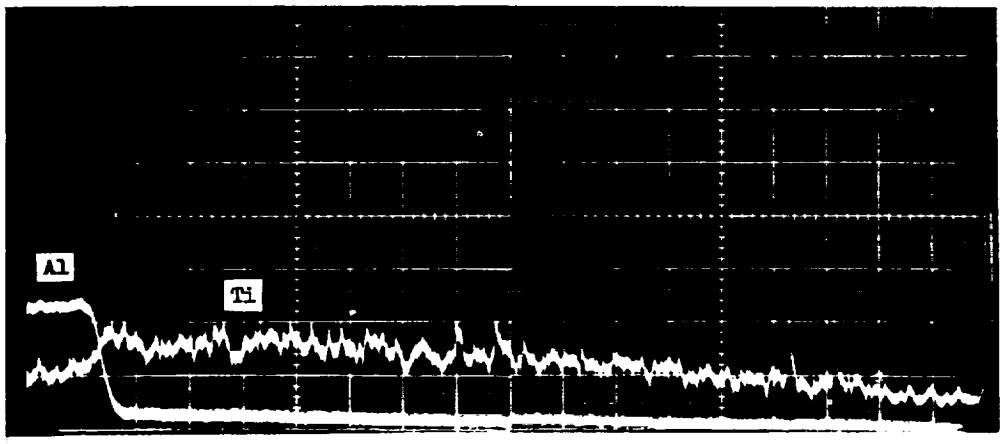

Sample C. Aged 500 hours at 1200°C
Line Profiles, Al and Ti, 800X

Figure 105. Braze Analysis Data: Braze System 10M (Cb-1Zr/64V-34Cb-2Ti/Mo/Al_2O_3) brazed at 1860° C for 2 minutes.

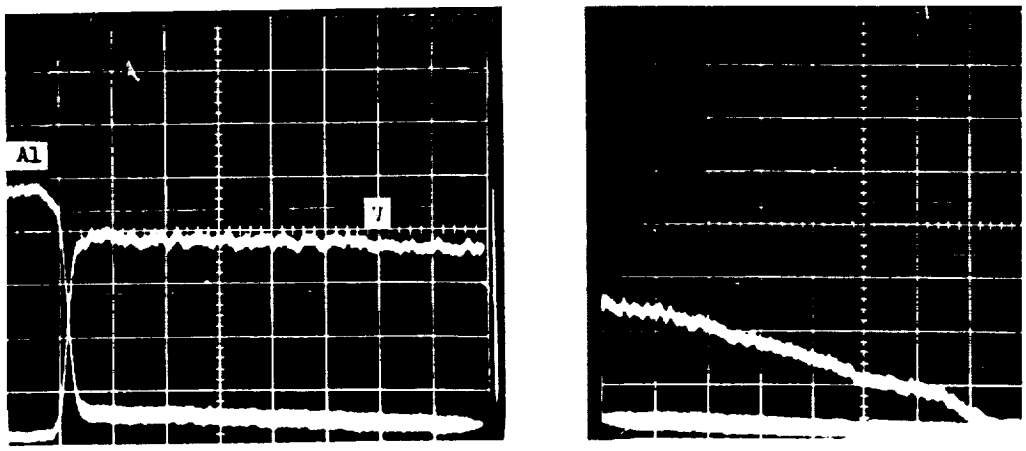

Sample D. Aged 1000 hours at 1200°C
Line Profiles, Al and V, 800X

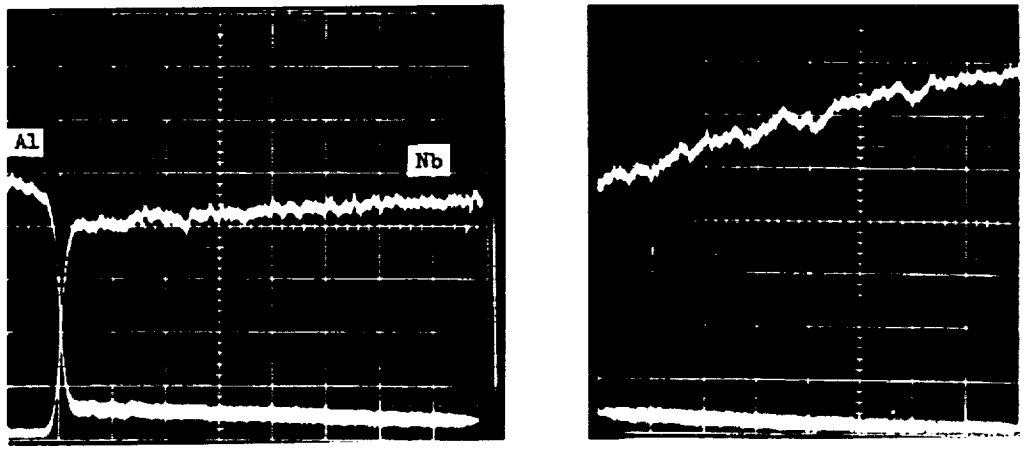

Sample D. Aged 1000 hours at 1200°C
Line Profiles, Al and Nb, 800X

Figure 106. Braze Analysis Data: Braze System 10M (Cb-1Zr/64V-34Cb-2Ti/Mo/Al_2O_3) brazed at 1860°C for 2 minutes.

A. Micrograph, 100X

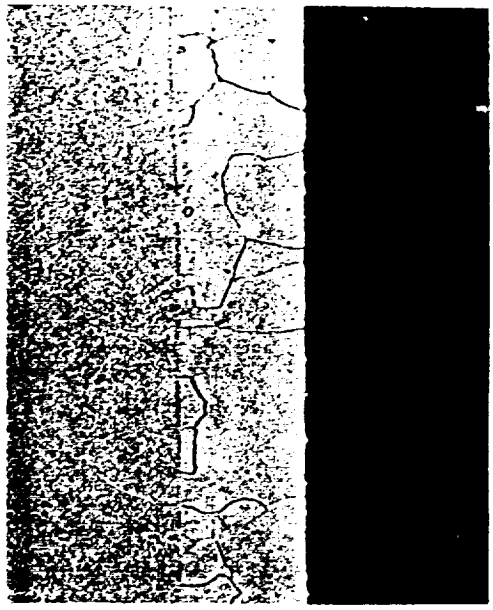

B. Micrograph, 100X

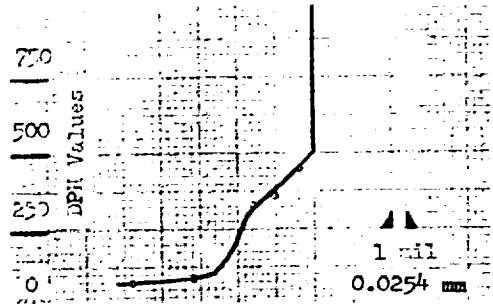

A. Microhardness Profile

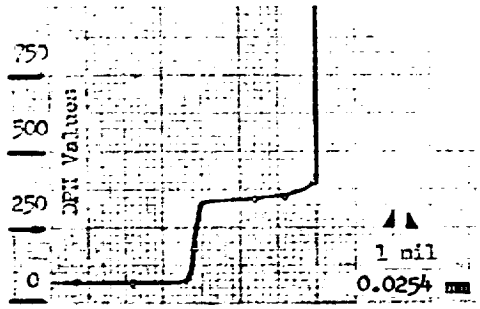

B. Microhardness Profile

V:	Figure 110
Cb(Nb):	Figure 110
Ti:	Similar to Figure 105
Zr:	Similar to Figure 105
W:	Similar to Figure 82
Al:	Figure 110

A. Electron Microprobe Line Profile Summary.

V:	Similar to Figure 75
Cb(Nb):	Similar to Figure 75
Ti:	Similar to Figure 105
Zr:	Similar to Figure 105
W:	Similar to Figure 82
Al:	Similar to Figures 103, 104

B. Electron Microprobe Line Profile Summary.

Figure 107. Braze Analysis Data: Braze System 10W (Cb-1Zr/64V-34Cb-2Ti/W/Al_2O_3) brazed at 1870°C for 120 s. Sample A aged for 10 hrs (3.6×10^4s) at 1200°C; Sample B aged for 100 hrs (3.6×10^5s) at 1200°C.

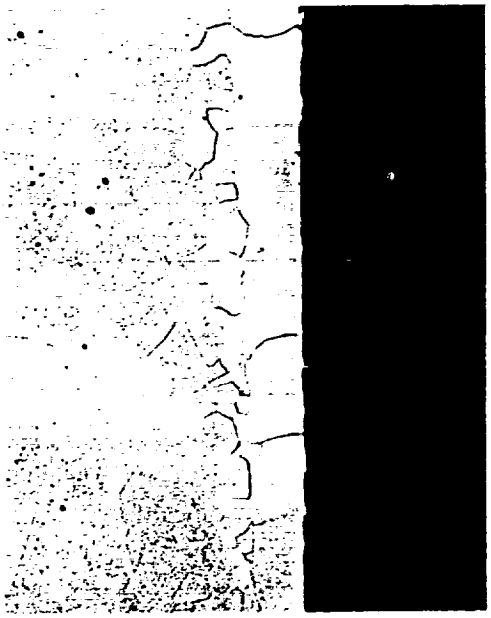

C. Micrograph, 100X

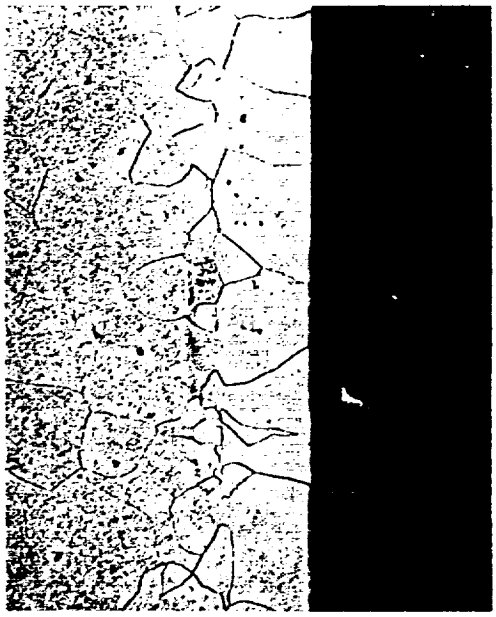

D. Micrograph, 100X

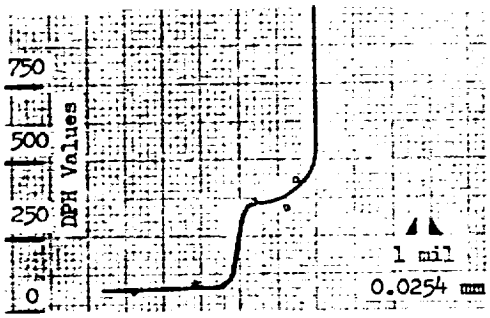

C. Microhardness Profile

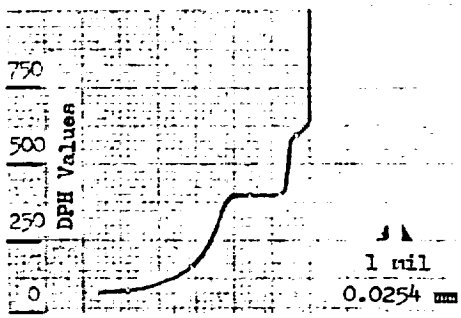

D. Microhardness Profile

V:	Figure 111
Cb(Nb):	Similar to Figure 75
Ti:	Similar to Figure 105
Zr:	Similar to Figure 105
W:	Similar to Figure 82
Al:	Figure 111

C. Electron Microprobe Line Profile Summary

V:	Figure 113
Cb(Nb):	Figure 113
Ti:	Figure 112
Zr:	Figure 112
W:	Similar to Figure 82
Al:	Figures 112, 113

D. Electron Microprobe Line Profile Summary

Figure 108. Braze Analysis Data: Braze System 10W (Cb-1Zr/64V-34Cb-2Ti/W/Al_2O_3) brazed at 1870°C for 120 s. Sample C aged for 500 hrs (1.8×10^6 s) at 1200°C; Sample D aged for 1000 hrs (3.6×10^6 s) at 1200°C.

10-hour (3.6×10^4s) aged A sample to be about 6.5 mils (0.165 mm) thick. There is no evidence of an interface layer at the Al_2O_3, and the hardness profile appears smooth and nearly linear through the braze with a maximum observed DPH value of 450 about one mil (0.0254 mm) from the Al_2O_3. Epitaxy is evident.

Figure 109 shows the Back-Scattered Electron Image for the A sample, and the microhardness indents. Figure 109 also shows an electron microprobe area-scan trace for vanadium in the braze region. The lightness of the region is indicative of the vanadium content, and one can see the rather uniform region near the Al_2O_3, and the region of decreasing V content at the Cb-1Zr interface.

Figure 110 shows the Nb(Cb) and V line profiles for Sample A. The curves are generally smooth, but several small dips appear in the Nb(Cb) and V traces at the same locations, and there are also corresponding peaks in the Al profile. This combination is typical of the presence of a small Al_2O_3 precipitate, whose particle size is smaller than the diameter of the microprobe test spot. Therefore, these are considered to be very small particles of Al_2O_3 in the braze. The line profiles for Ti, Zr, and W are rather uniform and are similar to those shown in Figures 105, 105, and 82, respectively.

The braze layer in the 100-hour (3.6×10^5s) aged B sample is shown in Figure 107 to be about 8 mils (0.203 mm) thick. No interface layer is present. The braze hardness is rather uniform at a DPH value of about 350, with a value of 70 in the Cb-1Zr alloy.

Figure 111 shows the Back-Scattered Electron Image of Sample B, and the hardness indents. The line profiles of Nb(Cb) and V are quite similar to those shown in Figure 75, and the Ti, Zr, and W line profiles resemble those shown in Figures 105, 105, and 82, respectively.

The braze layer in the 500-hour (1.8×10^6s) aged C sample is shown in Figure 108 to be about 5 mils (0.127 mm) thick. An interface layer of 0.5 mil (0.0127 mm) thickness appears adjacent to the Al_2O_3. The DPH hardness values begin at the typical 75 in the Cb-1Zr and rise sharply to 360 at the edge of the braze. Then a gradual rise to about 425 at 1.5 mil (0.038 mm) from the Al_2O_3 is seen. A Cb-1Zr-braze interface boundary with some epitaxial growth in the very large braze grains is present.

Figure 111 shows the V line profile, which is smooth and regular. The Nb(Cb) profile is also smooth and regular and resembles that shown in Figure 75. The Ti, Zr, and W profiles show uniform concentrations across the braze.

The braze layer in the 1000-hour (3.6×10^6s) aged D sample is shown in Figure 108 to be about 8 mils (0.203 mm) thick. A transition region between the braze and the Cb-1Zr alloy is apparent, although there are several grains that go completely through that region. The braze is quite large grained, possibly as a consequence of aging. A very thin reaction region is seen at the Al_2O_3 interface, but it is, at most, 0.1 mil (0.0025 mm) thick. The hardness profile is seen to rise from the typical DPH value of 75 in the Cb-1Zr

Sample A. Aged 10 hours at 1200°C
Back-Scattered Electron Image, 400X

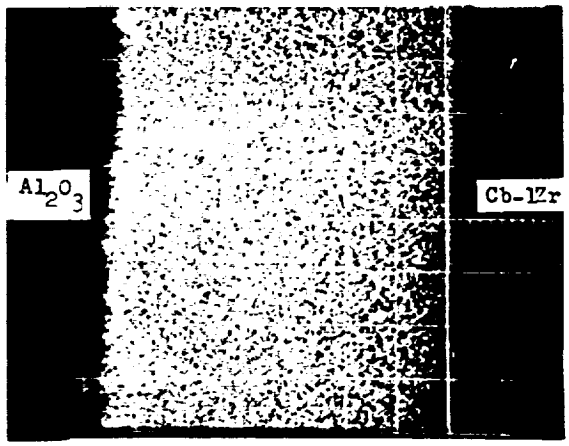

Sample A. Aged 10 hours at 1200°C
Area-Scan for Vanadium, 400X

Figure 109. Braze Analysis Data: Braze System 10W (Cb-1Zr/64V-34Cb-2Ti/W/Al_2O_3) brazed at 1870° C for 2 minut

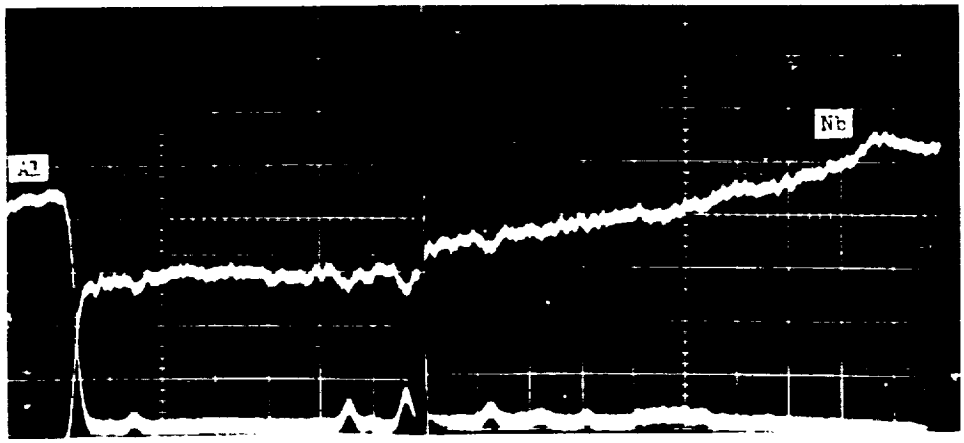

Sample A. Aged 10 hours at 1200°C
Line Profiles, Al and Nb, 300X

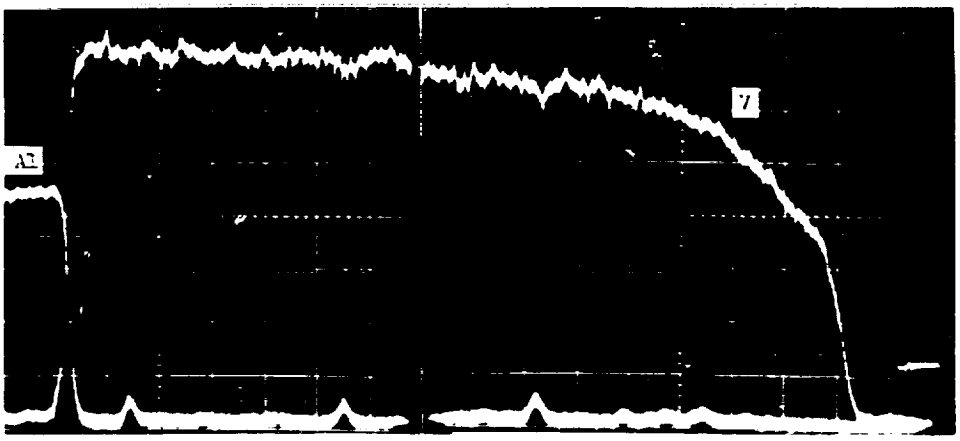

Sample A. Aged 10 hours at 1200°C
Line Profiles, Al and V, 800X

Figure 110. Braze Analysis Data: Braze System 10W (Cb-1Zr/64V-34Cb-2Ti/W/Al_2O_3) brazed at 1870°C for 2 minutes.

Sample B. Aged 100 hours at 1200°C
Back-Scattered Electron Image, 200X

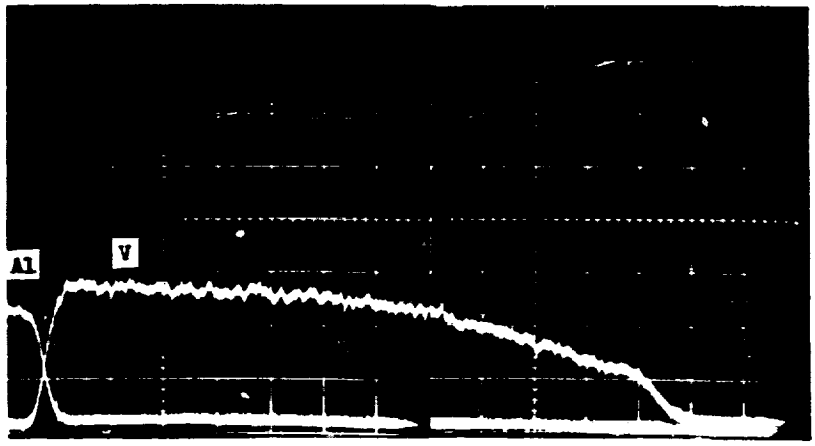

Sample C. Aged 500 hours at 1200°C
Line Profiles, Al and V, 800X

Figure 111. Braze Analysis Data: Braze System 10W (Cb-1Zr/64V-34Cb-2Ti/W/Al_2O_3) brazed at 1870°C for 2 minutes.

alloy to a value of 400 in the braze. There is a region of apparently uniform hardness in the middle of the braze, but then a rather high DPH value of 600 is found 1 mil (0.0254 mm) from the Al_2O_3 surface.

Figure 112 shows the Zr and the Ti line profiles for the D sample, and no tendency for concentration at the Al_2O_3 interface region is present. Figure 113 shows the Nb(Cb) and V line profiles, and they, too, appear smooth and uncomplicated.

In summary, Braze 10W yields wide braze regions, but with varying hardness character. Some of the DPH hardness values reach 600, although most are below 450. A modest tendency to form a reaction region is shown in Sample C, but the other three samples have rather thin reaction zone thicknesses. There is no tendency for the concentration of Zr or Ti at the Al_2O_3 surface, and the Nb(Cb) and V profiles are generally smooth and regular. A few indications of the presence of very small Al_2O_3 particles in the braze were found.

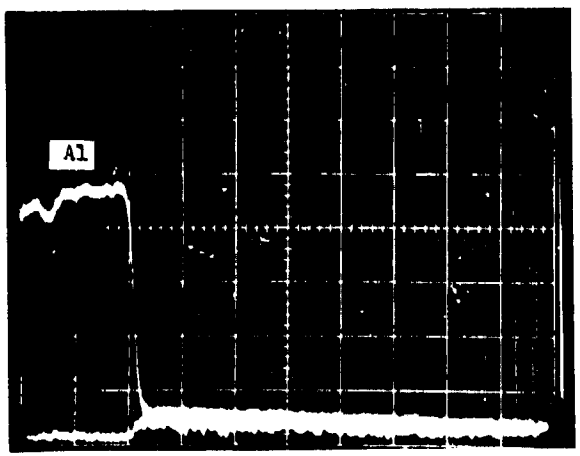

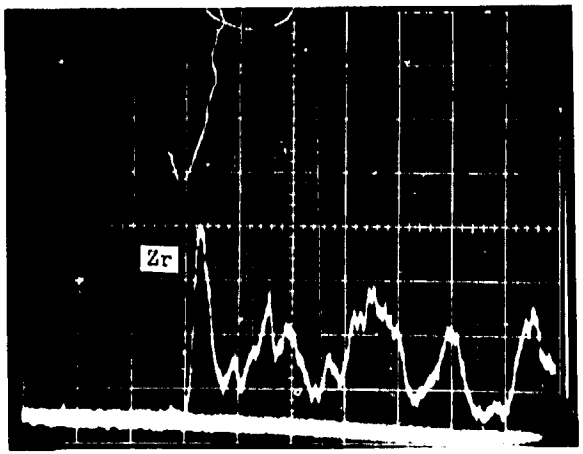

Sample D. Aged 1000 hours at 1200°C

Line Profiles, Al and Zr, 800X

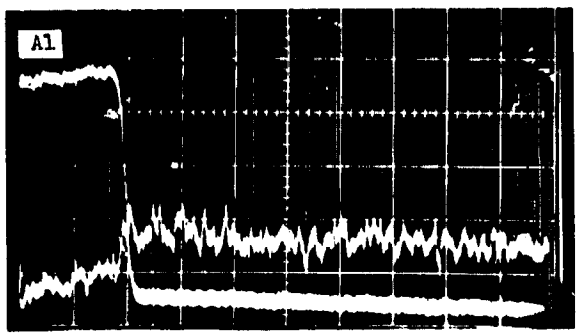

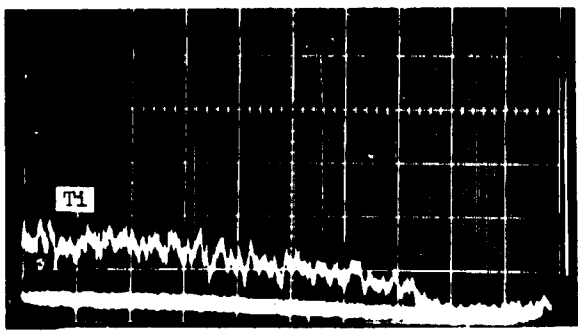

Sample D. Aged 1000 hours at 1200°C

Line Profiles, Al and Ti, 800X

Figure 112. Braze Analysis Data: Braze System 10W (Cb-1Zr/64V-34Cb-2Ti/W/Al_2O_3) brazed at 1870°C for 2 minutes.

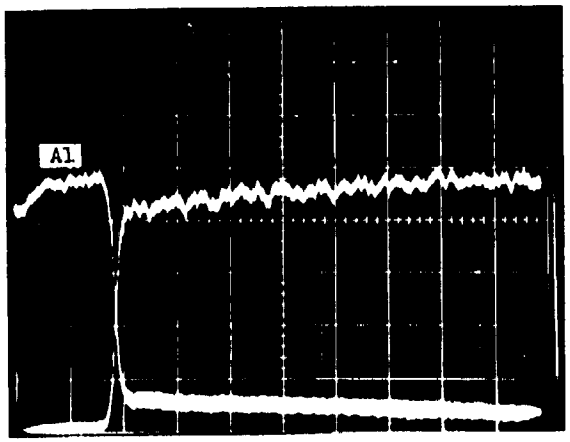

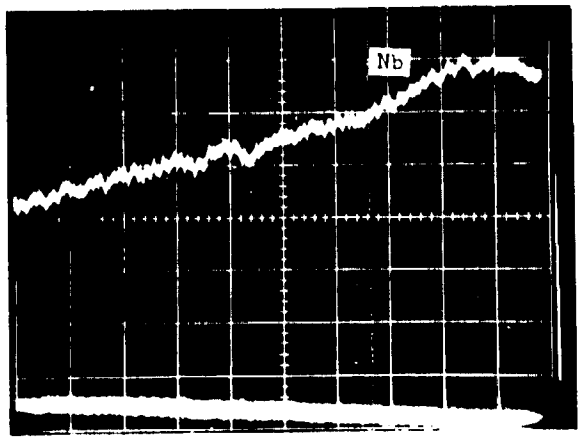

Sample D. Aged 1000 hours at 1200°C

Line Profiles, Al and Nb, 800X

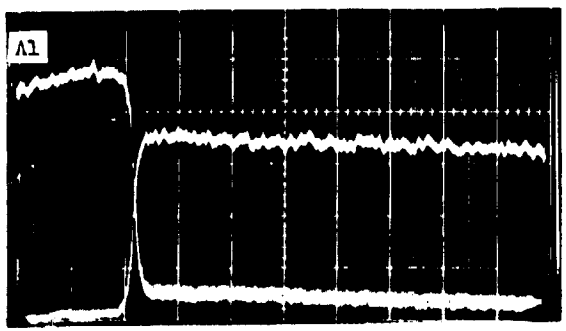

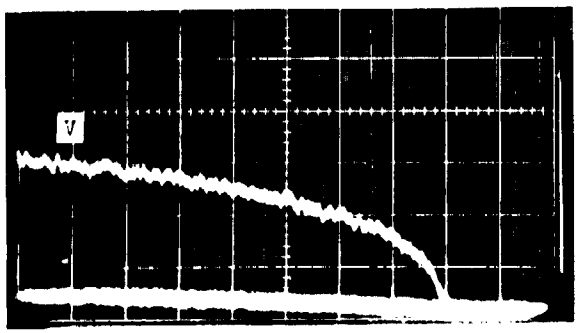

Sample D. Aged 1000 hours at 1200°C

Line Profiles, Al and V, 800X

Figure 113. Braze Analysis Data: Braze System 10W (Cb-1Zr/64V-34Cb-2Ti/W/Al_2O_3) brazed at 1870°C for 2 minutes.

APPENDIX XIII. CONCENTRATION PROFILE DATA SUMMARY

Because one criterion of a good braze alloy is its ability to survive for an extended service period, its stability with regard to diffusional changes is an important aspect of its performance evaluation. Therefore, an aging sequence was employed in these studies, with the expectation that the examination of concentration profiles of critical elements as a function of aging time would yield effective D-values for key elements. Such data would then enable one to predict the long-term behavior of braze systems and to establish probable service-lives of brazes. The first step in the evaluation of D-values was the quantitative determination of the concentration profiles of the elements of interest. Niobium (columbium), vanadium, and aluminum were selected as the most informative in these systems. Based upon examinations of the qualitative line profile oscilloscope traces, Braze Systems 4W, 6W, and 10M were chosen for more detailed examination. The data are tabulated in Tables XLII through LIII, and are plotted in Figures 114, 115, and 116.

The niobium (columbium) concentration curves for Braze System 4W in Figure 114 can be compared with the corresponding line profiles shown in Figures 66, 68, 69, and 71. The principal differences in the shapes of these curves are: (1) that the quantitative curves show a nominal (maximum/minimum) concentration ratio of 2, while the corresponding ratios in the line profiles range from 1.35 to 1.8; and (2) that the slopes of the quantitative curves in the braze-Cb-1Zr juncture are steeper than those of the line profiles. The vanadium curves of Figure 114 also show a greater slope at the juncture region than do the line profile curves. Both the line profile and the quantitative data show the Sample D (1000 hour, 3.6×10^6s) aluminum to be a significant component in the final braze. However, the Al line profiles of Sample B (100 hour, 3.6×10^5s) of Figures 67 and 68 do not indicate the Al to be present in as great an amount as is shown in Figure 114.

In comparing the data of Figure 115 with that of Figures 83, 84, 85, and 86, one again finds the quantitative Nb(Cb) maximum/minimum ratio to be 2, while that shown in the line profiles ranges from 1.35 to 1.65. Again, the Nb(Cb) curves in Figure 115 are steeper at the juncture region than are the line profiles. However, these comparisons should not be considered quantitative, because the line profiles and the concentration profile data were not necessarily taken along the same traverse line.

Although the quantitative concentration profiles of Figures 114, 115, and 116 indicate the slope of the Nb(Cb) curve at the juncture between the braze and the Cb-1Zr alloy to be steeper than is suggested by the line profiles, there is still a considerable slope present in even the 10-hour (3.6×10^4s) aged samples. The problem is that all of the brazes tend to dissolve large amounts of the refractory alloy so that the final braze composition has 45 to 55 weight percent niobium (columbium). If this dissolution were to occur so that the braze alloy mixture composition were

TABLE XLII

CONCENTRATION PROFILES OF Nb(Cb), V, AND Al IN BRAZE 4W AFTER 10 HR (3.6×10^4 s) AGING AT 1200°C

X Microns*	C, wt %		
	Nb(Cb)	V	Al
4.5	50.8	47.6	0.46
9.0	51.3	47.2	0.50
13.5	51.8	46.5	0.77
18.0	52.7	45.6	0.79
22.5	53.8	44.3	0.78
27.0	54.5	43.7	0.79
31.5	54.8	43.2	0.88
36.0	56.7	41.3	0.90
40.5	57.4	40.7	0.80
45.0	58.5	39.8	0.66
49.5	59.1	39.1	0.66
54.0	60.9	37.5	0.65
58.5	65.2	32.7	1.09
63.0	69.9	28.8	0.78
67.5	73.2	25.5	0.76
72.0	79.2	19.2	0.35
76.5	88.5	10.5	0.17
81.0	94.5	4.3	0.10
85.5	96.0	2.9	0.13
90.0	98.2	0.7	0.1
94.5	99.0	0	0

*Measured from Al_2O_3 Interface

TABLE XLIII

CONCENTRATION PROFILES OF Nb(Cb), V, and Al IN BRAZE 4W AFTER 100 HR (3.6×10^5 s) AGING AT 1200°C

X Microns*	C, wt %		
	Nb(Cb)	V	Al
4.5	46.2	49.1	3.67
9.0	46.5	48.9	3.49
13.5	46.9	48.8	3.22
18.0	47.5	48.5	3.60
22.5	47.8	48.3	2.99
27.0	48.2	43.0	2.64
31.5	48.8	47.7	2.46
36.0	51.0	46.6	2.43
40.5	50.9	45.9	2.14
45.0	52.2	44.6	2.03
49.5	53.8	43.8	1.72
54.0	54.5	42.9	1.72
58.5	56.1	41.5	1.49
63.0	57.5	40.1	1.40
67.5	59.7	38.1	1.23
72.0	60.7	37.5	1.10
76.5	62.5	35.7	0.85
81.0	63.6	34.4	0.94
85.5	65.6	32.4	0.92
90.0	68.0	30.2	0.70
94.5	71.0	27.5	0.57
99.0	73.4	25.1	0.59
103.5	78.6	20.2	0.23
108.0	83.1	15.5	0.26
112.5	98.0	1.0	0
117.0	99.0	0	0

*Measured from Al_2O_3 Interface

TABLE XLIV

CONCENTRATION PROFILES OF Nb(Cb), V, AND Al IN BRAZE 4W AFTER 500 HR (1.8×10^6 s) AGING AT 1200°C

Microns*	C, wt %			Microns*	C, wt %		
	Nb(Cb)	V	Al		Nb(Cb)	V	Al
4.5	49.8	47.2	2.01	162.0	72.5	25.6	0.68
9.0	49.9	47.4	1 78	164.5	74.1	24.3	0.58
13.5	49.0	48.1	1.86	169.0	77.0	21.4	0.52
18.0	49.7	47.7	1.59	173.5	79.5	19.2	0.35
22.5	50.0	47.3	1.62	178.0	83.0	16.0	0.17
27.0	49.6	47.8	1.58	182.5	89.7	9.15	0.09
31.5	50.0	47.5	1.60	187.0	97.5	1.47	0.09
36.0	50.0	47.3	1.65	191.5	98.0	1.0	0.09
40.5	50.6	47.0	1.32	196.0	99.0	0	0
45.0	50.6	47.2	1.40				
49.5	50.8	46.7	1.40				
54.0	50.1	47.6	1.35				
58.5	51.6	46.2	1.29				
63.0	51.2	46.5	1.20				
67.5	51.4	46.2	1.22				
72.0	53.0	45.0	1.15				
76.5	52.6	45.2	1.29				
81.0	53.1	44.7	1.21				
85.5	53.3	44.2	1.32				
90.0	54.0	43.8	1.32				
94.5	54.6	43.1	1.21				
99.0	55.3	42.4	1.22				
103.5	56.0	41.9	1.10				
108.0	56.6	41.0	1.25				
112.5	57.6	40.5	1.09				
117.0	58.5	38.9	1.10				
121.5	59.2	38.8	0.90				
126.0	60.6	37.6	1.05				
130.5	61.9	36.3	0.92				
135.0	63.1	35.2	0.91				
139.5	64.4	33.6	0.91				
144.0	65.1	33.0	0.87				
148.5	66.6	31.7	0.72				
153.0	68.2	30.0	0.71				
157.5	70.3	27.9	0.80				

*Measured from Al_2O_3 Interface.

TABLE XLV

CONCENTRATION PROFILES OF Nb(Cb), V, AND Al IN BRAZE 4W AFTER 1000 HR (3.6×10^6 s) AGING AT 1200°C

X Microns*	C, wt %		
	Nb(Cb)	V	Al
4.5	54.5	40.0	4.74
9.0	54.9	39.5	4.60
13.5	54.7	40.0	4.43
18.0	54.9	39.7	4.42
22.5	55.2	39.5	4.39
27.0	55.2	39.5	4.26
31.5	55.5	39.1	4.31
36.0	56.0	39.0	4.26
40.5	56.0	38.7	4.25
45.0	56.5	38.6	3.92
49.5	56.6	38.5	3.93
54.0	57.1	38.1	3.81
58.5	57.5	37.9	3.63
63.0	57.6	37.7	3.47
67.5	57.6	37.7	3.84
72.0	58.6	36.6	3.72
76.5	59.2	36.3	3.65
81.0	60.0	35.8	3.37
85.5	60.4	35.8	3.38
90.0	61.2	34.8	3.23
94.5	62.1	33.8	3.19
99.0	63.4	32.5	2.98
103.5	64.5	31.5	2.88
108.0	65.4	30.8	2.80
112.5	66.5	29.9	2.52
117.0	68.0	28.6	2.39
121.5	69.0	27.9	2.20
126.0	70.6	26.1	2.14
130.5	71.6	25.3	2.07
135.0	72.2	25.1	1.90
139.5	74.2	23.2	1.69
144.0	76.2	21.4	1.40
148.5	77.8	20.1	1.24
153.0	79.8	18.0	1.11
157.5	81.9	16.3	0.93
162.0	85.1	13.2	0.66
167.5	95.7	2.9	0.38
171.0	99.	0	0

*Measured from Al_2O_3 Interface

TABLE XLVI

CONCENTRATION PROFILES OF Nb(Cb), V, AND Al IN BRAZE 6W AFTER 10 HR (3.6×10^4 s) AGING AT 1200°C

X Microns*	C, wt %		
	Nb(Cb)	V	Al
4.5	52.1	43.6	3.37
9.0	52.7	43.5	2.91
13.5	53.0	43.8	2.27
18.0	53.0	44.0	2.03
22.5	53.0	44.0	2.02
27.0	54.1	43.0	2.08
31.5	54.5	42.1	2.27
36.0	54.7	42.2	2.13
40.5	55.2	41.6	2.20
45.0	55.3	41.5	2.17
49.5	55.9	41.0	2.10
54.0	56.2	40.5	2.21
58.5	57.7	39.3	2.07
63.0	59.0	38.0	1.94
67.5	59.6	37.5	1.88
72.0	61.4	36.0	1.80
76.5	64.0	33.5	1.61
81.0	65.7	31.7	1.60
85.5	68.2	29.2	1.62
90.0	72.3	25.6	1.01
94.5	75.7	22.3	0.91
99.0	80.2	18.1	0.72
103.5	83.3	14.8	0.60
108.0	89.0	9.46	0.45
112.5	95.9	2.94	0.18
117.0	99.0	0	0

*Measured from Al_2O_3 Interface

TABLE XLVII

CONCENTRATION PROFILES OF Nb(Cb), V, AND Al IN BRAZE 6W AFTER 100 HR (3.6×10^5 s) AGING AT 1200°C

X Microns*	C, wt %		
	Nb(Cb)	V	Al
4.5	50.6	44.5	3.93
9.0	51.1	44.4	3.64
13.5	50.8	44.9	3.30
18.0	51.0	44.8	3.08
22.5	51.3	44.7	2.97
27.0	51.5	45.0	2.66
31.5	51.2	45.3	2.48
36.0	51.4	45.5	1.97
40.5	50.7	46.0	2.14
45.0	52.4	44.8	1.82
49.5	52.5	44.6	1.92
54.0	53.8	43.4	1.82
58.5	55.4	41.9	1.82
63.0	56.4	41.1	1.60
67.5	58.5	39.0	1.62
72.0	58.7	38.5	1.70
76.5	61.5	36.0	1.58
81.0	63.6	33.9	1.34
85.5	65.5	32.3	1.30
90.0	67.2	30.3	1.23
94.5	69.9	27.9	1.05
99.0	72.5	25.6	0.80
103.5	75.6	22.9	0.60
108.0	76.4	21.6	0.92
112.5	82.0	16.4	0.60
117.0	84.2	14.2	0.65
121.5	91.0	7.4	0.42
126.0	96.8	1.9	0.22
130.5	98.1	0.8	0.18
135.0	98.8	0.2	0
139.5	99.0	0	0

*Measured from Al_2O_3 Interface.

TABLE XLVIII
CONCENTRATION PROFILES OF Nb(Cb), V, AND Al IN BRAZE 6W
AFTER 500 HR (1.8×10^6 s) AGING AT 1200° C

X Microns*	C, wt %		
	Nb(Cb)	V	Al
4.5	57.1	37.0	4.89
9.0	57.6	36.4	4.98
13.5	57.7	36.6	4.7
18.0	58.2	36.4	4.55
22.5	58.6	36.8	3.71
27.0	59.8	35.5	3.65
31.5	59.3	35.3	4.55
36.0	59.6	35.3	4.21
40.5	60.6	34.1	4.25
45.0	61.0	33.6	4.10
49.5	61.8	33.2	3.93
54.0	63.2	32.1	3.82
58.5	64.6	30.8	3.66
63.0	65.8	29.8	3.39
67.5	66.8	28.8	3.43
72.0	68.1	27.5	3.24
76.5	69.7	26.3	3.02
81.0	71.6	24.7	2.75
85.5	73.2	23.0	2.59
90.0	76.0	20.6	2.40
94.5	78.2	18.6	2.16
99.0	81.2	16.2	1.61
103.5	84.1	13.7	1.17
108.0	91.2	7.3	0.6
112.5	98.0	0.7	0.2
117.0	99.	0	0

*Measured from Al_2O_3 Interface.

TABLE XLIX

CONCENTRATION PROFILES OF Nb(Cb), V, AND Al IN BRAZE 6W AFTER 1000 HR (3.6×10^6 s) AGING AT 1200°C

X Microns*	C, wt %			X Microns*	C, wt %		
	Nb(Cb)	V	Al		Nb(Cb)	V	Al
4.5	50.7	44.1	4.27	162.0	54.2	42.5	2.50
9.0	50.7	44.3	4.00	166.5	54.2	42.6	2.43
13.5	50.6	44.6	3.93	171.0	54.1	42.4	2.43
18.0	50.1	44.9	4.00	175.5	54.5	42.0	2.35
22.5	50.5	44.8	3.88	180.0	55.0	41.7	2.30
27.0	50.2	44.7	4.00	184.5	55.3	41.6	2.18
31.5	50.2	44.8	3.74	189.0	56.2	40.7	2.25
36.0	50.5	44.7	3.95	193.5	56.6	40.2	2.09
40.5	50.3	43.9	3.89	198.0	56.8	40.1	2.05
45.0	50.5	43.8	3.69	202.5	57.7	39.2	2.05
49.5	51.0	44.2	3.81	207.0	58.2	38.9	1.90
54.0	50.4	44.1	3.72	211.5	58.3	38.8	1.89
58.5	51.0	44.4	3.50	216.0	59.6	37.4	1.91
63.0	51.4	44.1	3.47	220.5	60.0	37.0	1.90
67.5	50.7	44.7	3.54	225.0	60.6	36.8	1.75
72.0	51.1	44.3	3.52	229.5	61.3	36.0	1.63
76.5	51.2	44.5	3.48	234.0	61.6	35.7	1.60
81.0	51.2	44.2	3.50	238.5	63.1	34.3	1.42
85.5	51.1	44.5	3.37	243.0	63.8	33.9	1.35
90.0	51.0	43.8	3.35	247.5	64.5	33.2	1.23
94.5	51.1	43.6	3.30	252.0	64.5	33.3	1.13
99.0	51.7	43.9	3.34	256.5	66.3	31.1	1.14
103.5	51.5	44.1	3.32	261.0	67.3	30.4	1.12
108.0	51.1	44.5	3.37	265.5	67.9	29.9	1.10
112.5	51.6	44.3	3.17	270.0	69.1	28.5	1.11
117.0	51.5	44.2	3.16	274.5	70.2	27.8	0.96
121.5	52.0	43.9	3.23	279.0	71.0	26.9	0.96
126.0	52.3	43.8	2.96	283.5	72.7	25.4	0.82
130.5	52.1	43.9	2.84	288.0	73.9	24.3	0.71
135.0	52.5	44.0	2.82	292.5	75.2	23.0	0.70
139.5	52.5	43.6	2.84	297.0	76.9	21.7	0.48
144.0	52.5	43.7	2.82	301.5	78.1	20.2	0.57
148.5	52.8	43.5	2.63	306.0	79.9	18.8	0.44
153.0	53.1	43.3	2.64	310.5	82.1	16.4	0.38
157.5	53.6	42.5	2.61	315.0	83.9	14.8	0.38
				319.5	86.2	12.7	0.32
				324.0	88.1	10.6	0.19
				328.5	89.9	8.8	0.18
				333.0	93.0	5.8	0.15
				337.5	97.0	2.0	0
				342.0	98.2	0.7	0

*Measured from Al_2O_3 Interface.

TABLE L

CONCENTRATION PROFILES OF Nb(Cb), V, AND Al IN BRAZE 10M AFTER 10 HR (3.6×10^4 s) AGING AT 1200° C

X Microns*	C, wt %		
	Nb(Cb)	V	Al
4.5	51.9	42.6	4.54
9.0	53.5	44.6	1.05
13.5	53.4	44.6	1.01
18.0	53.3	44.5	1.27
22.5	53.3	44.3	1.35
27.0	53.5	44.5	1.12
31.5	53.1	44.2	1.64
36.0	52.5	42.3	4.10
40.5	54.1	43.9	0.97
45.0	54.2	43.6	1.15
49.5	54.8	42.9	1.41
54.0	54.4	41.6	3.03
58.5	56.1	41.7	1.02
63.0	55.8	42.0	1.04
67.5	57.4	40.5	1.15
72.0	57.8	40.4	1.09
76.5	58.0	40.1	0.81
81.0	56.9	38.7	3.38
85.5	59.8	38.3	0.95
90.0	61.5	36.7	0.87
94.5	62.1	34.9	1.95
99.0	64.0	33.5	1.56
103.5	66.1	31.6	1.15
108.0	68.7	29.0	1.11
112.5	71.8	25.9	1.12
117.0	75.5	22.5	0.85
121.5	79.6	18.4	0.76
126.0	86.3	12.1	0.47
130.5	96.8	2.1	0.0
135.0	98.5	0.4	0.0

*Measured from Al_2O_3 Interface

TABLE LI

CONCENTRATION PROFILES OF Nb(Cb), V, AND Al IN BRAZE 10M AFTER 100 HR (3.6×10^5 s) AGING AT 1200°C

X Microns*	C, wt %		
	Nb(Cb)	V	Al
4.5	49.0	47.0	3.26
9.0	48.9	47.3	2.94
13.5	49.4	47.0	2.68
18.0	49.7	46.7	2.63
22.5	49.6	46.9	2.25
27.0	50.8	46.4	1.97
31.5	51.4	45.7	2.01
36.0	52.0	45.7	1.66
40.5	52.3	45.0	1.70
45.0	53.4	44.0	1.55
49.5	52.3	45.0	1.70
54.0	53.4	44.0	1.55
58.5	54.5	43.3	1.24
63.0	55.5	42.6	0.96
67.5	56.5	41.5	0.93
72.0	57.3	40.7	0.85
76.5	59.5	38.8	0.81
81.0	61.1	37.2	0.84
85.5	63.2	35.0	0.74
90.0	66.2	32.2	0.66
94.5	68.2	30.2	0.69
99.0	70.7	27.8	0.45
103.5	73.0	25.3	0.43
108.0	75.9	22.8	0.23
112.5	78.9	19.7	0.32
117.0	83.1	15.7	0.10
121.5	87.0	11.8	0.15
126.0	90.3	8.75	0.1
130.5	93.1	5.75	0.03
135.0	95.6	3.12	0.11
139.5	96.9	1.94	0.09
144.0	98.8	0.12	0
148.5	99.0	0	0

*Measured from Al_2O_3 Interface

TABLE LII
CONCENTRATION PROFILES OF Nb(Cb), V, AND Al IN BRAZE 10M AFTER 500 HR (1.8×10^6s) AGING AT 1200°C

X Microns*	C, wt %		
	Nb(Cb)	V	Al
4.5	54.6	38.4	6.13
9.0	53.8	39.6	5.7
13.5	53.3	39.7	5.86
18.0	53.2	40.0	5.70
22.5	53.0	40.1	5.61
27.0	54.2	39.4	5.33
31.5	54.7	39.1	5.33
36.0	55.1	38.6	5.12
40.5	54.5	38.5	5.04
45.0	55.7	38.4	4.74
49.5	56.3	38.2	4.71
54.0	57.1	37.7	4.28
58.5	57.8	37.1	4.08
63.0	58.5	36.5	3.92
67.5	59.3	35.1	4.54
72.0	59.7	34.3	3.79
76.5	61.6	34.0	3.49
81.0	62.9	32.9	3.19
85.5	64.7	31.3	2.94
90.0	66.9	29.6	2.39
94.5	68.4	28.3	2.53
99.0	69.8	26.7	2.43
103.5	72.0	25.1	2.07
108.0	74.5	22.8	1.69
112.5	76.0	21.4	1.46
117.0	79.1	18.9	1.03
121.5	81.5	16.5	0.89
126.0	84.3	13.8	0.73
130.5	87.7	10.8	0.48
135.0	90.7	8.1	0.39
139.5	94.0	4.9	0.18
144.0	94.3	4.6	0.19
148.5	95.7	3.0	0.16
153.0	96.7	2.0	0.12
157.5	98.6	0.2	0
162.0	99.0	0	0

*Measured from Al_2O_3 Interface

TABLE LIII

CONCENTRATION PROFILES OF Nb(Cb), V, AND Al IN BRAZE 10M AFTER 1000 HR (3.6×10^6 s) AGING AT 1200°C

X Microns*	C, wt %			X Microns*	C, wt %		
	Nb(Cb)	V	Al		Nb(Cb)	V	Al
4.5	53.5	40.9	4.61	162.0	61.3	35.3	2.37
9.0	53.3	41.2	4.43	166.5	62.3	34.4	2.26
13.5	53.5	41.1	4.34	171.0	62.6	33.9	2.27
18.0	53.3	41.4	4.26	175.5	63.5	33.6	2.22
22.5	53.0	41.9	4.09	180.0	65.2	32.1	1.83
27.0	53.9	41.0	4.05	184.5	65.5	31.8	1.78
31.5	53.2	42.0	3.81	189.0	66.9	30.6	1.62
36.0	53.8	41.4	3.80	193.5	67.9	30.0	1.50
40.5	53.6	41.5	3.81	198.0	68.6	29.0	1.39
45.0	53.9	41.5	3.54	202.5	69.6	28.2	1.26
49.5	54.0	41.3	3.68	207.0	70.8	27.0	1.11
54.0	53.8	41.4	3.67	211.5	71.7	26.3	0.98
58.5	54.0	41.1	3.84	216.0	73.3	24.8	0.83
63.0	54.2	41.3	3.45	220.5	74.3	23.0	0.73
67.5	54.6	41.1	3.39	225.0	76.0	22.3	0.75
72.0	54.6	41.0	3.44	229.5	77.7	20.5	0.55
76.5	55.1	40.7	3.12	234.0	79.6	18.7	0.54
81.0	55.3	40.7	3.00	238.5	81.1	17.1	0.55
85.5	54.7	41.0	3.05	243.0	83.9	14.7	0.34
90.0	55.4	40.5	3.03	247.5	87.3	11.5	0.18
94.5	55.3	40.6	3.07	252.0	97.3	1.46	0.15
99.0	56.1	39.8	2.88	256.5	98.8	0.20	0
103.5	55.8	39.6	3.46	261.0	99.0	0	0
108.0	56.2	39.3	3.40				
112.5	56.2	39.4	3.32				
117.0	56.6	39.1	3.20				
121.5	57.2	38.6	3.13				
126.0	57.5	38.4	3.07				
130.5	57.6	38.3	3.05				
135.0	58.4	37.7	2.92				
139.5	58.9	37.4	2.80				
144.0	59.4	36.7	2.74				
148.5	59.9	36.3	2.65				
153.0	60.3	36.0	2.8				
157.5	60.7	35.7	2.52				

*Measured from Al_2O_3 Interface.

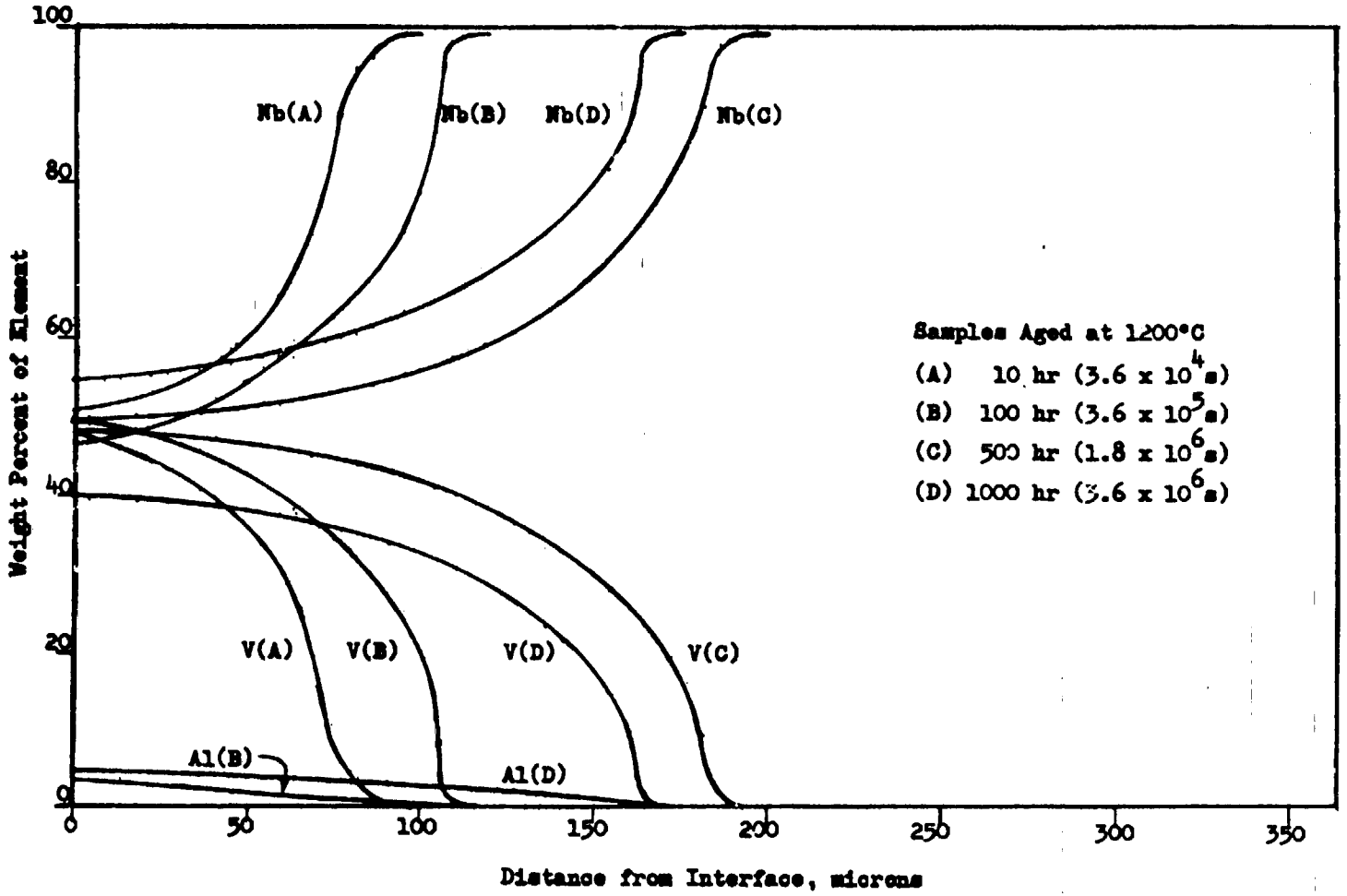

Figure 114. Concentration Profiles, Braze System 4W

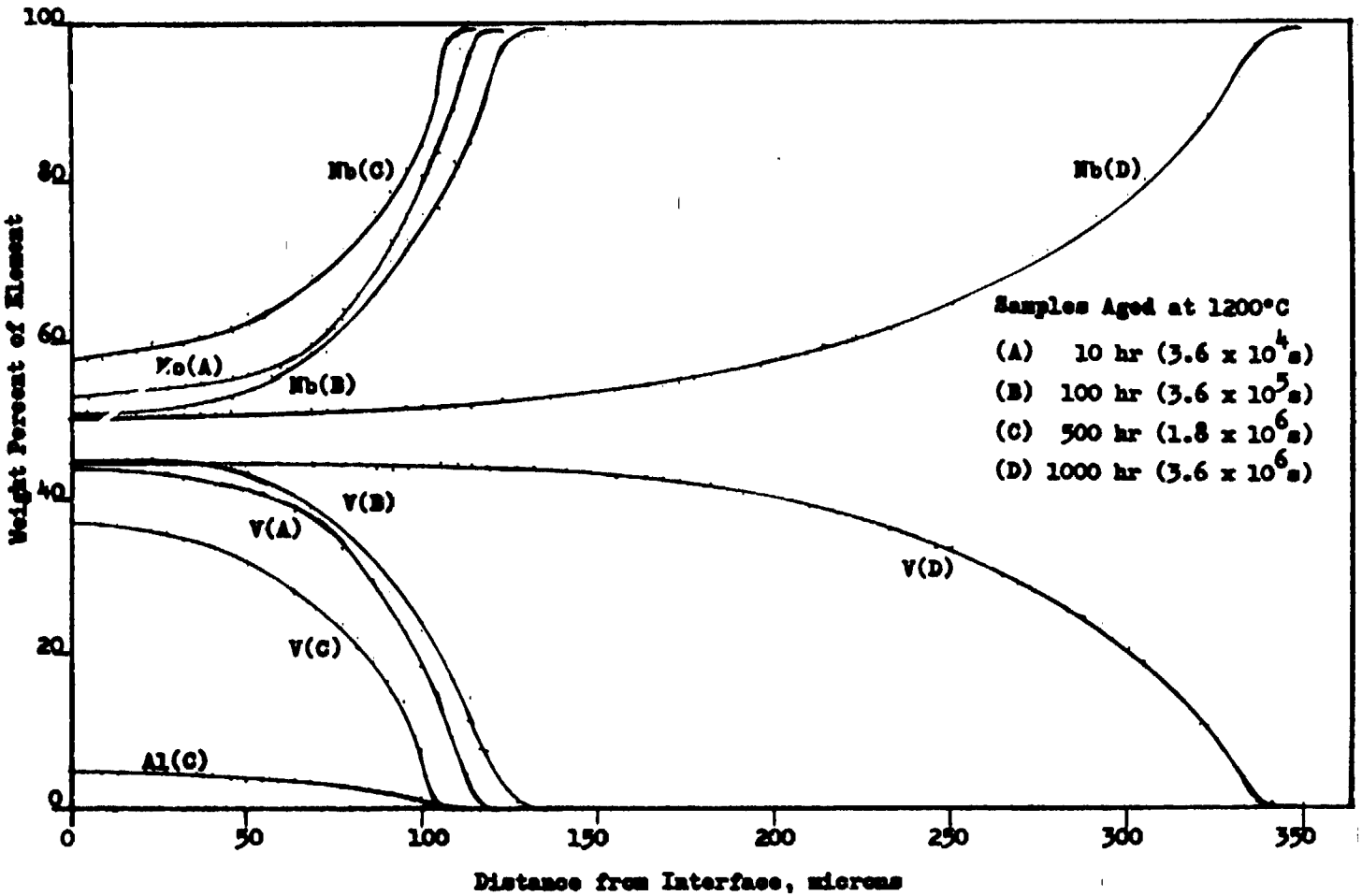

Figure 115. Concentration Profiles, Braze System 6W

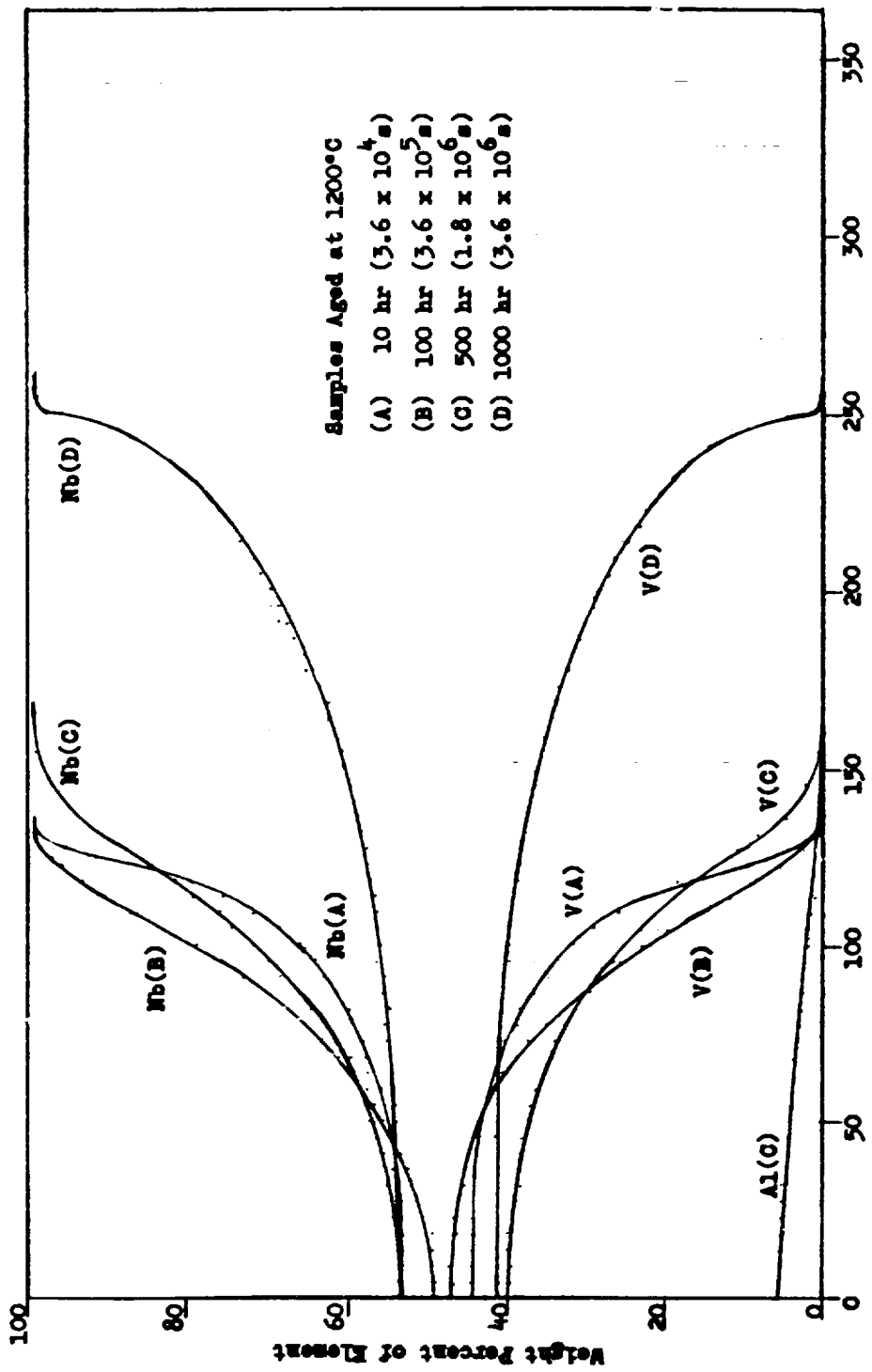

Figure 116. Concentration Profiles, Braze System 10M

uniform across the braze at the moment of freezing, then all of the systems would have a similar starting point for aging diffusion, but an examination of the several 10-hour (3.6×10^4s) Nb(Cb) concentration profiles shows a substantial curvature in the Nb(Cb) concentration curve near the juncture, such that it is obvious that the sloping gradient existed at the end of the brazing cycle.

APPENDIX XIV

BRAZING JIG, 0.5-INCH CAPSULE

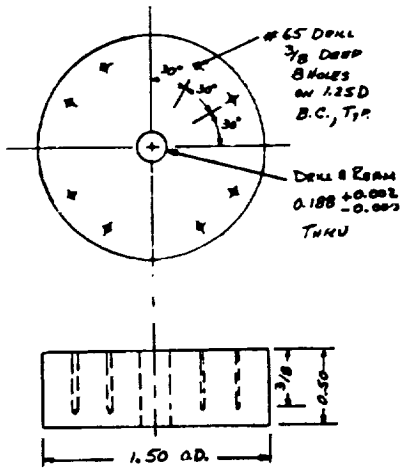

BASE

MAKE 1
MATERIAL: CB-1ZR ALLOY

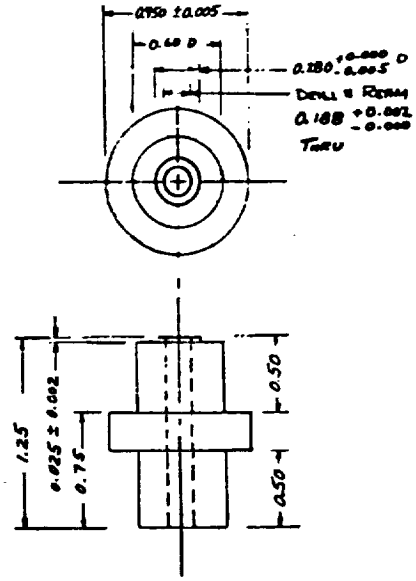

SPACER

MAKE 2
MATERIAL: CB-1ZR ALLOY

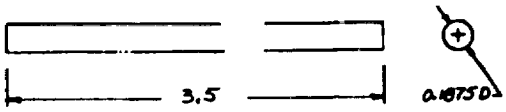

ALIGNMENT ROD

MAKE 1
MATERIAL: TUNGSTEN WELD ROD

NOTE: FOUR WIRE SUPPORTS ARE USED TO STEADY THE 0.20-INCH HIGH Al_2O_3 CERAMIC IN PLACE. THE WIRES ARE 0.030 INCH TANTALUM ABOUT 4 INCHES LONG AND BENT INTO A "U" SHAPE WITH THE ENDS INSERTED INTO THE #65 DRILL HOLES AND THE LOOP BENT OVER TO LIGHTLY TOUCH THE CERAMIC.

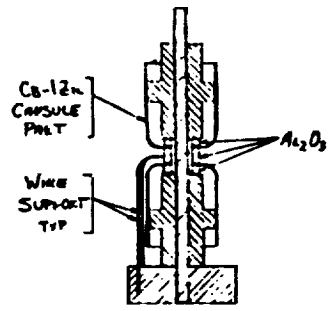

ASSEMBLY DRAWING

WITH CAPSULE PARTS IN PLACE

Figure 117. 0.5-Inch Capsule Brazing Jig Drawing

APPENDIX XV. PHASE II SAMPLE PREPARATION

The samples used in the Phase II studies were bulb-type capsules, as is shown in Figure 118, and button samples, which consist of one-inch (2.54 cm) lengths of 0.25-inch (0.635 cm) diameter Cb-1Zr rod, to the end of which an alumina button, 0.25-inch (0.635 cm) in diameter and 0.125 inch (0.318 cm) high is brazed. The best braze system as determined from the Phase I study was used in preparing the first set of bulb samples.

The seal joint as shown in Figure 118 consists of a 0.50-inch (1.27 cm) OD, 0.10-inch (0.254 cm) wall, ceramic cylinder 0.2-inch (0.508 cm) in length, brazed on each end to a cup-shaped Cb-1Zr section. In order to provide stress equalization across the braze/metal region, a ring of ceramic 0.50-inch (1.27 cm) OD, with an 0.10-inch (0.254 cm) wall, and 0.10-inch (0.254 cm) high is brazed to the inside of the Cb-1Zr sections in alignment with the ceramic section. Four braze regions are thus required although only two of them are required to be vacuum tight.

The Cb-1Zr cups were deep drawn in a single step from recrystallized sheet stock. The 2.5-inch (6.35 cm) diameter, 0.020-inch (0.051 cm) thick disc blanks were placed between an aluminum bronze female die and an air-hardened tool steel hold-down plate. The platen on a double-acting press was utilized to adjust the pressure on the periphery of the blank to prevent it from wrinkling during the draw. A flat-bottomed tool steel punch was used to form the cup. After the draw, and with the cup still on the punch, the punch was pressed against a tool steel plate to assure the flatness of the surface to be brazed.

The cup was removed from the punch by hand and visually inspected for evidence of galling or wrinkling. None was found. The cups were then degreased and washed in preparation for chemical cleaning in accordance with NASA Specification No. C-393666-2 (June 25, 1970). This procedure involves the use of a 20-20-60 mixture of HF-HNO_3-H_2O to etch the metal surface, a distilled water soak and rinse, and finally an absolute alcohol rinse.

Following the cleaning, the cups were heat treated in vacuum ($< 1 \times 10^{-5}$ torr or 1.33×10^{-3} N/m^2) for one hour at 2200°F (1204°C). The annealed cups were then handled with gloves and machined to their finished dimensions (Figure 118), inspected, and stored in a clean, covered, glass container. The braze joints were prepared as is described above, using the jig shown in Appendix XIV.

Figure 118. Capsule Assembly

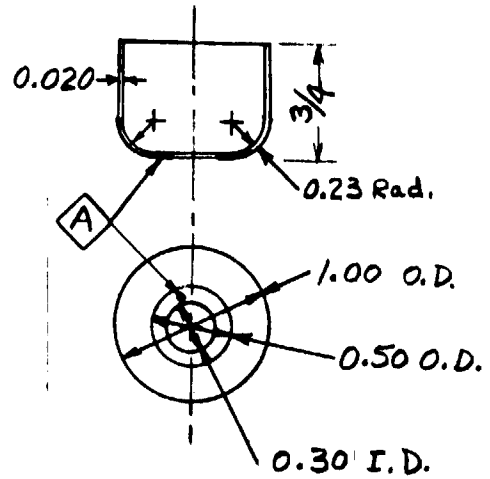

CUP
MAKE 2
MATERIAL Cb-1Zr

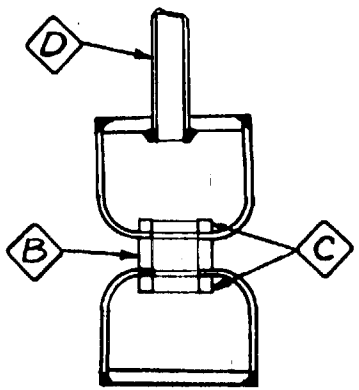

ASSEMBLY

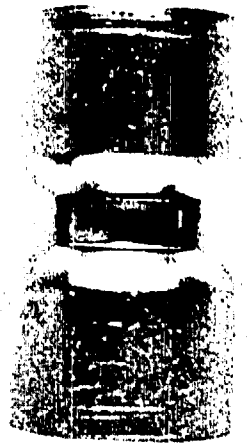

AS-BRAZED ASS'Y
1.5X

NOTES:

A. SURFACE FLAT TO 0.001
B. ALUMINA RING, 0.500 O.D. x 0.300 I.D x 0.20 HIGH
C. ALUMINA RING, 0.500 O.D. x 0.300 I.D. x 0.10 HIGH
D. Cb-1Zr TUBE, 0.257 O.D. x 0.020 WALL

APPENDIX XVI. SHEAR TEST DATA SUMMARY

As is indicated in Table XV, two button samples from each aging exposure condition were tested in shear. The test results are shown in Table LIV. All of the samples, except those from the 5000-hour, 1200°C test, showed shear values equivalent to the as-brazed samples. The lowest value was 5810 psi (4×10^7 N/m^2). However, the two samples which were exposed at 1200°C for 5000 hours showed shear strength values of 1590 and 1630 psi (1.09×10^7 and 1.12×10^7 N/m^2). This is a significant decrease in strength and must be attributed to a high temperature aging effect.

TABLE LIV

SHEAR TEST RESULTS FOR AGED SAMPLES

Sample	Aging Temp. °C	Shear Strength, psi, (N/m^2)		
		Before Aging	1000 hr Aging	5000 hr Aging
8	None	7 340 (5.05×10^7)		
38-2	800		8 250 (5.68×10^7)	
38-4	800		10 500 (7.24×10^7)	
35-4	800			8 360 (5.76×10^7)
36-1	800			11 940 (8.22×10^7)
37-2	1000		13 050 (9.0×10^7)	
37-1	1000		5 810 (4.0×10^7)	
37-3	1000			10 700 (7.38×10^7)
35-2	1000			8 060 (5.56×10^7)
36-2	1200		7 240 (4.99×10^7)	
36-3	1200		6 320 (4.35×10^7)	
36-4	1200			1 630 (1.12×10^7)
34-3	1200			1 590 (1.09×10^7)

APPENDIX XVII
METALLOGRAPHIC AND MICROHARDNESS DATA SUMMARY

The data from the Phase II metallographic and microhardness evaluations are presented below.

One button sample from each aging exposure condition was examined metallographically. In addition, a microhardness traverse of the braze region was made. These test results are shown in Figures 119, 120, 121, and 122. Figure 119 is an as-brazed sample. Figure 120 shows samples 37-4(A) and 34-4(B); Figure 121 shows samples 21-3(A) and 21-4(B); and Figure 122 shows samples 21-1(A) and 21-2(B).

The photomicrograph shown in Figure 119 shows a braze layer about 9 mils (0.228 mm) thick. This un-aged sample shows a reasonably flat hardness profile in the braze with an increase from 350 units to 450 units about 1 mil (0.0254 mm) from the braze-ceramic interface. A layer about 2 mils (0.0508 mm) thick can be seen at the alloy-braze interface, but its hardness is no different from that of the bulk of the braze. Epitaxy is evident in this pure vanadium braze, and from the width of the braze zone, the vanadium braze has obviously dissolved a large amount of the Cb-1Zr alloy. In this regard, it behaves just as did the vanadium alloy brazes tested in Phase I. A final observation is that the Cb-1Zr alloy in Figure 119 has the characteristic hardness value of 75 units. One thing that is different in the sample shown in Figure 119 is the presence of a rough line of imperfections about 1.5 mils (0.038 mm) from the ceramic interface. This is, however, characteristic of these vanadium brazes, and appears in many of them to varying degrees.

Figure 120 shows the 800°C exposed samples. Sample A was the 1000 hour aged button sample and shows a braze thickness of 8.5 mils (0.216 mm), a rather level microhardness trace of 410 DPH units, and the typical 75 DPH unit hardness in the Cb-1Ar alloy. Marked epitaxy is evident, as is the difference in appearance of the braze region and the base metal. The braze region appears clear, and suggests that it is more uniform than the Cb-1Zr which shows the presence of many fine particles. A slight indication of a layer at the metal/braze interface is evident, as are a number of imperfections near the ceramic.

Another region of the same 800°C-1000-hour exposed sample (#37-4) is shown as Sample A of Figure 123. The hardness traverse region (Figure 120) was chosen to be reasonably clear of voids, in order that they not perturb the hardness profile measurements. However, there are regions along the 0.25 inch (6.35 mm) width of the button sample in which voids appear. The voids are seen to be primarily on grain boundaries, although several of them are seen to be within the rather large grains. Although in Sample A of Figure 123 there was not yet an indication of the linking-up of voids, the tendency toward their joining, with the strong possibility of developing a leak, is clearly evident.

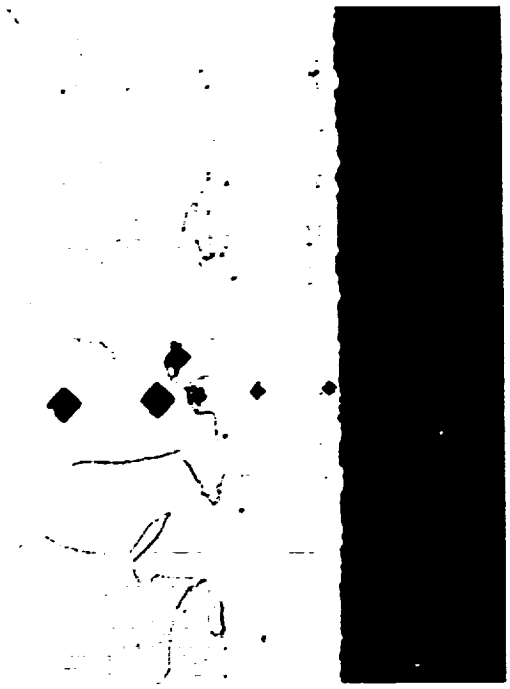

Micrograph, 100X

Microhardness Profile

Figure 119. Aging Test Analysis Data: Braze System 14W (Cb-1Zr/V/W/Al_2O_3). Brazed at 1860°C for 60s. As-Brazed Sample.

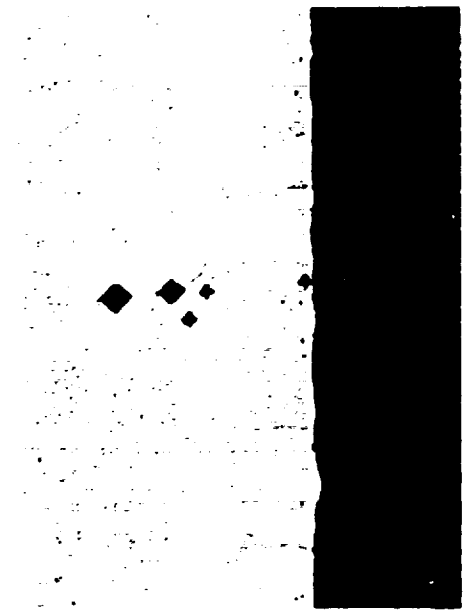

A. Micrograph, 100X

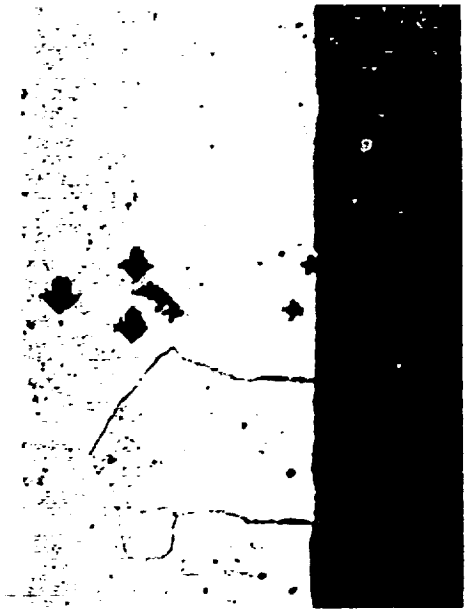

B. Micrograph, 100X

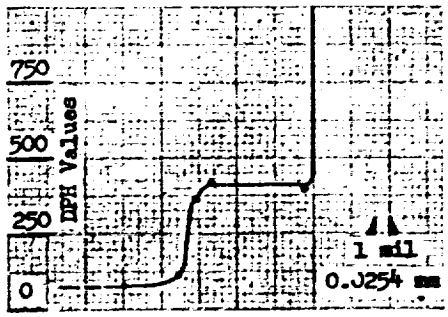

A. Microhardness Profile

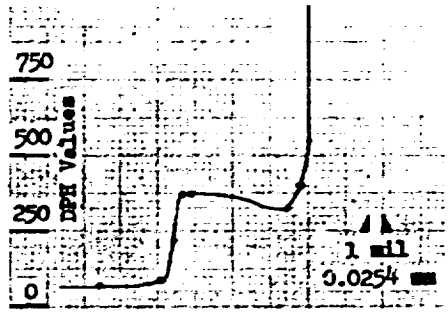

B. Microhardness Profile

Figure 120. Aging Test Analysis Data: Braze System 14W (Cb-1Zr/V/W/Al_2O_3) Brazed at 1860°C for 60s. Sample A aged for 1000 hours (3.6×10^6s) at 800°C; Sample B aged for 5000 hours (1.8×10^7s) at 800°C.

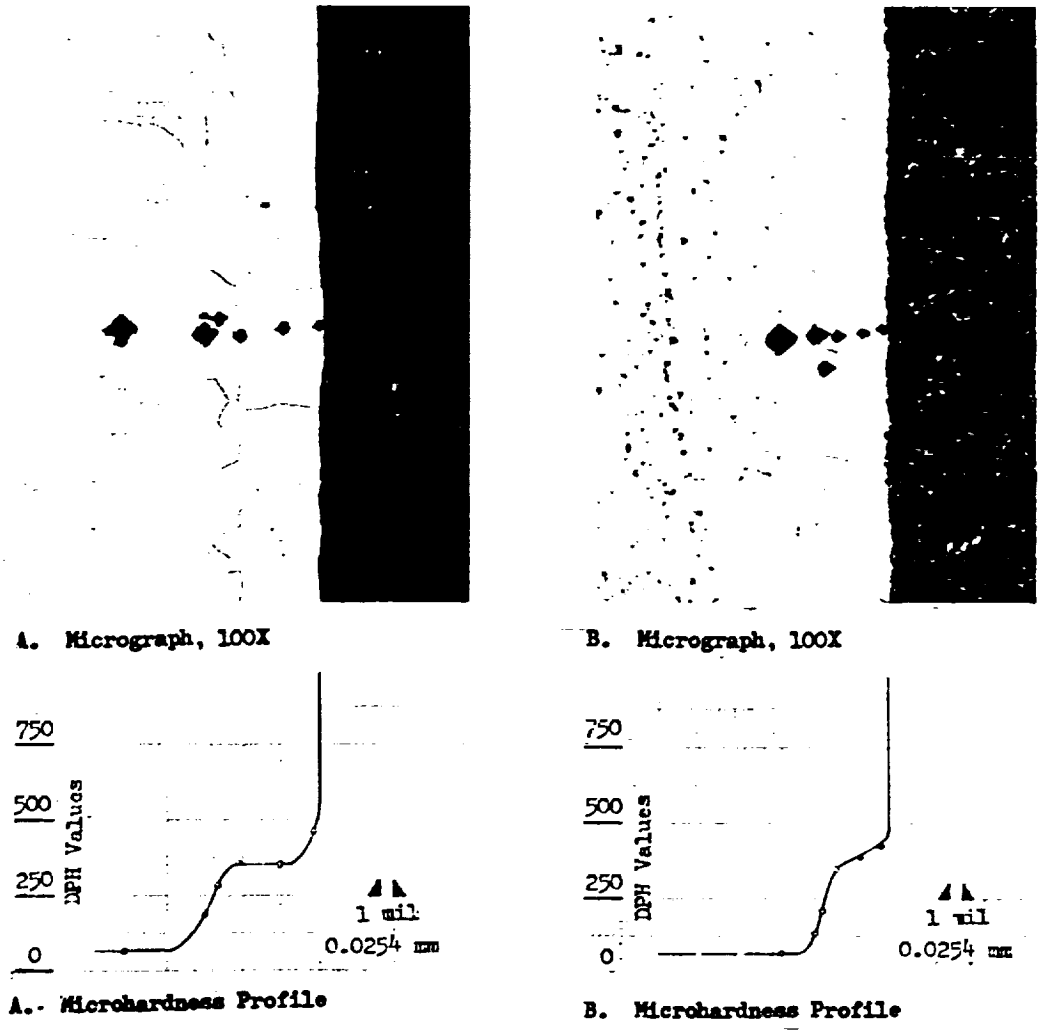

Figure 121. Aging Test Analysis Data: Braze System 14 W (Cb-1Zr/V/W/Al_2O_3) brazed at 1860°C for 60s. Sample A aged for 1000 hours (3.6×10^6s) at 1000°C; Sample B aged for 5000 hours (1.8×10^7s) at 1000°C.

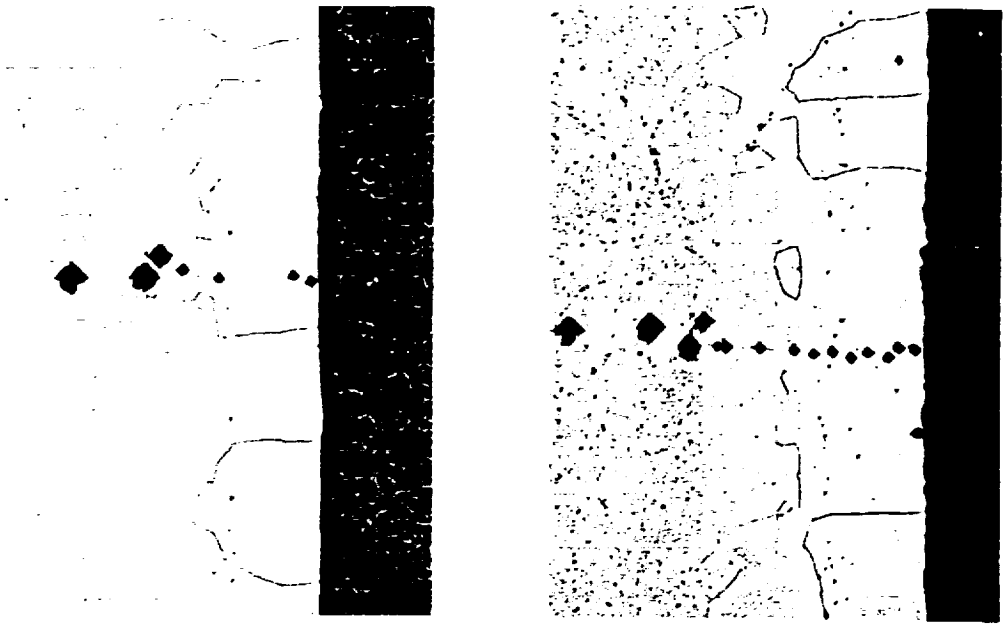

A. Micrograph, 100X

B. Micrograph, 100X

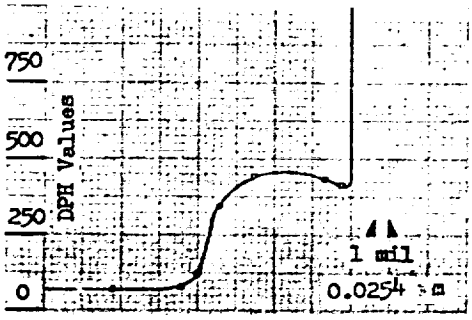

A. Microhardness Profile

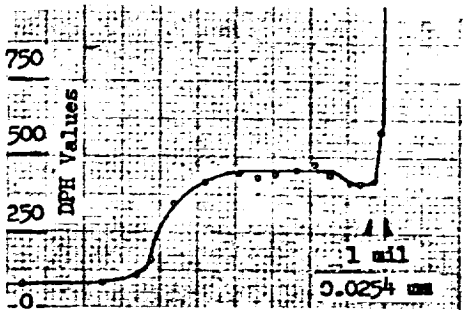

B. Microhardness Profile

Figure 122. Aging Test Analysis Data: Braze System 14 W (Cb-1Zr/V/W/Al_2O_3) brazed at 1860°C for 60 s. Sample A aged for 1000 hours (3.6×10^6s) at 1200°C; Sample B aged for 5000 hours (1.8×10^7s) at 1200°C.

A. Micrograph, 100X

B. Micrograph, 100X

C. Micrograph, 100X

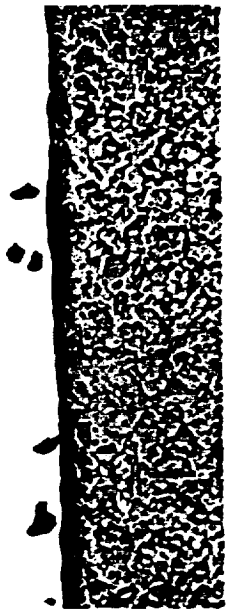

D. Micrograph, 100X

Figure 123. Aging Test Analysis Data: Braze System 14 W (Cb-1Zr/V/W/Al_2O_3) brazed at 1860°C for 60 s. Sample A aged at 800°C for 1000 hours, Sample B aged at 1000°C for 1000 hours, Sample C aged at 1200°C for 5000 hours, Sample D aged at 1200°C for 1000 hours.

Sample B of Figure 120 has aged for 5000 hours. Its hardness value is reversed in detail, being slightly softer near the Al_2O_3 (325 DPH units) than in the bulk of the braze (375 DPH units). Some imperfections which appear to be small voids are evident, as is a very thin interfacial layer between the braze and the ceramic.

Figure 122 shows the 1000°C exposed samples. Sample A was the 1000-hour aged button sample, and shows a nominal braze thickness of about 7 mils (0.178 mm). The microhardness of the braze is typical at 350 DPH units, but that of the Cb-1Zr alloy is about 70, which is lower than the 75 units usually seen. Epitaxy is clearly evident. Only a few imperfections are seen in this braze. One interesting aspect of Sample A is the wide region in which the hardness drops from 350 units to the 70 units. This width is 3 mils (0.076 mm) at least, and is not reflected in the photomicrograph, in which the braze appears 5-6 mils (0.127-0.152 mm) thick.

Another region of the same 1000°C - 1000-hour exposed sample (#21-3) is shown as Sample B of Figure 123. In this photomicrograph, a number of small voids on the grain boundary line parallel to the alumina surface have joined to form connected voids 4 to 7 mils (0.102 to 0.178 mm) in length. The line of the voids is 3 mils (0.076 mm) from the ceramic interface but the braze region thickness is nominally 7 mils (0.178 mm), and was produced by a braze foil which was originally 5 mils thick with the solution of Cb-1Zr during the 60 second brazing period. It is not unlikely that during the 1000-hour aging period some vanadium from the vanadium-rich braze diffused into the Cb-1Zr alloy, and simultaneously, some Cb (Nb) diffused from the niobium-rich alloy into the vanadium-rich braze. Because vanadium is a smaller atom than is a niobium atom, its diffusion coefficient and therefore its diffusion rate is greater than that of niobium. Such an imbalance in diffusion rates tends to form the well-known Kirkendall holes. If there had been an original line of imperfections, they could conceivably have caused the orientation of the voids seen in Sample B of Figure 123. The vanadium in the region nearer the alumina would be expected to be less mobile if the local impurity content (especially if the impurity were oxygen) in that layer were higher than that farther from the ceramic. Therefore, there would be less tendency for vanadium to move out of the 3-mil (0.076 mm) layer adjacent to the ceramic to replace or partially replace that which diffused toward the Cb-1Zr from the 3 to 4 mil (0.076 - 0.102 mm) region. The final result is then a depletion of vanadium at the 3 mil (0.076 mm) position, which depletion when coupled with a grain boundary already present leads to the formation of a line of holes, which ultimately become connected.

Sample B of Figure 121 shows a much thinner braze for this particular 5000-hour, 1000°C exposed sample. The hardness trace indicates a braze thickness of about 4.5 mils (0.114 mm), with a long transition region from the braze hardness value of about 400 DPH units to the annealed Cb-1Zr value of about 65 units. Epitaxy and large grains are again characteristic of the braze region, and as in Sample B of Figure 120, a very thin interfacial reaction zone appears to have developed.

Figure 122 shows the 1200° C exposed samples. Sample A, with a 1000-hour exposure, shows a region extending about 9.5 mils (0.241 mm) in thickness. Marked epitaxy and very large grains are also seen. The hardness profile shows a softer region adjacent to the ceramic at 400 DPH units, while the maximum value in the braze is 450 units, but with a gradual reduction in a nearly 3 mil (0.076 mm) thick region to the characteristic 75 DPH units for the Cb-1Zr. The photomicrograph shows a potential beginning of a row of imperfections about 6 mils (0.152 mm) from the ceramic interface, and a gradation of the imperfection pattern of the alloy from the clear region at the 6 mil point to the characteristic Cb-1Zr appearance beyond 10 or 11 mils (0.254 or 0.279 mm).

Sample D of Figure 123 shows another region of the 1200° C, 1000-hour exposed sample (#21-1). Several large voids are seen at grain boundaries. However, these are within 1 to 2 mils (0.0254 to 0.0508 mm) of the ceramic-braze interface, which is different from the behavior exhibited by Sample B of Figure 123. The difference here may be that there are no grain boundaries which lie parallel to the ceramic and closer than about 7 mils (0.178 mm) to the interface.

Sample B of Figure 122, with a 5000-hour exposure, shows a similar pattern to that of Sample A, but a much thicker region is affected. The photomicrograph suggests the braze region to be about 7 or 8 mils (0.178 or 0.203 mm) thick, but the microhardness traverse shows a well-defined hardness effect out to 15.5 mils (0.394 mm). Between the 8 mil and the 15.5 mil locations one can see the gradation in the Cb-1Zr material imperfection pattern. Again, epitaxy and extremely large grains are evident. In this case, there is no evidence of an interface reaction layer at the braze-alumina interface in this region of the 5000-hour aged sample. However, in Sample C of Figure 123, which is another region of the same sample (#21-2), a distinct interfacial layer is seen and several very large (1 to 2 mil) (0.0254 to 0.0508 mm) voids are also seen to lie on the grain boundaries.

Figure 124 shows two regions of the braze of Capsule #11 (64 thermal cycles followed by 5000 hours aging at 1200° C). These regions are relatively free of voids and were chosen for ease of obtaining microhardness plots of the braze. Sample A of Figure 124 is a region that showed no indication of a vacuum leak, and Sample B of Figure 124 is near a region that did show an indication of a vacuum leak. Figure 125 shows a leaky area of Capsule #11 and the very large voids that formed.

The hardness profiles of Capsule #11 (Figure 124) show a rather narrow 5 to 6 mil (0.127 to 0.152 mm) region of low hardness characteristic of the base Cb-1Zr alloy and the harder adjacent braze alloy regions. Sample A has a more gradual gradation of hardness through the braze region, but the curve is similar in character to those of some of the button samples. Sample B has constant-hardness regions in the braze, which behavior was also observed in several of the button samples. Sample A shows a minimum at about 80 DPH units, which is the typical value for Cb-1Zr alloy, but Sample B has a minimum hardness value of 175 DPH units.

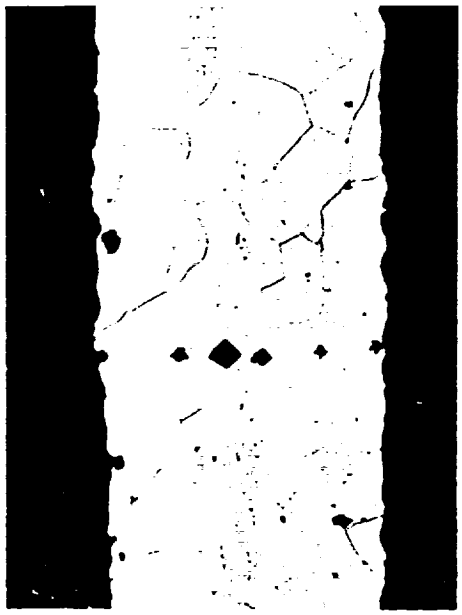

A. Micrograph, 100X

B. Micrograph, 100X

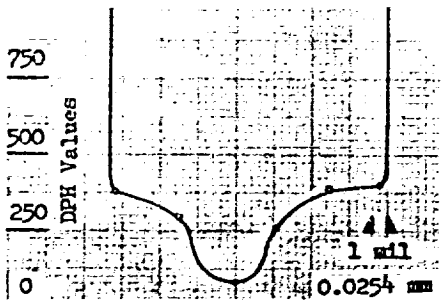

A. Microhardness Profile

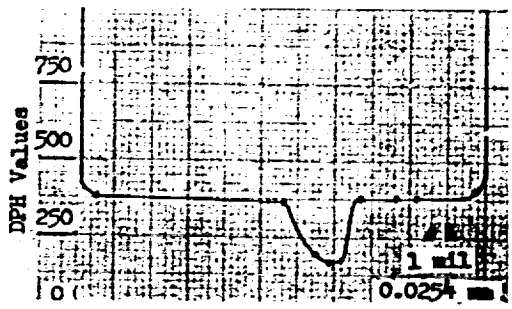

B. Microhardness Profile

Figure 124. Aging Test Analysis Data: Braze System 14 W (Cb-1Zr/V/W/Al_2O_3) brazed at 1860°C for 60s. Sample A was taken from Capsule #11 in a region which showed no evidence of vacuum leaks. Sample B was taken from Capsule #1 in a region which did show evidence of a vacuum leak.

Micrograph, 100X

Figure 125. Aging Test Analysis Data: Braze System 14 W (Cb-1Zr/V/W/Al_2O_3) brazed at 1860°C for 60 s. This sample was taken from Capsule #11 in a region which showed evidence of a vacuum leak. This region of the sample is adjacent to that shown in Sample B of Figure 124.

This may be the consequence of the rather thin residual "Cb-1Zr"-like region in Sample B, whose overall braze region is 27 mils (0.685 mm) thick. However, the "residual" Cb-1Zr region is only about 4 mils (0.107 mm). The braze region to the left on the photomicrograph in Sample B is 14 mils (0.356 mm) wide, and at least 10 mils (0.254 mm) of it (at the far left) appears to have been fully molten during brazing. The remaining 4 mils (0.102 mm) shows a very slight shadowing which suggests that an alloying of the vanadium with the Cb-1Zr has occurred, either by rapid diffusion during the brazing period, or by diffusion subsequent to the brazing operation. The former hypothesis seems more plausible, because the hardness profile is quite uniform across that region.

A similar suggestion of a molten/diffusion zone is seen on the right side of Sample B of Figure 124. However, the width of the molten zone is only 4 mils (0.102 mm), and that of the diffusion zone is about 5 mils (0.127 mm). The dissolution of the Cb-1Zr is quite evident, with about 15 mils (0.381 mm) being dissolved in Sample B. It is reasoned that because the residual Cb-1Zr area was so thin, the diffusion of the vanadium into that "Cb-1Zr" region during aging caused a hardening effect which extended to the centerline of the "Cb-1Zr."

Sample A of Figure 124 shows a thinner overall braze region, about 18 mils (0.457 mm) in all. Because there was a total metal thickness of 2 (5) plus 20 = 30 mils (0.76 mm) at the beginning of the braze period, some movement of material away from this particular location occurred. If the material which flowed away was largely vanadium (and that is most likely), then the remaining ratio of vanadium to Cb-1Zr is lower than that of Sample B, and may account for the wider "residual Cb-1Zr" region of about 6 or 7 mils (0.152 or 0.178 mm) as judged by the hardness trace. Again, a two-region braze layer can be seen on both sides of Sample A.

Figure 125 also shows the same thin "residual Cb-1Zr" layer as does Sample B of Figure 124, and the thick (26 mil or 0.65 mm) braze. The voids are very large and appear to have formed and linked up along grain boundaries.

The braze region of Capsule #15 is shown in Figure 126. This sample completed a 5000-hour exposure at 1200°C, and was initially exposed internally to cesium vapor at 5 torr (6.67×10^2 N/m^2). The braze is seen to be very thin at about 17 mils (0.43 mm), with a residual "Cb-1Zr" region which appears to be about 5 mils (0.127 mm) thick. A large amount of vanadium-rich braze material has obviously flowed out of the braze in this location, and further, this flowing material must have contained an appreciable amount of dissolved alloy. A few voids are observed in both the Sample A and Sample B and they again have a tendency to align themselves parallel to the ceramic. It is most interesting to note that the best-defined row of voids, which appears in Sample B, lies beyond the edge of the alumina, toward the outside of the braze joint. The reason for this is not understood, although it is clear that the vanadium braze flowed along the surface of the Cb-1Zr cup material and out of the joint.

A. Micrograph, 100X

B. Micrograph, 100X

Figure 126. Capsule #15. Sample A shows the inner surface of the braze region. Sample B shows the region of the braze and the Cb-1Zr alloy at the outside of the braze region.

In Sample B, there is a fillet-like extension of the braze that is seen to be adherent to the ceramic on the right side of the photomicrograph.

The metallographic and hardness data on aged samples shown in Figures 119 through 126 are self-consistent. The effects of both time and temperature on the brazes are clearly shown, with the most severe effects being observed on Capsule #11 (Figures 125 and 124). This is consistent with the thermal cycling plus the 5000-hour aging at 1200°C being the most severe treatment given any of the samples. The next most severe is the 5000-hour aging at 1200°C, as represented by Sample C of Figure 123, Sample B of Figure 122, and Figure 126. Void formation is evident, but the average size of the voids is less than appears in Capsule #11. The next most severe effects are those shown in Sample B of Figure 121 and Sample B of Figure 123. Here the voids are smaller, although they have already begun to become connected in Sample B of Figure 123. The least affected samples were Sample E of Figure 120 and Sample A of Figure 123.

Characteristically, the vanadium braze is seen to be very active in dissolving large amounts of the Cb-1Zr alloy, so that the final braze compositions involve an estimated 50 percent niobium (columbium), as did Brazes # 4W, 6W, and 10M (Figures 114, 115, and 116). Because of the strong dissolution effect, and because of the tendency to produce a final braze composition containing a nominal 50% Cb(Nb)-50% V, one might expect to find less attack of the Cb-1Zr (Nb-1Zr) alloy from Braze #8, which is initially 65% V with 35% Cb(Nb). In this system, then, less columbium (niobium) is required to bring the braze melt up to the observed nominal 50% Cb(Nb) composition.

A second feature of concern in braze system #14 (Cb-1Zr/V/W/Al_2O_3) is the strong tendency for the braze to develop voids under aging conditions. Even in the 1000-hour samples, voids are seen to be developing on the grain boundaries, and they enlarge as aging proceeds. In time, the individual voids tend to merge and to develop lines of voids, which ultimately would lead to failure.

If these voids are formed as a consequence of the net diffusion of vanadium from the braze toward the Cb-1Zr alloy being greater than the diffusion of the niobium (columbium) in the alloy back into the braze, then they will inexorably form as the braze joints age. Their rates of formation will depend, of course, on the diffusion coefficients of V and Nb(Cb) in the particular alloy compositions. In these systems, diffusion gradients will be present, and the atoms will move. However, the use of thinner braze foil should be beneficial in reducing the formation of voids. The thinner braze will develop a higher concentration of Nb(Cb) during the brazing step, during which the Nb dissolves in the molten vanadium. However, the amount of the dissolved niobium (columbium) is contained in less vanadium, so that the final concentration and concentration gradient of the vanadium will be less for a thin braze foil. With a lower gradient, there should be less tendency for vanadium to diffuse, and for voids to form.

APPENDIX XVIII. AGING CAPSULE DATA SUMMARY

The results of the Phase II aging tests are given in Table LV. an examination of the table shows that four of the six capsules that were originally leak tight survived their 5000-hour aging tests. Two of these six capsules developed leaks. Capsule #18, which on 6-23-70 had a leak of 30×10^{-10} std cc air/sec showed a continuous increase in the leak rate as it aged.

Capsule #11, which was subjected to 64 thermal cycles between 250 and 1200°C before being aged, survived 1000 hours aging at 1200°C without developing a leak. However, after 5000 hours (total) aging at 1200°C, a leak which was too large to measure on the Veeco MS-9 leak detector had developed.

Capsule #15, which was the cesium vapor test capsule, developed a leak in the braze during the 5000-hour test exposure. The time at which the leak developed is not known because when the samples were removed from the furnaces after the first 1000-hour increment, there was no evidence that the capsule had developed a leak, so it was returned to test with only the visual examination.

Capsules #14, #13, #16, and #19 all survived their aging exposures with no degradation in the vacuum integrity of the braze seal. Their final leak rates were all less than 2.3×10^{-10} std cc air/sec, which value is the lower limit of detection of the Veeco MS-9 helium leak detector instrument used.

It is of interest (Ref. 16) to briefly examine the aging behavior of Capsule #18, which began the 5000-hour test sequence with a measurable leak, as is indicated in Table LV. Table LVI shows a leak-rate history of the capsule with time, beginning with the date of fabrication and with the indications of the pertinent events of its life. The leak rate is seen to continually increase with time, but the fractional rate of change decreases with time.

The behavior of Capsule #15 can be shown in a similar fashion. Table LVII shows its aging behavior as indicated by its vacuum leak rates as a function of aging time at temperature (1200°C). Because a leak check could not be performed after the 1000-hour aging period, it is not known when the leak in the ceramic-to-metal seal first developed. However, its size, even after the 5000-hour period, was really quite small, and had there not been the much larger leaks in the metal-to-metal capsule weld, it is questionable whether all of the cesium would have escaped.

TABLE LV

VACUUM INTEGRITY TEST RESULTS OF BRAZE JOINTS

FOR AGED CAPSULE SAMPLES

Sample No.	Braze Date (1971)	Thermal Cycles to 1200°C	Aging Temp. °C	Leak Rates* (std cc air/sec) x 10^{10}						
				After Prep'n of Braze Joint	After Closure Weld		After Thermal Cycling	After 1000 hr Aging	After 5000 hr Aging	After 5000 hr Aging
				6-3-71	6-10-71	6-23-71	6-23-71	8-12-71	2-14-72	3-13-72
11	5-14	64	1200	< 2	< 2	-	< 2	< 2.3	> 10^4**	-
13	5-19	64	1000	< 2	< 2	-	< 2	< 2.3	< 2.3	-
14	5-20	None	1200	< 2	-	< 2	-	< 2.3	< 2.3	-
15***	5-21	None	1200	< 2	-	< 2	-	-	-	36
16	5-24	None	1000	< 2	-	< 2	-	< 2.3	< 2.3	-
18	5-27	None	R.T.	< 2	-	30	-	600	-	1630
19	6-1	None	800	< 2	-	< 2	-	< 2.3	-	< 2.3

* Values shown with < are below the minimum detectable value. Value given is the minimum detectable.

** Leak too large to measure on helium leak detector.

*** Cesium capsule.

TABLE LVI

LEAK RATE HISTORY OF CAPSULE #18

Date	Leak Rate (std cc air/sec)	Comment
5-27-71	$<2 \times 10^{-10}$	Braze date
6- 3-71	$<2 \times 10^{-10}$	Leak check
6- 4-71	$<2 \times 10^{-10}$	Ends of cups machined
6-18-71		e. b. weld of end caps
6-23-71	30×10^{-10}	Leak check
6-30-71 7- 2-71		Begin aging test at RT Slow initial pump-down
8-12-71	600×10^{-10}	Complete 1000 hour aging and leak check
8-18-71		Ion pump failed to develop adequately low system pressure. Installed an additional pump. SCR control failed, sent out for repair
9-24-71		Re-start aging tests
12-14-71		Vacuum pumps off 4 hrs
1-20-72		Vacuum pumps off ~ 4 hrs
3-10-72		5000-hour aging test concluded
3-13-72	1630×10^{-10}	Final leak check

TABLE LVII

LEAK RATE HISTORY OF CAPSULE #15

Date	Leak Rate (std cc air/sec)	Comment
5-21-71	$<2 \times 10^{-10}$	Braze date
6- 3-71	$<2 \times 10^{-10}$	Leak check
6- 4-71	$<2 \times 10^{-10}$	Ends of cups machined
6-10-71		e. b. weld of end caps
6-23-71	$<2 \times 10^{-10}$	Leak check
6-28-71		Cesium loading
6-30-71		Begin aging test at 1200°C
8-11-71		Conclude 1000 hrs aging
8-12-71		Remove sample for visual examination--no anomaly observed
8-17-71		Resume aging test at 1200°C
8-31-71		SCR Trigger unit failed, furnace cooled
9- 1-71		Replace SCR Trigger unit and re-start furnace
1-21-72		SCR unit failed
1-22-72		Re-start furnaces
2- 2-72		5000-hour aging test concluded
3-13-72		Opened capsule: no Cs remained very large vacuum leaks in e. b. weld regions.
3-15-72	36×10^{-10}	Remove end caps and re-test braze joint--final leak check

REFERENCES

1. National Aeronautics and Space Administration Negotiated Contract No. NAS3-11840 with North American Rockwell Corporation, Atomics International Division, February 10, 1969.

2. Phillips, W. M.: Metal-to-Ceramic Seals for Thermionic Converters, A Literature Survey. Technical Report 32-1420, Jet Propulsion Laboratory, November 1, 1969.

3. Kaufman, W. B.; Tichler, R. F.; and Breitwieser, R.: A High Temperature, Electrically Insulating Cermet Seal Having High Strength and Thermal Conductance. NASA TM X-52373, October 30, 1967.

4. Kirby, R. S.; and LaMotte, J. D.: Feasibility of Brazed Joints Between Cb-1Zr Alloy and Alumina Ceramics. LA-3302-MA, August 25, 1965.

5. Kueser, P. E.; et al.: Bore Seal Technology Topical Report. WAED-64-54E, also NASA-CR-54093, December, 1964.

6. Jost, W.: Diffusion in Solids, Liquids, Gases. Academic Press, Inc. New York, N. Y., p 16 ff.

7. Darken, L. S.; and Gurry, R. W.: Physical Chemistry of Metals. McGraw-Hill Book Co., Inc., New York, N.Y., p 437 ff.

8. Wells, C.: Chemical Techniques and Analysis of Diffusion Data in Atom Movements. Holloman, Ed., Am. Soc. Metals, Cleveland, Ohio (1951), p 26 ff.

9. Matano, C.: On the Relation Between the Diffusion Coefficients and Concentration of Solid Metals. J. Physics (Japan) 8, 109 (1933) as summarized in Ref. 7.

10. JANAF Thermochemical Tables, PB 168 370,PB 168 370-1, PB 168 370-2.

11. Glassner, A.: The Thermochemical Properties of the Oxides, Fluorides, and Chlorides to 2500°K. ANL-5750.

12. Shunk, F. A.: Constitution of Binary Alloys, Second Supplement. McGraw-Hill Book Co., Inc., New York, N.Y. (1969)

13. Hansen, M.: Constitution of Binary Alloys. McGraw-Hill Book Co., Inc., New York, N.Y. (1958).

14. McKisson, R.L.; and Bromley, L. A.: Heats of Formation of Intermetallic Compounds. UCRL-578 (1950).

15. Mechtly, E. A.: The International System of Units. NASA-SP-7012 (1964).

16. Lindberg, R. A., National Aeronautics and Space Administration Project Manager; personal communication, June (1972).

17. Ziebold, T. O.; and Ogilvie, R. E.: An Empirical Method for Electron Microanalysis. Anal. Chem., 36, (2), 322 (1964).

4